

ADVERTIMENT. L'accés als continguts d'aquesta tesi queda condicionat a l'acceptació de les condicions d'ús establertes per la següent llicència Creative Commons:  <https://creativecommons.org/licenses/?lang=ca>

ADVERTENCIA. El acceso a los contenidos de esta tesis queda condicionado a la aceptación de las condiciones de uso establecidas por la siguiente licencia Creative Commons:  <https://creativecommons.org/licenses/?lang=es>

WARNING. The access to the contents of this doctoral thesis it is limited to the acceptance of the use conditions set by the following Creative Commons license:  <https://creativecommons.org/licenses/?lang=en>

Role of two pathogenesis-related proteins (PRs)
in tomato plant defense against
Ralstonia solanacearum

Thesis submitted for the fulfilment of the requirements for the Doctoral Degree
(PhD) in Plant Biology and Biotechnology

Weiqi Zhang

Supervisor: Dr. Núria Sánchez Coll
Dr. Marc Valls

ACKNOWLEDGEMENT

Marc Valls and Nuria Sanchez, my supervisors in my PhD career. This doctoral dissertation would not have been accomplished without your guidance and resources. So many thanks for giving me the professional advice. Also, thank you giving me a lot of patience when my English was not good as well as the encouragement.

The lab. Many memories in the lab, Bacterial plant diseases and Plant cell death Lab, CRAG can't be forgot, I will always cherish funny and precious memories. And I thank you for giving me favors about this work and living in Spain. **Laia Armengot**, she is a very kind and nice person. She always gives me information about everything, like experiments,

SYNOPSIS

The plant pathogen *Ralstonia solanacearum* is the causal agent of the devastating disease known as bacterial wilt. *R. solanacearum* is a soil-borne and vascular pathogen that enters host plants through root wounds and lateral root emerging sites. Within the plant, the pathogen traverses the cortical apoplast until it reaches the vascular cylinder and proliferates rapidly the xylem vessels, reaching very high numbers. The combination of bacterial growth and the secretion of a mucus-like exopolysaccharide, clogs the infected vessels, blocking water flow and causing wilt disease symptoms that lead to the death of the plant. To date, the most effective method to control *R. solanacearum* is the use of genetic resistance.

In the apoplast, the initial battlefield between plant and pathogen, the host can perceive microbe-associated molecular patterns (MAMP) through receptors, activating pattern-triggered immunity (PTI). As part of their defense response, plant cells secrete proteases that can cleave pathogen proteins to make them detectable by the immune system. Secreted plant proteases can also trigger immunity by proteolyzing other plant proteins. However, pathogens can counteract proteolysis using protease inhibitors. In turn, plant hosts can deploy chitinase and peroxidases to combat pathogens. To explore proteomic responses in response to *R. solanacearum* in tomato plants, we extracted apoplast and xylem from susceptible (Marmande) and resistant (H7996) cultivars after infection. Comparative proteomics revealed high induction of the protease P69s (Chapter I) and PR1 proteins (Chapter II) during *R. solanacearum* infection.

In **chapter I**, we characterized the role of the Solanaceae-specific P69 subtilase family in the interaction between *R. solanacearum* and tomato. *R. solanacearum* infection post-translationally activated several tomato P69s. Among them, P69D was exclusively activated in resistant H7996 tomato plants. *In vitro* experiments showed that P69D activation by prodomain removal occurred in an autocatalytic and intramolecular reaction that does not rely on the residue upstream of the processing site. Importantly P69D-deficient tomato plants were more susceptible to bacterial wilt. Transient expression of *P69B*, *D* and *G* in *Nicotiana benthamiana* limited proliferation of *R. solanacearum*. Our study demonstrates that P69s have conserved features but diverse functions in tomato and that P69D is involved in resistance to *R. solanacearum* but not to other vascular pathogens like *Fusarium oxysporum*.

In **chapter II**, we characterised the role of the PR1 protein family in the interaction between tomato and *R. solanacearum*. Infection of tomato plants resulted in the accumulation of four different PR1 proteins PR1a, b, c and d. PR1s localized in multivesicular bodies. Mutation of the cleavage site trapped PR1b in the endoplasmic reticulum (ER), but not PR1c, that still could translocate into multivesicular bodies. PR1b and its variants did not have a direct antimicrobial function against *R. solanacearum*. However, a chemically

synthesized CAPE peptide, derived from PR1b, inhibited multiplication of *R. solanacearum* in tomato leaves and xylem through priming plant defense genes, such as jasmonic acid-responsive genes (*PI-I* and *PI-II*), and *PR1b*, its own precursor. Although the proteomics and N-terminomics in the chapter I indicated that PR1b could be a candidate substrate of P69D, we observed that the four PR1s tested were not cleaved by P69D *in vitro*. Importantly, two of the three tomato *pr1b* mutant lines generated in this study were slightly more resistant to *R. solanacearum* infection specifically when the pathogen was soil-inoculated.

RESUMEN EN ESPAÑOL

El patógeno vegetal *Ralstonia solanacearum* es el agente causal de la devastadora enfermedad conocida como marchitez bacteriana. *R. solanacearum* es un patógeno del suelo y vascular que ingresa en las plantas huésped a través de heridas en las raíces y sitios de emergencia de las raíces laterales. Una vez dentro de la planta, el patógeno atraviesa el apoplasto cortical hasta llegar al cilindro vascular y se multiplica rápidamente en los vasos del xilema, alcanzando números muy altos. La combinación del crecimiento bacteriano y la secreción de un exopolisacárido viscoso obstruye los vasos infectados, bloqueando el flujo de agua y causando síntomas de marchitez que conducen a la muerte de la planta. Hasta la fecha, el método más efectivo para controlar *R. solanacearum* es el uso de resistencia genética.

En el apoplasto, el primer campo de batalla entre la planta y el patógeno, el huésped puede percibir los patrones moleculares asociados a microbio (MAMP, por sus siglas en inglés) a través de los receptores, activando la inmunidad desencadenada por patrones (PTI, por sus siglas en inglés). Como parte de su respuesta de defensa, las células vegetales secretan proteasas que pueden cortar las proteínas del patógeno haciéndolas detectables por el sistema inmune. Las proteasas vegetales secretadas también pueden desencadenar la inmunidad proteolizando otras proteínas vegetales. Sin embargo, los patógenos pueden contrarrestar la proteólisis utilizando inhibidores de proteasas. A su vez, las plantas huésped pueden secretar quitinasa y peroxidasas para combatir a los patógenos en el apoplasto. Para explorar las respuestas proteómicas en respuesta a *R. solanacearum* en plantas de tomate, extrajimos apoplasto y xilema de cultivares susceptibles (Marmande) y resistentes (H7996) después de la infección. La proteómica comparativa reveló una alta inducción de la proteasa P69s (Capítulo I) y las proteínas PR1 (Capítulo II) durante la infección por *R. solanacearum*.

En el Capítulo I, caracterizamos el papel de la familia de subtilasas P69 específicas de las Solanáceas en la interacción entre *R. solanacearum* y el tomate. La infección por *R. solanacearum* activó post-traduccionamente varias P69s de tomate. Entre ellas, P69D se activó exclusivamente en las plantas de tomate resistentes H7996. Experimentos in vitro mostraron que la activación de P69D por la eliminación del prodominio tuvo lugar autocatalítica- e intramolecularmente, en una reacción no dependiente del residuo aguas arriba del sitio de procesamiento. Es importante señalar que las plantas de tomate deficientes en P69D fueron más susceptibles a la marchitez bacteriana. La expresión transitoria de *P69B*, *D* y *G* en *Nicotiana benthamiana* limitó la proliferación de *R. solanacearum*. Nuestro estudio demuestra que las P69s tienen características conservadas pero funciones diversas en plantas de tomate y que P69D está involucrada en la resistencia a *R. solanacearum* pero no a otros patógenos vasculares como *Fusarium oxysporum*.

En el Capítulo II, caracterizamos el papel de la familia de proteínas PR1 en la interacción entre el tomate y *R. solanacearum*. La infección de plantas de tomate resultó en la acumulación de cuatro proteínas PR1 diferentes PR1a, b, c y d. Las proteínas PR1s se localizaron en cuerpos multivesiculares. La mutación del sitio de corte atrapó a PR1b en el retículo endoplásmico (ER), pero no a PR1c, que aún podía translocarse a los cuerpos multivesiculares. PR1b y sus variantes no tenían una función antimicrobiana directa contra *R. solanacearum*. Sin embargo, un péptido CAPE sintetizado químicamente, derivado de PR1b, inhibió la multiplicación de *R. solanacearum* en hojas y xilema de tomate mediante la activación de genes de defensa de la planta, como genes sensibles al ácido jasmónico (*PI-I* y *PI-II*) y *PR1b*, su propio precursor. Aunque la proteómica y la N-terminómica en el Capítulo I indicaron que PR1b podría ser un sustrato candidato de P69D, observamos que los cuatro PR1s probados no fueron cortados por P69D *in vitro*. Es importante destacar que dos de las tres líneas mutantes de tomate *pr1b* generadas en este estudio fueron ligeramente más resistentes a la infección por *R. solanacearum*, específicamente cuando el patógeno fue inoculado en el suelo.

RESUM EN CATALÀ

El patogen vegetal *Ralstonia solanacearum* és l'agent causal de la devastadora malaltia coneguda com a marcimient bacterià. *R. solanacearum* és un patogen del sòl i vascular que ingressa a les plantes hostes a través de ferides a les arrels i llocs d'emergència de les arrels laterals. Un cop dins de la planta, el patogen travessa l'apoplast cortical fins arribar al cilindre vascular i es multiplica ràpidament als vasos del xilema, assolint nombres molt alts. La combinació del creixement bacterià i la secreció d'un exopolisacàrid viscos obstrueix els vasos infectats, bloquejant el flux d'aigua i causant símptomes de marcimient que condueixen a la mort de la planta. Fins a la data, el mètode més efectiu per controlar *R. solanacearum* és l'ús de resistència genètica.

A l'apoplast, el primer camp de batalla entre la planta i el patogen, l'hoste pot percebre els patrons moleculars associats a microbis (MAMP, per les seves sigles en anglès) a través dels receptors, activant la immunitat desencadenada per patrons (PTI, per les seves sigles en anglès). Com a part de la seva resposta de defensa, les cèl·lules vegetals secreten proteases que poden tallar les proteïnes del patogen fent-les detectables pel sistema immune. Les proteases vegetals secretes també poden desencadenar la immunitat proteolitzant altres proteïnes vegetals. No obstant això, els patògens poden contrarestar la proteòlisi utilitzant inhibidors de proteases. Alhora, les plantes hostes poden secretar quitinasa i peroxidases per combatre els patògens a l'apoplast. Per explorar les respostes proteòmiques en resposta a *R. solanacearum* en plantes de tomàquet, vam extreure apoplast i xilema de cultivars susceptibles (Marmande) i resistents (H7996) després de la infecció. La proteòmica comparativa va revelar una alta inducció de la proteasa P69s (Capítol I) i les proteïnes PR1 (Capítol II) durant la infecció per *R. solanacearum*.

Al Capítol I, vam caracteritzar el paper de la família de subtilases P69 específiques de les Solanàcies en la interacció entre *R. solanacearum* i les plantes de tomàquet. La infecció per *R. solanacearum* va activar post-traduccionament diverses P69s de tomàquet. Entre elles, P69D es va activar exclusivament a les plantes de tomàquet resistents H7996. Experiments in vitro van mostrar que l'activació de P69D per l'eliminació del prodomini es va produir de manera autocatalítica e intramolecular, en una reacció no dependent del residu aigües amunt del lloc de processament. És important assenyalar que les plantes de tomàquet deficientes en P69D eren més susceptibles al marcimient bacterià. L'expressió transitòria de *P69B*, *D* i *G* a *Nicotiana benthamiana* va limitar la proliferació de *R. solanacearum*. El nostre estudi demostra que les P69s tenen característiques conservades però funcions diverses en plantes de tomàquet i que P69D està involucrada en la resistència a *R. solanacearum* però no a altres patògens vasculars com *Fusarium oxysporum*.

Al Capítol II, vam caracteritzar el paper de la família de proteïnes PR1 en la interacció entre el tomàquet i *R. solanacearum*. La infecció de les plantes de tomàquet va donar lloc a l'acumulació de quatre proteïnes PR1 diferents PR1a, b, c i d. Les proteïnes PR1s es localitzaven en cossos multivesiculars. La mutació del lloc de tall va atrapar PR1b en el reticle endoplasmàtic (ER), però no a PR1c, que encara podia translocar-se als cossos multivesiculars. PR1b i les seves variants no mostren una funció antimicrobiana directa contra *R. solanacearum*. No obstant això, un péptid CAPE sintetitzat químicament, derivat de PR1b, va inhibir la multiplicació de *R. solanacearum* en fulles i xilema de tomàquet mitjançant l'activació de gens de defensa de la planta, com gens sensibles a l'àcid jasmònic (*PI-I* i *PI-II*) i *PR1b*, el seu propi precursor. Tot i que la proteòmica i la N-terminòmica al Capítol I indicaven que PR1b podria ser un substrat candidat de P69D, vam observar que els quatre PR1s provats no van ser tallats per P69D in vitro. És important destacar que dues de les tres línies mutants de tomàquet *pr1b* generades en aquest estudi eren lleugerament més resistents a la infecció per *R. solanacearum*, específicament quan el patògen va ser inoculat al sòl.

INDEX

SYNOPSIS.....	i
RESUMEN EN ESPAÑOL.....	iii
RESUM EN CATALÀ.....	v
INDEX	i
Introduction	1
1. Interaction between pathogens and plants	1
2. <i>Ralstonia solanacearum</i> , the causal agent of bacterial wilt	3
3. Plant defense in response to pathogen infection	5
3.1 Tomato resistance against bacterial wilt	5
3.2 Protein-based mechanisms of plant defense in the apoplast.....	6
Objectives	15
Characterization of the P69 family of plant subtilases.....	15
Characterization of the PR1 family of tomato plants.....	15
Chapter I (pre-publication).....	17
<i>Characterization of the P69 family of plant subtilases</i>	
I.1 Introduction	20
I.2 Results	21
I.3 Materials and Methods.....	35
I.4 Discussion	40
I.5 Supplementary	44
Chapter II	61
<i>Characterization of the PR1 family of tomato</i>	
II.1 Introduction	62
II.2 Results.....	65
II.3 Materials and methods.....	85
II.4 Discussion.....	94
Conclusions	100
References.....	102
Annex	116

Introduction

1. Interaction between pathogens and plants

In nature, plants face diverse microorganisms, many of which are beneficial for plants, like rhizobacteria and mycorrhizal fungi, and can help plants to absorb nutrients from environment and protect plants from different types of biotic and abiotic stress. However, danger microorganisms commonly co-exist in the environment. Pests and pathogens reduce by nearly 20% the yield of staple crops (rice, wheat, maize and potato), which constitute the major global source of human calorie intake (Savary *et al*, 2019). In this regard, disease control is essential to reduce the negative effect of the pathogens on the field and to ensure food production.

Plant pathogens acquired a wide variety of infection strategies in the evolutionary arms race of plant-pathogen interactions (Jones & Dangl, 2006). Many pathogens enter plants from natural openings, like stomata, and survive and multiply in this aqueous intercellular space, also called as the apoplastic space (Bai *et al*, 2015). For instance, various *Pseudomonas syringae* pathovars enter the host through open stomata, multiply in the apoplast and finally cause disease symptoms ranging from leaf spots to stem cankers (Melotto *et al*, 2008). Besides, some other plant pathogens are able to enter their host through root wounds caused by cultivation or by the feeding of insects and nematode. This is the case of the fungal pathogen *Fusarium oxysporum f. sp. lycopersici* and the bacterial pathogen *Ralstonia solanacearum*. Interestingly, these two root-infecting pathogens are considered vascular because they colonize and strongly multiply in the vascular tissue, finally causing irreversible wilt and destroying whole plants (Inoue *et al*, 2002; Vasse *et al*, 1995). The biological function and economic importance of vascular pathogens will be further explained in a section below.

Research on plant-pathogen interactions is essential to fight crop diseases. In the last two decades it has been discovered that upon pathogen attack plants activate a unique and sophisticated immune system. Each plant cell has developed an arsenal of cell

surface receptor to recognize microbial molecules. These receptors, called pattern recognition receptors (PRRs) induce pattern-triggered immunity (PTI) by perceiving non-self pathogen- or microbe-associated molecular patterns (MAMPs) (Jones & Dangl, 2006). For instance, the MAMPs, bacterial flagellin (flg22) and elongation factor Tu (elf18), are perceived by PRRs FLS2 and EFR, respectively (Gómez-Gómez & Boller, 2000; Zipfel *et al*, 2006). In addition, PRRs are able to recognize host-derived damage-associated molecular patterns (DAMPs), which are produced as a result of the damage inflicted by the pathogen. For example, oligogalacturonides (OGs) are generated as a product of cell wall degradation enzymes (CWDEs) from pathogens or by endogenous polygalacturonases, and are perceived by WAK1/WAK2 receptor (Brutus *et al*, 2010; Decreux *et al*, 2006). Plant endogenous immunomodulatory peptides, also named phytocytokines, are thought to be inducible DAMPs (iDAMPs). Phytocytokines mature and are released during activation of plant immune responses. For instance, the phytocytokines SMALL PHYTOCYTOKINES REGULATING DEFENSE AND WATER LOSS (SCREWs) are perceived by the cognate Arabidopsis receptor kinase PLANT SCREW UNRESPONSIVE RECEPTOR (NUT) (Liu *et al*, 2022). Upon perception of MAMPs/DAMPs by PRR PTI is initiated, including transient ROS burst, activation of mitogen-activated protein kinases (MAPKs) and elevation of cytosolic Ca²⁺ concentration (Bacete *et al*, 2018; Bigeard *et al*, 2015; Macho & Zipfel, 2014). This response is able to suppress the colonization and multiplication of most pathogens (Jones & Dangl, 2006). However, certain pathogens can successfully evade PTI responses via secretion of protein effectors. In the evolutionary arms race, plants have in turn evolved specialized receptors –mostly intracellular nucleotide-binding leucine-rich-repeat (NLRs) proteins– that can directly or indirectly recognize the activity of such effectors and induce what is known as effector-triggered immunity (ETI). Recent studies have shown crosstalk between PTI and ETI to potentiate a synergistic immune defense response against invading pathogens (Fig.1)(Ngou *et al*, 2021; Yuan *et al*, 2021).

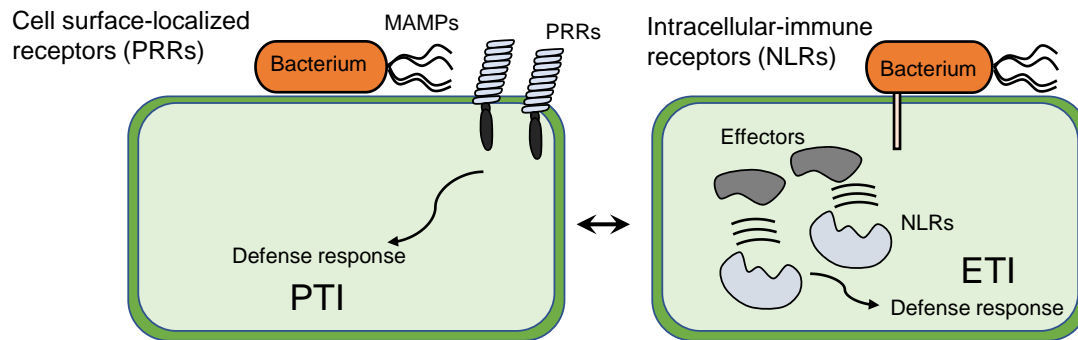


Fig. 1 The model of plant cell perceive bacterial pathogen to trigger PTI and ETI.

2. *Ralstonia solanacearum*, the causal agent of bacterial wilt

The plant pathogen *Ralstonia solanacearum* is the causal agent of the devastating disease known as bacterial wilt. This soil-borne gram-negative bacterium was initially described by Erwin F. Smith as “*Bacillus solanacearum*”, who portrayed it as a lethal wilt disease-causing bacterium of tomato, potato and eggplant (Smith, 1896). In the last century an increasing number of hosts has been identified, which currently encompass more than 200 plant species in over 50 families. Among them, important economical crops are threatened by *R. solanacearum* worldwide, owing to its aggressiveness, broad geographical distribution and long-persistence in soil and water environments (Genin, 2010; Mansfield *et al*, 2012).

As previously mentioned, *R. solanacearum* enter hosts through natural wounding of the root or lateral root emerging sites (Vasse *et al.*, 1995). In the root it can cross the cortical apoplast until reaching the vascular system and colonize the xylem vessels, where it multiplies rapidly reaching very high numbers (McGarvey *et al*, 1999). Meanwhile, *R. solanacearum* secretes a mucus-like component, known as exopolysaccharide (EPS), which can completely block the colonized xylem vessel, contributing to wilting (McGarvey *et al.*, 1999). After infected plants die, *R. solanacearum* returns to the soil or waterways to infect new hosts (Huang & Allen, 2000).

The major virulence determinants of *R. solanacearum* are the following:

A) The type III secretion system (T3SS). Pathogenic gram-negative bacteria have

developed this extremely efficient virulent strategy to avoid detection by the immune system. This ultrastructure forms a needle-liked channel that connects the cytoplasm of the bacterium and its hosts and allows the translocation of Type III effector proteins (T3Es). T3Es interfere the normal function of the host cell and suppress immune responses to facilitate pathogen invasion (Deng *et al*, 2017). The components of the T3SSs are highly conserved in many pathogens of animals and plants. In *R. solanacearum*, the T3SS is encoded by a cluster of more than 20 genes called the *hrp* operon and it is key for successful infection, colonization and multiplication in the host (Boucher *et al*, 1985; Vasse *et al*, 2000). This *hrp* operon is regulated by the PrhA - PrhI/R – PrhJ – HrpG - HrpB pathway, where only PrhA is a membrane receptor that perceives host signaling, the rest of them are transcriptional regulators (Brito *et al*, 2002; Valls *et al*, 2006). HrpB, the most downstream of the T3SS regulators, activates as well transcription of T3Es as well.

B) Exopolysaccharide (EPS). When *R. solanacearum* reaches high density levels, a large number of EPS is secreted. It contains the sugars N-acetylgalactosamine, 2-N-acetyl-2-deoxy-L-galacturonic acid and 2-N-acetyl-4-N-(3-hydroxybutanoyl)-2,4,6-trideoxy-D-glucose. *R. solanacearum* EPS-deficient mutants show impaired multiplication on tomato and tobacco and result in less symptoms (Denny & Baek, 1991). Interestingly, EPS help bacteria move within the stems as well (Saile *et al*, 1997), indicating that it might also play a protective and coating role, contributing to biofilm formation, movement in the vascular vessel and minimizing detection by plant defense mechanisms.

C) Biofilm formation. *R. solanacearum* can form biofilm structures in the surface of cells (Kumar *et al*, 2016; Mori *et al*, 2018; Mori *et al*, 2016). A mutation in *R. solanacearum* *lecM*, which encodes a lectin protein, severely affected biofilm formation in *in vitro* assays, and resulted in reduced colonization in the leaf apoplast and in the roots, and completely abolished virulence (Mori *et al*, 2016). The *lecM* mutation led to a reduced attachment ability of *R. solanacearum* on glass slides as well, indicating that biofilm formation guarantees the attachment or the

pathogen to the plant cells, possibly involving the lectin lecM and the deposition of EPS (Mori *et al.*, 2016). After attachment, the T3SS is assembled and T3Es are translocated into the host cells, suppressing immunity and favoring the invasion of *R. solanacearum*.

D) Cell wall degrading enzymes (CWDEs). CWDEs are generally secreted to the extracellular environment by the type II secretion system (T2SS). Until now, 6 CWDE have been found in the genome of *R. solanacearum* GMI1000, one 1,4- β -endoglucanase (*egl*), and one 1,4- β -cellobiohydrolase (*cbhA*) one pectin methyl-esterase (*pme*) and three polygalacturonases (*pehA*, *pehB* and *pehC*) (Liu *et al.*, 2005). The different combinations of mutants in three *pehs* and *egl* did not affect the virulence of *R. solanacearum*, while the one lacking one or both cellulolytic enzymes (*egl* or *cbhA*) caused wilting of tomato plants more slowly than the wild type strain (Liu *et al.*, 2005). Interestingly, the sextuple mutant lacking all six CWDEs was still found more virulent than the T2SS-impaired mutants (Liu *et al.*, 2005), suggesting except for known CWDES, there is some other secreted proteins by T2SS are crucial for *R. solanacearum* infection and colonization.

3. Plant defense in response to pathogen infection

The resistance to vascular pathogens is very complex as the processing of pathogen virulence. Since *R. solanacearum* is able to survive in the waterways and soil for long time and shelter inside of the host, like in the apoplast and xylem, it is difficult to find efficient chemical or biological method to manage and control the vascular pathogen in the crops. Additionally, their large host range limits the efficiency of crop rotation strategies that makes the management of disease control more difficult. Considering those reasons, the most reliable management strategy has been the use of genetic resistance. In the following sections, we summarize some researches that have been identified the molecular basis of resistance in different plant species.

3.1 Tomato resistance against bacterial wilt

In nature, the Hawaii lines, particularly H7996, are the tomato varieties with highest

levels of resistance to *R. solanacearum* known to date (Wang *et al*, 1998). However, the poor fruit produced by this cultivar makes it not suitable for the market. Although scientists have tried to introgress the resistance phenotype into more appealing commercial varieties, tomato breeders have not been successful in breaking the apparent genetic link between small fruit size and high levels of resistance (Scott *et al*, 2004). However, over thirty years, several studies focused on this variety to identify the molecules and special structure involved in resistance, and help us to understand the small molecules and structural mechanisms of defense against *R. solanacearum*.

H7996 was shown to be the most efficient cultivar in restricting colonization of *R. solanacearum* at different plant levels (McGarvey *et al.*, 1999; Nakaho *et al*, 2004), and an obvious delay symptom (Caldwell *et al*, 2017). A Comparison of histology and metabolite analysis between resistant and susceptible tomato plants under pathogen attack indicate that formation of tyloses, cell wall thickening, cell wall composition and over-lignification in H7996 cultivar are important determinants of resistance against *R. solanacearum* in this tomato variety (Grimault *et al*, 1994; Ishihara *et al*, 2012a; Wydra & Beri, 2007). Apart from that, suberin deposits accumulating around colonized xylem vessels seem to function as a physico-chemical barrier to block the spread of *R. solanacearum* (Kashyap *et al*, 2022). Additionally, H7996 cultivar can accumulate a large amount of some chemical compounds against *R. solanacearum* invasion. Hydroxycinnamic acid amides (HCAAs), constitute a class of phenolics that are highly expressed in H7996 compared with in the susceptible tomato cultivar Marmande (Kashyap *et al.*, 2022). Importantly, overexpression of N-hydroxycinnamoyl transferases (*THT*), which lead to accumulation of HCAAs, in the susceptible tomato cultivar could significantly enhance the resistance to *R. solanacearum* through formation a chemical barrier to limit vascular colonization, preventing bacterial spread and blocking the onset of disease (Kashyap *et al.*, 2022).

3.2 Protein-based mechanisms of plant defense in the apoplast

During the plant infection process, *R. solanacearum* colonizes two particular locations as consistently documented in the literature: the apoplast, also known as intercellular

space, which the bacterium colonizes during the initial stages of the infection, and the xylem, the main niche where the pathogen multiplies and spreads systemically. Most of works studying plant metabolites induced in response to pathogens have focused on foliar pathogens because of the ease in collecting the leaf's apoplastic fluid (Gupta *et al*, 2015a). In the apoplast, plants perceive MAMPs/PAMPs and DAMPs by plant PRRs, which triggers a series of plant immune responses. In addition, both plants and pathogens secrete an arsenal of molecules to suppress the opponent (Fig. 2)(Dixon *et al*, 2000; Lozano-Torres *et al*, 2012; Perez-Lopez *et al*, 2021; Wang *et al*, 2021). In the infection of xylem, CWDE secreted by vascular pathogens might digest the xylem walls and pit membranes of the vessels (Yadeta & J. Thomma, 2013). Besides constructing a physico-chemical barrier, plants also secrete some proteins and small molecules against pathogens, such as protease, chitinase, unknown function PR proteins (PR1/PR5x), oxidoreductases and peroxidases. Peroxidases are among the most abundantly secreted enzymes against vascular pathogens. They are involved in the production of reactive oxygen species (ROS) that are toxic for the pathogen (Passardi *et al*, 2005) and signaling molecules to regulate plant defense and acclimation to responses biotic and abiotic stress (Mignolet-Spruyt *et al*, 2016; Vaahtera *et al*, 2014).

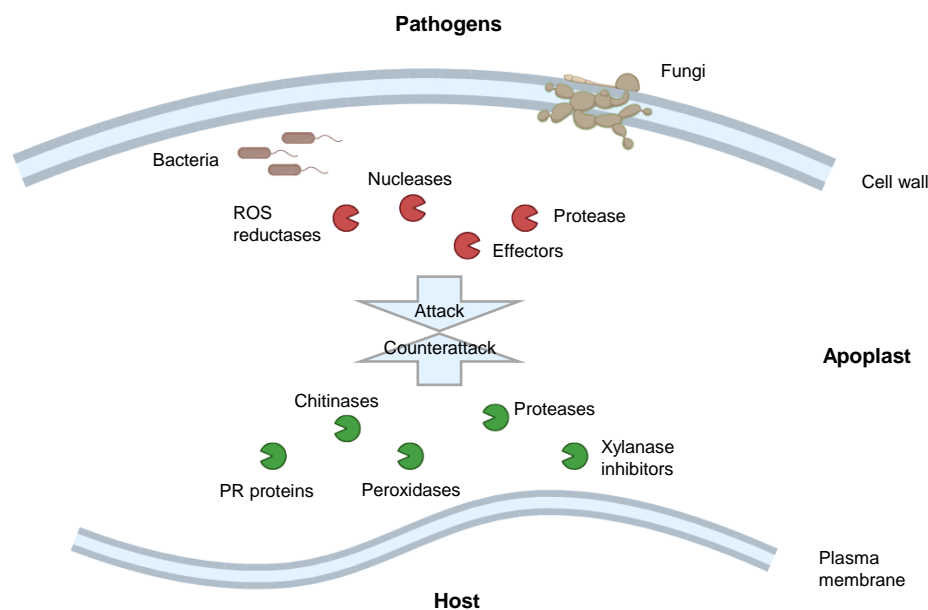


Fig.2 Overview of the enriched apoplastic proteins identified from in-plant secretome studies during host-pathogen interaction. High abundant secreted proteins derived from

pathogens are listed on top while host secreted proteins are listed at the bottom. Figure adapted from (Gupta *et al*, 2015b)

In our team, we extracted apoplast and xylem from susceptible (Marmande) and resistant (H7996) tomato plant under *R. solanacearum* infection to investigate the proteomic responses (Planas-Marques *et al*, 2018). Besides accumulation of peroxidases and oxidoreductases, the protease and PR proteins are also highly induced in the apoplast and xylem. Further, we characterized the P69s protease (Chapter I) and PR1 proteins (Chapter II) upon *R. solanacearum* infection.

3.2.1 Secreted plant proteases in response to pathogen infection

Proteases are enzymes that catalyze the cleavage of their substrates based on their ability to recognize and cut short specific amino acid sequences. Plant genomes encode hundreds of proteases that are distributed across all protease families, playing key roles in most aspects of plant physiology and development (van der Hoorn & Klemencic, 2021). Aspartic proteases, cysteine proteases, metalloproteases, and serine proteases are the most abundant superfamily proteases in plants. All these three types of proteases are involved in plant immunity and pathogen restriction responses (van der Hoorn, 2008).

Papain-like cysteine proteases affect plant defense indirectly or directly. One of the cysteine proteases, Rcr3 (Required for Cladosporium Resistance-3) was shown to act as a coreceptor of the tomato PRR-like protein Cf-2 (Dixon *et al.*, 2000). Rcr3 was targeted and inhibited by the effectors Avr2 and GrVAP1 secreted by the fungal pathogen *Cladosporium fulvum* and the nematode *Globodera rostochiensis*, respectively. The effector-Rcr3 complex was then sensed by Cf-2, triggering HR and rendering the plant resistant (Lozano-Torres *et al.*, 2012; Rooney *et al*, 2005). Another superfamily of proteases important for plant defense are subtilases (SBTs), members of the superfamily of subtilisin-like serine proteases (Schaller *et al*, 2018). Overexpression of the extracellular subtilase SBT3.3 leads to enhanced mitogen-activated protein kinase activation, defense gene expression, and resistance against

bacterial and fungal pathogens (Ramirez *et al*, 2013). Another example is a small cysteine-rich secreted protein PC2 from *Phytophthora infestans*. When it was secreted to the apoplast, it can induce plant immunity after cleaved by a subtilisin-like serine protease, the P69B (Wang *et al.*, 2021).

However, some pathogens have evolved effective weapons to inhibit the activity of plant defense-related proteases. For instance, the pathogen *Phytophthora infestans* secret a Kazal-like protease inhibitor (EPI1), to prevent PC2 cleavage and prohibit PC2 triggered plant immunity (Wang *et al.*, 2021). Pit2, an effector secreted by a biotrophic fungal pathogen *Ustilago maydis*, function as an inhibitor of a set of apoplastic cysteine proteases in maize, CP2, CP1A, CP1B and XCP2, lead to reduction of salicylic-acid-associated plant defenses (Mueller *et al*, 2013). SSPbP53, a putative apoplastic cystatin-like protein, interacts with xylem-associated PLCPs, XCP1, and the interaction suppress the plant immunity (Perez-Lopez *et al.*, 2021).

In addition to the interaction between plant proteases and pathogen effectors, plant proteases can target other plant proteins to activate immunity indirectly. In one hand, some plant proteases activate another protease by cleavage of the autoinhibitory prodomain. An example is the Rcr3 precursor is cleaved by P69B to form matured and activated Rcr3 (Paulus *et al*, 2020). In another hand, plant proteases can be necessary for formation of some phytocytokines. For instance, tomato systemin is processed at two aspartate residues from the C-terminus of a precursor protein, prosystemin (PS) by two tomato subtilases, SLPHYTASPASE 1 (SIPhyt1) and SIPhyt2, (Beloshistov *et al*, 2018). Metacaspase 4 and the other Type-II metacaspase are required for maturation of PEP1 from its precursor PROPEP1 (Hander *et al*, 2019). Interestingly, infection and cell wall damage can induce cleavage from PROPEP3 to PEP3 (Engelsdorf *et al*, 2018).

Identifying the protease-substrate pair is an important method to understand the mechanism of how protease triggers plant immunity. Nowadays, with the development of sequencing technology, the Proteomics Identification of Cleavage Sites (PICS) method provide a tool to test the cleavage e preference of target protein (Schilling *et*

al, 2011; Schilling & Overall, 2008), and the High-efficiency Undecanal-based N-Termini EnRichment (HUNTER) is a fast and sensitive method which is able to enrich protein N-termini from limited sample sources (Demir *et al*, 2022).

In this thesis we have identified new members of the P69 family in tomato and other members of the Solanaceae family and have harmonized its nomenclature system. Further, we have characterized the mode of action of these proteases, finding their substrate by PICS and Hunter, and their potential role in defense (Chapter I).

3.2.2 Phyto cytokine signaling as modulators of plant defense

Phyto cytokines are plant endogenous peptides that regulate plant defense. Generally, when plants are under stress, the precursor protein containing phyto cytokine will be highly induced and, after processing in the cytosol, will be released into the apoplast. The downstream signaling will be activated, when phyto cytokine is perceived by receptors. The first report about a signaling peptide acting this way was systemin in tomato (Pearce *et al*, 1991). In recent years, research in this field has boomed, with different types of peptide signals identified, which regulate plant immune responses, growth and development. Basically, phyto cytokines can be classified into two main groups depending on the absence or presence of a signal peptide to be secreted into the intercellular space (Table 1). Phyto cytokines whose precursors harbor a signal peptide, include phytosulfokines (PSKs), plant peptide containing sulphated tyrosine 1 (PSY1) and PAMP-induced secreted peptide 1 (PIP1)/PIP2. Due to the presence of the signal peptide, these phyto cytokine precursors enter the secretory pathway after translation, and they are finally secreted into the apoplast as mature phyto cytokines possessing biological activity. In the secretory pathway involving endoplasmic reticulum (ER), Golgi, late endosome (LE) and multivesicular body (MVB) or the apoplast, the signal peptide and prodomains are removed by proteolytic cleavage from phyto cytokine precursors. Subsequently, post-translational modifications, like tyrosine sulfation, proline hydroxylation, hydroxyproline arabinosylation, and intramolecular disulfide bond formation, are required for their maturation (Matsubayashi, 2014; Olsson *et al*, 2019). A second type of phyto cytokines, such as systemin, *Z. mays*

immune signaling peptide 1 (ZIP1) and plant elicitor peptide (PEP1), are processed in the cytoplasm or apoplast. Since they lack a signal peptide, they cannot be secreted by the canonical ER-Golgi secretory pathway, but instead they may use an unknown secretory pathway or take advantage of a compromised plasma membrane caused by damage (Ding *et al*, 2012).

Table 1 Classification, perception, processing and functions of phyto cytokines.

Type	Phyto cytokines	Receptor	Processing enzyme	Functions	Reference
Non-secreted peptides	Systemin	SYR1	Phytaspase	Induction of proteinase inhibitors, extracellular alkalization, and ethylene emission, mediation of systemic defense response, defense against insect herbivory	(Pearce <i>et al.</i> , 1991; Ryan & Pearce, 2003; Wang <i>et al.</i> , 2018)
	Pep1, Pep2, Pep3	PEPR1, PEPR2	METACASPASE 4	Activation of PTI responses, and plant resistance to <i>B. cinerea</i> , <i>P. syringae</i> , and <i>P. irregular</i> , activation of ET, JA, and SA signaling pathways, mediation of systemic immunity	(Hander <i>et al.</i> , 2019; Huffaker <i>et al.</i> , 2011; Huffaker <i>et al.</i> , 2006; Liu <i>et al.</i> , 2013; Ross <i>et al.</i> , 2014; Yamaguchi <i>et al.</i> , 2010)
	ZIP1	Unknown	CP1/2	Activation of SA defense signaling, maize resistance against <i>U. maydis</i> and susceptibility to <i>B. cinerea</i>	(Ziemann <i>et al.</i> , 2018)
Secreted peptides	PSK	PSKR1	SBT1.1	Attenuation of PTI and SA signaling, activation of JA signaling, increase resistance to necrotrophic pathogens and susceptibility to biotrophic pathogens	(Amano <i>et al.</i> , 2007; Igarashi <i>et al.</i> , 2012; Mosher <i>et al.</i> , 2013; Rodiuc <i>et al.</i> , 2016; Zhang <i>et al.</i> , 2018)
	PSY1	PSYR	Unknown		
	PIP1, PIP2	RLK7	Unknown	Activation of PTI responses and plant resistance to <i>P. syringae</i> and <i>F. oxysporum</i>	(Hou <i>et al.</i> , 2014)
	IDA	HAE, HSL2	SBT4.12, SBT4.13, SBT5.2	Regulation of plant resistance to <i>P. syringae</i>	(Butenko <i>et al.</i> , 2003; Patharkar & Walker, 2016; Schardon <i>et al.</i> , 2016; Stenvik <i>et al.</i> , 2008; Wang <i>et al.</i> , 2017)
	IDL6	HAE, HSL2	Unknown	Suppression of PTI responses and SA signaling, attenuation plant resistance to <i>P. syringae</i>	
	SCOOP12	MIK2	Unknown	Activation of PTI responses, plant resistance to <i>P. syringae</i> and <i>F. oxysporum</i> , and susceptible to <i>E. amylovora</i>	(Gully <i>et al.</i> , 2019; Hou <i>et al.</i> , 2021; Rhodes <i>et al.</i> , 2021)
	RGF7/GLV4	RGI3/4	Unknown	Activation of PTI responses	(Matsuzaki <i>et al.</i> , 2010; Ou <i>et al.</i> , 2016; Stegmann <i>et al.</i> , 2022; Wang <i>et al.</i> , 2021; Whitford <i>et al.</i> , 2012)
	RGF9/GLV2	RGI3	Unknown	Activation of PTI responses Promotion of FLS2 accumulation	
	HypSys	Unknown	Unknown	Induction of proteinase inhibitors, extracellular alkalization, and ethylene emission, activation of resistance to insect herbivory	(Pearce <i>et al.</i> , 2001; Ryan & Pearce, 2003)
	RALF1	FER-LLG	Unknown	Attenuation of PTI, activation of JA signaling	(Guo <i>et al.</i> , 2018; Haruta <i>et al.</i> , 2014; Li <i>et al.</i> , 2015; Stegmann <i>et al.</i> , 2017)
	RALF17	Unknown	Unknown	Activation of PTI responses	
	RALF22, RALF23	FER-LLG	S1P	Attenuation of PTI signaling	
	CAPE1	Unknown	XCP1	Activation of PTI responses and SA signaling, enhance plant resistance to <i>P. syringae</i>	(Chen <i>et al.</i> , 2014; Chen <i>et al.</i> , 2023)
	SCREW	NUT	Unknown	Suppression of phytohormone abscisic acid (ABA)- and microbe-associated molecular pattern (MAMP)-induced stomatal closure	(Liu <i>et al.</i> , 2022)
	IRP1	Unknown	Unknown	Induction of the chitin signaling pathway	(Wang <i>et al.</i> , 2023)

Most phyto cytokines are perceived by cell surface-resident receptor-like kinases (RLKs), which contain an extracellular domain, a single transmembrane region and the cytoplasmic kinase domain (Couto & Zipfel, 2016; Escocard de Azevedo Manhaes *et al*, 2021). Over past decade, more phtocytokine-receptor pairs have been discovered. Tomato systemin is perceived by SYSTEMIN RECEPTOR 1 (SYR1) and SYR2 (Wang *et al*, 2018), HAESA and HAESA-LIKE2 (HSL2) recognize IDA (Santiago *et al*, 2016), the phyto cytokine SMALL PHYTOCYTOKINES REGULATING DEFENSE AND WATER LOSS (SCREWs) and the cognate receptor kinase PLANT SCREW UNRESPONSIVE RECEPTOR (NUT) (Liu *et al*, 2022). Interestingly, these cell surface receptors often form complexes with the same coreceptors of multiple PRRs, and activate downstream signaling upon ligand perception. Like PEPs, PIPs, and SCOOPs are perceived by EP RECEPTOR 1 (PEPR1)/PEPR2, ECEPTOR-LIKE KINASE 7 (RLK7) and MALE DISCOVERER 1-INTERACTING RECEPTOR-LIKE KINASE 2 (MIK2), respectively, and interact with the coreceptor BAK1 (Hou *et al*, 2014; Rhodes *et al*, 2021; Yamaguchi *et al*, 2010). Noticeably, perception of ROOT MERISTEM GROWTH FACTOR 9/ GOLVEN 2 (RGF9/GLV2) by ROOT MERISTEM GROWTH FACTOR INSENSITIVE 3 can promote flg22-induced FLS2-BAK1 complex formation (Stegmann *et al*, 2022), suggesting some phyto cytokines modulate plant immunity indirectly, by increasing PRR abundance independently of transcriptional regulation.

Some phyto cytokines, like Pep1, PIP1 and SCOOP12 can also activate PTI responses, including ROS production, the activation of mitogen-activated protein kinases (MAPKs) and induction of some defense genes expression (Gully *et al*, 2019; Hou *et al*, 2014; Ranf *et al*, 2011). Usually, phyto cytokines are considered to enhance MAMP responses. However, some of them, like SCOOP-MIK2 signaling promotes flg22- but antagonizes Pep1-induced ROS production, showing a more complicated crosstalk between MAMP- and phyto cytokine-mediated immune signaling (Rhodes *et al*, 2021). In the plant defense related hormones, signaling crosstalk between SA and ET/JA commonly is thought to function as a reciprocal antagonism to against biotrophic and necrotrophic pathogens (Thaler *et al*, 2012). PIP1 and ZIP1 activate SA signaling pathway and contribute to against biotrophic pathogens (Hou *et al*, 2019; Ziemann *et al*, 2018), while PSK and PSY1 activate JA signaling pathway, but suppress SA signaling pathway, to enhance plant resistance to necrotrophic pathogens (Mosher *et al*, 2013). It is worth noting that PEP1 is able to activate both SA and JA signaling pathway and facilitate plant against both biotrophic and necrotrophic pathogens (Liu *et al*, 2013; Ross *et al*, 2014; Tintor *et al*, 2013; Yamaguchi *et al*, 2010).

Objectives

Characterization of the P69 family of plant subtilases

1. To define P69 subtilase family and its conservation in several plant species.
2. To decipher the mode of action and specificity of cleavage of P69 subtilases.
3. To investigate the role of P69D during *R. solanacearum* infection.

Characterization of the PR1 family of tomato plants

4. To verify the antimicrobial function of the CAP domain and the CAPE peptide.
5. To investigate the role of PR1b during *R. solanacearum* infection.
6. To characterize PR1b protein cleavage and release of the CAPE peptide.
7. To investigate the impact of PR1b and the CAPE peptide on plant immune responses.

Objectives

Chapter I (pre-publication)

Characterization of the P69 family of plant subtilases

The tomato P69 subtilase family is involved in resistance to bacterial wilt

Running title: P69D is involved in tomato resistance to *R. solanacearum*

Weiqi Zhang^{*1}, Marc Planas-Marquès^{*1,2}, Marianne Mazier³, Margarita Šimkovicová⁴, Melissa Mantz^{5,6}, Pitter F Huesgen^{5,6,7}, Frank L W Takken⁴, Annick Stintzi⁸, Andreas Schaller⁸, Nuria S. Coll^{1,9}, Marc Valls^{1,2}

¹ Centre for Research in Agricultural Genomics (CRAG), CSIC-IRTA-UAB-UB, Campus UAB, Bellaterra, Spain

² Department of Genetics, Microbiology and Statistics, Universitat de Barcelona, Barcelona, Spain

³ GAFL UR 1052, INRAE F84143 Montfavet, France.

⁴ Molecular Plant Pathology, Faculty of Science, Swammerdam Institute for Life Sciences, University of Amsterdam, Amsterdam, Netherlands.

⁵ Central Institute for Engineering, Electronics and Analytics, ZEA-3, Forschungszentrum Jülich, Jülich, Germany.

⁶ CECAD, Medical Faculty and University Hospital, University of Cologne, Cologne, Germany

⁷ Institute for Biochemistry, Faculty of Mathematics and Natural Sciences, University of Cologne, Cologne, Germany

⁸ Department of Plant Physiology and Biochemistry, University of Hohenheim, Stuttgart, Germany

⁹ Consejo Superior de Investigaciones Científicas (CSIC), Barcelona, Spain.

Authors for correspondence:

Marc Valls, e-mail: marcvalls@ub.edu

Nuria S. Coll, e-mail: nuria.sanchez-coll@cragenomica.es

Summary

The intercellular space or apoplast constitutes the main interface in plant-pathogen interactions. Apoplastic subtilisin-like proteases -subtilases- may play an important role in defence and they have been identified as targets of pathogen-secreted effector proteins. Here, we characterise the role of the Solanaceae-specific P69 subtilase family in the interaction between tomato and the vascular bacterial wilt pathogen *Ralstonia solanacearum*. *R. solanacearum* infection post-translationally activated several tomato P69s. Among them, P69D was exclusively activated in tomato plants resistant to *R. solanacearum*. *In vitro* experiments showed that P69D activation by prodomain removal occurred in an autocatalytic and intramolecular reaction that does not rely on the residue upstream of the processing site. Importantly P69D-deficient tomato plants were more susceptible to bacterial wilt and transient expression of *P69B*, *D* and *G* in *Nicotiana benthamiana* limited proliferation of *R. solanacearum*. Our study demonstrates that P69s have conserved features but diverse functions in tomato and that P69D is involved in resistance to *R. solanacearum* but not to other vascular pathogens like *Fusarium oxysporum*.

Key words: Apoplast, plant defence, *Ralstonia solanacearum*, serine protease, *Solanum lycopersicum*

I.1 Introduction

The extracellular space or apoplast plays a key role in plant-pathogen interactions. Both plants and pathogens secrete proteases, protease inhibitors, glycoside hydrolases (GHs), peroxidases, and antioxidant enzymes into this compartment (Du *et al*, 2016). Plant Pattern Recognition Receptors (PRRs) recognize Microbe- and Danger-Associated Molecular Patterns (MAMPs and DAMPs) in the apoplast and activate immune responses (Macho & Zipfel, 2014). However, due to the ease in collecting the leaf apoplastic fluid (Gupta *et al*., 2015b), most of these studies have been limited to foliar pathogens and the role of apoplastic enzymes in the interaction with vascular pathogens is largely unexplored.

Two families of proteases are of particular interest with respect to their role in plant defense: the papain-like cysteine proteases (PLCPs), and the subtilisin-like proteases (subtilases). Subtilases are serine proteases present in all living organisms and involved in various processes, from embryogenesis to senescence (Schaller *et al*., 2018). Subtilases possess an aspartate, histidine, serine catalytic triad (Smith *et al*, 1966) and are synthesized as pre-pro-enzymes with an N-terminal signal peptide and an auto-inhibitory prodomain that needs to be cleaved for secretion and activation of the protease (Meyer, 2016; Schaller *et al*., 2018). This prodomain processing is an intra-molecular (autocatalytic) processing event (Cedzich *et al*, 2009; Meyer, 2016; Nebes & Jones, 1991; Power *et al*, 1986; Vey *et al*, 1994) and depends on the active-site serine (Cedzich *et al*., 2009; Chichkova *et al*, 2010). Thus, the amino acid sequence at the cleavage site is expected to reflect the substrate specificity of the protease (Muller *et al*, 2000). This is observed for the aspartate-specific phytaspases, which feature an aspartic acid residue upstream of the cleavage site (Chichkova *et al*., 2010; Reichardt *et al*, 2018), while in other plant subtilases the TTXS/T motif at the N-terminus of the mature protease appears to be more relevant for cleavage site recognition (Meyer, 2016). The mature sequence of subtilases contains a subtilase catalytic domain, a protease-associated domain, and a fibronectin III-like domain (Schaller *et al*., 2018). The protease-associated domain has been implicated in protein-protein interactions (Mahon & Bateman, 2000) and substrate binding specificity (Schaller *et al*., 2018; Tan-Wilson *et al*, 2012), while the fibronectin III-like domain appears to confer stability to the enzyme (Ottmann *et al*, 2009).

Tomato P69A, initially named Pathogenesis Related protein 7 (PR-7), is the first subtilase for which a role in plant defence was reported (Vera, 1989; Vera & Conejero, 1988). The protein localizes in the extracellular space and occasionally inside the vacuole (Vera *et al*, 1989). Subsequent studies identified a total of six P69 genes in tomato, which were named P69A to F (Jorda *et al*, 1999; Jorda *et al*, 2000; Meichtry *et al*, 1999). P69B and P69C, are systemically induced by *Pseudomonas syringae* infection and salicylic acid treatment

(Jorda *et al.*, 2000; Meichtry *et al.*, 1999). Of note, P69C cleaves a leucin-rich repeat protein (LRP) located in the extracellular matrix, which was speculated to trigger immune signalling (Tornero *et al.*, 1996). Recently, other P69 genes were shown to be upregulated upon infection with various pathogens, including *Phytophthora infestans* (Tian *et al.*, 2004) and *Ralstonia solanacearum* (Ishihara *et al.*, 2012b; Zuluaga *et al.*, 2015). P69B was recently reported to participate in the maturation-by-cleavage of the Rcr3 protease (Paulus *et al.*, 2020), thereby constituting the first proteolytic cascade identified in plants. Of note, Rcr3 and Pip1 papain-like cysteine proteases are inhibited by *Cladosporium fulvum* Avr2 effector and *P. infestans* EPIC1 and EPIC2B (Song *et al.*, 2009; Tian *et al.*, 2007). In addition, *P. infestans* secretes the Kazal-like protease inhibitors EPI1 and EPI10 that were shown to bind and inhibit P69B (Gupta *et al.*, 2015b; Paulus *et al.*, 2020; Tian *et al.*, 2005; Tian *et al.*, 2004). The recent identification of P69B inhibitors in *Cladosporium fulvum*, *Fusarium oxysporum* and *Xanthomonas perforans* suggests that inactivation of P69B may be a general virulence strategy of diverse microbial pathogens (Homma *et al.*, 2023).

R. solanacearum (some strains are also called *R. pseudosolanacearum*) is a bacterial vascular pathogen that causes wilt disease in over 200 plant species, including economically important crops such as tomato, potato, banana and pepper (Hayward, 1991). This soil-borne pathogen infects plants through the roots and eventually colonises the xylem, where it clogs infected vessels, causing plant wilting (Vasse, 1995). Before reaching the xylem, *R. solanacearum* multiplies in the intercellular spaces of the roots (Grimault, 1994).

We previously demonstrated that resistant tomato plants limit early root colonization by *R. solanacearum* (Planas-Marques *et al.*, 2020). As a first step to dissect the underlying mechanisms we analysed the apoplast proteome upon challenge with *R. solanacearum* strain GMI1000 in susceptible (Marmande) and resistant (Hawaii 7996) tomato cultivars (Planas-Marques *et al.*, 2018). Amongst all papain-like cysteine proteases and serine hydrolases, two closely related subtilases (P69D and P69J) were the most highly activated after infection. More recently, we identified a total of ten P69 subtilases in the tomato genome (Reichardt *et al.*, 2018). Here, we study the P69s most highly induced upon infection and we demonstrate that they have conserved features but diverse functions in tomato. We further show that P69D is involved in resistance to *R. solanacearum* but not to other vascular pathogens like *Fusarium oxysporum*.

I.2 Results

P69s are conserved subtilases present only in the nightshade family and activated in tomato upon *R. solanacearum* infection

Ten genes encoding P69 proteases have been annotated in the tomato genome (Reichardt *et al.*, 2018) (Table S1). These cluster in a single 60Kb region on chromosome 8, without any interspaced genes (Fig.1A). A neighbour-joining tree of the encoded amino acid sequences, including the closest non-P69 tomato subtilase (Soly08g007680) as an outgroup, revealed that the most divergent proteins (P69E and F) occupy a distal position at one end of the genomic cluster (Fig.1B). The encoded proteins share a high percentage of identity (>82%). Comparison with other subtilisin-like proteases showed that they all possess the same conserved domains (Fig.1C) including a predicted N-terminal signal peptide and autoinhibitory prodomain, the subtilase domain with the conserved catalytic triad, the protease-associated domain (Mahon & Bateman, 2000) and the fibronectin-3-like domain (Cedzich *et al.*, 2009) (Fig.1C). Although the N-terminal TTHT sequence motif of mature subtilases (Reichardt *et al.*, 2018) was conserved, both the amino acid preceding the cleavage site, and the specificity-conferring residue in the S1 binding pocket of the enzyme (Vartapetian *et al.*, 2011) differed among P69s (Table. S1).

BLASTp searches identified orthologues in potato, eggplant, pepper, *Nicotiana tabacum* and *N. attenuata* with 91.8% to 83.1% sequence identity to P69D, while in non-solanaceous genomes the closest proteins shared less than 68% sequence identity. *S. pimpinellifolium* were found to be identical to those of tomato. All *bona fide* P69s were identified in each species as candidate orthologs that clustered with tomato P69 sequences in neighbour-joining trees (Fig. S1). P69A and P69D are conserved in all analysed species of the nightshade family. P69B, P69C, P69E and P69I were only found in tomato and potato, whereas P69G, P69H, P69J and P69F are unique in tomato (Fig. S2).

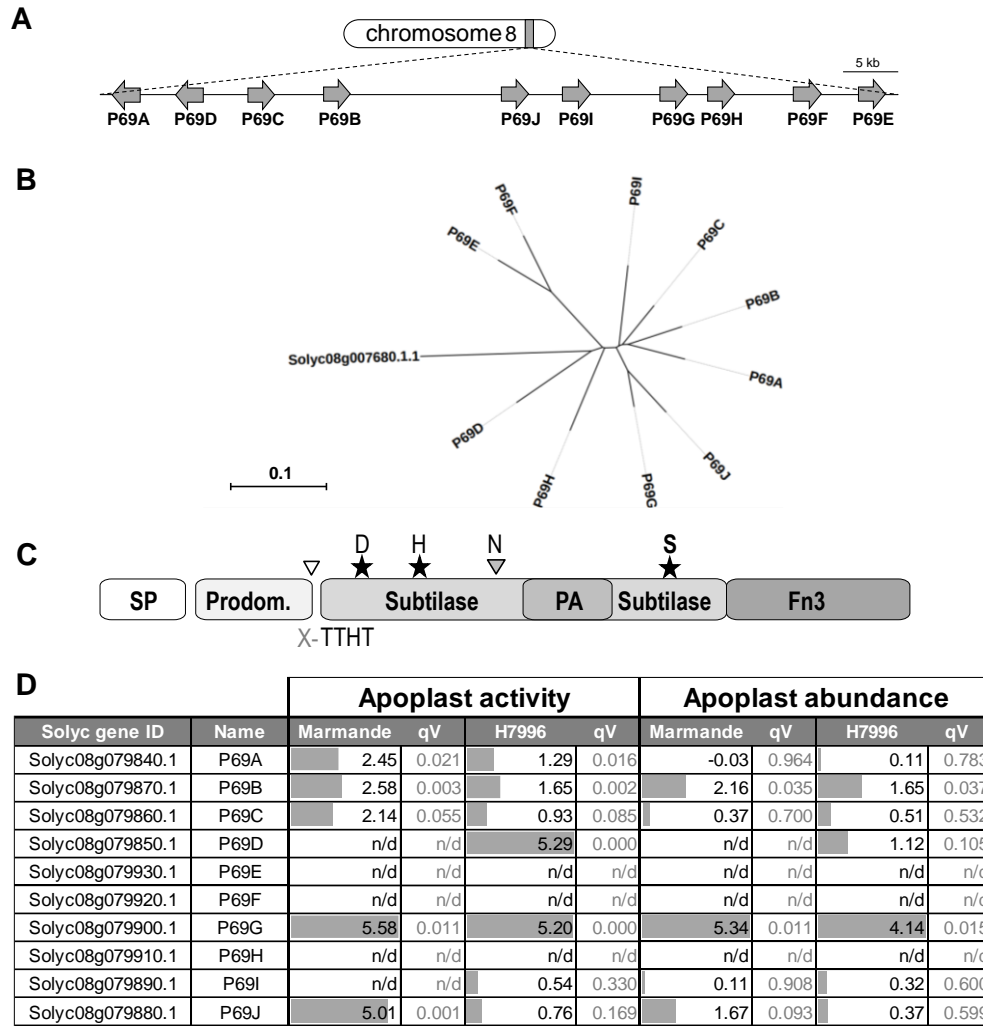


Figure 1: Genomic and protein features of the tomato P69 subtilases. (A) Schematic representation of the genomic locus of tomato P69 subtilases. (B) Neighbour-joining protein similarity tree of tomato P69 subtilases generated from a ClustalO alignment. The most highly related non-P69 tomato subtilase Solyc08g007680 was added as outgroup. Scale bar indicates 0.1 changes per site per 100 nucleotides. (C) Representation of the tomato P69 protein domains and conserved features. The predicted prodomain cleavage site marked by a white triangle. The position of the catalytic triad (D, H, S, asterisks), the conserved TTHT motif and the putative oxyanion hole residue (N) (gray triangle) are indicated. SP, signal peptide; Prodom., prodomain; PA, protease-associated domain; Fn3, fibronectin III-like domain. (D) Differential activation or accumulation of P69 subtilases in the apoplastic fluid. Log2 FC of abundance for the active proteins ('Apoplast activity' and general proetin abundance 'Apoplast abundance') in *R. solanacearum*-inoculated vs non-inoculated samples in susceptible (Marmande) and resistant (Hawaii 7996) tomato apoplast is shown for all P69s. Gray bars inside each cell are proportional to log2 FC values. The q-value (qV) statistic is also indicated. n/d, not detected.

To analyse changes in activity and abundance of P69 proteins in tomato in response to *R. solanacearum*, we reanalysed our activity-based proteome profiling dataset (Planas-

Marques *et al.*, 2018) where a biotinylated active-site probe was used to pull down active serine hydrolases and to quantify their abundance in the tomato apoplast. We found that the activity of seven P69s increased in response to the pathogen in the resistant variety Hawaii 7996 while five proteases were also activated in susceptible plants (Fig. 1D). P69D, G and J showed the highest increase in activity, while P69D and to a lesser extent P69I were uniquely activated in the resistant cultivar (Fig. 1D).

Cleavage specificity of *R. solanacearum*-induced P69 proteases

To investigate the activity and substrate specificity of tomato P69 subtilases, C-terminally His-tagged recombinant proteins were purified from apoplastic fluid after transient expression in *N. benthamiana* (Fig. 2A and S3). We confined our study to the members activated in the apoplast upon *R. solanacearum* infection: P69A, P69B, P69C, P69D, P69G and P69J (Fig. 1D). The activity of the purified proteins at neutral pH was measured using two fluorogenic substrates, a synthetic 11-mer peptide and casein. All enzymes effectively cleaved both substrates but P69A, P69C and P69D showed preference for the synthetic peptide while P69B, P69G, and P69J were more active on casein (Fig. 2B). The protease activity was measured for each protein over a range of pH using the preferred substrates. P69B, C and D were most active at neutral pH, while P69A, G and J also remained fully active at alkaline conditions (Fig. 2C).

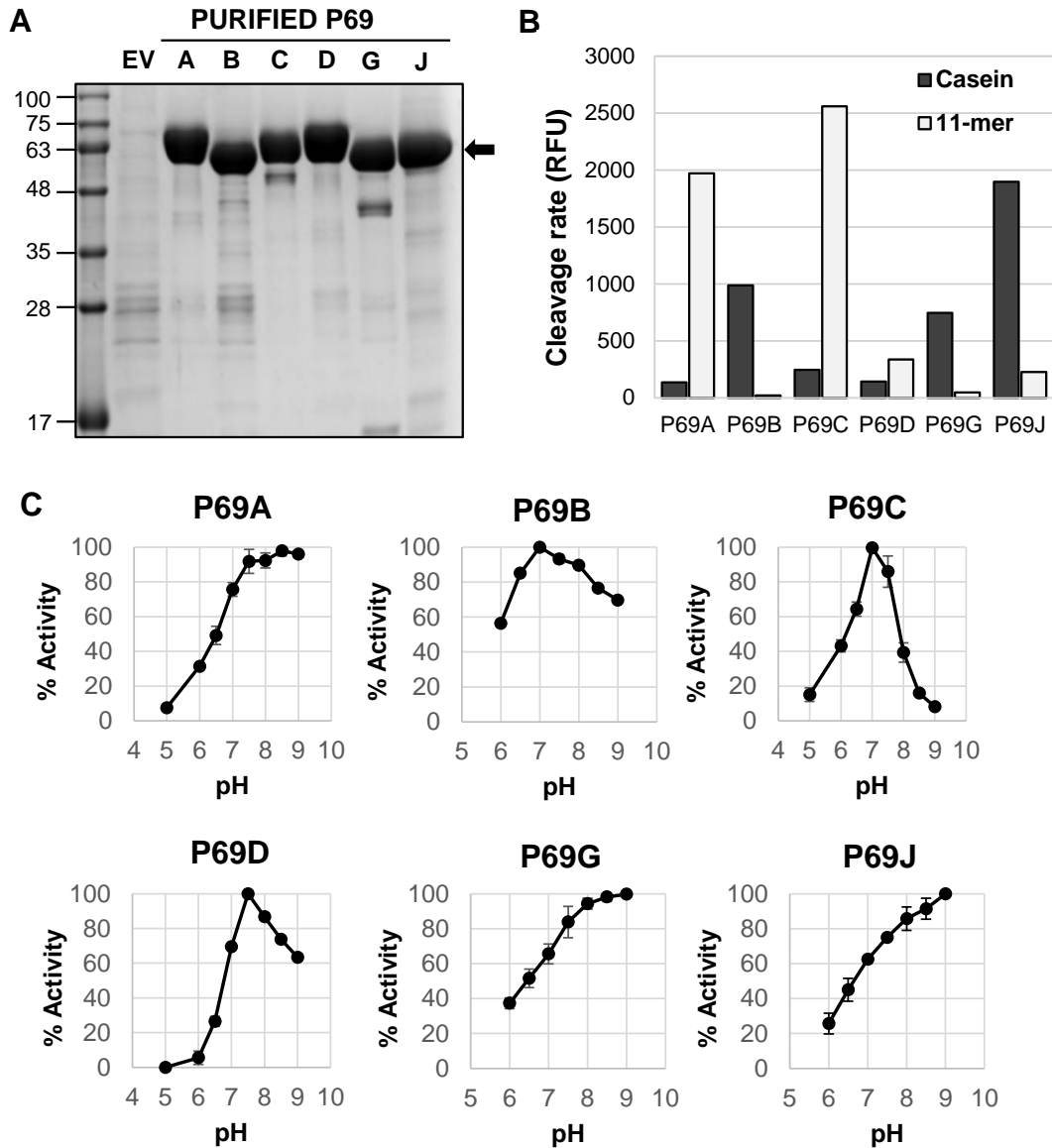


Figure 2: Enzymatic activity of recombinant tomato P69 subtilases. (A) SDS-PAGE separation of purified P69 proteins (arrow) stained with Coomassie Brilliant Blue. The coding sequence of representative tomato P69s were fused to a C-terminal hexa-His tag and transiently expressed in *N. benthamiana* leaves. Proteins were purified by metal chelate affinity chromatography from apoplastic fluid harvested 5 days after agroinfiltration. A mock-purified fraction from empty-vector infiltrated plants is shown as control (EV) (B) Activity assay of recombinant P69s at pH 7 using a synthetic 11-mer peptide or casein as substrates. RFU, Relative Fluorescent Units. (C) P69 activity at different pH. Activity in a three-component buffer system using the 11-mer peptide (P69A, P69C, P69D) or casein (P69B, P69G, P69J) as fluorogenic substrates is shown as percentage of maximum activity at optimal pH. Average values of two technical replicates from two independent enzyme purifications ($n=4$) is shown. Error bars indicate standard deviation.

Next, we investigated substrate specificity of the selected P69s using the PICS (Proteomics Identification of Cleavage Sites) approach (Schilling *et al.*, 2011; Schilling & Overall, 2008). Overall, all proteins exhibited similar selectivity for the five amino acids upstream of the scissile bond, where cleavage occurs (Fig. 3). However, some particularities were observed. Firstly, P69A and P69B were the only P69s with a preference for aspartate in the P1 position (the position immediately upstream of the scissile bond). Secondly, P69D showed clear selectivity for the hydrophobic aliphatic residues isoleucine and valine in P2, while other P69s preferred proline in this position (Fig. 3). All P69s showed a preference for hydrophobic aliphatic residues (isoleucine, leucine and/or valine) in P4, which was most pronounced for P69A and P69B. Overall, P69s showed similar cleavage site selectivity and considerable cleavage promiscuity, suggesting that additional mechanisms may contribute to cleavage specificity *in vivo*.

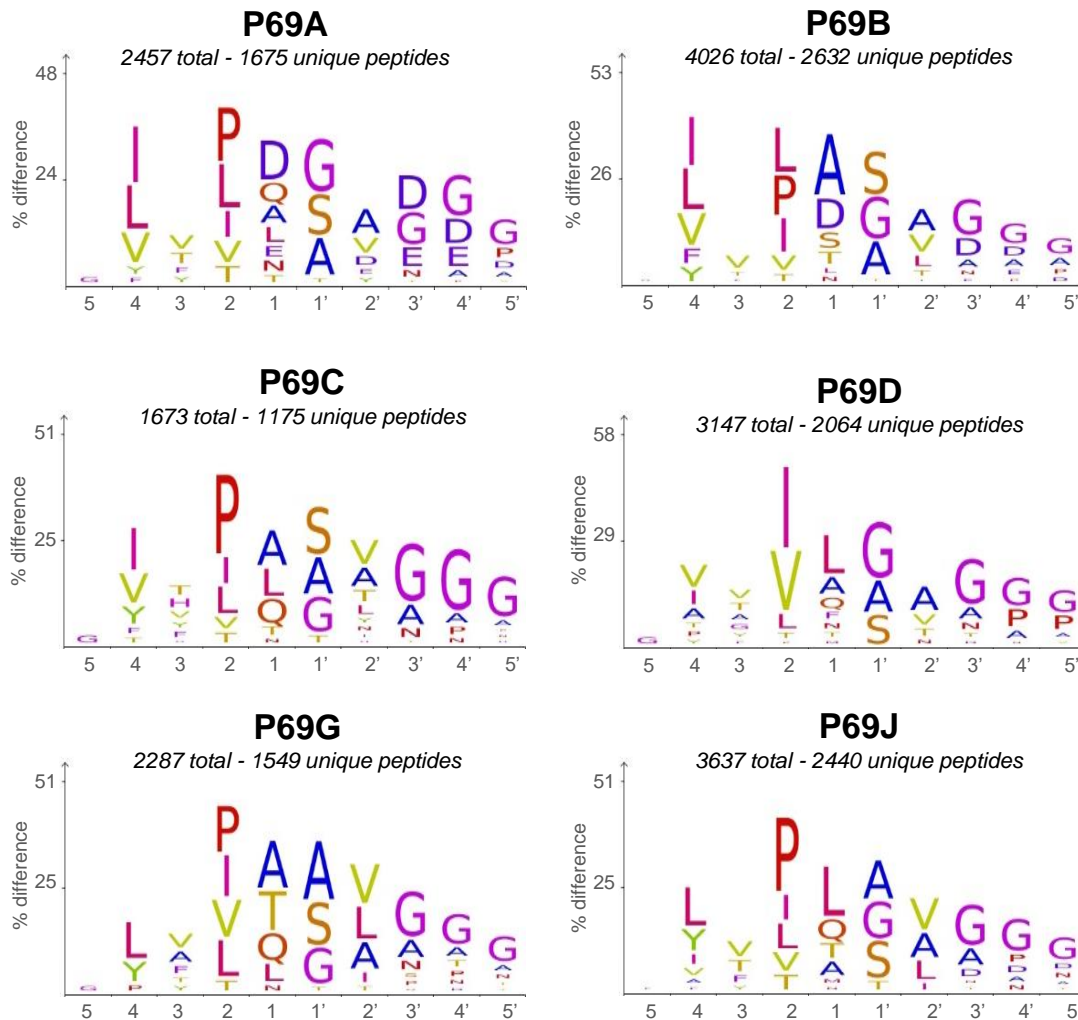


Figure 3: Substrate cleavage specificity of tomato P69s analysed by PICS. IceLogo graphs showing the amino acids observed upstream (positions 1 to 5) and downstream (positions 1' to 5') of the scissile bond. Letter size reflects the relative frequency of an amino acid at a given position as compared to natural abundance in the tomato proteome.

Only residues that are significantly different from natural abundance at $p < 0.05$ are shown. The number of total and unique peptides identified by mass spectrometry is indicated in each panel.

P69B, P69D and P69G inhibit *R. solanacearum* growth

To investigate whether the P69s induced by *R. solanacearum* play a role in plant defence, we inoculated the pathogen in *N. benthamiana* leaves overexpressing the proteases and recorded bacterial growth over time. A *R. solanacearum* strain that is pathogenic on *N. benthamiana* was used for these experiments (GM11000 devoid of the effectors AvrA and PopP2) (Poueymiro *et al*, 2009). Bacterial growth was impaired two days post-inoculation in leaves overexpressing P69B, C, D and G but not P69A or J, when compared to the empty-vector control (Fig. 4). The strongest effect was seen for P69D, which is the one most highly and specifically activated by pathogens in resistant plants (Fig. 1D). Thus, we concentrated on this protein for further characterisation.

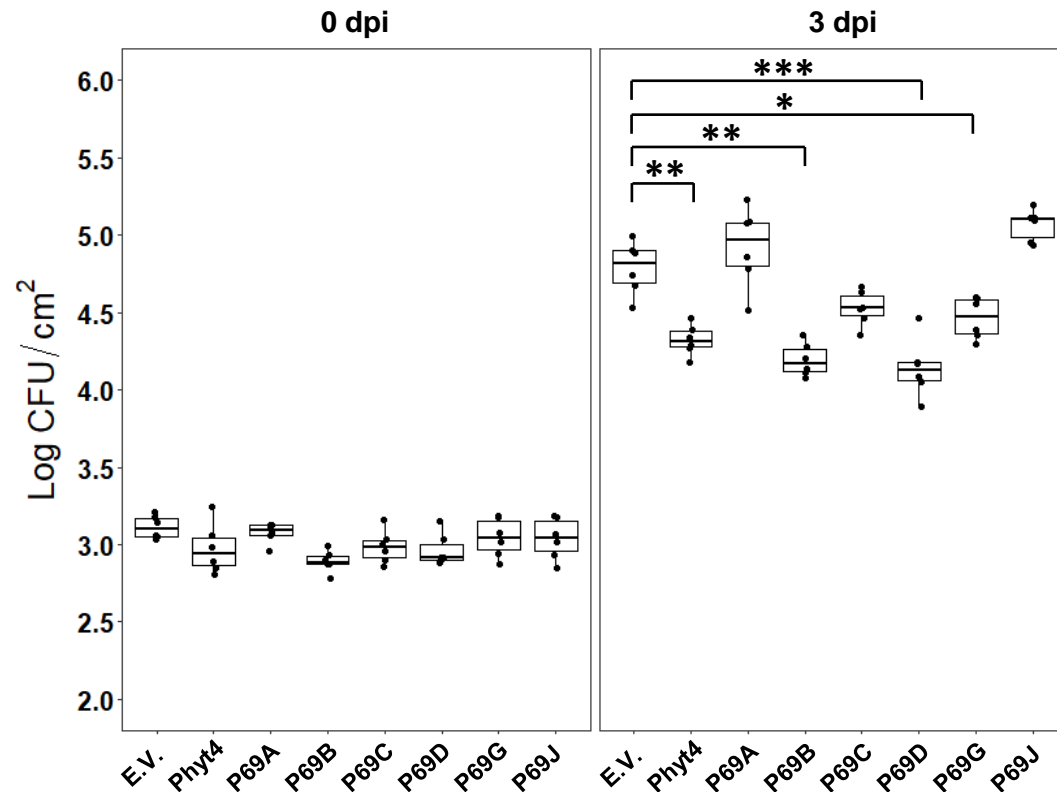


Figure 4: Phenotypes caused by overexpression of P69s. Multiplication of *R. solanacearum* in *N. benthamiana* leaves transiently overexpressing P69s. *Agrobacterium* C58C1 harbouring plasmid pART27 (EV) or the same plasmid including P69s expression constructs were infiltrated into *N. benthamiana* leaves and 2 days later, inoculated by infiltration with 10^5 CFU/ml of a virulent *R. solanacearum* strain defective in the avirulence genes *avrA* and *popP1*. Bacterial multiplication in leaves was assessed at 2 days post inoculation (dpi). Each dot corresponds to a biological replica from an independent leaf.

Significant differences to the empty vector are shown as, **P < 0.01 and ***P < 0.001 (Student's t-test, n=6).

Characterization of P69D self-processing, secretion and glycosylation

To investigate the requirements for prodomain self-removal in P69D, we generated a mutant replacing the putative catalytic serine and the histidine preceding TTHT by alanine (S532A and H114A, respectively). Contrary to WT P69D, the S532A mutant was not secreted into the apoplast (Fig. 5A) upon transient expression in *N. benthamiana* and was retained in the cells in its unprocessed form (Fig. 5B), indicating that this serine was required for enzyme maturation and secretion. Moreover, co-expression of WT P69D and S532A showed that prodomain removal occurred in an autocatalytic and intramolecular reaction since the mutant proteins could not be processed *in trans* by WT P69D (Fig. 5A, B, *rightmost lanes*). On the contrary, the H114A variant was processed and secreted into the apoplast, yet less efficiently than WT P69D (Fig. 5A). This indicated that, unlike tobacco phytaspase, prodomain cleavage in P69D does not rely on the residue upstream of the processing site, which is consistent with our PICS analysis showing that histidine is tolerated but not preferred in P1 (Fig. 3).

Secreted P69s transiently expressed in *N. benthamiana*, showed bigger and varying sizes in SDS-PAGE likely due to post-translational modifications (Fig. 2A). We therefore analysed if *N*-glycosylation could explain these apparent size differences. We predicted five putative *N*-glycosylation sites in P69D, four of which were previously confirmed experimentally for P69B (Bykova *et al*, 2006) (Fig. S4A). Next, we estimated P69D molecular weight assuming that all putative sites were glycosylated either with the lighter, the most abundant or the heaviest glycans identified in P69B (Fig. S4B). Since these estimated weights were still 7 to 20 KDa smaller than those observed in the SDS-PAGE (Fig. S4B), we suggest that P69D may be subject to additional post-translational modifications or larger glycans that account for the observed mass differences.

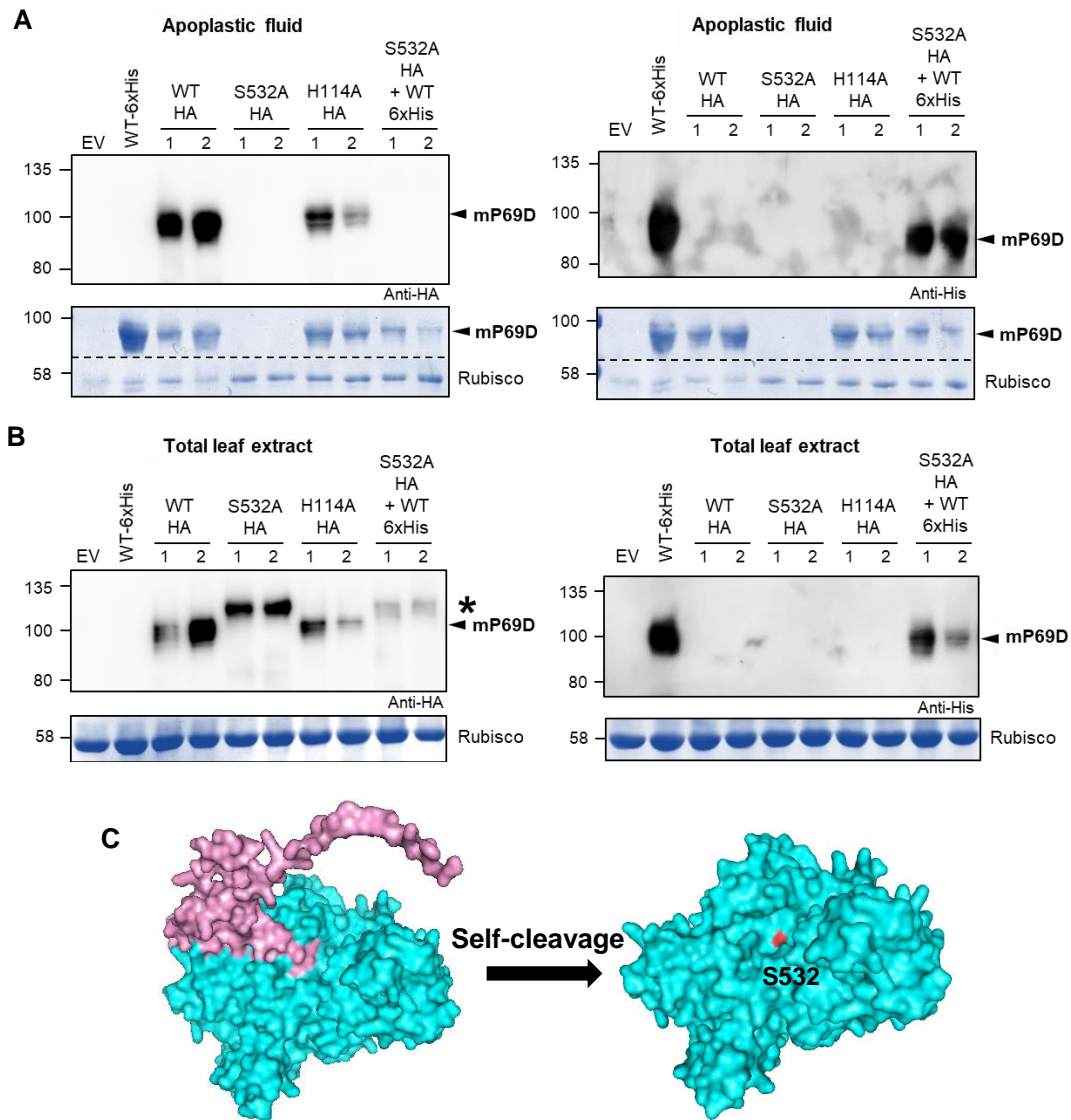


Figure 5: Serine-532 is required for P69D self-processing and secretion. Hexahistidine- (6xH) or hemagglutinin- (HA) tagged wild type (WT) P69D and its mutant variants S532A and H114A were transiently expressed in *N. benthamiana* leaves. Apoplastic fluids (A) and total leaf extracts (B) were sampled five days after agro-infiltration and blotted using either α -His tag or α -HA antibodies. The results of two biological replicas using different transformed *Agrobacterium* clones were used. Arrowheads and asterisk indicate the position of mature (mP69D) and immature P69D, respectively. An empty vector (EV) control was included. Bottom loading panels correspond to SDS-PAGE of the same samples stained with Coomassie brilliant blue. (C) Modelled structures of tomato P69D full length (left) and its prodomain-less mature form using AlphaFold2. Signal peptide and prodomain are coloured in pink, the mature P69D protein in cyan and the catalytic site serine 532 in red.

Identification of candidate P69D substrates using proteomics and N-terminomics

To determine putative tomato P69D protein substrates, P69D-deficient tomato plants were generated using CRISPR/Cas9 technology (Danilo *et al.*, 2018) (Fig. S5). Cas9-free homozygous mutants were obtained in the resistant tomato cv Hawaii 7996. Two sibling lines that carried a 202bp deletion (P69D^{Δ202}) giving rise to a truncated P69D protein lacking the catalytic site serine were selected for analysis (Fig. S5B).

We next isolated apoplastic proteomes from WT and P69D-deficient plants after infection with *R. solanacearum*. Quantitative apoplast proteome comparison identified 530 proteins that were quantified in at least two of the three independent replicates (Dataset S1). Of these, nine proteins were significantly over-represented in WT ($\pi > 1.1082$), most prominently P69D itself (Fig. 6A). Sixteen proteins were more abundant in the knock-out apoplast ($\pi < 1.1082$), including several defense-related proteins such as PR1b, an osmotin-like protein, an aspartic protease of the A1 family and a carboxypeptidase (Fig. 6A). HUNTER N-terminome analysis (Demir *et al.*, 2022) further identified 419 N-terminal peptides from 249 proteins that were quantified in two of three replicates (Dataset S2), of which 50 showed significantly different accumulation (Fig. 6B). Nineteen of the N-terminal peptides accumulating in WT and 22 of the N-terminal peptides more abundant in the P69D knock-out mutant arose from proteolytic processing *in vivo*, as their newly generated N-termini were dimethylated (modified during the enrichment procedure) and matched to positions within the protein sequences. Strikingly, 19 N-terminal peptides came from the pathogenesis-related protein 1B (PR-1B), of which three were more abundant in wild type while five were more prevalent in the absence of P69D. Also, three peptides derived from cleaved PR2, which accumulated in the wild type, but not in the mutant (Fig. 6B). This suggested that P69D may be involved in the processing of PR1B and PR2. In addition, we also observed a variety of differentially processed N-terminal peptides arising from P69 proteases, and other subtilases (Dataset S2).

To identify direct P69D-mediated cleavages, we isolated aploplastic proteomes under non-denaturing conditions from P69D-deficient plants after infection with *R. solanacearum* and incubated this apoplast proteome with recombinant P69D or a control purification *in vitro*. Subsequent HUNTER N-terminome analysis determined 459 N-terminal peptides that were quantified in two of four replicates, of which 38 derived from PR-proteins (Fig. S6A, Dataset S3). To our surprise, only three putative cleavage products (dimethylated N-terminal peptides) moderately increased (LIMMA-moderated t-test p-value < 0.05 and $\log_2 > 1$) after incubation with P69D and all were from proteins that appeared as likely contaminants. In contrast, 10 N-terminal peptides, including 6 termini derived from PR proteins cleavage (4 from PR1B and 2 from PR2), showed significantly lower abundance,

suggesting that other proteases are responsible for initial processing and that the cleavage products are then further degraded by P69D.

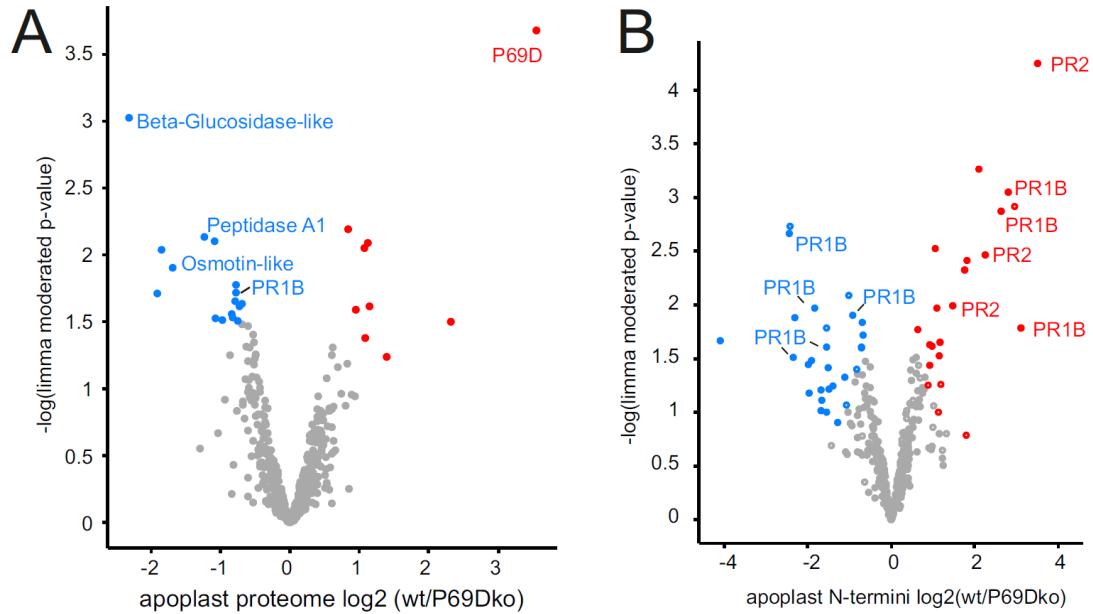


Figure 6. P69D proteome and N-terminome analyses. (A) Volcano plot depicting changes in the apoplast leaf proteome of P69D-deficient plants compared to wild type, both infected with *R. solanacearum*. Red and blue, proteins significantly accumulating ($\pi > 1.1082$) and depleted ($\pi < -1.1082$), respectively, in wild type compared to P69D-deficient plants. (B) N-terminome analysis of the same samples as in A. Open circles, N-termini mapping to canonical protein termini (position 1 or 2 with intact or removed Met, known signal- or transit peptide sequences); filled circles, non-canonical protein termini mapping to positions within their protein sequence; red and blue, N-terminal peptides significantly accumulating or depleted ($\pi > 1.1082$ or < -1.1082 respectively) after addition of P69D.

To verify that the added recombinant P69D was active and could cleave intact protein substrates, we additionally extracted total proteomes under non-denaturing conditions from leaves of *R. solanacearum*-infected P69D-deficient mutant plants and incubated them with recombinant P69D. HUNTER N-terminome analysis identified 617 N-terminal peptides that were quantified in 2 or 4 replicates (Dataset S4), of which 134 matching to internal positions corresponding protein sequences accumulated significantly (LIMMA-moderated t-test p-value < 0.05 and $\log_2 > 1$), thus representing likely 69D cleavage sites (Fig. S6B). Icelogo analysis of these P69D-generated cleavage sites showed strong agreement with the sequence logos derived from the peptide-based PICS analysis with Ile and Val preferred at P2 and small amino acids at P1', demonstrating that P69D can cleave intact proteins that present this motif (Fig. S6C). However, none of these identified cleavage sites came from proteins with known apoplastic location.

Taken together, apoplast proteome and N-terminome analyses suggest that P69D-deficiency results in altered proteolytic processing of pathogenesis-related proteins, particularly PR1B and PR2 in the apoplast *in vivo* (Fig. S6A). However, this is likely not a direct effect as incubation of apoplast proteomes with recombinant P69D resulted in the degradation of some of the differentially cut PR1B protein termini, but not generation of new termini (Fig. S6C).

Deletion of P69D in resistant tomato cv Hawaii 7996 compromises its resistance to *R. solanacearum*

To determine the functional relevance of P69D in the tomato-*R. solanacearum* interaction, we inoculated wild-type and P69D-deficient tomato lines with *R. solanacearum* by soil drenching. Mutant lines were more susceptible than the Hawaii 7996 wild type, although not as susceptible as cv Marmande (Fig. 7A). Quantification of *R. solanacearum* concentrations in the roots or the base of the hypocotyl 5 days post-inoculation (dpi) revealed that hypocotyls of P69D-deficient Hawaii 7996 plants contained 3-4 times more bacteria than the resistant WT, but clearly less than the susceptible cv Marmande. On the contrary, no differences in bacterial loads could be observed in the roots of the WT and the *P69D* mutant lines (Fig. 7B). Interestingly, when the pathogen was inoculated directly into the stem, no significant wilting differences between the P69-deficient plants and wild-type H7996 were observed (Fig. S7).

To check the specificity of the P69D-mediated disease resistance, we inoculated WT and P69D mutant plants with *Fusarium oxysporum* f.sp. *lycopersici* (*Fol*). Analyses of the disease index and fresh weight revealed that the absence of functional P69D did not affect resistance to *Fol* (Fig. S8) Thus, P69D is important for tomato resistance against bacterial wilt but not against fungal vascular pathogens like Fusarium wilt.

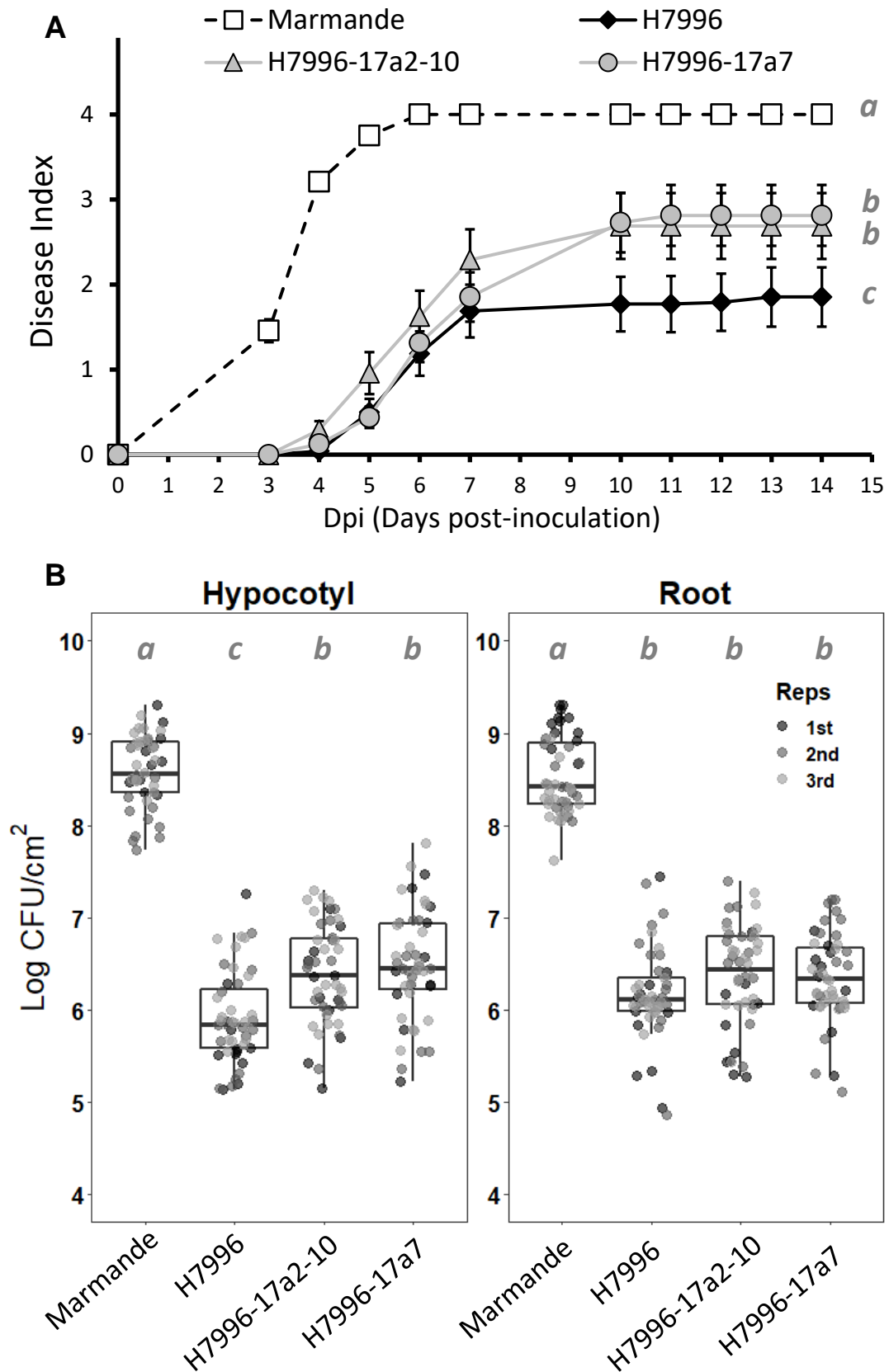


Figure 7: Pathogenicity assays of the P69D single mutant. The susceptible tomato cv Marmande, the resistant cv. Hawaii 7996 (H7996) and two independent H7996 lines with the same CRISPR mutation disrupting the P69D gene (17A2-10 and 17a7) were used. (A)

Evolution of disease symptoms over time. 3-week-old tomato plants were soil-drenched with a 10^8 CFU/ml *R. solanacearum* suspension and wilting symptoms scored for two weeks. The graph shows the results of a representative experiment out of the three biological replicas performed using at least 20 plants of each variety and line. (B) Bacterial multiplication in the roots and hypocotyls of 3-week-old plants assessed 5 days after soil-drench inoculation with a luminescent *R. solanacearum* strain (n=16-20 plants). The roots and the base of the hypocotyls were excised and bacteria was quantified by emitted luminescence and transformed to CFU/ml. Each dot shows the bacterial count in one plant. Different letters next to each graph or above each boxplot indicate statistically significant differences ($\alpha=0.05$, Fisher's least significant difference test). The results from three independent experiments are shown as dots of different shading colours

I.3 Materials and Methods

In silico analyses

BLASTn/p searches to identify tomato P69 genes were performed on the SolGenomics and NCBI databases (<https://solgenomics.net>, <https://www.ncbi.nlm.nih.gov/>). Orthologue candidates were selected as proteins with >55% identity (60% for potato) and >50% alignment score to P69C. Databases used to identify P69 orthologues in each species are indicated in Table S2, and the equivalence between gene and protein identifiers of tomato P69s in the SGN, NCBI and UniprotKB is indicated in Table S1.

P69 subtilases were located on the tomato genome using the genome browser webtools from the SGN database (Jbrowse). Neighbour-joining trees and amino acid sequence identity matrices were constructed from the respective ClustalO sequence alignments and visualized either with GSTree (<http://genestudio.com>) or iTOL (<https://itol.embl.de>).

Putative *N*-glycosylation sites in P69 proteins were predicted using the NetNGlyc 1.0 Server (<http://www.cbs.dtu.dk/services/NetNGlyc/>) with a threshold of significance of 0.5. Structure homology models of P69 subtilases were built in the Alpha Fold server AlphaFold2.ipynb (Mirdita *et al.*, 2022) (<https://colab.research.google.com/github/sokrypton/ColabFold/blob/main/AlphaFold2.ipynb>). The structures were visualized with PyMOL 2.5 (<https://pymol.org/2/>).

DNA cloning and transient expression

The coding sequences (ORFs) of P69B, P69C, P69D, P69G and P69J were amplified from tomato H7996 by PCR using the primer combinations specified in Table S3. and cloned into pJET1.2/blunt (Thermo Scientific™). ORFs confirmed by Sanger sequencing were cloned downstream of the CaMV 35S promoter in pART7 (Gleave, 1992) using the restriction enzymes *Sma*I and *Bam*HI. Expression cassettes were mobilized to the binary vector pART27 (Gleave, 1992) using *Not*I. The expression vector for P69A with a C-terminal His-tag (Solyc08g079840) was previously described (Reichardt *et al.*, 2018).

Transient expression in *N. benthamiana* was performed as previously described (Reichardt *et al.*, 2018), with some modifications. Briefly, *Agrobacterium tumefaciens* C58C1 containing the constructs and collected from plates were resuspended in 10 ml of 10 mM MES pH 5.6, 10 mM MgCl₂. Strains were mixed to a final OD₆₀₀ of 0.7 for pART27-P69 and 0.3 for p19 and infiltrated in the leaves of 3 to 4-week-old *N. benthamiana* using a blunt syringe. Five days after agro-infiltration, leaves were harvested and the apoplastic fluid collected in 50 mM NaH₂PO₄/Na₂HPO₄, pH 6.5, 200 mM KCl as described (Reichardt *et al.*, 2018).

Protein purification and activity assays

Apoplastic fluids were subjected to metal chelate affinity chromatography with Ni-NTA agarose (Qiagen) on Poly-Prep® chromatography columns (Bio-Rad). The apoplastic fluid obtained from P69J-expressing leaves was subjected to gel filtration using a Superdex 200 column on an Äkta Purifier chromatography system (GE Healthcare). Finally, eluate fractions resulting from the affinity purification (P69A-D and P69G) and the fractions from the gel filtration purification (P69J) were concentrated using Vivaspin® concentrators (MW cutoff 10 kDa, Sartorius).

Activity of recombinant P69s was monitored using a fluorogenic 11-mer peptide (aminobenzoyl-SKRDPPKMQTD(NO₂)Y) (JPT Peptide Technologies) and casein as substrates at 25 µM and 10 µg/ml, respectively. Assays were performed in 50 mM acetic acid, 50 mM MES, 100 mM Tris/HCl (pH 7.5 unless otherwise indicated) and relative fluorescence increase was monitored using a SPARK® microplate reader (Tecan).

For substrate identification *in vitro*, recombinant P69D purified from *N. benthamiana* was incubated with total or apoplast protein extracts for 30 min at RT at an enzyme: proteome ratio of 1:200. No apparent overall protein degradation was observed in these conditions.

PICS analyses

Proteomics Identification of Cleavage Sites (PICS) (Schilling *et al.*, 2011; Schilling & Overall, 2008) was used to analyse the substrate specificity of tomato P69s, with slight modifications detailed in (Reichardt *et al.*, 2018). 100 µg of the chemically modified peptide library was digested at 25°C with purified P69s in 50 mM NaH₂PO₄/Na₂HPO₄, pH 6.5, at an enzyme to library ratio of 1:1000 (w/w) for 2h. Purified peptides were subjected to LC-MS/MS and cleavage sites were reconstructed using WebPICS (<http://clipserve.dentistry.ubc.ca/pics>) and cleavage specificity preferences were visualized using IceLogos (<https://iomics.ugent.be/icelogoserver/>) (Colaert *et al.*, 2009).

Proteome and N-terminome sample preparation

For quantitative analysis of the apoplast proteomes, purified proteins were dissolved and denatured in 6M guanidine buffered with 100 mM HEPES to pH7.2, cysteine residues reduced with 10 mM DTT and alkylated with 30 mM IAA and digested with proteomics-grade trypsin at an enzyme:proteome ratio of 1:100 for 16 h at 37°C. Peptides were differentially stable isotope labelled by reductive dimethylation (Boersema *et al.*, 2009) with light labelling (20 mM CH₂O and 20 mM NaBH₃CN, +28.0313 Da) of wild type proteomes and heavy isotope labelling (20 mM ¹³CD₂O and 20 mM NaBH₃CN, +34.0631 Da) of 17a7 P69D-knock out proteomes. Labelling reactions were incubated for X h at 37°C, then quenched with 100 mM Tris-HCl pH 6.8 for 1h at RT, pooled, purified using reverse-phase STAGE tips (Rappsilber *et al.*, 2007), dried in a vacuum concentrator and reconstituted in

0.1% formic acid prior to LC/MS analysis.

HUNTER N-terminome analyses were performed as described (Demir *et al.*, 2022). Briefly, free primary amines at the protein N-termini and lysine side chains were differentially stable isotope-labelled by reductive dimethylation, using the light isotopes for WT and heavy isotope for 17A7 proteomes for the *in vivo* experiment. In the *in vitro* experiments, proteomes treated with a mock-purified *N. benthamiana* apoplast extract were labelled with light isotopes and proteomes treated with enriched recombinant P69D labelled with heavy isotope. Proteins were then digested with trypsin and new peptide alpha-amines generated by the tryptic digest modified with undecanal. N-terminal peptides were then selectively enriched by depletion of the undecanal-modified peptides using HRX reverse phase cartridges (Macherey and Nagel). Enriched N-terminal peptides were desalted with STAGE tips as described above.

Mass spectrometry data analysis

Peptides were analysed using an UltiMate 3000 RSCL nano-HPLC system (Thermo) online coupled to an Impact II Q-TOF mass spectrometer (Bruker) via a CaptiveSpray ion source boosted with an ACN-saturated nitrogen gas stream as described (Beck *et al.*, 2015). Peptides were loaded on a μ PAC pillar array trap column (1 cm length, PharmaFluidics) and separated on a μ PAC pillar array analytical column (50 cm flowpath, PharmaFluidics) using a 2 h elution protocol that included an 80 min separation gradient from 5% to 35% solvent B (solvent A: H₂O+0.1% FA, solvent B: ACN+0.1% FA) at a flow rate of 300 nl min⁻¹ at 60 °C. Line-mode MS spectra were acquired in mass range 200–1400 m/z with a Top14 method.

Acquired tandem mass spectra were queried with MaxQuant (Tyanova *et al.*, 2016) v.2.0.3 against a database consisting of the UniProt *R. solanacearum* database (release 2022_04) and the UniProt *Solanum lycopersicum* database (release 2023_03), with the 7 entries A0A3Q7HVI0; A0A3Q7HTM2; A0A3Q7HVI4; A0A3Q7F3D9; A0A3Q7HHX1; A0A3Q7HI18; A0A3Q7HKM1 (incorrect annotations of P69 sequences) replaced by the eight P69 sequences listed in Figure 1 downloaded from the Solanaceae Genomics Network (see above) and entry A0A3Q7HXL1 (incorrect annotation of PR1 proteins as fusion protein) removed and replaced by manually annotated PR1 protein homolog sequences (12 entries). For the apoplast shotgun proteome analysis, duplex dimethyl labelling at Lys and peptide N-termini was set as label, trypsin as digestion protease with up to three missed cleavage sites, and label-free quantification enabled. Protein quantification required 1 unique peptide per protein group, razor proteins were not used for abundance calculations. Shotgun data analysis was based on the individual LFQ intensities of heavy and light

channels to allow for imputation of missing values and determination of differentially expressed proteins using the LIMMA-moderated t-test as plug.in in Perseus (Yu *et al*, 2020) v. 2.0.10.0. For HUNTER data, search settings were set as described (Demir *et al.*, 2022) and MaxQuant results further analysed using MANTI (Demir *et al*, 2021) using the graphical user interface as implemented in v5.4 (Demir & Huesgen, 2022). For *in vivo* comparisons, the π value, calculated by multiplying the fold-change as a measure of protein abundance with the -log limma-moderated t-test p-value, was used as a test criterion (Xiao *et al*, 2014). Proteins were considered significantly different in abundance at $\pi > 1.1082$ or < -1.1082 . For *in vitro* experiments, N-terminal peptide abundance was considered significantly different at a >2-fold change and a limma-moderated p-value <0.05.

Plant material and growth conditions

The tomato (*Solanum lycopersicum*) susceptible variety Marmande and the highly resistant line Hawaii 7996 were used. To generate the CRISPR/Cas9 mutant in the Hawaii7996 background (designated 17a7 and 17a2-10), single guide RNA (sgRNA) sequences were designed with high specificity score and the lowest number of off-targets using CRISPOR (Haeussler *et al*, 2016), synthesized (Integrated DNA Technologies) and cloned as described (Danilo *et al.*, 2018) (Table S3). The Hawaii 7996 genotype was transformed using *A. tumefaciens* C58 pGV2260 (Mazier *et al*, 2011). Leaf samples from regenerating plants or their progenies were screened by PCR using specific primers (Table S3). Deletions were confirmed by DNA sequencing (Macrogen).

Plants were grown in controlled growth chambers at 60% relative humidity, 12 h: 12 h, day: night and 27°C (light-emitting diode (LED) lighting) or 25°C (fluorescent lighting). Three-week-old plants were used for pathogenicity assays and developmental observation.

Bacterial material and pathogenicity assays

A *R. solanacearum* luminescent reporter derivative carrying the *PpsbA::LuxCDABE* construct (Cruz *et al*, 2014) was used for all experiments carried out with the wild type GMI1000 strain. Multiplication of *R. solanacearum* in *N. benthamiana* leaves was analysed using a $\Delta avrA$ and $\Delta popP1$ mutant, pathogenic on this plant. *R. solanacearum* was routinely grown on rich B medium (10 g/l bactopectone, 1 g/l yeast extract and 1 g/l casaminoacids) using gentamicin (10 µg/ml) for selection.

For soil-drenching inoculations, plants were inoculated by pouring 40 ml of a 10^8 CFU/ml bacterial suspension on every pot after root wounding (Planas-Marques *et al.*, 2020). For petiole inoculation, 10 µl of a 10^6 CFU/ml suspension was placed onto the petiole-stem boundary in the cotyledons or first internode and poked into the stem with a needle. Infected plants were scored for wilting symptoms using a scale from 0 to 4, where 0=healthy plant with no wilt, 1=25%, 2=50%, 3=75% and 4=100% of the canopy wilted. For

bacterial inoculation in the apoplast, plants were vacuum-infiltrated with a bacterial suspension of 10^5 CFU/ml as described (Planas-Marques *et al.*, 2018). Necrotic symptoms were evaluated in the third and fourth leaves using a scale: no necrosis, mild necrosis (<25% of leaf area), and severe necrosis (>75% of leaf area). Assessment of bacterial multiplication was performed in four independent plants per time point per genotype as follows: four 5 mm-diameter leaf disks were excised from each plant. CFUs in homogenized leaf samples were counted and bacterial growth was calculated as CFU·cm⁻² of leaf.

***Fusarium* inoculation assay**

Fungal strains *FoI007* and *FoI029* were inoculated from glycerol stocks to potato dextrose agar (Becton, Dickinson and Company) and grown for five days at 25°C in darkness (Marlatt M *et al.*, 1996; Mes *et al.*, 1999). A single agar plug (~1cm²) was put into a 250ml flask containing 100 ml of minimal nitrate liquid medium (100mM KNO₃, 3% sucrose and 0,17 % Yeast Nitrogen Base without amino acids or ammonia) and placed in a shaker incubator (25°C, 150rpm). Five days after inoculation, the fungal suspension was filtered through sterile miracloth (Millipore), spun down, washed and diluted with sterilized Milli-Q water (10^7 spores/ml) (Rep *et al.*, 2004). Ten-day-old tomato cv. Hawaii 7996 (H7996) and CRISPR/Cas9 knockout lines were uprooted and trimmed (remaining root length approx. 1,5 cm long). Seedlings were root dip-inoculated by placing them for two minutes in water (mock) or the spore suspension. The plants were grown in a greenhouse at 25 °C, 65% relative humidity and a 16-hour photoperiod. Three weeks post-inoculation fresh weight and disease index were scored as described (de Lamo *et al.*, 2021). Statistical analyses were done using the software PRISM 9.3.0 (GraphPad).

Statistical analyses

Statistical analyses were performed using the STATGRAPHICS Centurion XVI software. All statistical tests are indicated in the respective figure legends.

I.4 Discussion

Conservation and function of P69 subtilase sequence identity and substrate specificity

Since the discovery of the first P69 family member as a protein induced by the Citrus Exocortis Viroid (Granell, 1987), these proteins have been implicated in all sorts of plant-pathogen interactions, including bacteria, fungi and oomycete infections (French *et al.*, 2018; Gawehns *et al.*, 2015; Ishihara *et al.*, 2012b; Jorda *et al.*, 1999; Planas-Marques *et al.*, 2018; Tian *et al.*, 2005; Tian *et al.*, 2004; Tornero *et al.*, 1997; Zuluaga *et al.*, 2016). P69B and P69G are the two members most responsive to pathogens, being highly accumulated during *R. solanacearum* infection (Fig.1D). P69 B, C and G are also induced by the vascular pathogen *Fusarium oxysporum* (de Lamo *et al.*, 2018; Gawehns *et al.*, 2015). Although potential substrates of P69s have been proposed during the last thirty years, including RuBisCO for P69A (Vera & Conejero, 1988) and a leucine-rich repeat (LRR) protein for P69C (Tornero *et al.*, 1996), their function in immunity has remained elusive. Recently, the secreted tomato PLCP Rcr3 has been reported as a substrate of P69B (Paulus *et al.*, 2020). Rcr3, involved both in basal and gene-for-gene resistance against various pathogens, is also targeted by a distantly related subtilase, suggesting that redundant protease activities are required to ensure robust Rcr3-dependent immune responses (Paulus *et al.*, 2020). Other P69s, such as P69A that also shows a preference for aspartate in position P1 (Reichardt *et al.*, 2018), could also participate in this process.

Interrogation of our activity-based protease profiling data highlighted several P69 family members as good protease candidates with a potential role in defence against *R. solanacearum* in tomato (Planas-Marques *et al.*, 2018). Specifically, the activity of seven P69s increased in response to the pathogen in the resistant variety Hawaii 7996 while five members of this family were also activated in susceptible plants (Fig. 1D). P69D, G and J showed the highest increase in activity, and P69D was uniquely activated in the resistant cultivar (Fig. 1D). We thus confined our study to the members specifically activated in the apoplast upon *R. solanacearum* infection: P69A, P69B, P69C, P69D, P69G and P69J (Fig. 4). We carried out PICS to determine the substrate cleavage site of these P69s. This methodology serves as an indicator of preferred amino acids in protease cleavage sites, but it has two major limitations: i) the short length of the peptides in the library, which facilitates access to the protease active site, and ii) the lack of other interacting proteins present *in vivo*. Our PICS results for P69A were slightly different from those previously obtained (Reichardt *et al.*, 2018), in which a very strong preference for aspartate (close to 90%) was found in position P1. We believe that the differences between the two experiments can be attributed to the larger size of the peptide library used here, which increases the number of cleavable sequences and may favour less preferred residues. In

effect, the robustness of our results is clearly exemplified by the fact that for P69D a very similar cleavage site logo is observed using PICS and the HUNTER approach, where cleavage of intact proteins was observed *in vitro* (Fig. 3 and Fig. S6C).

P69D is the most conserved P69 gene across the four *Solanaceae* species investigated, and it exhibited the most distinct PICS profile (Fig. 3), suggesting a function divergent from the other family members. P69B was reported to cleave aspartate residues present in the junction between the autoinhibitory prodomain of Rcr3 and its mature form, but it could also cleave synthetic peptides with an alanine residue in this position (Paulus *et al.*, 2020). The latter observation correlates with our PICS analysis (Fig. 3) and suggests that aspartic-containing proteins might not be the exclusive target(s) of P69B. Overall, P69s showed similar cleavage site selectivity and considerable cleavage promiscuity, suggesting that specificity *in vivo* may rather be provided by other mechanisms.

The tomato genome codes for 10 P69s that share more than 71% sequence identity (Reichardt *et al.*, 2018). The highest sequence variability is observed in the protease-associated (PA) and Fn3-like domains (Fig. 1C). The PA domain has been described as a protein-protein interaction module in many different and unrelated proteins, contributing to substrate recognition and selectivity (Schaller *et al.*, 2018). In plants, the interaction between the PA domains and β -hairpin motifs of two tomato SBT3 protomers was proposed to mediate homodimerization and to regulate SBT3 activity by lifting a presumed autoinhibition (Ottmann *et al.*, 2009). In the soybean protease C1, the PA domain was proposed to determine the length of the targeted substrates (Tan-Wilson *et al.*, 2012) and in Arabidopsis SBT1.8, two residues of the PA domain (R302 and S333; numbers referring to the mature protease) are required for recognition of sulfo-tyrosine at the cleavage site and proteolytic maturation of the TWS1 peptide (Royek *et al.*, 2022). In sum, the little divergence observed within the subtilase domain suggests that the PA domain might contribute to functional specialization in different P69 family members, although differential tissue expression may also contribute to the presumed functional diversity of P69 proteins.

P69D function and mutant phenotype

P69D was found to accumulate and be activated in *R. solanacearum*-infected apoplast of resistant H7996 (Fig. 1), while it was neither detected in the susceptible variety Marmande, nor in the xylem sap of any of the two varieties (our unpublished results). In order to identify P69D substrate candidates we undertook a two-pronged degradomics approach (Demir *et al.*, 2018), comparing i) apoplast proteome and N-terminome of P69D knock-out and wild type plants *in vivo* and ii) searching for direct P69D cleavages *in vitro*. The comparison of

the apoplast proteomes indicated a lower abundance of immune-responsive proteins in P69D-deficient plants, while the N-terminome analysis showed altered proteolytic processing patterns particularly in PR1B and PR2. Interestingly, the CAPE peptide released from the C-terminus of PR1B after wounding is a well-known immune signalling peptide (Chen *et al.*, 2014). The altered processing of PR1B observed here therefore may perturb the release of PR1B-derived peptides -such as CAPE- and possibly PR2-derived peptides as well. These peptides would signal plant defence responses and could contribute to the weaker immune response in P69D knock-out plants. All cleavages that we observed using HUNTER were at the N-terminus of PR1B and CAPE is located at the C-terminal end. However, CAPE or any other short C-terminal peptide would most likely be undetectable because they are lost during the protein purification step after the initial HUNTER labelling. In any case, the CAPE cleavage site (CNYD-PVGN) with P at position P1' does not match the P69 PICS cleavage site profiles.

Strikingly, few P69D-dependent cleavage products accumulated after incubation with recombinant P69D in the apoplast (Fig. S6A), while few N-terminal peptides derived from PR1B or PR2 cleavage were further degraded. This may indicate that i) P69D degrades fragments of PR proteins cleaved by other proteases to attenuate generated signals, or ii) that P69D is required to activate other proteases required for processing of intact apoplast proteins. The related subtilase P69B has previously been shown to activate the papain-like cysteine protease Rcr3, suggesting that this may be a more general function of P69 proteases. Incubation with total leaf extracts demonstrated that recombinant P69D can cleave isolated protein *in vitro*, suggesting that the assay works (Fig. S6B). However, we cannot exclude that, endogenous or bacterium-derived inhibitors were present in higher concentration in the apoplast that may have inhibited the added recombinant P69D, or that P69D may have been degraded, as we did not observe peptides mapping uniquely to P69D in these samples. Also, apoplast proteins may be stably folded in the used isolation buffer that and therefore not processed, whereas proteins in total leaf extracts may have partially denatured during isolation due to change in pH and concentration and therefore may have been be more amenable to P69D cleavage. Taken together, the proteome and N-terminome data point to widespread changes in protease activity in the apoplast of P69D-deficient plants that result in altered processing of PR1B, which likely affects immune signalling mediated by the release of CAPE or other still unknown peptides.

Phenotypic characterization of P69-deficient plants indicate that this protein participates in the response of resistant tomato plants against *R. solanacearum* infection (Fig. 7). During the early stages of colonization, *R. solanacearum* occupies the root apoplastic space, while it is restricted to the xylem in the stem of H7996 (Planas-Marques *et al.*, 2020). The

stronger phenotype of the P69 mutation at late disease stages (wilting symptoms) and in bacterial numbers in the hypocotyl, compared to the weak effect observed in the root (Fig. 7) thus seems contradictory. However, this can be explained by an accumulative effect produced by restriction of bacterial multiplication in the root apoplast and the other bottlenecks encountered by the bacterium during colonisation (Planas-Marques *et al.*, 2020). P69-deficient plants were as susceptible as wild-type H7996 when the pathogen was directly inoculated into the stem, (Fig. S7). This strengthens a role of P69D in the root apoplast during the first stages of *R. solanacearum* infection, which are overcome when the bacterium is directly injected into the stem. Interestingly, the proposed role of P69D in defence does not seem to constitute a general mechanism against vascular pathogens, since P69D-deficient plants responded as WT to infection with *F. oxysporum* (Fig. S8).

When it was first discovered, P69D was thought to have a role in development because of its expression in flowers, expanding cotyledons and leaves, and its lack of induction by salicylic acid or pathogen treatments (Jorda *et al.*, 1999). This pattern of expression correlated with transcriptomic data, where *P69D* expression was particularly induced in young tissues of *S. pimpinellifolium* but not by *Pseudomonas syringae* pv tomato DC3000 (<http://ted.bti.cornell.edu/>). It is tempting to speculate that a potential role of P69D in cell elongation by changing cell wall properties may have been co-opted for plant defence. P69D could indeed act as a surveillance protein that regulates downstream processes, such cell wall remodelling to respond to pathogen attack. This correlates with the quantitative nature of bacterial wilt resistance in tomato, whereby P69D would be one of the multiple layers of defence whose absence only partially abolishes resistance (Fig. 7).

I.5 Supplementary

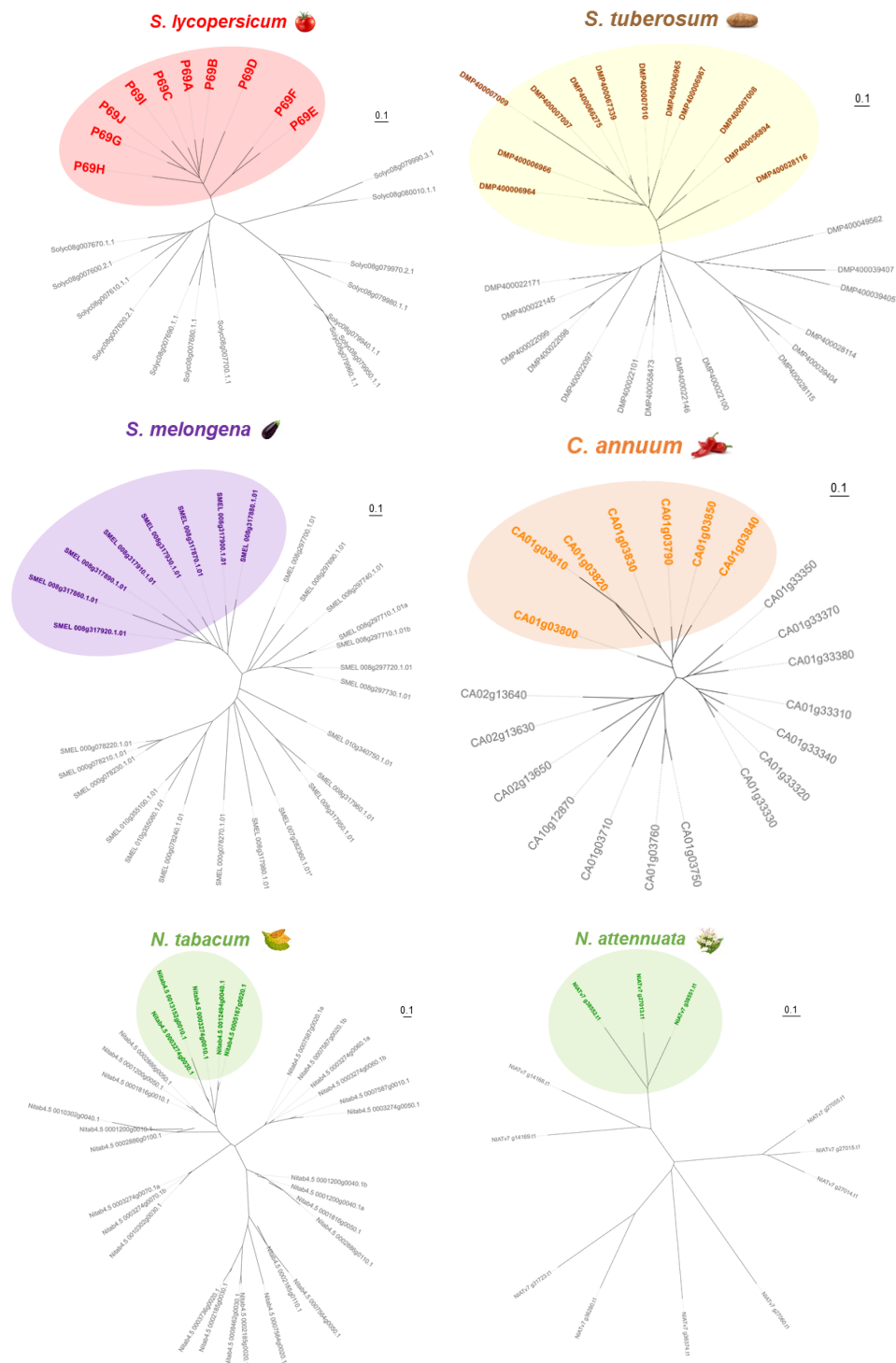
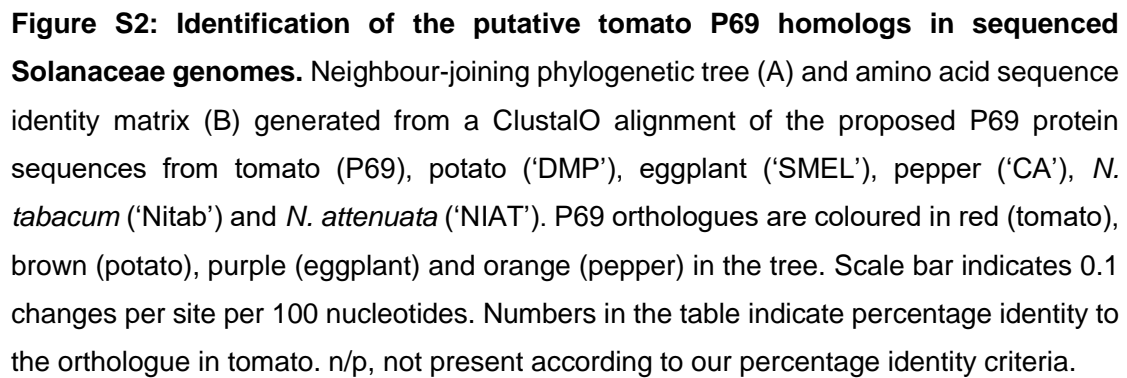


Figure S1: Phylogenetic analysis of the conserved P69 clade across different *Solanaceae* species. Neighbour-joining protein similarity trees generated from a ClustalO alignment of protein sequences sharing >55% identity with P69C (>60% identity for potato) and >50% of the alignment's maximum score. Identified P69 clades in each species are coloured, while non-P69 subtilases are shown in grey. Scale bar indicates 0.1 nucleotide changes.



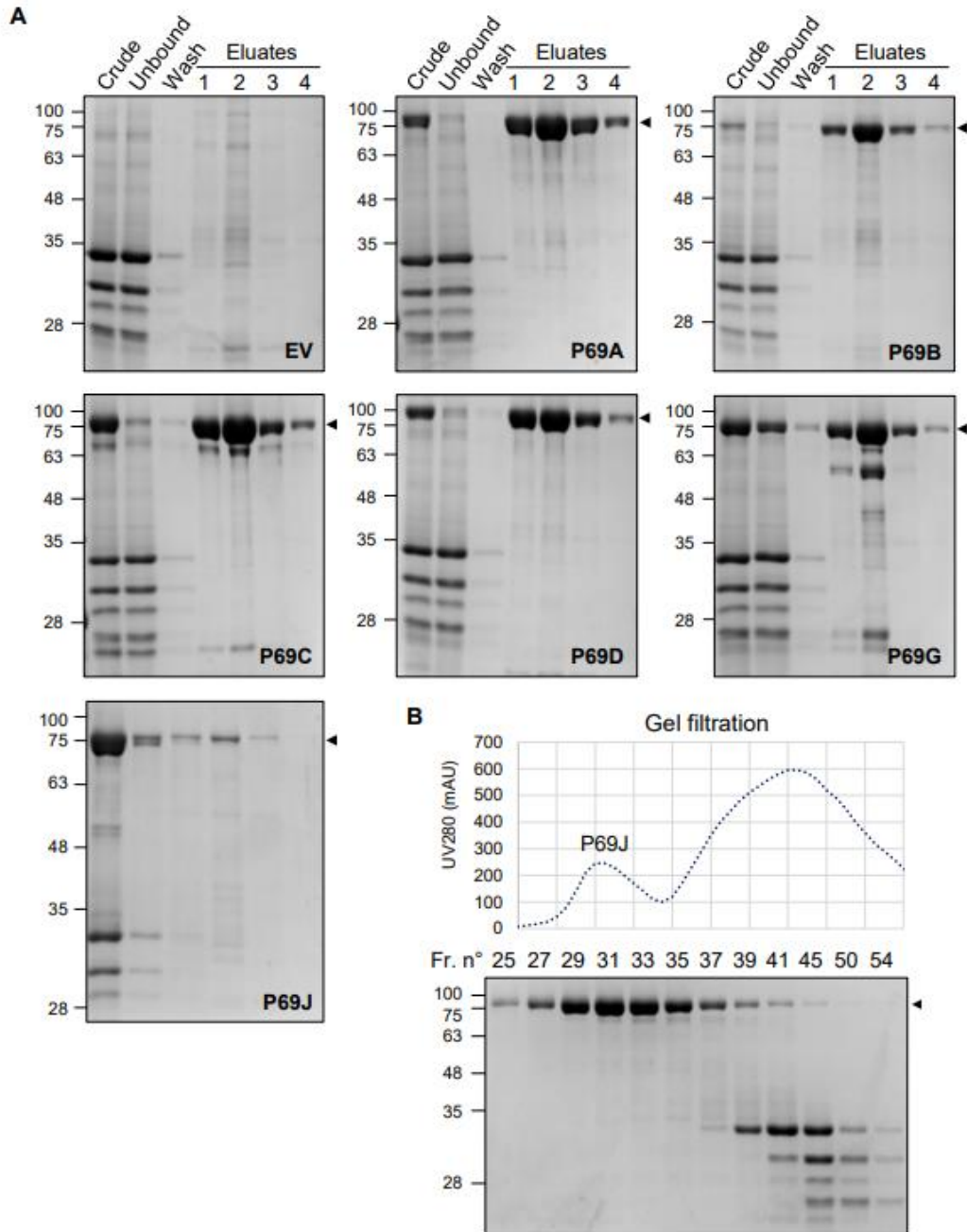


Figure S3: Purification of recombinant P69 enzymes. (A) Tomato P69A to D, P69G and P69J were transiently expressed in *N. benthamiana* leaves by agro-infiltration, the apoplastic fluids were collected 5 days later and subjected to metal chelate affinity chromatography. Fractions of each purification step were analysed by SDS-PAGE. An empty vector (EV) was included as a control. (B) Gel filtration chromatography of apoplastic fluid collected from P69J-expressing leaves. Eluate fractions 1-4 (A) and gel filtration fractions 25-33 (B) were pooled and concentrated using centrifugal concentrators.

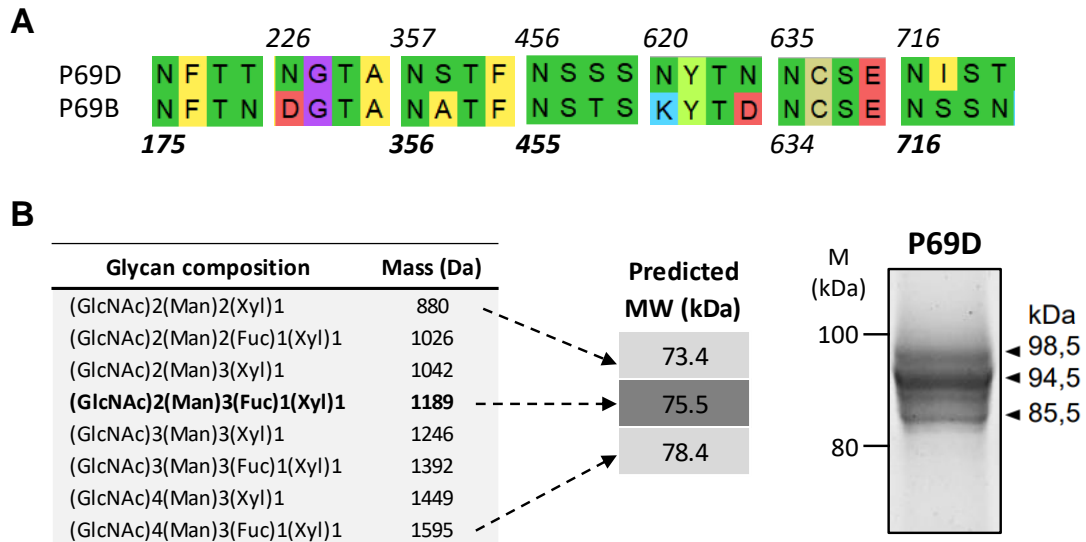


Figure S4: Analysis of putative P69G *N*-glycosylation sites. (A) Putative *N*-glycosylation sites predicted on mature P69G with NetNGlyc 1.0 Server (<http://www.cbs.dtu.dk/services/NetNGlyc/>) using a threshold of 0.5 significance. P69B was included as a control. Amino acid sequences were aligned by ClustalW and visualized using MEGA-X (<https://www.megasoftware.net/>). Asparagine residues (N) predicted to be *N*-glycosylated are indicated by numbered position on the aligned sequences. Experimentally proven glycosylation sites in P69B are marked in bold. (B) Comparison of predicted glycosylations and detected P69G protein species. Left panel: Glycan composition and estimated molecular mass of differentially glycosylated asparagine residues detected by Bykova *et al.* in P69B (Bykova *et al.*, 2006). In bold, most abundant glycan structure based on relative intensities of ion peaks. Center panel: predicted molecular weights of P69D variants fused with His tag modified at all putative *N*-glycosylation sites with the lightest, the most abundant and the heaviest glycan. Right image, SyproRuby-stained SDS-PAGE of purified hexa-His tagged P69D. Arrowheads indicate apparent mass for the observed protein bands.

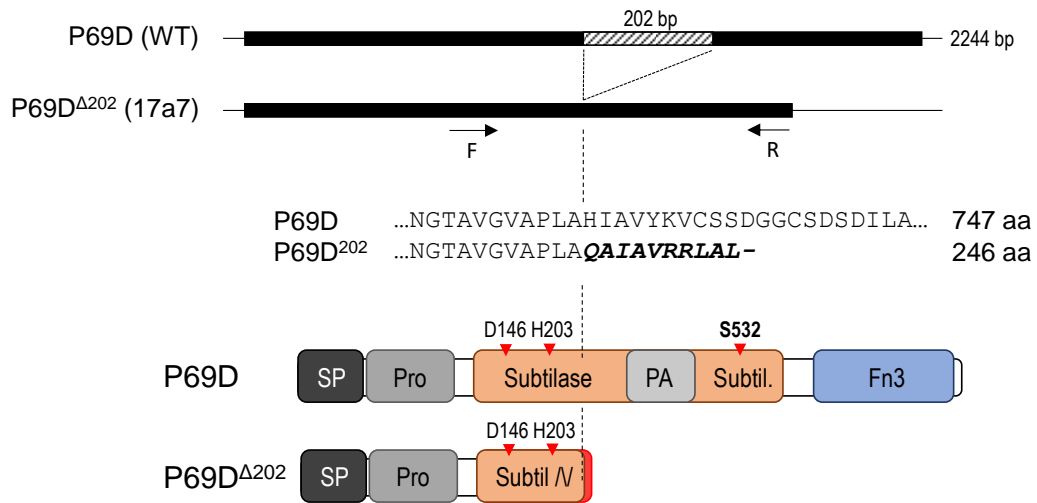
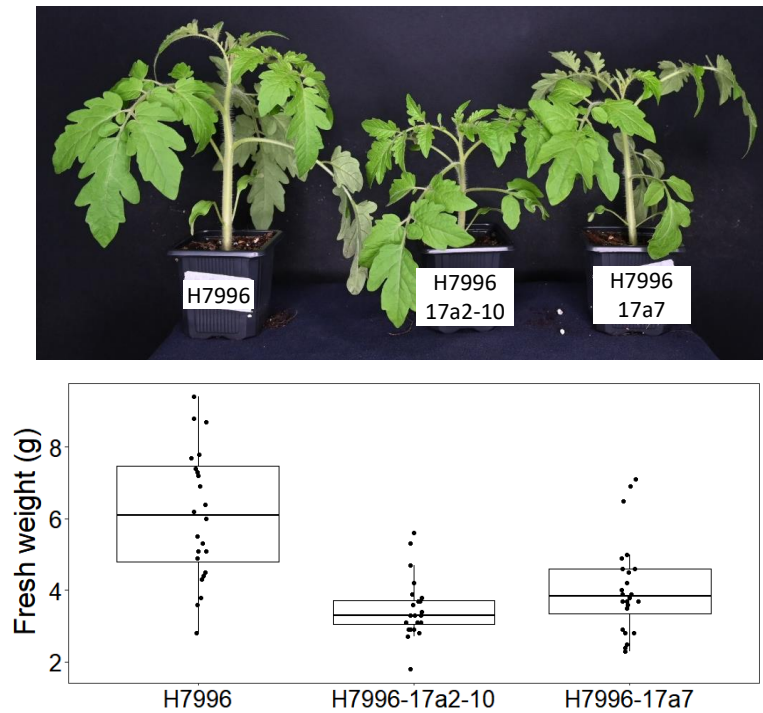
A**B**

Figure S5: Generation of a *p69d* CRISPR/Cas9 deletion mutant. (A) Schematic representation showing the 202 bp deletion obtained by CRISPR/Cas9 in the *P69D* gene. The mutation results in a premature stop codon, resulting in a truncated protein variant. D, H and S indicate the putative aspartate, histidine and serine residues from the active site. Arrowheads indicate genotyping primers (F, Forward; R, Reverse). Dashed lines indicate the double-strand break site used by Cas9. (B) Phenotype of Hawaii 7996 tomato plants and the derived *P69D* mutant lines. Representative pictures and fresh weight of the wild type Hawaii 7996 (H7996) and the two genome edited plant lines used in this work three weeks after germination.

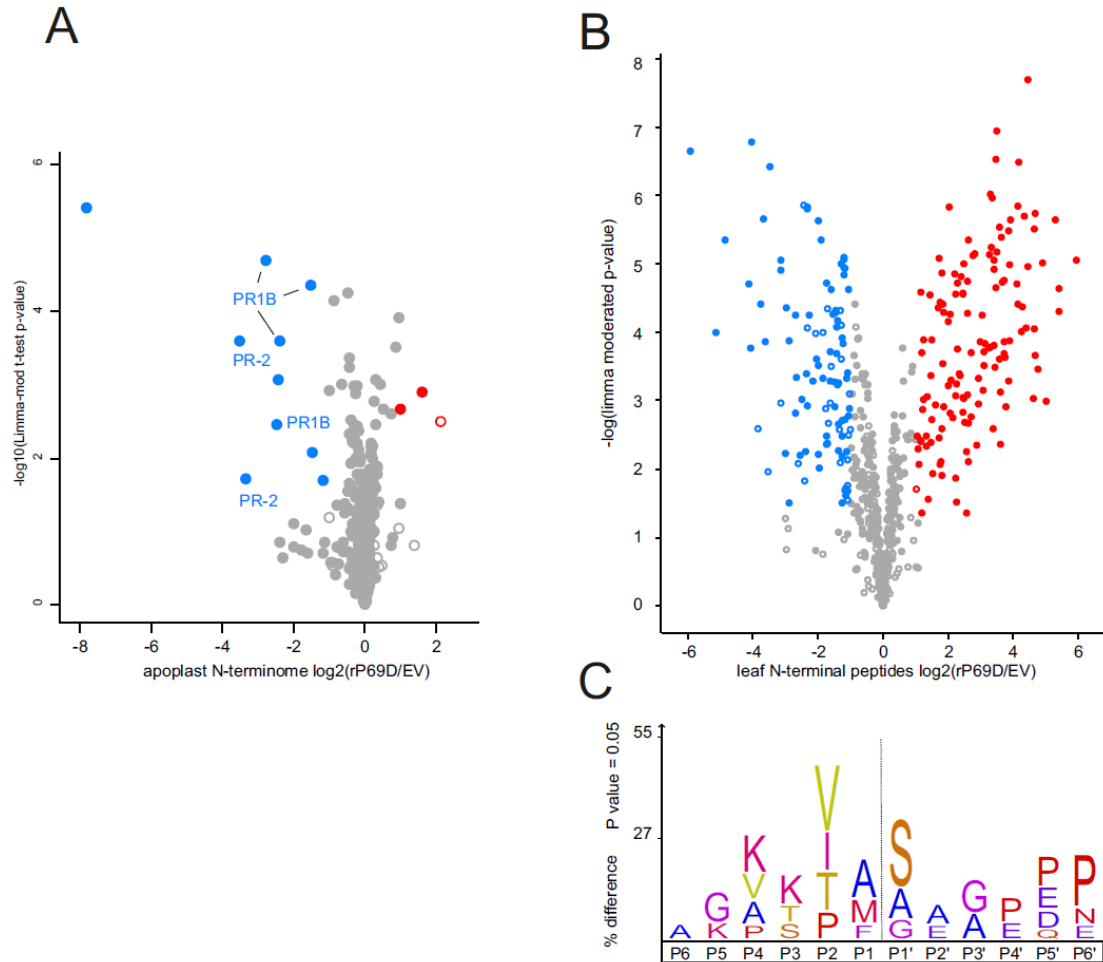


Figure S6. N-terminome analysis of P69D-deficient plants after incubation with recombinant P69D *in vitro*. (A) Volcano plot depicting N-terminal peptide abundance in apoplastic extracts from P69D-deficient plants infected with *R. solanacearum* after incubation with recombinant P69D (P69D) or empty vector control (EV). Open circles, N-termini mapping to canonical protein termini mapping to positions 1 or 2 with intact or removed Met, known signal- or transit peptide sequences; filled circles, non-canonical protein termini mapping to positions within their protein sequence; red and blue, N-terminal peptides significantly accumulating or depleted (moderated t-test p-value<0.05, 2-fold change in abundance) after incubation with recombinant P69D. (B) Volcano plot depicting changes in N-terminal peptide abundance after incubation of total leaf proteome isolated from *R. solanacearum*-infected P69D-deficient plants with recombinant P69D or mock purification after empty vector (EV) expression as control. Open circles, N-termini mapping to canonical protein termini mapping to positions 1 or 2 with intact or removed Met, known signal- or transit peptide sequences; filled circles, non-canonical protein termini mapping to positions within their protein sequence; red and blue, N-terminal peptides significantly accumulating or depleted (moderated t-test p-value<0.05, 2-fold change in abundance) after incubation with recombinant P69D. (C) Icelogo depicting the amino acid prevalence of 133 aligned P69D cleavage sites derived from dimethylated, noncanonical N-terminal

peptides identified in (B).

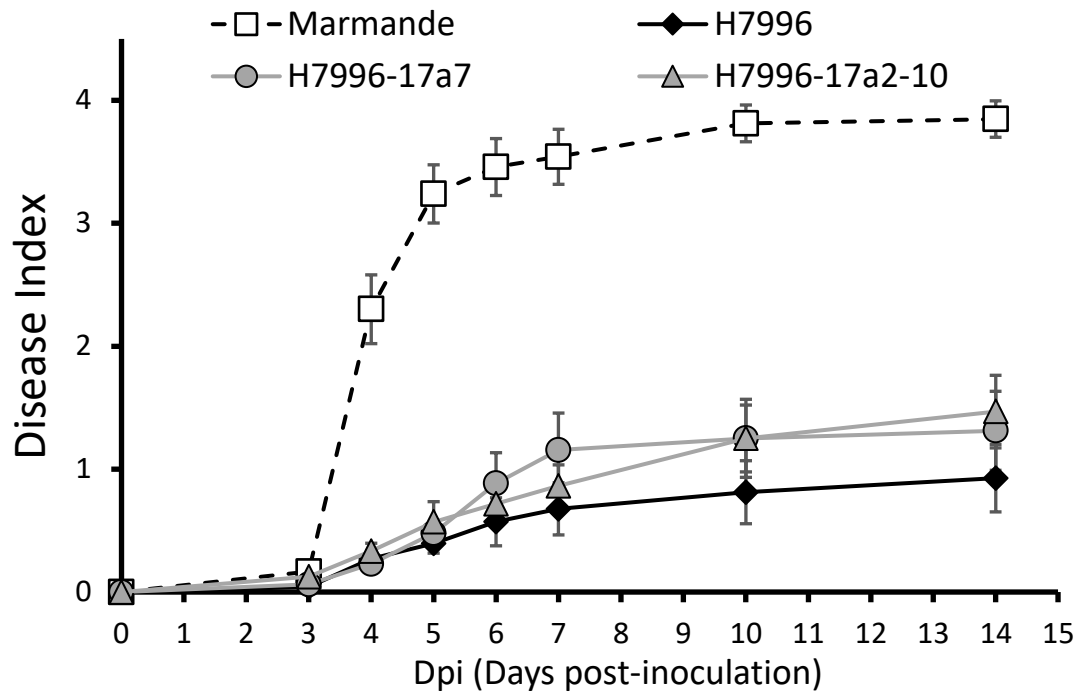
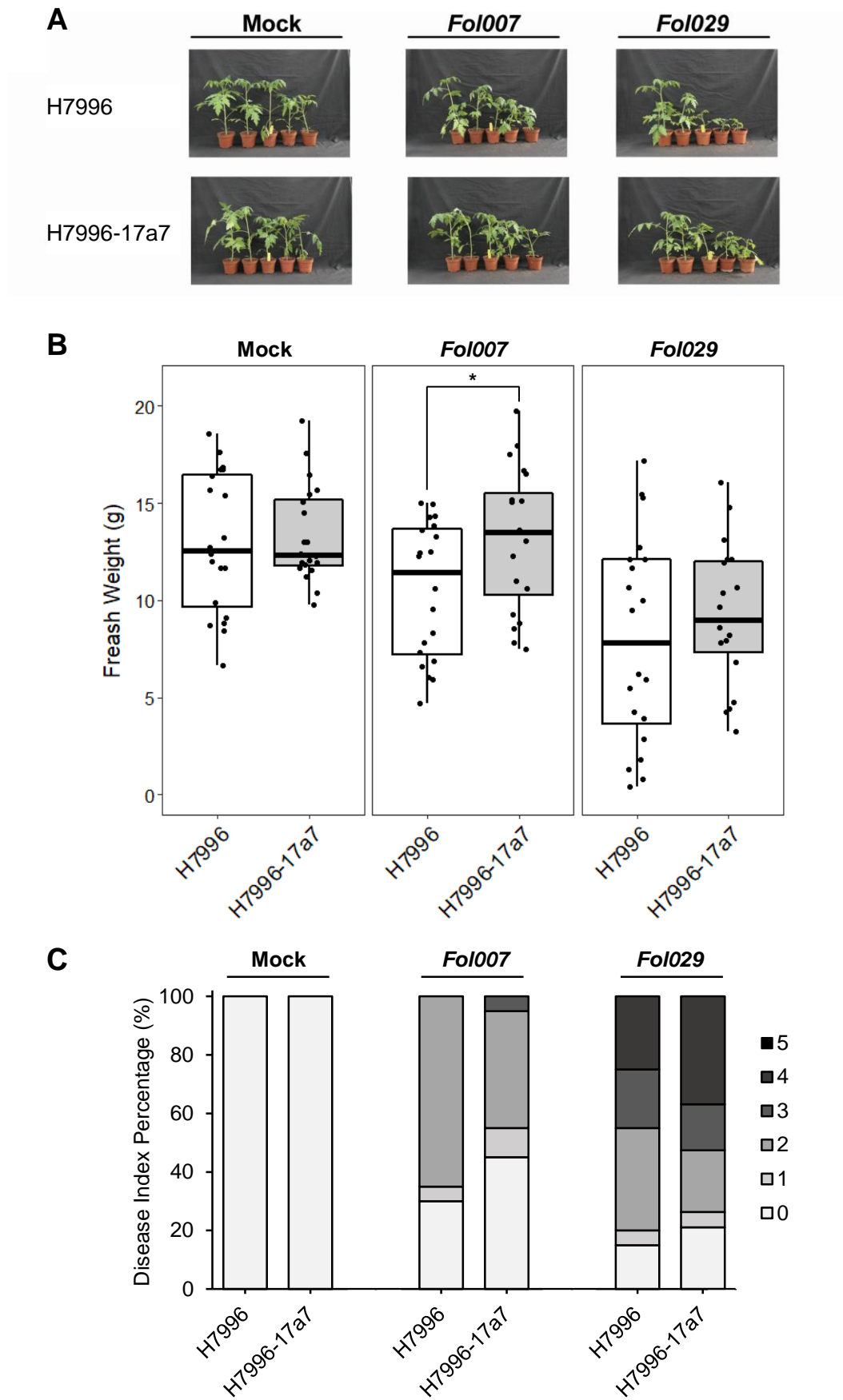


Figure S7. Pathogenicity assays of the P69D single mutant by petiole-inoculation. Four or six-weeks-old tomato plants were petiole-inoculated with 10^6 CFU/ml *R. solanacearum* suspension as indicated. Wilting symptoms were scored over time for two weeks. The graph shows the results of a representative experiment out of the three biological replicas performed using at least 20 plants of each variety and line. Different letters next to each graph or above each boxplot indicate statistically significant differences ($\alpha=0.05$, Fisher's least significant difference test).



Hawaii 7996 (H7996) and the *P69D* knockout tomato lines were root dip inoculated with mock, *FolI007* or *FolI029*. Three weeks post-inoculation five representative plants per treatment were photographed (A), their fresh weight was measured (B) and disease index (C) were scored on a scale from 0 (healthy plant) to 5 (dead plant). Statistical analyses were performed using an Ordinary One-way ANOVA for fresh weight and a Mann-Whitney U test for disease index data. The assay was repeated twice using approximately 20 plants per treatment yielding similar results.

Table S1. Gene and protein identifiers for tomato P69s.

Identifier (SGN)	LOC ID (NCBI)	UniprotKB	P69 name
Solyc08g079840	LOC544111	K4CNY4	P69A
Solyc08g079870	LOC544296	O04678	P69B
Solyc08g079860	LOC108511949	K4CNY6	P69C
Solyc08g079850	LOC101255226	O65836	P69D
Solyc08g079930	LOC109118744	K4CNZ3	P69E
Solyc08g079920	LOC101253407	Q9LWA3	P69F
Solyc08g079900	LOC778308	K4CNZ0	P69G
Solyc08g079910	LOC109120848	K4CNZ1	P69H
Solyc08g079890	LOC101254322	K4CNY9	P69I
Solyc08g079880	LOC101254622	O65834	P69J

Table S2. Databases used for the construction of P69-like gene phylogeny in *Solanaceae* species.

Organism	Database	Ref.
<i>Solanum lycopersicum</i>	Tomato Genome proteins (ITAG release 4.0)	(56)
<i>Solanum pimpinellifolium</i>	Wild tomato <i>S. pimpinellifolium</i> protein sequences LA1589 (draft genome)	(56)
<i>Solanum tuberosum</i>	Potato PGSC DM v3.4 Protein sequences	(57)
<i>Capsicum annuum</i>	Pepper cv. CM334 Genome protein sequences (release 1.55)	(58)
<i>Solanum melongena</i>	Eggplant genome v3 protein sequences	(59)
<i>Nicotiana tabacum</i>	Tobacco Nitab v4.5 proteins Edwards 2017 (draft genome)	(60)
<i>Nicotiana attenuata</i>	Wild tobacco <i>N. attenuata</i> v2 annot v5 proteins (draft genome)	(61)

Table S3. Oligonucleotides used in this study

Primer Name	Primer Sequence (5' to 3')
P69B F	GGCCCGGGATGGGATTATTGAAAATCCTTCTTGTTTTC
P69B R	GGGGATCCTTAATGGTGATGATGATGGTGGGCAGACACAACGCAATTG
P69C F	GGCCCGGGATGGGATTCTTCAAAATCCTTTTTGTTTTCATC
P69C R	GGGGATCCTTAATGGTGATGATGATGGTGGGCTAACACAACGCAATTG
P69D F	GGCCCGGGATGGGATTCTTGAAAATTCTTCTTATCTTCATATTTTGC
P69D R	GGGGATCCTTAATGGTGATGATGATGGTGTTGAGCAGACACTCTAACTG
P69G F	GGCCCGGGATGGGATTCTTGAAAATCCTTTTTGTTTTCATC
P69G R	GGGGATCCTTAATGGTGATGATGATGGTGCTTAGCCAATGCCAACACAAC
P69J F	GGCCCGGGATGGGATTCTTCAAAATCCTTTTTGTTTTCATC
P69J R	GGGGATCCTTAATGGTGATGATGATGGTGAATGTCTGAATACTTTGTAGC
P69D U3-SG1	CCGCTATGTGGGCTAGAGGGGCA
P69D U6-SG2	CGGACCGCTATTGCCTGCTGAGG
P69D U6-SG9	TTAGCTACAGTGCCAAGCGACGG
P69D U3-SG10	TGCTACGCTTGGTCCTCGTGAGG
P69D F5	GTCCTCGAGAGCCATCTCAC
P69D R4	ACAAGCTCATTGGAGCCAGG
Cas9 F	TCCCTTACTACGTGGGACCTC
Cas9 R	ATCTGCCTGGTTTCCACAAG

References

1. Du Y, Stegmann M, Misas Villamil JC. The apoplast as battleground for plant-microbe interactions. *New Phytol.* 2016;209(1):34-8.
2. Macho AP, Zipfel C. Plant PRRs and the activation of innate immune signaling. *Mol Cell.* 2014;54(2):263-72.
3. Gupta R, Lee SE, Agrawal GK, Rakwal R, Park S, Wang Y, *et al.* Understanding the plant-pathogen interactions in the context of proteomics-generated apoplastic proteins inventory. *Front Plant Sci.* 2015;6:352.
4. Schaller A, Stintzi A, Rivas S, Serrano I, Chichkova NV, Vartapetian AB, *et al.* From structure to function - a family portrait of plant subtilases. *New Phytol.* 2018;218(3):901-15.
5. Smith EL, Markland FS, Kasper CB, DeLange RJ, Landon M, Evans WH. The complete amino acid sequence of two types of subtilisin, BPN' and Carlsberg. *J Biol Chem.* 1966;241(24):5974-6.
6. Meyer M, Leptihn, S., Welz, M., Schaller, A. Functional Characterization of Propeptides in Plant Subtilases as Intramolecular Chaperones and Inhibitors of the Mature Protease*. *J Biol Chem* 2016;291(37):19449-61.
7. Nebes VL, Jones EW. Activation of the proteinase B precursor of the yeast *Saccharomyces cerevisiae* by autocatalysis and by an internal sequence. *J Biol Chem.* 1991;266(34):22851-7.
8. Vey M, Schafer W, Berghofer S, Klenk HD, Garten W. Maturation of the trans-Golgi network protease furin: compartmentalization of propeptide removal, substrate cleavage, and COOH-terminal truncation. *J Cell Biol.* 1994;127(6 Pt 2):1829-42.
9. Power SD, Adams RM, Wells JA. Secretion and autoproteolytic maturation of subtilisin. *Proc Natl Acad Sci U S A.* 1986;83(10):3096-100.
10. Cedzich A, Huttenlocher F, Kuhn BM, Pfannstiel J, Gabler L, Stintzi A, *et al.* The protease-associated domain and C-terminal extension are required for zymogen processing, sorting within the secretory pathway, and activity of tomato subtilase 3 (SISBT3). *J Biol Chem.* 2009;284(21):14068-78.
11. Chichkova NV, Shaw J, Galiullina RA, Drury GE, Tuzhikov AI, Kim SH, *et al.* Phytaspase, a relocatable cell death promoting plant protease with caspase specificity. *EMBO J.* 2010;29(6):1149-61.
12. Muller L, Cameron A, Fortenberry Y, Apletalina EV, Lindberg I. Processing and sorting of the prohormone convertase 2 propeptide. *J Biol Chem.* 2000;275(50):39213-22.
13. Reichardt S, Reppe D, Tuzhikov AI, Galiullina RA, Planas-Marques M, Chichkova NV, *et al.* The tomato subtilase family includes several cell death-related proteinases with caspase specificity. *Sci Rep.* 2018;8(1):10531.
14. Mahon P, Bateman A. The PA domain: a protease-associated domain. *Protein Sci.* 2000;9(10):1930-4.

15. Tan-Wilson A, Bandak B, Prabu-Jeyabalan M. The PA domain is crucial for determining optimum substrate length for soybean protease C1: structure and kinetics correlate with molecular function. *Plant Physiol Biochem.* 2012;53:27-32.
16. Ottmann C, Rose R, Huttenlocher F, Cedzich A, Hauske P, Kaiser M, *et al.* Structural basis for Ca²⁺-independence and activation by homodimerization of tomato subtilase 3. *Proc Natl Acad Sci U S A.* 2009;106(40):17223-8.
17. Vera P, Conejero V. Pathogenesis-related proteins of tomato : p-69 as an alkaline endoproteinase. *Plant Physiol.* 1988;87(1):58-63.
18. Vera P, and Conejero, V. The induction and accumulation of the pathogenesis-related P69 proteinase in tomato during citrus exocortis viroid infection and in response to chemical treatments. *Physiological and Molecular Plant Pathology.* 1989;34(4):323-34.
19. Vera P, Yago JH, Conejero V. Immunogold localization of the citrus exocortis viroid-induced pathogenesis-related proteinase p69 in tomato leaves. *Plant Physiol.* 1989;91(1):119-23.
20. Jorda L, Coego A, Conejero V, Vera P. A genomic cluster containing four differentially regulated subtilisin-like processing protease genes is in tomato plants. *J Biol Chem.* 1999;274(4):2360-5.
21. Jorda L, Conejero V, Vera P. Characterization of P69E and P69F, two differentially regulated genes encoding new members of the subtilisin-like proteinase family from tomato plants. *Plant Physiol.* 2000;122(1):67-74.
22. Meichtry J, Amrhein N, Schaller A. Characterization of the subtilase gene family in tomato (*Lycopersicon esculentum* Mill.). *Plant Mol Biol.* 1999;39(4):749-60.
23. Tornero P, Mayda E, Gomez MD, Canas L, Conejero V, Vera P. Characterization of LRP, a leucine-rich repeat (LRR) protein from tomato plants that is processed during pathogenesis. *Plant J.* 1996;10(2):315-30.
24. Tian M, Huitema E, Da Cunha L, Torto-Alalibo T, Kamoun S. A Kazal-like extracellular serine protease inhibitor from *Phytophthora infestans* targets the tomato pathogenesis-related protease P69B. *J Biol Chem.* 2004;279(25):26370-7.
25. Ishihara T, Mitsuhara I, Takahashi H, Nakaho K. Transcriptome analysis of quantitative resistance-specific response upon *Ralstonia solanacearum* infection in tomato. *PLoS One.* 2012;7(10):e46763.
26. Zuluaga AP, Sole M, Lu H, Gongora-Castillo E, Vaillancourt B, Coll N, *et al.* Transcriptome responses to *Ralstonia solanacearum* infection in the roots of the wild potato *Solanum commersonii*. *BMC Genomics.* 2015;16:246.
27. Paulus JK, Kourelis J, Ramasubramanian S, Homma F, Godson A, Horger AC, *et al.* Extracellular proteolytic cascade in tomato activates immune protease Rcr3. *Proc Natl Acad Sci U S A.* 2020;117(29):17409-17.
28. Tian M, Win J, Song J, van der Hoorn R, van der Knaap E, Kamoun S. A *Phytophthora infestans* cystatin-like protein targets a novel tomato papain-like apoplastic protease. *Plant Physiol.* 2007;143(1):364-77.

29. Song J, Win J, Tian M, Schornack S, Kaschani F, Ilyas M, *et al.* Apoplastic effectors secreted by two unrelated eukaryotic plant pathogens target the tomato defense protease Rcr3. *Proc Natl Acad Sci U S A.* 2009;106(5):1654-9.
30. Tian M, Benedetti B, Kamoun S. A Second Kazal-like protease inhibitor from *Phytophthora infestans* inhibits and interacts with the apoplastic pathogenesis-related protease P69B of tomato. *Plant Physiol.* 2005;138(3):1785-93.
31. Homma F, Huang J, Hoorn RALvd. Alphafold-multimer predicts cross-kingdom interactions at the plant-pathogen interface. *bioRxiv.* 2023:2023.04.03.535425.
32. Hayward AC. Biology and epidemiology of bacterial wilt caused by *Pseudomonas solanacearum*. *Annu Rev Phytopathol.* 1991;29:65-87.
33. Vasse J, Frey, P., and Trigalet, A. . Microscopic studies of intercellular infection and protoxylem invasion of tomato roots by *Pseudomonas solanacearum*. . *Molecular Plant-Microbe Interactions.* 1995;8:241-51.
34. Grimault V, G  lie, B., Lemattre, M., Prior, P., and Schmit, J. Comparative histology of resistant and susceptible tomato cultivars infected by *Pseudomonas solanacearum*. *Physiological and Molecular Plant Pathology.* 1994;44:105-23.
35. Planas-Marques M, Kressin JP, Kashyap A, Panthee DR, Louws FJ, Coll NS, *et al.* Four bottlenecks restrict colonization and invasion by the pathogen *Ralstonia solanacearum* in resistant tomato. *J Exp Bot.* 2020;71(6):2157-71.
36. Planas-Marques M, Bernardo-Faura M, Paulus J, Kaschani F, Kaiser M, Valls M, *et al.* Protease Activities Triggered by *Ralstonia solanacearum* Infection in Susceptible and Tolerant Tomato Lines. *Mol Cell Proteomics.* 2018;17(6):1112-25.
37. Vartapetian AB, Tuzhikov AI, Chichkova NV, Taliansky M, Wolpert TJ. A plant alternative to animal caspases: subtilisin-like proteases. *Cell Death Differ.* 2011;18(8):1289-97.
38. Schilling O, Overall CM. Proteome-derived, database-searchable peptide libraries for identifying protease cleavage sites. *Nat Biotechnol.* 2008;26(6):685-94.
39. Schilling O, Huesgen PF, Barre O, Auf dem Keller U, Overall CM. Characterization of the prime and non-prime active site specificities of proteases by proteome-derived peptide libraries and tandem mass spectrometry. *Nat Protoc.* 2011;6(1):111-20.
40. Poueymiro M, Cunnac S, Barberis P, Deslandes L, Peeters N, Cazale-Noel AC, *et al.* Two type III secretion system effectors from *Ralstonia solanacearum* GMI1000 determine host-range specificity on tobacco. *Mol Plant Microbe Interact.* 2009;22(5):538-50.
41. Danilo B, Perrot L, Botton E, Nogue F, Mazier M. The DFR locus: A smart landing pad for targeted transgene insertion in tomato. *PLoS One.* 2018;13(12):e0208395.
42. Demir F, Perrar A, Mantz M, Huesgen PF. Sensitive Plant N-Terminome Profiling with HUNTER. *Methods Mol Biol.* 2022;2447:139-58.
43. Granell A, Bell  s, J. M., and Conejero, V. Induction of pathogenesis-related proteins in tomato by citrus exocortis viroid, silver ion and ethephon. *Physiological and Molecular Plant Pathology.* 1987;31(1):83-90.

44. French E, Kim BS, Rivera-Zuluaga K, Iyer-Pascuzzi AS. Whole Root Transcriptomic Analysis Suggests a Role for Auxin Pathways in Resistance to *Ralstonia solanacearum* in Tomato. *Mol Plant Microbe Interact.* 2018;31(4):432-44.
45. Gawehns F, Ma L, Bruning O, Houterman PM, Boeren S, Cornelissen BJ, *et al.* The effector repertoire of *Fusarium oxysporum* determines the tomato xylem proteome composition following infection. *Front Plant Sci.* 2015;6:967.
46. Zuluaga AP, Vega-Arreguin JC, Fei Z, Matas AJ, Patev S, Fry WE, *et al.* Analysis of the tomato leaf transcriptome during successive hemibiotrophic stages of a compatible interaction with the oomycete pathogen *Phytophthora infestans*. *Mol Plant Pathol.* 2016;17(1):42-54.
47. Tornero P, Conejero V, Vera P. Identification of a new pathogen-induced member of the subtilisin-like processing protease family from plants. *J Biol Chem.* 1997;272(22):14412-9.
48. de Lamo FJ, Constantin ME, Fresno DH, Boeren S, Rep M, Takken FLW. Xylem Sap Proteomics Reveals Distinct Differences Between R Gene- and Endophyte-Mediated Resistance Against *Fusarium* Wilt Disease in Tomato. *Front Microbiol.* 2018;9:2977.
49. Bykova NV, Rampitsch C, Krokhin O, Standing KG, Ens W. Determination and characterization of site-specific N-glycosylation using MALDI-Qq-TOF tandem mass spectrometry: case study with a plant protease. *Anal Chem.* 2006;78(4):1093-103.
50. Royek S, Bayer M, Pfannstiel J, Pleiss J, Ingram G, Stintzi A, *et al.* Processing of a plant peptide hormone precursor facilitated by posttranslational tyrosine sulfation. *Proc Natl Acad Sci U S A.* 2022;119(16):e2201195119.
51. Demir F, Niedermaier S, Villamor JG, Huesgen PF. Quantitative proteomics in plant protease substrate identification. *New Phytol.* 2018;218(3):936-43.
52. Chen YL, Lee CY, Cheng KT, Chang WH, Huang RN, Nam HG, *et al.* Quantitative peptidomics study reveals that a wound-induced peptide from PR-1 regulates immune signaling in tomato. *Plant Cell.* 2014;26(10):4135-48.
53. Mirdita M, Schutze K, Moriwaki Y, Heo L, Ovchinnikov S, Steinegger M. ColabFold: making protein folding accessible to all. *Nat Methods.* 2022;19(6):679-+.
54. Gleave AP. A versatile binary vector system with a T-DNA organisational structure conducive to efficient integration of cloned DNA into the plant genome. *Plant Mol Biol.* 1992;20(6):1203-7.
55. Colaert N, Helsens K, Martens L, Vandekerckhove J, Gevaert K. Improved visualization of protein consensus sequences by iceLogo. *Nat Methods.* 2009;6(11):786-7.
56. Boersema PJ, Raijmakers R, Lemeer S, Mohammed S, Heck AJ. Multiplex peptide stable isotope dimethyl labeling for quantitative proteomics. *Nat Protoc.* 2009;4(4):484-94.
57. Rappsilber J, Mann M, Ishihama Y. Protocol for micro-purification, enrichment, pre-fractionation and storage of peptides for proteomics using StageTips. *Nat Protoc.* 2007;2(8):1896-906.

58. Beck S, Michalski A, Raether O, Lubeck M, Kaspar S, Goedecke N, *et al.* The Impact II, a Very High-Resolution Quadrupole Time-of-Flight Instrument (QTOF) for Deep Shotgun Proteomics. *Mol Cell Proteomics*. 2015;14(7):2014-29.
59. Tyanova S, Temu T, Cox J. The MaxQuant computational platform for mass spectrometry-based shotgun proteomics. *Nat Protoc*. 2016;11(12):2301-19.
60. Yu SH, Ferretti D, Schessner JP, Rudolph JD, Borner GHH, Cox J. Expanding the Perseus Software for Omics Data Analysis With Custom Plugins. *Curr Protoc Bioinformatics*. 2020;71(1):e105.
61. Demir F, Kizhakkedathu JN, Rinschen MM, Huesgen PF. MANTI: Automated Annotation of Protein N-Termini for Rapid Interpretation of N-Terminome Data Sets. *Anal Chem*. 2021;93(13):5596-605.
62. Demir F, Huesgen PF. A User Guide to Validation, Annotation, and Evaluation of N-Terminome Datasets with MANTI. *Methods Mol Biol*. 2022;2447:271-83.
63. Xiao Y, Hsiao TH, Suresh U, Chen HI, Wu X, Wolf SE, *et al.* A novel significance score for gene selection and ranking. *Bioinformatics*. 2014;30(6):801-7.
64. Haeussler M, Schonig K, Eckert H, Eschstruth A, Mianne J, Renaud JB, *et al.* Evaluation of off-target and on-target scoring algorithms and integration into the guide RNA selection tool CRISPOR. *Genome Biol*. 2016;17(1):148.
65. Mazier M, Flamain F, Nicolai M, Sarnette V, Caranta C. Knock-down of both eIF4E1 and eIF4E2 genes confers broad-spectrum resistance against potyviruses in tomato. *PLoS One*. 2011;6(12):e29595.
66. Cruz AP, Ferreira V, Pianzola MJ, Siri MI, Coll NS, Valls M. A novel, sensitive method to evaluate potato germplasm for bacterial wilt resistance using a luminescent *Ralstonia solanacearum* reporter strain. *Mol Plant Microbe Interact*. 2014;27(3):277-85.
67. Mes JJ, Weststeijn EA, Herlaar F, Lambalk JJ, Wijbrandi J, Haring MA, *et al.* Biological and Molecular Characterization of *Fusarium oxysporum* f. sp. *lycopersici* Divides Race 1 Isolates into Separate Virulence Groups. *Phytopathology*. 1999;89(2):156-60.
68. Marlatt M, Correll JC, Kaufmann P, Cooper P. Two genetically distinct populations of *Fusarium oxysporum* f. sp. *lycopersicirace* 3 in the united states. *Plant Disease*. 1996;80(12):1336.
69. Rep M, van der Does HC, Meijer M, van Wijk R, Houterman PM, Dekker HL, *et al.* A small, cysteine-rich protein secreted by *Fusarium oxysporum* during colonization of xylem vessels is required for I-3-mediated resistance in tomato. *Mol Microbiol*. 2004;53(5):1373-83.
70. de Lamo FJ, Simkovicova M, Fresno DH, de Groot T, Tintor N, Rep M, *et al.* Pattern-triggered immunity restricts host colonization by endophytic fusaria, but does not affect endophyte-mediated resistance. *Mol Plant Pathol*. 2021;22(2):204-15.
71. Deutsch EW, Bandeira N, Perez-Riverol Y, Sharma V, Carver JJ, Mendoza L, *et al.* The ProteomeXchange consortium at 10 years: 2023 update. *Nucleic Acids Res*. 2023;51(D1):D1539-D48.

72. Perez-Riverol Y, Bai J, Bandla C, Garcia-Seisdedos D, Hewapathirana S, Kamatchinathan S, *et al.* The PRIDE database resources in 2022: a hub for mass spectrometry-based proteomics evidences. *Nucleic Acids Res.* 2022;50(D1):D543-D552.

Chapter II

Characterization of the PR1 family of tomato

II.1 Introduction

II.1.1 PR1 superfamily protein

The pathogenesis-related (PR) proteins of plants have been proven to be highly induced upon abiotic and biotic stresses. Until now, these proteins are classified into 17 superfamilies (PR1-PR17). They are often toxic to invading phytopathogens, such as PR2 (β -1,3-glucanases), PR3 (chitinases), PR4 (antifungal), PR6 (proteinase inhibitors), PR7 (P69s, subtilisin-like proteases, subtilases). The mode of action of most PR proteins has been well characterized (Green & Ryan, 1972; Lagrimini *et al*, 1987; Van Loon, 1982), except for PR1. PR1 proteins were first identified from leaves of *Nicotiana tabacum* infected with tobacco mosaic virus (TMV) (Van Loon & Van Kammen, 1970). At the end of last century, numerous PR1 family proteins were identified as highly induced upon infection or treatment with plant hormones in Solanaceae plants (De Wit *et al*, 1986; Eyal *et al*, 1992; Tornero *et al*, 1994; van Kan *et al*, 1992). With the widespread application of genome sequencing, additional PR1-like proteins were identified. Interestingly, even though there are dozens of PR1 proteins spread across various species, not all PR1 proteins are upregulated during infection (Cornelissen *et al*, 1987). According to their theoretical isoelectric point, PR1 family proteins were classified as either acidic or basic proteins. At first, many researchers named PR1 family proteins depending on this characterization (Eyal *et al*, 1992; Tornero *et al*, 1994).

Since the upregulation of PR1 has been well characterized as part of the salicylic acid-dependent host defense activation, PR1 is widely used as a defense marker in plants (Durrant & Dong, 2004). For instance, PR1 proteins constitute around 2% of the total leaf protein found in infected tobacco (Alexander *et al*, 1993). Recent functional studies showed a potential role for PR1 proteins as antimicrobial. Niderman *et al*. sowed in 1995 impaired growth of *Phytophthora infestans* zoospores after adding purified PR1 proteins from tomato and tobacco (Niderman *et al*, 1995). Recently, ectopic expression of *PR1* from crop plants in tobacco and *Arabidopsis thaliana* conferred increased resistance to bacterial and fungal pathogens through priming plant defense (Fang *et al*, 2019; Li *et al*, 2011; Sarowar *et al*, 2005; Shin *et al*, 2014).

II.1.2 CAP domain

PR1 proteins are members of the CAP protein family (cysteine-rich secretory proteins from humans -CRISP-, antigen 5 -Ag5-, and pathogenesis-related 1 proteins), found in bacteria, fungi, plants and animals. Most PR1 family proteins only contain the CAP domain and a relatively short N-, C- terminal domains, suggesting that this domain

possesses antimicrobial function in plant defense.

CAP superfamily proteins have a conserved lipid binding function (Choudhary & Schneider, 2012; Darwiche *et al.*, 2017). Sterols are a main component of membranes, particularly of fungal plasma membranes. The sterol-binding activity of PR1 proteins from tomato is essential for their antimicrobial function *in vitro* (Gamir *et al.*, 2017), supporting the suggested role of PR1 to cause cellular leakage of fungi. The 146th cysteine residue of CAP domain is necessary sterol-binding in PR1 (Gamir *et al.*, 2017). However, sterols are rare in bacteria, which suggests that the antimicrobial function of PR1 against bacterial pathogens is provided by a different domain or mechanism.

II.1.3 Plant PR1s are proteolytically cleaved to generate a signaling peptide

Besides the previously mentioned direct antimicrobial action of PR1 through the sequestration of sterols from the fungal pathogen membrane, PR1 has been shown to possess anti-bacterial activity. Since the bacterial cell membrane does not contain sterol, PR1 may enhance plant immunity differently. An 11-amino acid peptide derived from PR1b was reported to be highly accumulated in wounding and methyl jasmonate-treated tomato leaves (Chen *et al.*, 2014). Subsequent analysis by mass spectrometry revealed that it was originated from the C-terminus of PR1b, and was termed CAP-derived peptide 1 (CAPE1). Interestingly, plants sprayed with CAPE1 showed more resistance to the bacterial phytopathogen *Pseudomonas syringae* and the fungal pathogen *Fusarium oxysporum f. sp. lycopersici* (Fol) (Chen *et al.*, 2014; Li *et al.*, 2022). In addition, gene expression studies of treated CAPE1 leaves showed that multiple defense genes, including protease inhibitor and pathogenesis-related proteins, like PR7 and PR1b itself, were induced by adding exogenous CAPE1 peptide. Noticeably, the CAPE1 peptide did not upregulate the expression of WRKY TRANSCRIPTION FACTOR53 (WRKY53), which is highly upregulated by the application of the pathogen-associated molecular pattern (PAMP) peptide flg22 (Chen *et al.*, 2014). These data suggested that CAPE1 may activate a damage-associated molecular pattern (DAMP) signaling pathway to induce plant defense response genes and immunity.

In addition, the CAPE peptide PxGNxxxxxPY motif is highly conserved in monocots and dicots. The Arabidopsis CAPE was experimentally proven to enhance plant immunity in treated tomato leaves (Chen *et al.*, 2014). The CAPE peptide derived from mulberry PR1 also plays a role in activating plant resistance against bacterial and fungal pathogens (Fang *et al.*, 2019). Similarly, the CAPE peptide of wheat PR1 suppressed the multiplication of *Parastagonospora nodorum* (Sung *et al.*, 2021). Besides the CAPE sequence, the conserved CNYx motif upstream of the CAPE peptide, was proposed as a putative cleavage motif to generate the CAPE1 peptide.

Processing of PR1 in wheat is likely performed by an unknown serine protease, since treatment of the apoplastic fluid with a serine protease inhibitor repressed the accumulation of CAPE peptide (Sung *et al.*, 2021). However, in *Arabidopsis* this process involves a caspase-like enzyme, Xylem cysteine peptidase 1 (XCP1) (Chen *et al.*, 2023).

II.1.4 Translocation of PR1

Most PR1 proteins are thought to be secreted into the apoplastic space, via their N-terminal signal peptide, and accumulate adjacent to the area of lesion (Carr *et al.*, 1987; Lincoln *et al.*, 2018). Transiently expressed *Arabidopsis* PR1 co-localized with the late endosome (LE)/multivesicular body (MVB) FYVE marker, but both the C-truncated version PR1 Δ C and cleavage motif-mutated version PR1YDPR/AAAA predominantly localized to the endoplasmic reticulum (ER) (Pecenкова *et al.*, 2022; Pecenкова *et al.*, 2017). Thus, the cleavage motif also plays an important role in translocation of PR1. Secreted PR1 was shown to translocate through an unknown mechanism into *Phytophthora infestans* cells to target AMPK kinase complex, repressing growth, proliferation and virulence (Luo *et al.*, 2023). Interestingly, the fungal pathogen *Fusarium oxysporum f. sp. lycopersici* (Fol) can secrete a pathogen effector, Fol-Secreted Virulence-related Protein1 (FolSvp1), which directly binds PR1, translocating from the extracellular and plasma membrane to the host nucleus (Li *et al.*, 2022).

II.2 Results

II.2.1 Identification of PR1s proteins of tomato

At the start of this work, a total of four PR1 genes had been identified in tomato, which were named PR1a, b, c and d. These tomato CAP proteins had been studied simultaneously by two independent laboratories that followed different nomenclature systems, causing considerable confusion in the literature (Eyal *et al.*, 1992; Niderman *et al.*, 1995; Tornero *et al.*, 1994). In addition, their work was performed before the sequenced tomato genome was publicly available (Tomato Genome, 2012). We thus decided to identify all tomato PR1 genes and name them consistently. A BLASTn on the Sol Genomics Network and the NCBI databases using the coding sequence (CDS) of PR1b (Solyc00g174340) as the main PR1 gene, retrieved ten highly similar genes (>82% sequence identity), five of which corresponded to the previously reported PR1 proteins. A neighbor-joining tree of the encoded amino acid sequences, including the closest non-PR1 in tomato (Solyc02g065470.1.1) as an outgroup, revealed that the PR1a, b and d occupy a distal position at one end of the genomic cluster (Fig.1B).

We then set to analyze the protein sequence of the distinct PR1s to check the conservation of important domains and residues of the catalytic site. We retrieved and aligned the protein sequences of all annotated PR1s using ClustalO. Most PR1s were featured the predicted N-terminal signal peptide, a CAP domain and the CAPE peptide. In the mature proteins, PR1 lost the N-terminal signal peptide. As previously described, the CAP domain was involved in degradation of sterol, which is a main component of fungal cell wall, contributing to defense against fungi in tomato plants (Gamir *et al.*, 2017). The putative catalytic cysteine was conserved in all PR1s. At the C-termini of PR1s, there is a CAPE peptide, containing 11 amino acids, accumulated in wounding and methyl jasmonate treated tomato leaves (Chen *et al.*, 2014)(Fig. 1A). The predicted cleavage site before the CAPE peptide was conserved in all PR1s, though the CAPE peptide sequence is not identical. Further, PR1c shows additional amino acids after CAPE peptide (Fig. 3A).

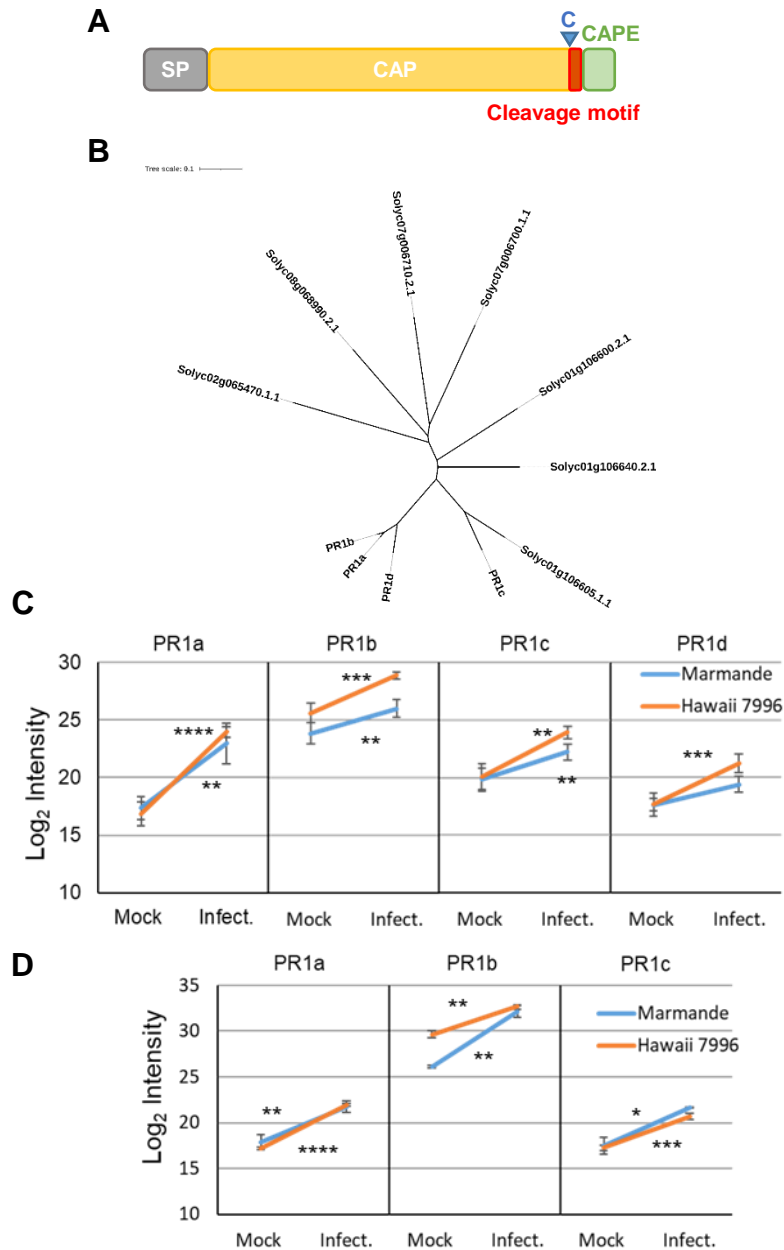


Fig.1 Protein features and abundance of the tomato PR1 proteins. (A) Representation of the tomato PR1 protein domains and conserved features. The position of catalytic site (C, blue triangle) and the putative cleavage motif (red region) are indicated. SP, signal peptide; CAP, Cysteine-rich secretory proteins, Antigen 5, and Pathogenesis-related 1 proteins domain; CAPE, CAP-derived peptide. (B) Neighbor-joining protein similarity tree of tomato PR1 proteins generated from a ClustalO alignment. The most highly related non-PR1 Solyc02g065470.1.1 was added as outgroup. Scale bar indicates 0.1 amino acid changes per site. Log₂ abundance intensity of PR1s of Marmande and Hawaii 7996 upon mock treatment and *R. solanacearum* infection in the xylem (C) and apoplast (D). Error bars indicate standard error of three biological replicates. Asterisks indicate activity or abundance significant differences on infection by *t*-test ($\alpha=0.05$).

To compare the abundance of PR1 proteins in the tomato apoplast and xylem in response to *R. solanacearum*, we analyzed previously obtained proteome data (Planas-Marques *et al.*, 2018). We found that the high abundance of four PR1s increased in response to the pathogen in the xylem of resistant variety Hawaii 7996 and susceptible plants, while three PR1s highly accumulated in the apoplast of both resistant and susceptible plants Marmande. Notably, in the xylem, the PR1s proteins are more abundance in Hawaii 7996 than in Marmande. (Fig. 1C and 1D)

II.2.2 Conservation of the PR1s in the Solanaceae family

Subsequently, we investigated how conserved PR1 family proteins are in other plant species. We chose another three Solanaceae family plants, pepper, potato and tobacco, and another two species, Arabidopsis and wheat, where PR1s have already been studied.

First, proteins sharing more than 40% sequence identity to PR1b were identified by BLASTp searches in the Sol Genomics genome databases (pepper, potato and tobacco) and Arabidopsis (TAIR 10) (Table M1, Methods section). Then, in order to identify the putative PR1 members in each plant genome, we constructed an independent neighbor-joining tree for each specie (Fig. 2). PR1s containing a C-terminal extension are highlighted in grey, and occupy a distal position in the tree.

To compare the C-terminal sequence of PR1s from different species, we aligned representative PR1s from different species and constructed a neighbor-joining phylogenetic tree (Fig.3). The cleavage site (CNYD) is highly conserved in Solanaceae and Arabidopsis, while the cleavage motif of wheat is variable, only cysteine and tyrosine are conserved (Fig.3A), indicating that the mechanism of cleavage of the CAPE peptide in Solanaceae plant could be the same as in Arabidopsis, rather than wheat. The neighbor-joining tree showed that in Solanaceae, PR1 with and without C-terminal extension clustered in different branches shown as blue and orange region, respectively (Fig. 3B).

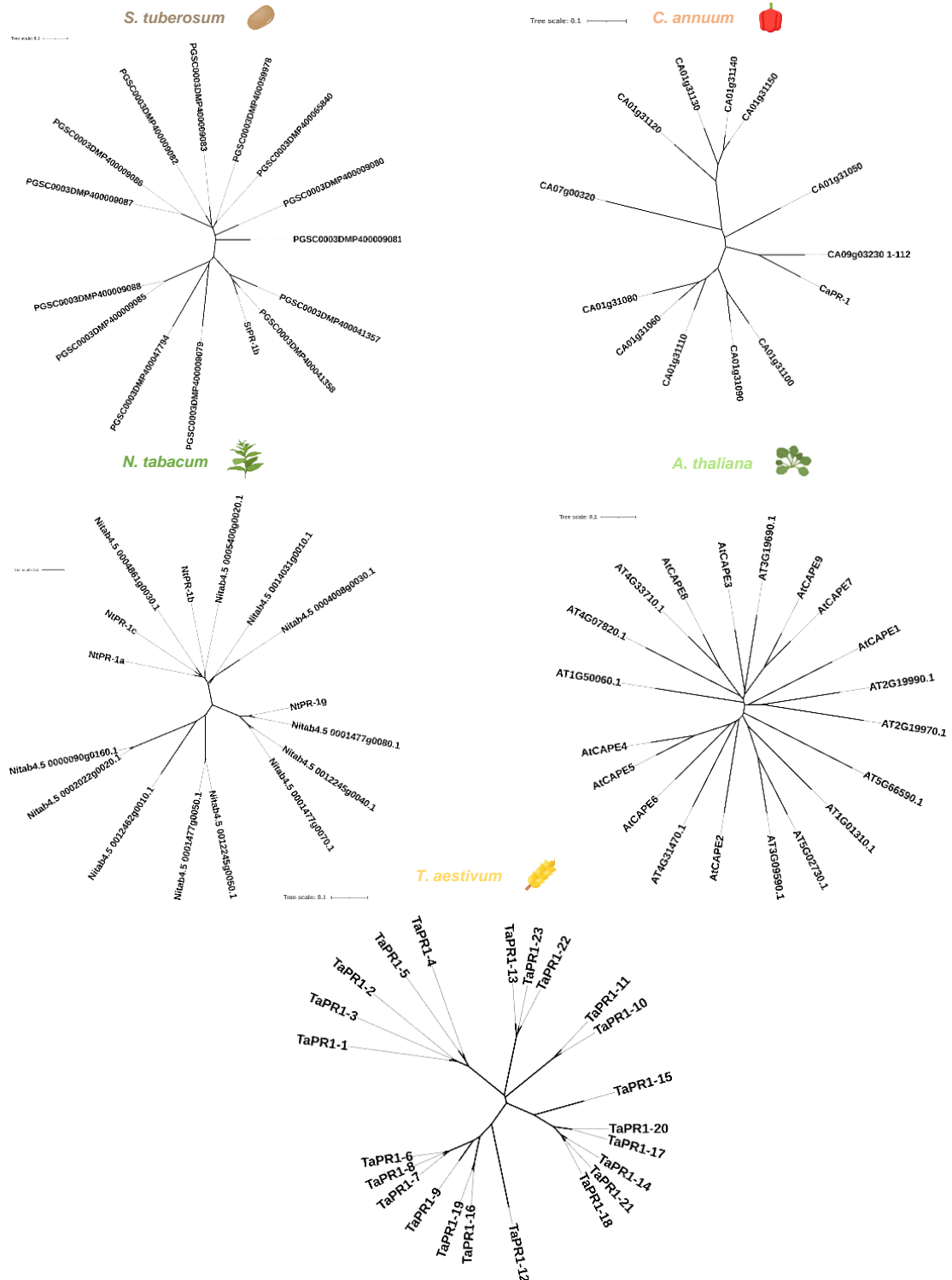


Fig. 2 Phylogenetic analysis of the conserved PR1 clade across different plant species. Neighbor-joining phylogenetic trees generated from a ClustalO alignment of the most similar proteins to tomato PR1b (>40% sequence identity). Scale bar indicates 0.1 amino acid changes per site.

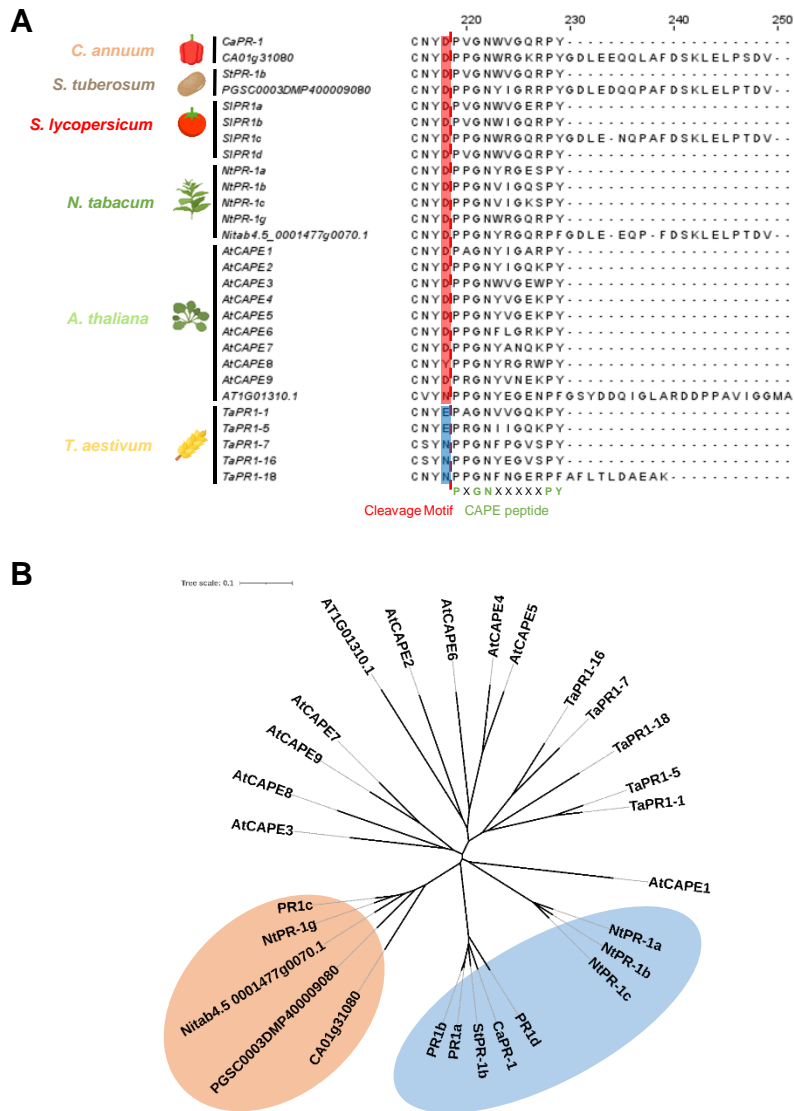


Fig.3 Alignment of the representative PR1s across different plant species. Alignment of amino acids (A) and Neighbor joining phylogenetic tree (B) are generated from a ClustalO alignment of the representative PR1 proteins from tomato (*S. lycopersicum*), potato (*S. tuberosum*, 'St'), pepper (*Capsicum annuum*, 'CA'), tobacco (*N. tabacum*, 'Nitab'), Arabidopsis (*A. thaliana*, 'At') and wheat (*Triticum aestivum*, 'Ta'). For simplicity, 'PGSC0003DMP4000' was omitted from the potato protein identifiers. In panel (A), the red dashed line indicates the putative CAPE peptide cleavage site, red and blue (wheat) regions show the last amino acid before the CAPE peptide. The conserved CAPE peptide sequence was also shown at the bottom in green. In panel (B), the blue and orange region indicate the extended amino acid sequence of PR1b and PR1b after the CAPE peptide, respectively. Scale bar indicates 0.1 amino acid changes per site.

II.2.3 Subcellular localization of PR1 in *N.Benthamiana* leaves

To uncover the cellular localization of plant PR1s and discover the location where the

CAPE peptide is cleaved, we cloned four *PR1s* with the wild type sequence or a mutation at the predicted cleavage site and fused the coding sequences with *GFP*. After transient expression in *N. benthamiana* and fluorescence microscopy analysis, we observed that PR1b-GFP showed a pattern compatible with its localization at the multivesicular body (MVB), while the PR1b^{CNAD}-GFP localized to the endoplasmic reticulum (ER) (Fig. 4A), which corresponded with previous studies performed in *Arabidopsis* (Pecenkova *et al.*, 2022). To confirm the ER location and the MVB location, we also co-infiltrated PR1b with ER marker ER-rk CD3-959 and MVB marker ARA6, respectively. We observed that the ER marker colocalized with PR1b^{CNAD}-GFP (Fig. 4B). However, we did not detect the signal for the MVB marker. In the future, we will change another MVB marker to check localization of wild type of PR1s. Subsequently, we checked the subcellular localization of PR1c-GFP and PR1b^{CNAD}-GFP, which has long extension after CAPE peptide, with the ER marker. Interestingly, both wild type version PR1c-GFP and its mutant version PR1c^{CNAD}-GFP localized in the MVB (Fig. 4B). These results indicate that PR1b seems to be secreted to the apoplast through the ER/Golgi/MVB secretory pathway, and its cleavage site plays a key role on translocation of PR1b from ER to MVB.

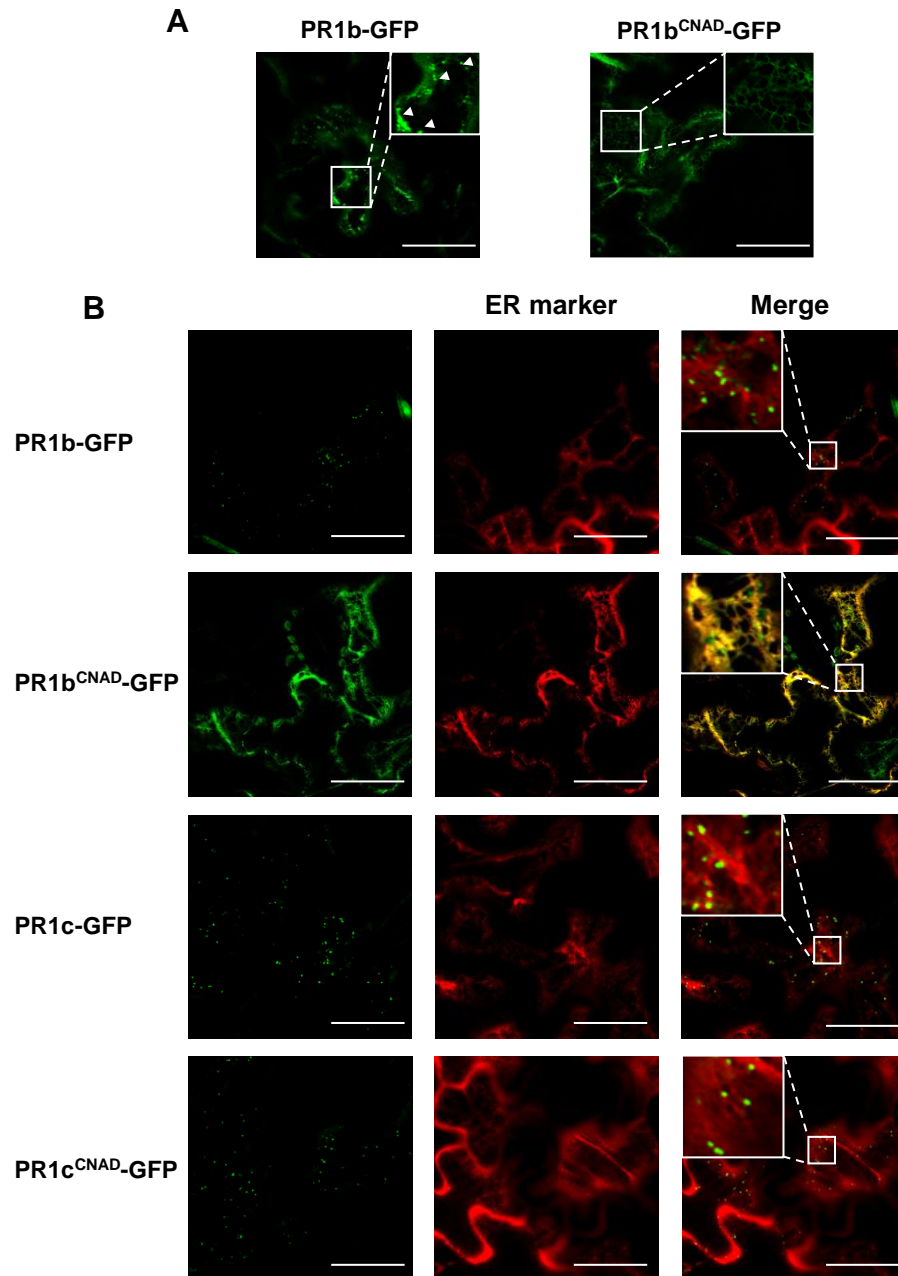


Fig.4 Subcellular localization of PR1s and PR1s^{CNAD} mutant. (A) PR1b and PR1b^{CNAD} fused to GFP transiently expressed in *Nicotiana benthamiana*. Arrows point to multivesicular body (MVB). (B) Co-localization of PR1b and PR1c-GFP and their mutant versions with the marker of endoplasmic-reticulum (ER). Scale bar: 20 μ m. Insets depict a magnified view of the signal in the solid squares.

II.2.4 Characterization of the role of the CAPE peptide in response to *R. solanacearum*

To understand the function of CAPE peptide, we chemically synthesized it and checked its antimicrobial activity *in vitro*. We added increasing concentrations of CAPE peptide in rich medium and measured growth of *R. solanacearum* over time. The

results showed CAPE peptide did not affect the growth of *R. solanacearum* (Fig. 5A).

We subsequently tested the antimicrobial activity of CAPE peptide *in planta*. CAPE peptide (500 nM) and water, as a control, were sprayed on the surface of leaves from 4 weeks-old susceptible tomato plants (Marmande). Three hours later, *R. solanacearum* was infiltrated into the tomato leaves at a concentration of 10^5 CFU/mL using vacuum. Multiplication of *R. solanacearum* was significantly decreased in CAPE pre-sprayed leaves after 3 days, compared with leaves sprayed with water (Fig. 5B).

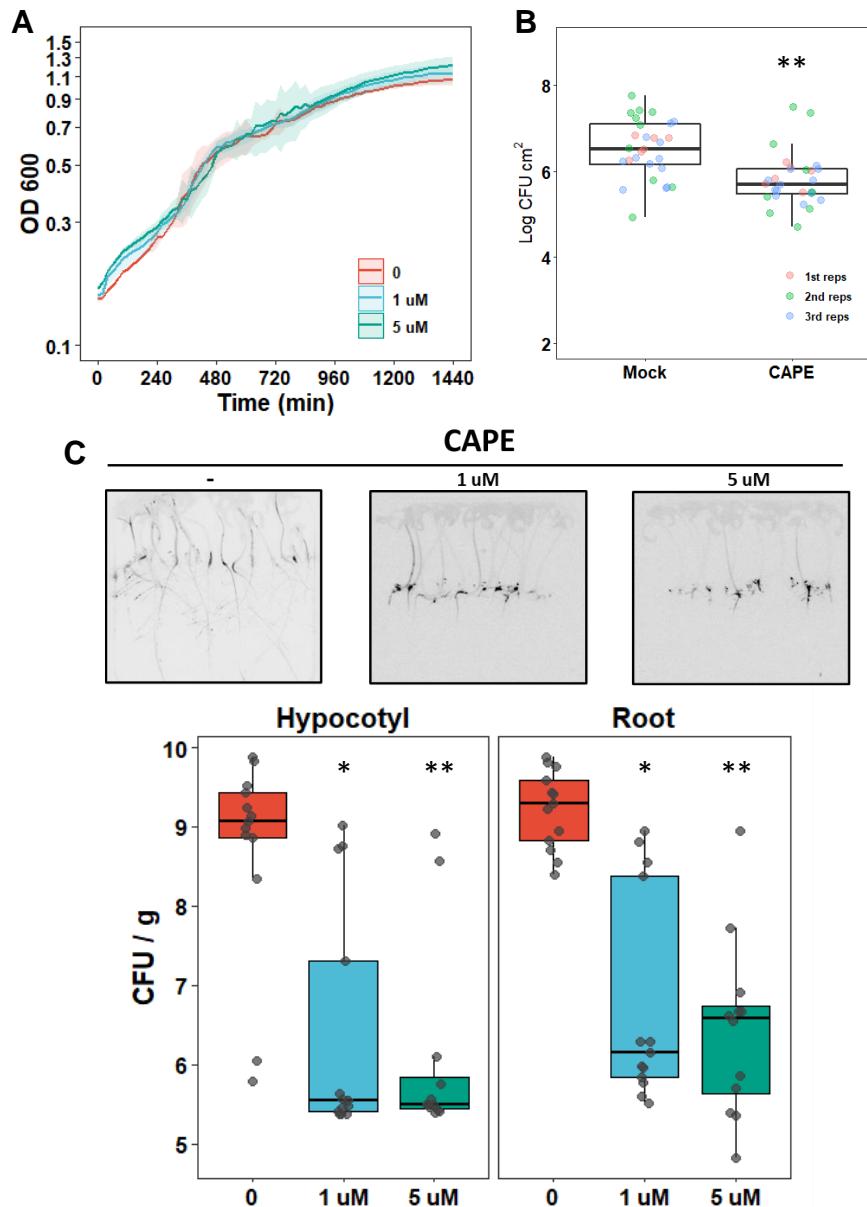


Fig.5 Antimicrobial function of CAPE peptide. (A) Growth of *R. solanacearum* in rich medium adding different concentration of CAPE peptide. The light area means standard deviation. (B) The aerial part of four-week-old tomato plants was vacuum-infiltrated with a 10^5 CFU/mL suspension of *R. solanacearum* before spraying 500 mM CAPE peptide 3 hours and bacterial loads were evaluated after 3 days infection. Three biological replicates were

performed; asterisks indicate significant differences with and without CAPE peptide using t test. (C) Seedlings of Marmande grew in the MS plates containing different concentrations of CAPE peptide and 10 days later they were pin-inoculated in the taproot with the luminescent *R. solanacearum* strain. A representative photograph is shown for each treatment at 7 dpi. Bacterial loads in the hypocotyl and root of the plants were calculated based on the luminescence signal and are expressed as log CFU/g tissue.

Considering that *R. solanacearum* is a soil-borne pathogen, we also analyzed whether the CAPE peptide could affect *R. solanacearum* from root colonization. MS plates supplemented or not with CAPE peptide were used to grow plants. Ten days after germination, *R. solanacearum* was inoculated at 10^6 CFU/mL at the intersection between the hypocotyl and the taproot with a pasteur pipette (aprox 10^4 inoculated cells). For this, the luminescent *R. solanacearum* was used so that it could be visualized by chemiluminescence. At 7 dpi, *R. solanacearum* spread from the infection site to the bottom part of the root and upper part of the hypocotyl of seedlings grown in MS plate without CAPE peptide. In comparison, plates supplemented with 1 μ M CAPE peptide, showed less *R. solanacearum* on hypocotyls and roots of seedlings. When seedlings were grown in the MS plate with 5 μ M of CAPE peptide, the bacterium remains confined at infection sites, unable to spread in the plant tissues (Fig. 5C). These data suggest that the CAPE peptide could reduce proliferation of *R. solanacearum* in tomato seedlings root and hypocotyl. Together, these results show that the CAPE peptide can only affect multiplication of *R. solanacearum in planta*, but not in the medium, suggesting an antimicrobial function through triggering plant immunity.

II.2.5 Purification of recombinant PR1 proteins in *E. coli*

In order to characterize the role of PR1b protein in the tomato-*R. solanacearum* interaction, we decided to purify recombinant PR1 proteins in *E. coli*. First, we tried the expression vector pBAD to express PR1b proteins, which is induced by L-arabinose. We generated PR1b constructs without signal peptide of N-terminus. Three versions of PR1b were generated: PR1b^{fl} (the full length), PR1b^{wo} (without the CAPE peptide) and PR1b^{KK} (mutation at the putative cleavage site, CNYD to CNKK). Most purified proteins accumulated in the insoluble fraction after sonication. We could only detect a small portion soluble PR1s after purification by His-trap and size exclusive chromatography (SEC) (Fig. 6A). Considering that the planned experiments required a large amount of protein, we decided to change to another protein expression vector.

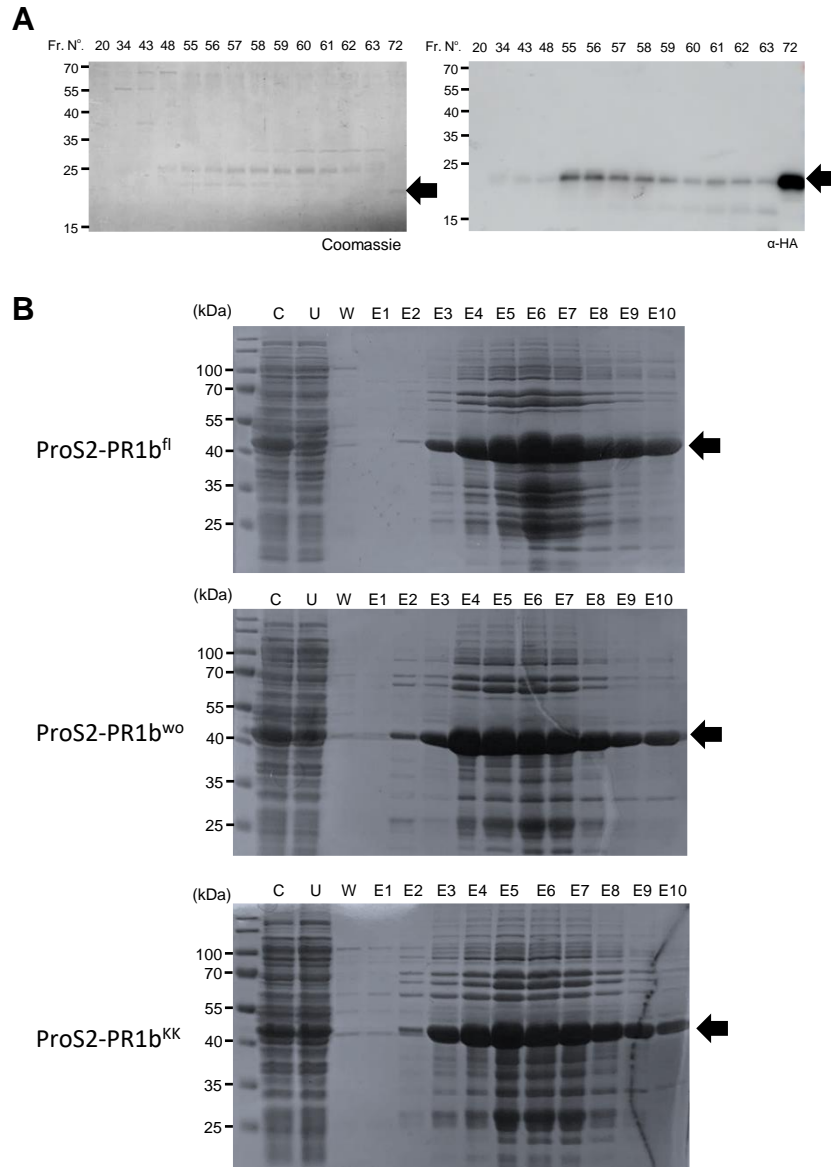


Fig.6 Purification of recombinant PR1b and derivatives enzymes. (A) Size exclusive chromatography of PR1b were collected by pBAD system and induced by L-arabinose. The size exclusive chromatography fractions were loaded on SDS-PAGE and stained using Coomassie Brilliant Blue (left panel) or western-blot with anti-HA (right panel). (B) PR1b proteins were collected by pCold vectors in *E. coli* induced by IPTG and subjected to metal chelate affinity chromatography. Fractions of each purification step were loaded on SDS-PAGE and stained using Coomassie Brilliant Blue (CBB). C: Crude; U: Unbound; W: Wash, E: Elution fraction. Arrows indicate target proteins.

The pCold vector contains the ProS2 domain at the N-terminus, which can increase the solubility of target proteins. The pCold plasmids containing the PR1 fused with HA tag were transformed into Rosetta *E. coli* strain to recombinantly produce the proteins. Through optimized parameters of expression condition, we finally observed abundant

target proteins in the soluble fraction after cell lysis. Subsequently, 500 mL culture of *E. coli* expressing the PR1b^{fl}, PR1b^{wo} and PR1b^{KK} versions were lysed and purified using His-trap, generating clean and abundant target proteins at elution fraction 9 and 10 (Fig. 6B).

II.2.6 Processing of PR1b with candidate protease P69s

In wheat, PR1 proteins have been shown to be cleaved by serine proteases to release CAPE peptide, while in Arabidopsis CAPE can be released from PR1 by a cysteine protease (Chen *et al.*, 2023; Sung *et al.*, 2021). As our N-terminomics studies with pointed PR1 as a possible target (see chapter I), we checked if two candidate serine proteases of the P69 family, P69B and P69D, could cleave PR1 proteins.

First, we tested PR1c transiently expressed in *N. benthamiana* incubated with purified P69B and P69D proteins. We chose PR1c because it has extension after CAPE peptide that allows detecting cleavage by immunodetection of free GFP versus GFP with CAPE. *Agrobacterium tumefaciens* expressing PR1c and PR1c mutated at cleavage motif (CNAD), both C-terminally fused with GFP, were injected into *N. benthamiana* leaves and 2 days later we extracted total proteins leaf extract. These extracts were incubated with purified P69B and P69D for 30 to 60 minutes. Counterintuitively, the PR1c mutant version was cleaved by P69D and P69B, but not the wild type version (Fig. 7A). Similarly, when other transiently expressing PR1s in *N. benthamiana* leaf were incubated with the purified P69D protein, only PR1s mutant versions were cleaved by P69D, not wild type versions (Fig. 7B).

In order to avoid possible interference by other proteases or by endogenous protein inhibitors in *N. benthamiana* leaves, we then incubated purified ProS2-PR1b^{fl} from *E. coli* with purified P69s. Since the CNAD mutant could be cleaved by P69s, we generated an additional cleavage site mutant: CNYD to CNKK. We tested either incubation of 1 µg of PR1b protein with increasing concentrations of P69D protein or incubation of 1 µg of each protein and analyzed them over time. Western blot with HA, 6xHis and PR1 antibody and Coomassie stainings showed that PR1 without ProS2 accumulated over time when incubated with P69D, and also accumulated with increasing concentration of P69D (Fig. 7C). This may indicate that P69D cleaves the fusion PR1-ProS2 protein at ProS2, and not at PR1. All these results show that the P69s serine proteases are unable to cleave PR1s to release the CAPE peptide in tomato plants.

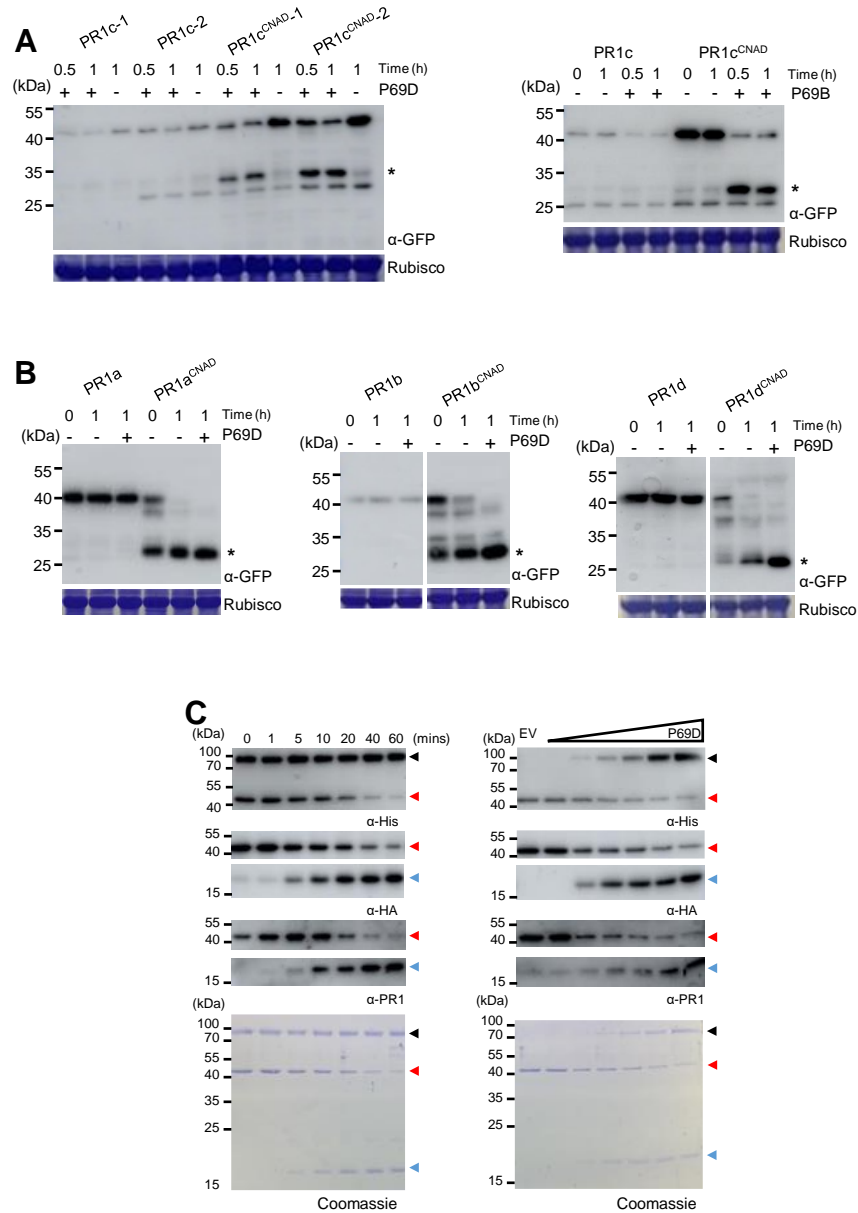


Fig. 7 Processing of PR1b with candidate protease P69s. (A) Incubated extract of *N. benthamiana* leaves transiently expressing *PR1c* or *PR1c^{CNAD}* fused to GFP with P69D and P69B, respectively, over time. (B) *N. benthamiana* leaves transiently expressing other PR1s or *PR1s^{CNAD}* fused to GFP incubated with purified P69D over time. Bottom loading panels correspond to SDS-PAGE of the same samples stained with Coomassie brilliant blue. (C) Incubation of purified PR1b with purified P69D. In the left panel, 1 µg of each protein was added and analyzed over time. In the right panel, 1 µg of PR1b protein was incubated for 1 hour with increasing concentration of P69D. Different colors of arrows indicate different proteins. (Black: P69D; Red: ProS2-PR1b; Blue: cleaved PR1b).

II.2.7 Effect of recombinant PR1 proteins on *R. solanacearum* growth

To test the antimicrobial function of PR1b, *R. solanacearum* was grown in rich medium with different versions of purified PR1b proteins, ProS2-PR1b^{fl}, PR1b^{wo} and PR1b^{KK},

respectively and OD₆₀₀ was measured every 20 minutes. None of the PR1 variants tested affected the growth of *R. solanacearum* (Fig. 8), indicating that PR1b cannot inhibit growth of *R. solanacearum* directly.

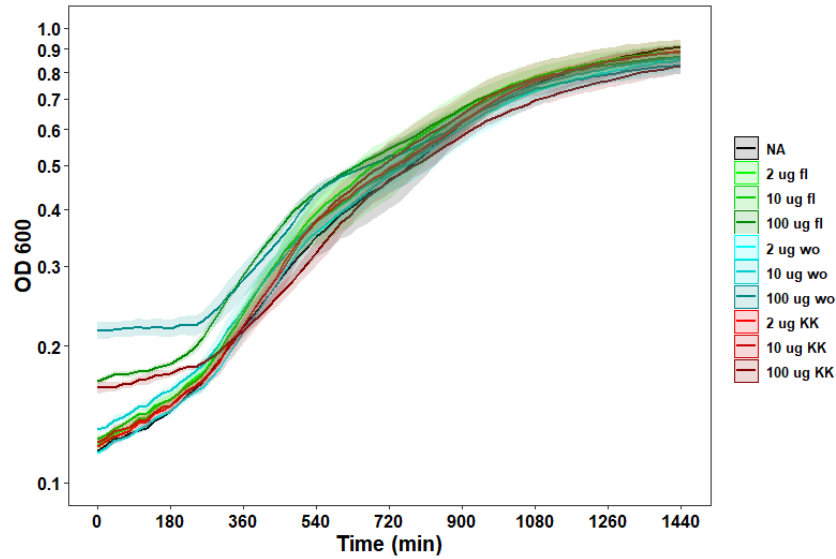


Fig. 8 Effect of purified PR1 variants on *R. solanacearum* growth. PR1b^{fl}: PR1b full length, green. PR1b^{wo}: PR1b without CAPE peptide, blue. PR1b^{KK}: PR1b CNKK, red. The light area means standard error.

II.2.8 Generation of PR1b mutant and overexpression lines in tomato

To study the role of PR1b in the interaction between tomato-*R. solanacearum*, we generated PR1b-defective mutant tomato plants. We designed small guide RNAs (sgRNAs, SG) to target the *PR1b* gene and induce intragenic deletions. Considering the similarity between different *PR1* genes (especially *PR1a* with *PR1b*), we used the most specific guide RNAs (instead of higher scores on the CRISPOR web tool). On the other hand, one guide-RNA targeted a region near the DNA sequence encoding for the cleavage site of CAPE, to make sure CAPE peptide was mutated. We chose both the resistant tomato line H7996 and susceptible tomato cultivar Marmande as the background genotypes, expecting them to become more susceptible when *PR1b* are deleted.

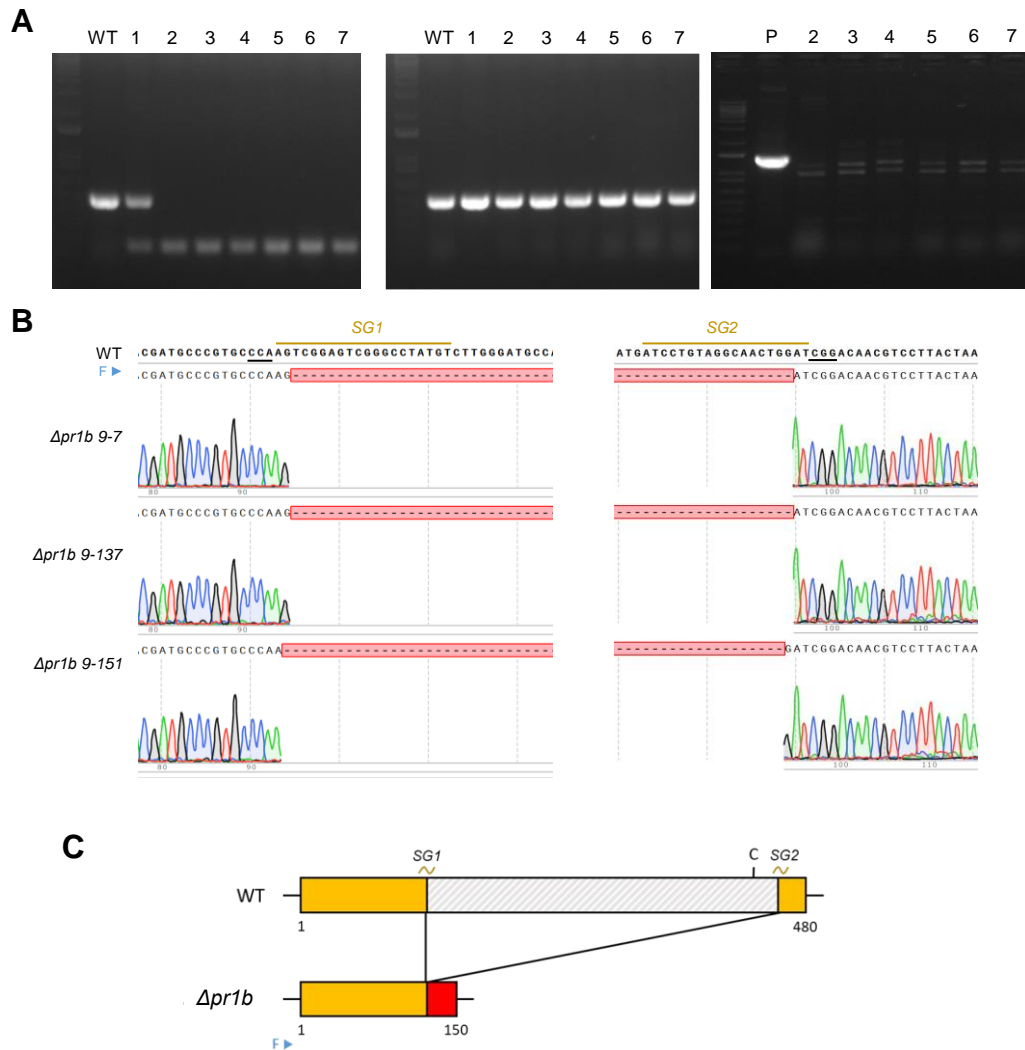


Fig. 9 Generation of *pr1b* CRISPR/Cas9 deletion mutants in Marmande. (A) Electropherograms of results of PCR amplification of the *PR1b* CRISPR/Cas9 deletion mutants with *PR1b* primers, *PR1a* primers and *Cas9* primers, respectively. WT line: wild type, 1: known heterozygous *pr1b* mutant, 2-3: ΔPR1b 9-7, 4-5: ΔPR1b 9-137, 6-7: ΔPR1b 9-151. P: positive control of *Cas9*. (B) Sequence results of *pr1b* mutant corresponding panel A. Arrowheads indicate genotyping forward primers. Protospacer-adjacent motif (PAM) sequence is underlined. Arrows and dashed lines indicate the putative double-strand break site used by *Cas9*. (C) Schematic representation showing the 112 bp deletion obtained by CRISPR/Cas9 in the *PR1b* gene. The mutation results in a late stop codon, which is then translated into a truncated protein variant. C indicates the cysteine residues from the putative active site.

Once all the CRISPR/Cas9 constructs were constructed and verified by sequencing, we generated stable tomato mutant lines by *Agrobacterium* transformation of leaf explants. We were only able to obtain transformed calli from susceptible tomato plants Marmande, but none from Hawaii plants. Successfully regenerated explants were

screened for deletions. We detected shift deletions and Cas9 in the *PR1b* gene in 2 out of 63 plants analyzed. *Cas9* was segregated out from the genome in subsequent generations. Presence of deletions and *Cas9* absence were later confirmed by DNA sequencing (Fig. 9A, 9B). We finally obtained three lines that carried a 112 bp deletion in homozygosity without *Cas9*, named as $\Delta pr1b$ 9-7, $\Delta pr1b$ 9-137, $\Delta pr1b$ 9-151. This out-of-frame deletion generated a late stop codon and, in turn, a truncated protein lacking the CAPE peptide (Fig. 9C).

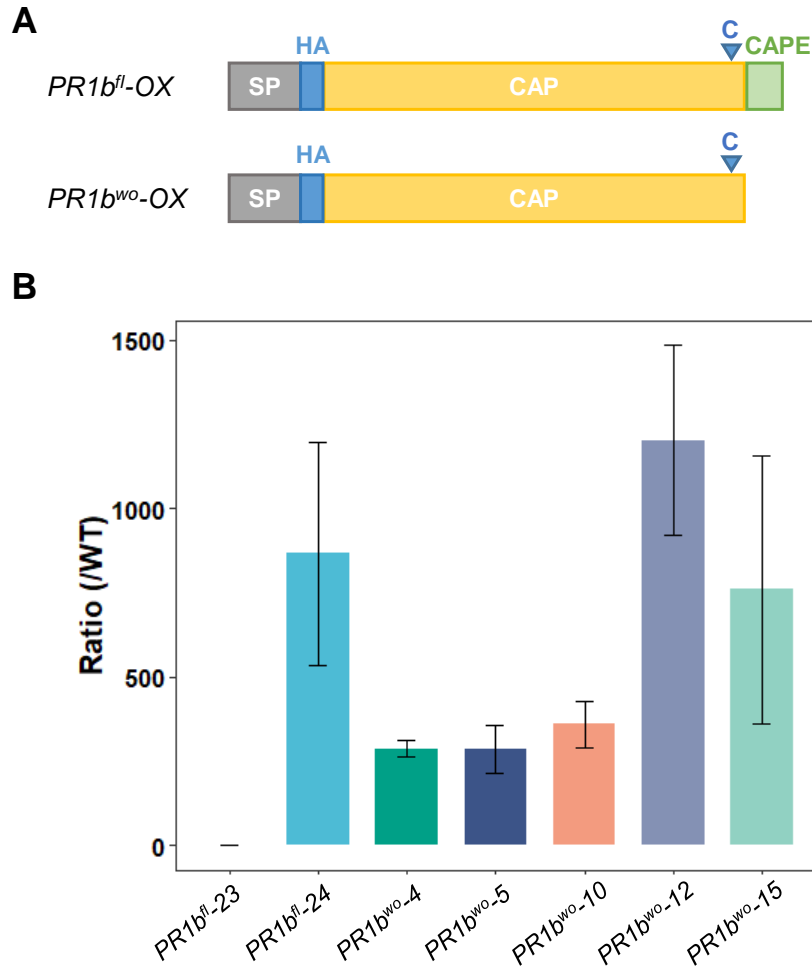


Fig.10 Generation of *PR1b^{fl}* and *PR1b^{wo}* overexpression lines in Marmande. (A) Schematic representation of PR1 versions used in the overexpression lines. SP, signal peptide; CAP, Cysteine-rich secretory proteins, Antigen 5, and Pathogenesis-related 1 proteins domain; CAPE, CAP-derived peptide. (B) *PR1b* gene expression levels comparing overexpression lines with wild type by qRT-PCR. The *Actin* gene (*SlAct2*) was used as endogenous reference. Three biological replicates were performed.

For overexpression lines of *PR1b*, considering *PR1b* has two signal peptides that could be cleaved at both the N- and C-terminal sites, we decided to create an HA-tag after

the N-terminal signal peptide. On the other hand, PR1b without CAPE peptide also was created (Fig. 10A). We chose susceptible tomato cultivar Marmande as the background genotype, expecting *PR1b* overexpression lines to become more resistant when the *PR1b* gene is expressed massively. We generated stable mutant lines by *Agrobacterium* transformation of leaf explants and obtained one *PR1b^{fl}* (full length) overexpression line and four *PR1b^{wo}* (devoid of the CAPE peptide) overexpression lines, verified by qRT-PCR (Fig. 10B). After segregation, we kept two of four *PR1b^{wo}* overexpression lines and only one *PR1b^{fl}* overexpression line to obtain homozygous lines in the future.

II.2.9 Investigation of the role of PR1s in plant defense

In order to investigate the role of PR1b in plant defense, we analyzed the responses to *R. solanacearum* of the *pr1b* mutant lines compared to wild type. First, we used soil drenching to mimic natural *R. solanacearum* colonization. Surprisingly, two independent experiments showed that tomato *pr1* mutant lines $\Delta pr1b$ 9-7 and $\Delta pr1b$ 9-151 were slightly more resistant than wild type Marmande, while a third line, $\Delta pr1b$ 9-137, always showed wild type-like symptoms (Fig. 11A). If PR1b played an essential role in the apoplast, we would expect that *pr1b* deletion in the susceptible Marmande cultivar resulted in enhanced colonization due to defective defense mechanisms. To test this hypothesis, we vacuum-infiltrated the aerial part of four-week-old plants and evaluated the growth of *R. solanacearum* over time. On two independent experiments, there is no significant difference of multiplication of *R. solanacearum* between wild type and all the three *pr1* mutant lines (Fig. 11B). In conclusion, mutation of *pr1b* in a susceptible Marmande background did not enhance susceptibility.

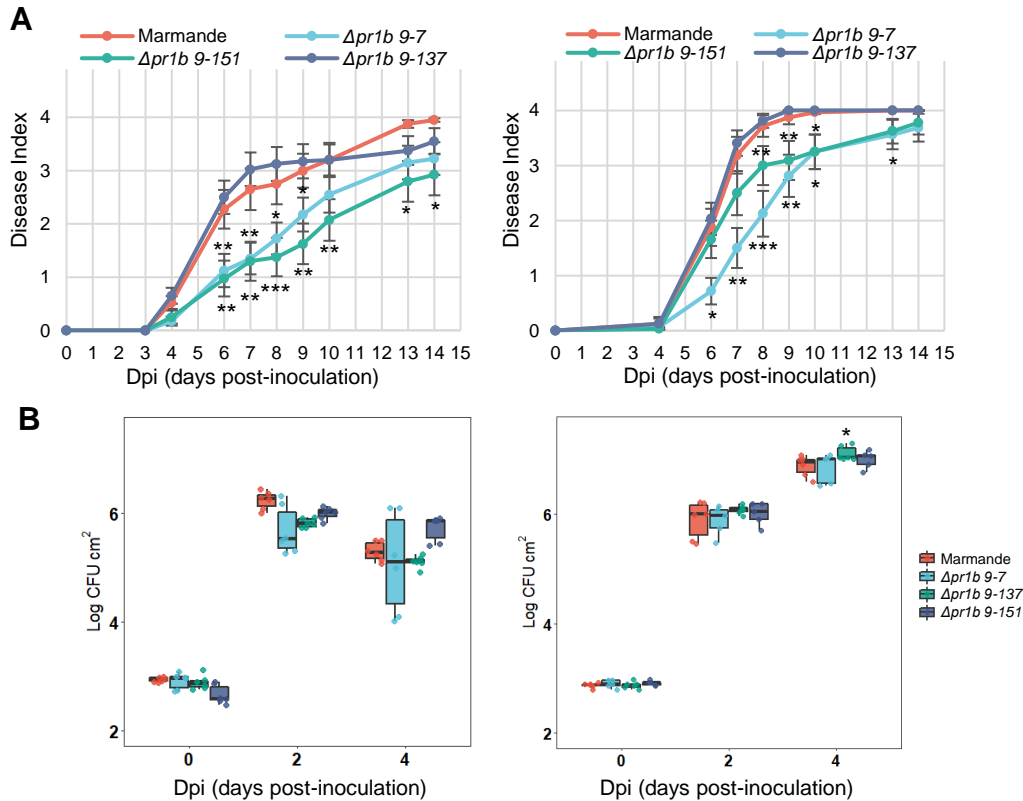


Fig. 11 Pathogenicity assays of the *pr1b* mutant. (A) Tomato plants were soil-drenched with a 10^7 CFU/mL *R. solanacearum* suspension at the age of 4-weeks-old. Wilting symptoms were scored over time for two weeks. At least 20 plants of each variety and line were inoculated. Asterisks indicate statistically significant differences between wild type and each of the *pr1b* mutant lines analyzed using a paired Student's t-test (* $p < 0.05$, ** $P < 0.01$ and *** $P < 0.001$). (B) The aerial part of four-week-old tomato plants was vacuum-infiltrated with a 10^5 CFU/mL suspension of *R. solanacearum*, and bacterial loads were evaluated over time. Six biological replicates were assayed per day and plant genotype. Each dot corresponds to a biological replica from an independent leaf. Significant differences to wild type were shown as, * $p < 0.05$ (Student's t-test).

II.2.10 Analysis of the role of tomato PR1b in defense priming

It has been previously shown that the CAPE peptide derived from PR1b can prime plant defense (Chen *et al.*, 2014). Thus, we analyzed by qRT-PCR expression of genes in the leaves used as markers for defense priming after CAPE peptide exposure over time, such as jasmonic acid-responsive genes Proteinase Inhibitors I and II (*PI-I* and *PI-II*), salicylic acid-responsive genes Pathogenesis Related protein 1b, 2 and 5x (*PR1b*, *PR2* and *PR5x*), abscisic acid-responsive genes Abscisic acid and environmental stress-inducible protein (*TAS14*) and Abscisic acid-Responsive

Element Binding Protein 1 (*AREB1*), and an ethylene-responsive gene Ethylene Response Factor 5 (*ERF5*). Six hours after spraying 500 nM CAPE, we observed a strong induction of JA-responsive genes, *PI-I* and *PI-II*. *TAS14*, *AREB1* and *ERF5* showed a slight induction 3 hours after spraying the CAPE peptide (Fig. 12A and 12D). Surprisingly, CAPE peptide induced expression of its own precursor gene *PR1b* dramatically, while suppressing SA-responsive genes, *PR2* and *PR5x* (Fig. 12B) at 3 hours. In order to understanding the reason behind the differential behavior of SA-responsive genes after CAPE treatment, we analyzed the expression of SA biosynthesis genes Isochorismate Synthase (*ICS*) and Phenylalanine Ammonia Lyase 5 (*PAL5*). The expression of *ICS* and *PAL5* was slightly inhibited 3 h after CAPE treatment similar to *PR2* and *PR5x* (Fig. 12C). In contrast, CAPE treatment did not affect the expression of ABA-responsive genes (*TAS14* and *AREB1*) or ethylene-responsive gene (*ERF5*) (Fig. 12D).

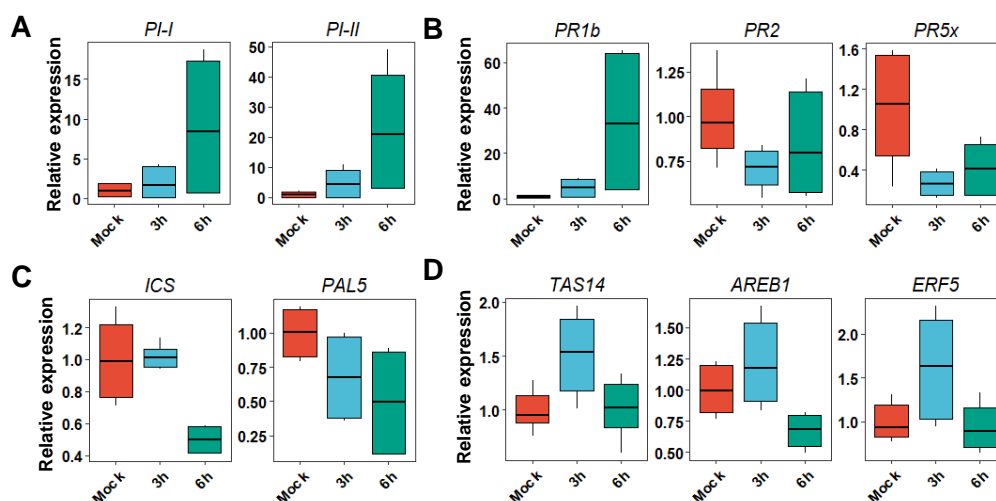


Fig. 12 Effect of CAPE treatment on the expression of plant defense genes involved in priming in tomato leaves. Expression of hormone-related genes involved in plant defense was analyzed by qPCR in leaves sprayed with water or 500 nM CAPE peptide. The *Actin* gene (*SlAct2*) was used as endogenous reference. One disk of a CAPE- or water-sprayed leaf was collected after 3 and 6 hours for RNA extraction and cDNA synthesis.

We also check the expression of these hormone-related priming marker genes in the *PR1b* mutant and overexpression lines. Since the *PR1b* overexpression lines were heterozygous, we used the selection plate to make sure the plants used were *PR1b*-overexpressors. The *pr1b* mutant showed inhibition of JA-responsive genes, while *PR1b^{fl}* overexpression line showed induction of those (Fig. 13A and B). For *PR1b* expression, as expectation, the *pr1b* deficient plants did not express *PR1b* (Fig. 13A), and *PR1b^{fl}* overexpression line showed high *PR1b* expression (Fig. 13B). Surprisingly,

PR1b^{wo} overexpression line showed lower *PR1b* levels compared with their previous generation (Fig. 13B and Fig. 10B), indicating that *PR1b* silencing could be taking place over generations. Interestingly, the SA-responsive genes *PR2* and *PR5x* and SA-synthesis gene *PAL5* were highly induced in the *PR1b* overexpression line, especially *PR1b^{fl}* line (Fig. 13B). However, no differences of expression were observed between wild type and *pr1b* mutants (Fig. 13A). *PR1b^{fl}* overexpression line did not affect the expression of ABA-responsive genes (*TAS14* and *AREB1*) and ethylene-responsive gene (*ERF5*), similar to what we previously observed after CAPE treatment (Fig. 13A and 13B).

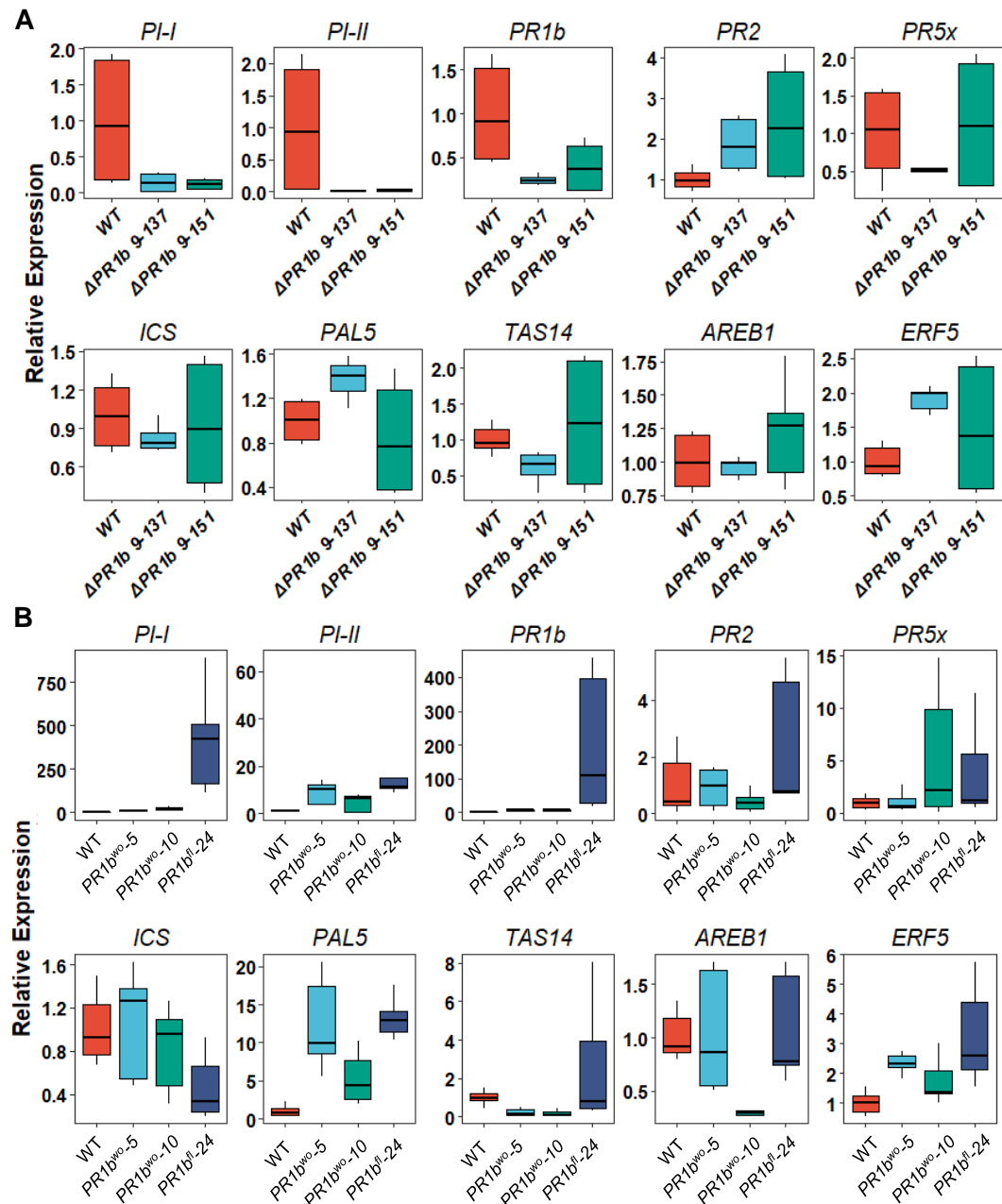


Fig. 13 The expression of plant defense genes involved in priming in tomato leaves from

***pr1b* mutant and *PR1b* overexpression lines.** Expression of hormone-related genes involved in plant defense was analyzed of *pr1b* mutant and *PR1b* overexpression lines by qPCR. The *Actin* gene (*SlAct2*) was used as endogenous reference. One leaf disk of wild type, *pr1b* mutant and *PR1b* overexpression lines was collected for RNA extraction and cDNA synthesis.

Together, these results show that PR1b or the application of CAPE peptide derived from PR1b enhance the expression of JA-responsive genes and SA-responsive genes, while they do not affect the expression of ABA-responsive genes and the ethylene-responsive gene.

II.3 Materials and methods

Phylogenetic analysis of PR1 proteins

BLASTn/p searches to identify new tomato PR1 genes and putative orthologs were performed on the Sol Genomics (SGN) database (<https://solgenomics.net/>), and in combination with the NCBI databases (<https://www.ncbi.nlm.nih.gov/>) and UniProt (<https://www.uniprot.org/>) when indicated. To identify the tomato PR1s, the SGN searches were performed using Tomato Genome proteins (ITAG release 4.0) database. The species' specific databases used to identify putative PR1 orthologues are indicated in Table M1, and the equivalence between gene and protein identifiers of tomato PR1s in the SGN, NCBI and UniprotKB databases is indicated in Table M2.

Table M1. Databases used for the construction of PR1-like phylogeny in different species.

Organism	Database	Ref.
<i>Solanum lycopersicum</i>	Tomato Genome proteins (ITAG release 4.0)	(Tomato Genome, 2012)
<i>Solanum tuberosum</i>	Potato PGSC DM v3.4 Protein sequences	(Potato Genome Sequencing <i>et al</i> , 2011)
<i>Capsicum annuum</i>	Pepper cv. CM334 Genome protein sequences (release 1.55)	(Kim <i>et al</i> , 2014)
<i>Nicotiana tabacum</i>	Tobacco Nitab v4.5 proteins Edwards 2017 (draft genome)	(Edwards <i>et al</i> , 2017)
<i>Arabidopsis thaliana</i>	Arabidopsis TAIR10 protein	https://www.arabidopsis.org/index.jsp
<i>Triticum aestivum</i>	NCBI: AEH25616.1	(Lu <i>et al</i> , 2011)

Neighbor-joining phylogenetic trees and amino acid sequence identity matrices were constructed from the respective ClustalO sequence alignments (<https://www.ebi.ac.uk/Tools/msa/clustalo/>). Phylogenetic analyzes were performed using highly similar proteins (>40% sequence identity for potato, pepper, Arabidopsis, tobacco and the wheat species), with an alignment score greater than 50% of the maximum score, which considers both identity and coverage. Phylogenetic trees were visualized by the Interactive Tree of Life (iTOL) webtool (<https://itol.embl.de>). Alignment analysis was performed by MEGA-X with the clustalO method, and visualized by Java Tree.

Table M2. Gene and protein identifiers for tomato PR1s.

Gene Accession (NCBI)	UniprotKB	SGN	PR1 name
NP_001234314	P04284	Solyc00g174340.1.1	PR1b
NP_001234523	Q04108	Solyc09g007010.1.1	PR1a
NP_001307969	O24026	Solyc09g007020.1.1	PR1d
NP_001234358	B2LW68	Solyc01g106620.2.1	PR1c
NP_001234128	K4B2M8	Solyc01g106605.1.1	
XP_004230669	K4B2N1	Solyc01g106640.2.1	
XP_004230668	K4B2M7	Solyc01g106600.2.1	P4-like
XP_004242676	K4CBE2	Solyc07g006710.2.1	PR1-like
XP_004242675	K4CBE1	Solyc07g006700.1.1	PR1-like
XP_004245428	A0A3Q7HSC4	Solyc08g068990.2.1	

Plant material and growth conditions

The tomato (*Solanum lycopersicum*) lines used were the highly resistant breeding line Hawaii 7996, the highly susceptible commercial variety Marmande. In addition, PR1b mutant lines generated by CRISPR/Cas9 and PR1b overexpression lines on the Marmande genetic background were used. The wild type *Nicotiana benthamiana* was used as transient expression. For pot experiments, plants were grown on soil (Substrate 2, Klasmann-Deilmann GmbH) (Planas-Marques *et al.*, 2020). Briefly, the soil was mixed with perlite and vermiculite (30:1:1) and the plants were grown in the greenhouse at around 26°C. For pathogenicity assays, plants were transferred to a chamber set at 27°C, 60% relative humidity and 12h day/night photoperiod 2 days prior to inoculation with *R. solanacearum*.

For *in vitro* experiments, tomato seeds were surface sterilized in 35% bleach and 0.02% Triton-X 100 () for 10 minutes and then rinsed with sterile distilled water five times before sowing them on semi-solid medium [Murashige and Skoog (MS) with agar] in square culture plates (Sudelab S.L.). Plates were placed standing upright in a walk-in tissue culture growth chamber set at 25 °C under long-day light conditions.

Cloning of the PR1 proteins

For transient expression in *N. benthamiana*, the open reading frames (ORFs) of PR1a, PR1b, PR1c and PR1d were amplified from the tomato H7996 line by PCR using the primer combination specified in Table M3. PCR products were cloned into pJET1.2/blunt (Thermo Scientific™) and amplified in *E. coli* TOP10. The identity of each PR1 construct was confirmed by sequencing (Macrogen). Inserts were then cloned in between the CaMV 35S promoter and terminator of pART7 (Gleave, 1992) using the restriction enzymes *SmaI* and *BamHI*, whose restriction sites were included in the forward and reverse primers, respectively (underlined in Table M3). The expression cassettes were then transferred to the binary vector pART 27 (Gleave,

1992) using *NotI*. The vectors were ultimately introduced into *Agrobacterium tumefaciens* strain C58C1 for transient expression in *N. benthamiana*.

For generation of overexpression *PR1b* lines, the open reading frames (ORFs) of *PR1b^{fl}* and *PR1b^{wo}* (*PR1b* without CAPE peptide) driven by 35S promoter were amplified from the pART7-*PR1b* by PCR using primers in Table M3. An HA-tag (in italics) was inserted between N-terminal signal peptides as determined by SignalP (Almagro Armenteros *et al*, 2019) and CAP domain by overlapping PCR with primers in Table M3. The final fragments were cloned into pART27 vectors with *NotI* restriction enzyme.

For purification of *PR1b* proteins, open reading frames (ORFs) of *PR1b^{fl}* and *PR1b^{wo}*, lacking their N-terminal signal peptides, were amplified from the tomato H7996 line by PCR using the primer combination specified in Table M3. An HA-tag codon (in italics) was included in the forward PCR primers to facilitate detecting of the recombinant proteins. PCR products were cloned into pJET1.2/blunt and amplified in *E. coli* TOP10. The identity of the *PR1* construct was confirmed by sequencing (Macrogen). For generation of *PR1b^{KK}*, based on pJET1.2- *PR1b^{fl}* site, QuikChange II Site-Directed Mutagenesis Kit (Agilent), were used with complementary primers in Table M3. The 148th tyrosine and 149th aspartic acid residues of *PR1b* were substituted to lysine. Inserts were then cloned in MCS of pCold using the restriction enzymes *NdeI* and *HindIII*, whose restriction sites were included in the forward and reverse primers, respectively (underlined in Table M3). The vectors were subsequently introduced into *E. coli* Rosetta, which is engineered to enhance the production of disulphide-bonded proteins, for protein expression.

Table M3. Primers used in this chapter.

Primer name	Sequence (5' to 3')
PI-I F	CCGGTTCCTTCACTCTTTACAAC
PI-I R	GCCCATCAATTTCTTTTCGTGC
PI-II F	CACAGGGTACAAGGGTTGCTAT
PI-II R	GAAGATGGACAAGTCTAGAGTCACA
PAL5 F	ACCTATCTCGTGGCGCTTTG
PAL5 R	TCTTTTGGCTACTTGGCTTACAG
ICS F	TGATGAACTTGAGGCACCTCTT
ICS R	GTCTACTAAATACGATGCGGCAG
ERF5 F	ACATCGCAAGCTTCTTTAATGCT
ERF5 R	TCCGTTCTCTCAAGTTACTCTGT
PR1b F	GGTGTCCGAGAGGCCAAG
PR1b R	TGCCCCGACCACAACCTAGT
PR2 F	TCGGAAAGTGGTTGGCCTTC
PR2 R	GTTCTGCCCCCTCCTTTCAC
PR5x F	ACAAAGGTGCCCTAATGCGTA
PR5x R	TGTGGCATCAATTATGGGCAA
TAS14 F	TCGTGATCCGACAGCTCTA

TAS14 R	ACCTTCATGTTGTCCAGGCA
AREB1 F	GTTGGTGTTCAGGTGGTCA
AREB1 R	CCACCACCATGCTCCTTTGA
PR1a F GG	AACAGGTCTCAAACAATGGGGTTGTTCAACATCTCAT
PR1a R GG	AACAGGTCTCTAGCCATAAGGACGTTCTCCAACCCAGTT
PR1b R GG	AACAGGTCTCTAGCCGTAAGGACGTTGTCCGATCCAGTT
PR1c F GG	AACAGGTCTCAAACAATGGGATACTCCAATATTGCTT
PR1c R GG	AACAGGTCTCTAGCCGACATCAGTTGGAAGTTCCAACCTT
PR1d F GG	AACAGGTCTCAAACAATGGGGTTGTTTAACATGTCAT
PR1d R GG	AACAGGTCTCTAGCCGTAAGGACGTTGTCCGACCCAATT
PR1a CNAD F	GGTGGTTCATTTCTTGCAACGCCGATCCTGTAGGCAACTGGGT
PR1a CNAD R	ACCCAGTTGCCTACAGGATCGGCGTTGCAAGAAATGAACCACC
PR1b CNAD F	GGTGGTTCATTTCTTGCAACGCCGATCCTGTAGGCAACTGGAT
PR1b CNAD R	ATCCAGTTGCCTACAGGATCGGCGTTGCAAGAAATGAACCACC
PR1c CNAD F	GGTACTTTATAACTTGTAAATGCCGATCCACCAGGTAACCTGGAG
PR1c CNAD R	CTCCAGTTACCTGGTGGATCGGCATTACAAGTTATAAAGTACC
PR1d CNAD F	GGTGGTTTATTTCTTGCAACGCCGATCCTGTAGGCAATTGGGT
PR1d CNAD R	ACCCAATTGCCTACAGGATCGGCGTTGCAAGAAATAAACCACC
35S <i>NotI</i>	ATGCGGCCGCTGAGACTTTTCAACAAAG
PR1b ol R	GAAGCGTAATCTGGAACATCGTATGGGTAATTTTGGGCCTCACAA GA
PR1b ol F	ATTACCCATACGATGTTCCAGATTACGCTTCACCCCAAGACTATCT T
PR1b ^{fl} <i>NotI</i>	ATGCGGCCGCTTAGTAAGGACGTTGTCCGAT
PR1b ^{wo} <i>NotI</i>	ATGCGGCCGCTTAATAGTTGCAAGAAATGAA
PR1b <i>XhoI</i> HA	ATCTCGAGATACCCATACGATGTTCCAGATTACGCTGCCCAAAT CACCCCAAGA
PR1b ^{fl} <i>HindIII</i> HA	GTAAGCTTTTAGTAAGGACGTTGTCCGA
PR1b ^{wo} <i>HindIII</i> HA	GTAAGCTTTAATCATAGTTGCAAGAAATGA
PR1b ^{KK} F	GGTGGTTCATTTCTTGCAACAAGAAGCCTGTAGGCAACTGGGTTG G
PR1b ^{KK} R	CCAACCCAGTTGCCTACAGGCTTCTTGTTGCAAGAAATGAACCAC C

Transient expression PR1 proteins in N. benthamiana

Transient expression in *N. benthamiana* was performed as previously described by Reichardt & collaborators (Reichardt *et al.*, 2018), with some modifications. Briefly, *A. tumefaciens* ASE containing pSoup and the PR1s and PR1s-wo expression construct in pART27 or the p19 suppressor of silencing were grown on LB plates with appropriate antibiotics (rifampicin, tetracycline and spectinomycin for C58C1 carrying pART27; kanamycin instead of spectinomycin for C58C1 carrying p19). Bacteria were collected from the plate with a 1 mL disposable pipette tip and resuspended in 10 mL infiltration buffer (10 mM MES pH 5.6, 10 mM MgCl₂). Constructs were mixed to a final OD₆₀₀ of 0.3 for C58C1 carrying pART27- PR1s and 0.3 for C58C1 carrying p19 and infiltrated in the leaves of 3 to 4-week-old *N. benthamiana* using a blunt syringe.

Purification of PR1b proteins and derivatives

The PR-1 proteins were expressed in *E. coli* Rosetta-competent cells. The Rosetta cells containing the target construct were grown in 50 mL LB medium with Ampicillin at 37 °C. shaker overnight, transfer all to 450 mL fresh LB medium with Ampicillin for another 3 hours, then adding 200 mM IPTG before transferring the flask into a 16 °C. shaker overnight. The 500 mL cell culture was resuspended in 50 mL lysis buffer consisting of 50 mM HEPES pH 8.0 (Sigma Aldrich), 500 mM NaCl, and lysed by two sequential passes through a French press cell at around 15,000–20,000 psi. The lysate was then clarified by centrifugation at 12,000 $\times g$ at 4°C for 30 minutes. After passing the lysate through a 0.45 μ m filter, the proteins of interest were separated by using immobilized metal affinity chromatography (IMAC) (His-trap 5 mL, Cytiva), facilitated by the presence of an N-terminal cleavable 6 histidine tag. The proteins were eluted from the IMAC column with the elution buffer (consisting of 50 mM HEPES pH 8.0 - SIGMA ALDRICH-, 500 mM NaCl and 300 mM imidazole). After elution, excess imidazole was removed by a 10 kDa MWCO ultrafiltration device (Vivaspin 500).

For removing the ProS2 domain and the histidine e tag, PR1s fractions were treated with the P69 protease for 3 hours at room temperature, leaving a 22-residue N-terminal overhang (Ser–Asp–Ala). The cleaved solution was reapplied to the Ni-NTA beads to remove His-ProS2, His-P69 and uncleaved target proteins. Fractions corresponding to the PR1b proteins were collected and visualized by Coomassie-stained SDS-PAGE, before being concentrated using 10 kDa MWCO ultrafiltration devices (Vivaspin 500) to appropriate concentrations for further analysis.

Extraction of apoplast and total extract from tomato leaves and N. benthamiana leaves

For extraction of apoplastic fluid of tomato leaves, full-size true leaves were excised, immersed in 50 mL of cold distilled water and infiltrated by vacuum for 1 min. After vacuum, leaves were surface-dried with paper, wrapped in 5 mL tips-cut pipette tips, and placed side up in a 50 mL centrifuge tube. After centrifugation (3,000 $\times g$, 10 min, 4°C), around 300 μ L of apoplastic fluid was harvested. The apoplastic fluid was finally passed through a 0.22 μ m filter to get rid of any bacteria, diluted to 1 mg/mL, after measured protein concentration by Protein Assay Dye Reagent (Bio-Rad), and stored at -80°C.

For total extract isolation, the main vein was cut from whole leaves, and the rest of the leaves was quickly frozen by liquid nitrogen. After grinding, leaf material was mixed with 5 mL of G-TEN buffer [10% glycerol, 100 mM Tris-HCl pH 7.5, 1 mM EDTA, 150 mM NaCl and 1 \times Protease inhibitor cocktail (SIGMA, P599)] and centrifuged for 20

min at 10,000 x *g* at 4 °C. After centrifugation, the supernatant was passed through Miracloth (EMD Millipore Corp.) to filter debris. 5x Laemmli sample buffer was added to 100 µl filtrate and boiled for 5 min. Equal amounts of supernatant were loaded on 12% SDS-PAGE gels.

PR1 cleavage assay

Total protein extract of *N. benthamiana* leaves transiently expressing PR1 or 1 µg/µl purified recombinant PR1b protein were incubated with or without 1 µg/µl of purified P69B or P69D proteins (purified in chapter I) at room temperature over time. 5x Laemmli sample buffer was added to incubated samples and boiled for 5 min. Equal amounts of supernatant were loaded on 10% SDS-PAGE gels. Coomassie staining or western blot with anti-HA, His and PR1 antibodies were performed afterwards.

Generation of CRISPR/Cas9 *pr1b* mutant tomato plants

The CRISPR/Cas9 vectors and the cloning methodology used in this study was described by Danilo and coworkers (Danilo *et al.*, 2018). Briefly, small guide RNA (sgRNA) sequences targeting *PR1b* gene were designed based on high specificity score and the lowest number of off-target genes on the CRISPOR web tool (Haeussler *et al.*, 2016) (<http://crispor.tefor.net/>), and are indicated in Table M4. The sgRNA sequences were placed under the control of U3 or U6 sgRNA promoters in a resulting sequence flanked by gateway recombinant sites (attB1 and attB2). The sequence of the U3- and U6-sgRNA backbones used is detailed in Danilo *et al.* (Danilo *et al.*, 2018). The sgRNA cassettes were synthesized by Twist Bioscience (<https://www.twistbioscience.com/>) and were introduced into pDONR207 by BP Gateway recombination. To generate deletions in each particular gene (Table M4), U3- and U6-sgRNA cassettes were combined into single vectors. For this, the U6-sgRNA cassette targeting one specific gene was excised from pDONR207 with *XhoI* and *PstI* and mobilized into the U3-sgRNA cassette-containing pDONR207 plasmid previously digested with *Sall* and *PstI*. The resulting vectors (pDONR207-U3-sgRNA-U6-sgRNA) were then introduced by LR Gateway recombination into the binary vectors pDe-Cas9-*NptII* or pDe-Cas9-*Hpt* described in Danilo *et al.* for later selection with kanamycin (Danilo *et al.*, 2018).

Table M4. Guide sequences (sgRNA) used for the generation of tomato PR1b mutants by CRISPR/Cas9 and primers for verifying. The protospacer adjacent motif (PAM) sequence recognized by Cas9 is underlined.

Strategy	Sequence (5' to 3')
sgRNA for PR1b mutant	U3-SG1: ACATAGGCCCGACTCCGACT <u>TGG</u>
	U6-SG2: ATCCTGTAGGCAACTGGAT <u>CGG</u>
Detecting PR1b mutant	F: ATGGGGTTGTTCAACATCTC
	R: TTAGCAACATCAAAAGGGAA
Detecting PR1a mutant	F: ATGGGGTTGTTCAACATCTC
	R: CATGAACATATGGTACGTGG
Detecting Cas9	F: TCCCTTACTACGTGGGACCTC
	R: ATCTGCCTGGTTTCCACAG

The tomato H7996 genotype and Marmande genotypes were transformed using *A. tumefaciens* C58 pGV2260 as previously described (Mazier *et al.*, 2011). Briefly, the plants were grown on semi-solid ½MS medium in a chamber set at 22°C/18°C and long-day light conditions. Cotyledon and leaf segments were excised from 8 to 12-day-old seedlings and were incubated abaxial side up with *A. tumefaciens* C58 pGV2260 containing the respective pDeCas9 binary vectors in the dark in plates of MS medium supplemented with 0.9 mg/l thiamine, 0.2 mg/l 2,4-D, 0.1 mg/l kinetin and 0.2 mM acetosyringone. After three days, the explants were transferred to the regeneration medium (MS containing 2 mg/l zeatin and 225 mg/l timentin and supplemented with the respective antibiotic for selection (100 mg/l kanamycin). The explants were transferred to fresh medium every two weeks until callus formed. Calli were then transferred to elongation medium (same composition as the regeneration medium where the MS salts had been reduced to half) until shoots developed. Shoots were excised from the surrounding callus and transferred to individual culture tubes that contained elongation medium until rooting. Shoots that rooted were screened for the desired PR1b deletion and were subsequently acclimated to greenhouse growing conditions. Successfully regenerated CRISPR/Cas9 plantlets were screened by PCR. For this, leaf samples were collected and genomic DNA was extracted. Deletions were screened using the genotyping primers listed in Table M4. The identity of the deletions was confirmed by DNA sequencing.

Generation of PR1b overexpression tomato plants

Transient expression in *N. benthamiana* was performed as previously described by Reichardt & collaborators (Reichardt *et al.*, 2018), with some modifications. Briefly, *A.*

tumefaciens C58C1 containing the *PR1b^{fl}* and *PR1b^{wo}* expression construct in pART27 or the p19 suppressor of silencing were grown on LB plates with appropriate antibiotics (rifampicin, tetracycline and spectinomycin for C58C1 carrying pART27; rifampicin, tetracycline and kanamycin for C58C1 carrying p19). Bacteria were collected from the plate with a 1 mL disposable pipette tip and resuspended in 10 mL infiltration buffer (10 mM MES pH 5.6, 10 mM MgCl₂). Constructs were mixed to a final OD₆₀₀ of 0.5 for C58C1 carrying pART27- PR1 and 0.5 for C58C1 carrying p19 and infiltrated in the leaves of 3 to 4-week-old *N. benthamiana* using a blunt syringe.

Confocal microscopy

For live-cell imaging, infiltrated parts of *N. benthamiana* leaves were used for observation under the Olympus FV1000 confocal microscope using ×60 water immersion objective. Excitation wavelengths used were 488 nm for GFP and 561 nm for m-cherry. The images were analyzed using ImageJ.

Bacterial material, plant inoculations and pathogenicity assays

All assays were performed using a *R. solanacearum* GMI1000 (Phylotype I, race 1, biovar 3) luminescent reporter strain carrying the *PpsbA:LuxCDABE* construct generated by Cruz *et al.* (Cruz *et al.*, 2014). *R. solanacearum* was routinely grown on rich B medium (10 g/l bactopectone, 1 g/l yeast extract and 1 g/l casaminoacids) using gentamicin (10 µg/mL) for selection.

For soil-drenching infections, plants were inoculated as previously described (Planas-Marques *et al.*, 2020). Briefly, 40 mL of a 10⁸ CFU/mL (OD₆₀₀=0.1) bacterial suspension of *R. solanacearum* was poured on every pot after making four holes in the soil with a disposable 1 mL pipette tip. For petiole inoculation, 10 µl of a 10⁶ CFU/mL (OD₆₀₀=0.001) suspension was pin-inoculated in the cotyledons or first internode of plants by placing a droplet of the suspension in the petiole-stem boundary and poking it through the stem with a needle (25G, BD Microlance, Becton Dickinson). Infected plants were scored for wilting symptoms using a scale from 0 to 4, where 0=healthy plant with no wilt, 1=25%, 2=50%, 3=75% and 4=100% of the canopy wilted. Assessment of bacterial multiplication in the roots and hypocotyls (3 cm sections) was performed by placing the respective tissues in an empty 2 mL tube and measuring the luminescence (RLU·s⁻¹) emitted by the bacteria in a luminometer (FB 12, Berthold Detection Systems). The value was referred as log RLU·s⁻¹g⁻¹ tissue.

For bacterial inoculation in the apoplast, plants were vacuum-infiltrated with a bacterial suspension of 10⁵ CFU/mL (OD₆₀₀=0.0001) as previously described (Planas-Marques *et al.*, 2018). Assessment of bacterial multiplication was performed in four independent

-plants per time point as follows: four 5 mm-diameter leaf disks were excised from each plant, the disks were grinded in 200 μ l sterile water-containing 1.5 mL tubes, and 10-fold dilutions were plated on rich B medium plates. CFUs were counted and bacterial growth was calculated as CFU \cdot mm⁻² of leaf. For CAPE peptide treatment, CAPE peptide, synthesized by pepMic (<https://www.pepmic.com/>), was sprayed on the surface of tomato leaves at 500 nM before inoculation with *R. solanacearum*.

For infection assay *in vitro*. Seeds were germinated on the MS plate with or without CAPE peptide. 10-day-old plantlets were pin-inoculated 1 cm below the root collar using a pasteur pipettes (HIRSCHMANN) submerged in a 10⁶ colony-forming units (CFU) \cdot mL⁻¹ (OD₆₀₀=0.001) luminescent *R. solanacearum* suspension. Wilting symptoms were recorded and bacterial invasion visualized a live imaging system (ImageQuant™ LAS 4000), using a 10-minute exposure time with high binning setting.

In all cases, infected plants were kept in chambers set at 27°C, 60% humidity and 12h day/night photoperiod during the course of the experiment.

Antimicrobial assay *in vitro*

Testing for antimicrobial activity of recombinant PR1 proteins was carried out as described by Gamir *et al.* (Gamir *et al.*, 2017). Briefly, *R. solanacearum* at 10⁸ CFU/mL (OD₆₀₀=0.1) in a total volume of 200 μ l rich B medium with different concentrations of CAPE peptide and recombinant PR1b and derivatives, were incubated in a 96-well microtiter plate (Greiner). Bacterial growth was recorded over time using VICTOR Nivo device (PerkinElmer).

RNA extraction and quantitative reverse transcription–PCR (qRT-PCR) analysis

The Maxwell® RSC Plant RNA kit (Promega) was used to isolate RNA from leaves from 3 different plants. 2 μ g of RNA were reverse transcribed into cDNA with the High-Capacity cDNA Reverse Transcription Kit with RNase inhibitor (Applied Biosystems™). RT-qPCRs were performed with LightCycler® SYBRgreen I master (Roche) in a LightCycler® 480 System (Roche). All gene expression were normalized to expression of *S/Act2* (Solyc11g005330.1) and data was analyzed using the $\Delta\Delta$ CT method. Primers for qRT-PCR used in this study were previously described and are listed in Table M3.

Statistical analysis

Statistical analyzes were performed using the corresponding R package. All statistical tests are indicated in the respective figure legends.

II.4 Discussion

Conservation of PR1s sequence identity in different plant species

Since the first PR1 protein was identified from leaves of *Nicotiana tabacum* infected with tobacco mosaic virus (Van Loon & Van Kammen, 1970), this family of proteins have been always connected with plant-pathogen interaction, including bacteria, fungi and virus (Niderman *et al.*, 1995; Tornero *et al.*, 1994; van Kan *et al.*, 1992). In our proteomic data, PR1a, b and c are the three members most responsive to the bacterial pathogen *R. solanacearum*, being highly accumulated both in the apoplast and xylem upon infection (Fig. 1C and 1D), which may suggest that the function of these different PR1 proteins is redundant. Even though there are dozens of PR1s in each species, not all PR1 proteins accumulate during infection (Cornelissen *et al.*, 1987). For instance, PR1d is only abundant in the xylem, but not in the apoplast (Fig. 1C and 1D). Blasting tomato genome against PR1b, we found that, besides PR1a, b, c and d, there are other 6 PR1-like proteins. Although we identified 10 PR1 proteins in tomato plants, only PR1a, b, c and d were detected in the apoplast or xylem (Fig. 1C and 1D).

All these PR1 family proteins feature a conserved signal peptide, CAP domain and CAPE peptide (Fig. 1A). In many proteins, the signal peptide facilitates their secretion into the extracellular space (Lauge *et al.*, 2000; Ziegler *et al.*, 2000). The CAP domain has a conserved lipid binding function, which has been shown to act as an anti-fungal (Choudhary & Schneiter, 2012; Darwiche *et al.*, 2017; Gamir *et al.*, 2017). The CAPE peptide, PxGNxxxxxPY, and the amino acid before the CAPE peptide (aspartic acid) are highly conserved in Solanaceae and in most PR1s from Arabidopsis, recent studies have proven that the cysteine protease cleave PR1b to release CAPE peptide (Chen *et al.*, 2023). However, for some monocots, like wheat, the cleaved amino acid is different from dicots (Sung *et al.*, 2021), indicating the way to release CAPE peptide is different in different plant species (Fig. 3A). Noticeably, all plant species present some PR1 proteins featuring an amino acid extension after CAPE peptide, such as PR1c in tomato plant, and they are highly conserved across the Solanaceae plants (Fig. 3). In sum, strong conservation of the CAPE peptide across plants species suggest that it may have an important contribution to the function of PR1 proteins. However, divergence observed within cleavage site in different plant species, suggest that there may be some degree of functional specialization, with different cleavage mechanisms used to release CAPE peptide.

Processing and translocation of PR1s to release the CAPE peptide

Most PR1 proteins are thought to be secreted to the apoplastic space, due to their N-terminal signal peptide (Carr *et al.*, 1987; Lincoln *et al.*, 2018). PR1 of Arabidopsis is synthesized in the endoplasmic reticulum, and then secreted into the apoplast through the late endosome (LE)/multivesicular body (MVB) pathways (Pecenкова *et al.*, 2017). However, a PR1 version with the cleavage motif mutated (YDPR to AAAA) or a C-terminal truncated version PR1 Δ C, including deficient cleavage motif, are stuck in the ER (Pecenкова *et al.*, 2022; Pecenкова *et al.*, 2017). Similarly, the tomato PR1b and its cleavage motif mutant fused to GFP showed the same localization as Arabidopsis PR1, suggesting that the cleavage motif plays an important role in translocation of PR1 in different plant species. However, both the wild type and cleavage site mutant version of PR1c were localized in the MVB (Fig. 4), demonstrating that the amino acid extension after CAPE peptide in this protein may prevent translocation of PR1 through divergent structures and recognition.

Wheat PR1 is cleaved by an unknown serine protease to release the CAPE peptide (Sung *et al.*, 2021). Our previous N-terminomics studies using P69 (Chapter I), suggested that PR1 could be a substrate of P69. Therefore, we tested if P69 could cleave PR1 to release CAPE peptide. Surprisingly, P69s showed a preference towards cleaving PR1 versions with mutations in the cleavage site predicted to render the protein uncleavable (PR1s^{CNAD}, which cleavage site change from CNYD to CNAD), instead of the wild type of PR1 proteins (Fig. 7A and 7B). PICS data from P69s (Chapter I), showed that certain members of this family showed a preference to cleave after an alanine, which would explain the preference towards the mutated versions of PR1. In light of that, we generated an alternative cleavage site mutant, CNYD to CNKK for subsequent experiments. However, we did not observe the cleavage within PR1b when we incubated purified ProS2-PR1b and purified P69s (Fig. 7C). As we mentioned in the last section, the cleavage site of PR1 in monocots is different than in dicots. In sum, P69 is not the protease cleaving PR1 to release the CAPE peptide. A recent study showed that the cysteine protease Xylem cysteine peptidase 1 (XCP1) could cleave PR1 to release CAPE peptide in Arabidopsis (Chen *et al.*, 2023). Since the cleavage sites are the same between Arabidopsis and Solanaceae plants, we hypothesize that the tomato homolog of XCP1 may be the protease cleaving PR1 to generate CAPE peptide in tomato. We tried to purify two XCPs homologs in tomato, however we did not manage to obtain the purified proteins due to time limits. Future work in the lab will help determine whether tomato XCPs cleave PR1s.

XCP1 is a tracheary Element Vacuolar Protein, which localizes in the vacuole, while PR1b is mostly localized in the apoplast. However, PR1 has also been shown to locate

in the vacuole (Dixon *et al.*, 1991; Funk *et al.*, 2002; Pecenkova *et al.*, 2022), implying that cleavage could also occur in the vacuole. Additionally, XCP1 facilitates processing of PR1b to release CAPE peptide, thus deficient *xcp1* has impaired response to pathogen *Pst DC3000* (Chen *et al.*, 2023). On the other hand, XCP2 impaired Arabidopsis, the paralog of XCP1, showed more resistant to the vascular pathogen *R. solanacearum*, and less colonization of *R. solanacearum* compared with wild type (Zhang *et al.*, 2014). Overall, XCP maybe play dual roles in plant defense to against different types of pathogens.

Function of CAPE peptide in priming plant defense

The CAPE peptide derived from PR1b has been shown to act as an antimicrobial against bacterial and fungal pathogens (Chen *et al.*, 2014; Li *et al.*, 2022; Sung *et al.*, 2021). Here, we also showed that spraying leaves with the CAPE peptide before inoculation with *R. solanacearum* limit multiplication (Fig. 5B). Growing seedlings on MS plates supplemented with CAPE peptide also enhanced plant defenses as well (Fig. 5C), suggesting that recognition of CAPE peptide could occur both at the root and leaves. In contrast, the CAPE peptide did not affect growth of *R. solanacearum* in rich medium (Fig. 5A). Together, these results indicate that the CAPE peptide may limit multiplication of *R. solanacearum* in plants through priming plant defense.

To understand signalling triggered upon CAPE perception, we tested expression of different hormone-related plant defense genes. The results show that until 6 hours after CAPE treatment, the peptide could highly induce JA-responsive genes *PI-I* and *PI-II* and PR1b, the precursor gene of CAPE peptide (Fig. 12A). However, other SA-responsive genes (*PR2* and *PR5x*) were not induced, but slightly suppressed at 3 hours after CAPE treatment (Fig. 12B). Additionally, CAPE did not affect the expression of neither ABA-responsive genes nor ethylene-responsive gene *ERF5* (Fig. 12D). Expression of upstream of SA signalling pathway, SA-synthesis genes *ICS* and *PAL5* was inhibited by CAPE treatment after 6 hours, like *PR2* and *PR5x* (Fig. 12C), indicating there is an unknown feedback loop of PR1b independent salicylic acid signalling pathway. Chen *et al.* showed the JA-responsive and PR1b are highly induced by CAPE peptide treatment, while CAPE peptide suppresses other SA-responsive genes expression at early stage of CAPE treatment. However, after 24 hours of CAPE treatment, the peptide highly induced both SA-responsive genes and JA-responsive genes (Chen *et al.*, 2014). The JA and SA biosynthesis pathways have a very complex interrelation, having shown to act antagonistically (Robert-Seilaniantz *et al.*, 2011; Thaler *et al.*, 2012), although in some instances they may also function synergistically, as in the SA-JA-ethylene backbone of the plant immune signalling

network, thereby redirecting defense output (Verhage *et al*, 2010). In light of our results in the context of *R. solanacearum* infection of tomato, one could speculate that CAPE can inhibit the multiplication of the hemibiotrophic pathogen *R. solanacearum* by inducing SA-triggered pathway during the biotrophic phase and JA-triggered pathway during the necrotrophic phase. Since in a natural infection setting these two lifestyles of the bacteria may occur concomitantly, it is not surprising that these different pathways are activated simultaneously.

Understanding the role of PR1 in tomato defense against *R. solanacearum*

The *PR1* genes, and especially the *PR1a*, are frequently used as markers of SA-mediated defense and systemic acquired resistance (SAR) against biotrophic pathogens (Breen *et al*, 2017; Mosher *et al.*, 2013). However, the exact function and mode of action of PR1s in defense is still unknown. Recent studies showed the CAP domain has a conserved lipid binding function, contributing to anti-fungal defense, since PR1 can limit sterol-auxotroph organisms through competition of sterol (Choudhary & Schneider, 2012; Darwiche *et al.*, 2017; Gamir *et al.*, 2017). However, sterol is not necessary for growth of *R. solanacearum*; in consequence, the purified PR1b^{fl}, PR1b^{wo} and PR1b^{KK} did not affect growth of *R. solanacearum* (Fig. 8). Hence, we will test the effect of these purified proteins on the inhibition of *R. solanacearum* in planta, by directly infiltrating purified proteins into the leaves.

Additionally, we tried to get *pr1b*-deficient plants both in susceptible Marmande and resistant Hawaii 7996 cultivars using CRISPR-Cas9. Unfortunately, we failed to obtain PR1b-deficient plants in Hawaii 7996, which would have provided more information as this variety is highly resistant to *R. solanacearum*. Still, we obtained 3 *pr1b* mutant lines in Marmande (Fig. 9). Li J. *et al* tried numerous times and still failed to obtain the desired *pr1b* knockout mutant (Li *et al.*, 2022), pinpointing the difficulty of deleting *PR1b*. *R. solanacearum* pathogenicity assays using soil drenching inoculation showed that deletion of *pr1b* resulted in a slight increase of resistance in two of the three lines analyzed (Fig. 11). The result seems contradictory, since the PR1b is supposed to facilitate plant defense. More replicates will be performed in the future to try to clarify these phenotypes. For leaf infiltration inoculation method, no significant differences were observed between wild type and these three mutant lines (Fig. 11). We hypothesized that there are redundant PR1s in tomato plant possessing the conserved CAPE peptide and same cleavage site, like PR1a and PR1d, these PR1s could function normally in *pr1b*-deficient tomato plants. We then checked the hormone-responsive genes expression of mutant lines. In contrast with CAPE treatment, *pr1b*

mutant lines showed severe inhibition of JA-responsive genes, and no effect on other hormone-related genes (Fig. 13A).

We also generated *PR1b^{fl}* and *PR1b^{wo}* (without CAPE peptide) overexpression lines on a susceptible Marmande background. *PR1b^{fl}*, but not *PR1b^{wo}*, displayed more resistance to fungal pathogen *Fusarium oxysporum* f. sp. *lycopersici* (Fol) (Li *et al.*, 2022). Expression analysis of defense hormone-responsive genes in the progeny of *PR1b^{fl}* and *PR1b^{wo}* lines revealed that other SA-responsive genes and SA-synthesis genes in *PR1b* overexpression lines (Fig. 13B). Besides, *PR1b* overexpression may have been partially silenced over generations, since the line used to perform this experiment the level of *PR1b* was only 5 times more than in wild type plants, while in a previous generation it was 100 times (Fig. 10B, Fig. 13B).

In sum, we hypothesize *PR1b^{fl}* enhance plant defense to *R. solanacearum*, but not *PR1b^{wo}*. We tried to use the progeny of T1 lines to check pathogenicity assays, however these plants germinated from selection plates seem under stress when we transferred them from green house to cabin. Therefore, we decided to perform the pathogenicity assays after obtaining the homozygous lines. Until now, we obtained the progeny of heterozygous lines, which shows a segregation of 3:1. With the present data we can conclude that determining the role of PR1 proteins in plant defense against *R. solanacearum* needs further experiments, which will be performed in the near future in our group.

Conclusions

From the main goals of this work, we extract the following conclusions:

Characterization of the P69 family of plant subtilases

1. The P69 family of subtilases contains 10 genes in tomato showing a protein sequence identity higher than 71%. They are arranged in a genomic cluster in chromosome 8. Homologs of P69A-D, P69I and P69E are found in potato, while only P69A and P69D are conserved in eggplant and pepper.
2. P69B, P69D and P69G can enhance plant defense to *R. solanacearum* in *N. benthamiana* leaves by transient expression.
3. The catalytic serine-532 of P69D, which is conserved in other P69S, is required for the autocatalytic removal of the inhibitory prodomain and secretion to the apoplast.
4. Apoplast proteome and N-terminome analyses suggest that P69D-deficiency results in altered proteolytic processing of pathogenesis-related proteins, particularly PR1B and PR2 in the apoplast *in vivo*.
5. A tomato P69D deficient line is slightly more susceptible to *R. solanacearum* infection specifically when the pathogen is soil-inoculated, and limit multiplication of *R. solanacearum* in the hypocotyl. However, it does not affect the virulence of the fungal vascular pathogen, like *Fusarium oxysporum* f.sp. *lycopersici* (Fol).

Characterization of the PR1 family of tomato plants

6. The PR1 family contains 10 genes in tomato. However, only 4 of them are induced upon *R. solanacearum* infection. The cleavage site to release CAPE peptide and the CAPE peptide are highly conserved in the Arabidopsis and Solanaceae plants.
7. PR1b and PR1c of tomato localize in multivesicular bodies. However, the cleavage site mutant version of PR1b is retained in the endoplasmic reticulum (ER).
8. The CAPE peptide can inhibit multiplication of *R. solanacearum* in tomato leaves and xylem through priming plant defense genes, like jasmonic acid-responsive genes (*PI-I* and *PI-II*), and *PR1b*, its own precursor.
9. Purified PR1 proteins do not affect the growth of *R. solanacearum* in rich medium.

Conclusions

10. The serine proteases P69B and P69D cannot cleave PR1 proteins to release CAPE peptide.
11. A tomato *pr1b* deficient line is slightly more resistant to *R. solanacearum* infection specifically when the pathogen is soil inoculated.
12. The expression of Jasmonic acid-responsive genes and salicylic synthesis-related genes is highly induced in the *PR1b* full length overexpression lines.

References

- Alexander D, Goodman RM, Gut-Rella M, Glascock C, Weymann K, Friedrich L, Maddox D, Ahl-Goy P, Luntz T, Ward E (1993) Increased tolerance to two oomycete pathogens in transgenic tobacco expressing pathogenesis-related protein 1a. *Proceedings of the National Academy of Sciences* 90: 7327-7331
- Almagro Armenteros JJ, Tsirigos KD, Sonderby CK, Petersen TN, Winther O, Brunak S, von Heijne G, Nielsen H (2019) SignalP 5.0 improves signal peptide predictions using deep neural networks. *Nat Biotechnol* 37: 420-423
- Amano Y, Tsubouchi H, Shinohara H, Ogawa M, Matsubayashi Y (2007) Tyrosine-sulfated glycopeptide involved in cellular proliferation and expansion in Arabidopsis. *Proc Natl Acad Sci U S A* 104: 18333-18338
- Bacete L, Melida H, Miedes E, Molina A (2018) Plant cell wall - mediated immunity: cell wall changes trigger disease resistance responses. *The Plant Journal* 93: 614-636
- Bai Y, Muller DB, Srinivas G, Garrido-Oter R, Potthoff E, Rott M, Dombrowski N, Munch PC, Spaepen S, Remus-Emsermann M *et al* (2015) Functional overlap of the Arabidopsis leaf and root microbiota. *Nature* 528: 364-369
- Beck S, Michalski A, Raether O, Lubeck M, Kaspar S, Goedecke N, Baessmann C, Hornburg D, Meier F, Paron I *et al* (2015) The Impact II, a Very High-Resolution Quadrupole Time-of-Flight Instrument (QTOF) for Deep Shotgun Proteomics. *Mol Cell Proteomics* 14: 2014-2029
- Beloshistov RE, Dreizler K, Galiullina RA, Tuzhikov AI, Serebryakova MV, Reichardt S, Shaw J, Taliany ME, Pfannstiel J, Chichkova NV *et al* (2018) Phytaspase-mediated precursor processing and maturation of the wound hormone systemin. *New Phytol* 218: 1167-1178
- Bigeard J, Colcombet J, Hirt H (2015) Signaling mechanisms in pattern-triggered immunity (PTI). *Molecular plant* 8: 521-539
- Boersema PJ, Raijmakers R, Lemeer S, Mohammed S, Heck AJ (2009) Multiplex peptide stable isotope dimethyl labeling for quantitative proteomics. *Nat Protoc* 4: 484-494
- Boucher CA, Barberis PA, Trigalet AP, Demery DA (1985) Transposon mutagenesis of *Pseudomonas solanacearum*: isolation of Tn 5-induced avirulent mutants. *Microbiology* 131: 2449-2457
- Breen S, Williams SJ, Outram M, Kobe B, Solomon PS (2017) Emerging Insights into the Functions of Pathogenesis-Related Protein 1. *Trends Plant Sci* 22: 871-879
- Brito B, Aldon D, Barberis P, Boucher C, Genin S (2002) A signal transfer system through three compartments transduces the plant cell contact-dependent signal controlling *Ralstonia solanacearum* hrp genes. *Molecular plant-microbe interactions* 15: 109-119
- Brutus A, Sicilia F, Macone A, Cervone F, De Lorenzo G (2010) A domain swap approach reveals a role of the plant wall-associated kinase 1 (WAK1) as a receptor of oligogalacturonides. *Proc Natl Acad Sci U S A* 107: 9452-9457
- Butenko MA, Patterson SE, Grini PE, Stenvik GE, Amundsen SS, Mandal A, Aalen RB (2003) *Inflorescence deficient in abscission* controls floral organ abscission in Arabidopsis and identifies a novel family of putative ligands in plants. *Plant Cell* 15: 2296-2307

References

- Bykova NV, Rampitsch C, Krokhn O, Standing KG, Ens W (2006) Determination and characterization of site-specific N-glycosylation using MALDI-Qq-TOF tandem mass spectrometry: case study with a plant protease. *Anal Chem* 78: 1093-1103
- Caldwell D, Kim B-S, Iyer-Pascuzzi AS (2017) *Ralstonia solanacearum* differentially colonizes roots of resistant and susceptible tomato plants. *Phytopathology* 107: 528-536
- Carr JP, Dixon DC, Nikolau BJ, Voelkerding KV, Klessig DF (1987) Synthesis and localization of pathogenesis-related proteins in tobacco. *Mol Cell Biol* 7: 1580-1583
- Cedzich A, Huttenlocher F, Kuhn BM, Pfannstiel J, Gabler L, Stintzi A, Schaller A (2009) The protease-associated domain and C-terminal extension are required for zymogen processing, sorting within the secretory pathway, and activity of tomato subtilase 3 (SISBT3). *J Biol Chem* 284: 14068-14078
- Chen YL, Lee CY, Cheng KT, Chang WH, Huang RN, Nam HG, Chen YR (2014) Quantitative peptidomics study reveals that a wound-induced peptide from PR-1 regulates immune signaling in tomato. *Plant Cell* 26: 4135-4148
- Chen YL, Lin FW, Cheng KT, Chang CH, Hung SC, Efferth T, Chen YR (2023) XCP1 cleaves Pathogenesis-related protein 1 into CAPE9 for systemic immunity in *Arabidopsis*. *Nat Commun* 14: 4697
- Chichkova NV, Shaw J, Galiullina RA, Drury GE, Tuzhikov AI, Kim SH, Kalkum M, Hong TB, Gorshkova EN, Torrance L *et al* (2010) Phytaspase, a relocatable cell death promoting plant protease with caspase specificity. *EMBO J* 29: 1149-1161
- Choudhary V, Schneider R (2012) Pathogen-Related Yeast (PRY) proteins and members of the CAP superfamily are secreted sterol-binding proteins. *Proceedings of the National Academy of Sciences* 109: 16882-16887
- Colaert N, Helsens K, Martens L, Vandekerckhove J, Gevaert K (2009) Improved visualization of protein consensus sequences by iceLogo. *Nat Methods* 6: 786-787
- Cornelissen BJ, Horowitz J, van Kan JA, Goldberg RB, Bol JF (1987) Structure of tobacco genes encoding pathogenesis-related proteins from the PR-1 group. *Nucleic Acids Research* 15: 6799-6811
- Couto D, Zipfel C (2016) Regulation of pattern recognition receptor signalling in plants. *Nat Rev Immunol* 16: 537-552
- Cruz AP, Ferreira V, Pianzola MJ, Siri MI, Coll NS, Valls M (2014) A novel, sensitive method to evaluate potato germplasm for bacterial wilt resistance using a luminescent *Ralstonia solanacearum* reporter strain. *Mol Plant Microbe Interact* 27: 277-285
- Danilo B, Perrot L, Botton E, Nogue F, Mazier M (2018) The DFR locus: A smart landing pad for targeted transgene insertion in tomato. *PLoS One* 13: e0208395
- Darwiche R, Mène-Saffrané L, Gfeller D, Asojo OA, Schneider R (2017) The pathogen-related yeast protein Pry1, a member of the CAP protein superfamily, is a fatty acid-binding protein. *Journal of Biological Chemistry* 292: 8304-8314
- de Lamo FJ, Constantin ME, Fresno DH, Boeren S, Rep M, Takken FLW (2018) Xylem Sap Proteomics Reveals Distinct Differences Between *R* Gene- and Endophyte-Mediated Resistance Against Fusarium Wilt Disease in Tomato. *Front Microbiol* 9: 2977
- de Lamo FJ, Simkovicova M, Fresno DH, de Groot T, Tintor N, Rep M, Takken FLW (2021) Pattern-triggered immunity restricts host colonization by endophytic fusaria, but does not affect endophyte-mediated resistance. *Mol Plant Pathol* 22: 204-215

References

- De Wit PJ, Buurlage MB, Hammond KE (1986) The occurrence of host-, pathogen-and interaction-specific proteins in the apoplast of *Cladosporium fulvum* (syn. *Fulvia fulva*) infected tomato leaves. *Physiological and Molecular Plant Pathology* 29: 159-172
- Decreux A, Thomas A, Spies B, Brasseur R, Van Cutsem P, Messiaen J (2006) In vitro characterization of the homogalacturonan-binding domain of the wall-associated kinase WAK1 using site-directed mutagenesis. *Phytochemistry* 67: 1068-1079
- Demir F, Huesgen PF (2022) A User Guide to Validation, Annotation, and Evaluation of N-Terminome Datasets with MANTI. *Methods Mol Biol* 2447: 271-283
- Demir F, Kizhakkedathu JN, Rinschen MM, Huesgen PF (2021) MANTI: Automated Annotation of Protein N-Termini for Rapid Interpretation of N-Terminome Data Sets. *Anal Chem* 93: 5596-5605
- Demir F, Niedermaier S, Villamor JG, Huesgen PF (2018) Quantitative proteomics in plant protease substrate identification. *New Phytol* 218: 936-943
- Demir F, Perrar A, Mantz M, Huesgen PF (2022) Sensitive Plant N-Terminome Profiling with HUNTER. *Methods Mol Biol* 2447: 139-158
- Deng W, Marshall NC, Rowland JL, McCoy JM, Worrall LJ, Santos AS, Strynadka NC, Finlay BB (2017) Assembly, structure, function and regulation of type III secretion systems. *Nature Reviews Microbiology* 15: 323-337
- Denny TP, Baek S-R (1991) Genetic Evidence that Extracellular Polysaccharide Is a Virulence Factor. *Molecular Plant-Microbe Interactions* 4: 198-206
- Ding Y, Wang J, Wang J, Stierhof YD, Robinson DG, Jiang L (2012) Unconventional protein secretion. *Trends Plant Sci* 17: 606-615
- Dixon DC, Cutt JR, Klessig DF (1991) Differential targeting of the tobacco PR-1 pathogenesis-related proteins to the extracellular space and vacuoles of crystal idioblasts. *EMBO J* 10: 1317-1324
- Dixon MS, Golstein C, Thomas CM, Van der Biezen EA, Jones JD (2000) Genetic complexity of pathogen perception by plants: the example of Rcr3, a tomato gene required specifically by Cf-2. *Proceedings of the National Academy of Sciences* 97: 8807-8814
- Du Y, Stegmann M, Misas Villamil JC (2016) The apoplast as battleground for plant-microbe interactions. *New Phytol* 209: 34-38
- Durrant WE, Dong X (2004) Systemic acquired resistance. *Annu Rev Phytopathol* 42: 185-209
- Edwards KD, Fernandez-Pozo N, Drake-Stowe K, Humphry M, Evans AD, Bombarely A, Allen F, Hurst R, White B, Kernodle SP *et al* (2017) A reference genome for *Nicotiana tabacum* enables map-based cloning of homeologous loci implicated in nitrogen utilization efficiency. *BMC Genomics* 18: 448
- Engelsdorf T, Gigli-Bisceglia N, Veerabagu M, McKenna JF, Vaahtera L, Augstein F, Van der Does D, Zipfel C, Hamann T (2018) The plant cell wall integrity maintenance and immune signaling systems cooperate to control stress responses in *Arabidopsis thaliana*. *Sci Signal* 11
- Escocard de Azevedo Manhaes AM, Ortiz-Morea FA, He P, Shan L (2021) Plant plasma membrane-resident receptors: Surveillance for infections and coordination for growth and development. *J Integr Plant Biol* 63: 79-101

References

- Eyal Y, Sagee O, Fluhr R (1992) Dark-induced accumulation of a basic *pathogenesis-related* (*PR-1*) transcript and a light requirement for its induction by ethylene. *Plant Molecular Biology* 19: 589-599
- Fang L-J, Qin R-L, Liu Z, Liu C-R, Gai Y-P, Ji X-L (2019) Expression and functional analysis of a *PR-1* Gene, *MuPR1*, involved in disease resistance response in mulberry (*Morus multicaulis*). *Journal of Plant Interactions* 14: 376-385
- French E, Kim BS, Rivera-Zuluaga K, Iyer-Pascuzzi AS (2018) Whole Root Transcriptomic Analysis Suggests a Role for Auxin Pathways in Resistance to *Ralstonia solanacearum* in Tomato. *Mol Plant Microbe Interact* 31: 432-444
- Funk V, Kositsup B, Zhao C, Beers EP (2002) The Arabidopsis Xylem Peptidase XCP1 Is a Tracheary Element Vacuolar Protein That May Be a Papain Ortholog. *Plant Physiology* 128: 84-94
- Gamir J, Darwiche R, Van't Hof P, Choudhary V, Stumpe M, Schneiter R, Mauch F (2017) The sterol-binding activity of PATHOGENESIS-RELATED PROTEIN 1 reveals the mode of action of an antimicrobial protein. *Plant J* 89: 502-509
- Gawehns F, Ma L, Bruning O, Houterman PM, Boeren S, Cornelissen BJ, Rep M, Takken FL (2015) The effector repertoire of *Fusarium oxysporum* determines the tomato xylem proteome composition following infection. *Front Plant Sci* 6: 967
- Genin S (2010) Molecular traits controlling host range and adaptation to plants in *Ralstonia solanacearum*. *New Phytol* 187: 920-928
- Gleave AP (1992) A versatile binary vector system with a T-DNA organisational structure conducive to efficient integration of cloned DNA into the plant genome. *Plant Mol Biol* 20: 1203-1207
- Gómez-Gómez L, Boller T (2000) FLS2: an LRR receptor-like kinase involved in the perception of the bacterial elicitor flagellin in Arabidopsis. *Molecular cell* 5: 1003-1011
- Granell A, Bellés, J. M., and Conejero, V (1987) Induction of pathogenesis-related proteins in tomato by citrus exocortis viroid, silver ion and ethephon. *Physiological and Molecular Plant Pathology* 31: 83-90
- Green TR, Ryan CA (1972) Wound-Induced Proteinase Inhibitor in Plant Leaves: A Possible Defense Mechanism against Insects. *Science* 175: 776-777
- Grimault V, Gélie B, Lemattre M, Prior P, Schmit J (1994) Comparative histology of resistant and susceptible tomato cultivars infected by *Pseudomonas solanacearum*. *Physiological and molecular plant pathology* 44: 105-123
- Grimault V, Gélie, B., Lemattre, M., Prior, P., and Schmit, J (1994) Comparative histology of resistant and susceptible tomato cultivars infected by *Pseudomonas solanacearum*. *Physiological and Molecular Plant Pathology* 44: 105-123
- Gully K, Pelletier S, Guillou MC, Ferrand M, Aligon S, Pokotylo I, Perrin A, Vergne E, Fagard M, Ruelland E *et al* (2019) The SCOOP12 peptide regulates defense response and root elongation in *Arabidopsis thaliana*. *J Exp Bot* 70: 1349-1365
- Guo H, Nolan TM, Song G, Liu S, Xie Z, Chen J, Schnable PS, Walley JW, Yin Y (2018) FERONIA Receptor Kinase Contributes to Plant Immunity by Suppressing Jasmonic Acid Signaling in *Arabidopsis thaliana*. *Curr Biol* 28: 3316-3324 e3316
- Gupta R, Lee SE, Agrawal GK, Rakwal R, Park S, Wang Y, Kim ST (2015a) Understanding the plant-pathogen interactions in the context of proteomics-generated apoplastic proteins inventory. *Frontiers in plant science* 6: 352

References

- Gupta R, Lee SE, Agrawal GK, Rakwal R, Park S, Wang Y, Kim ST (2015b) Understanding the plant-pathogen interactions in the context of proteomics-generated apoplastic proteins inventory. *Front Plant Sci* 6: 352
- Haeussler M, Schonig K, Eckert H, Eschstruth A, Mianne J, Renaud JB, Schneider-Maunoury S, Shkumatava A, Teboul L, Kent J *et al* (2016) Evaluation of off-target and on-target scoring algorithms and integration into the guide RNA selection tool CRISPOR. *Genome Biol* 17: 148
- Hander T, Fernandez-Fernandez AD, Kumpf RP, Willems P, Schatowitz H, Rombaut D, Staes A, Nolf J, Pottier R, Yao P *et al* (2019) Damage on plants activates Ca(2+)-dependent metacaspases for release of immunomodulatory peptides. *Science* 363
- Haruta M, Sabat G, Stecker K, Minkoff BB, Sussman MR (2014) A peptide hormone and its receptor protein kinase regulate plant cell expansion. *Science* 343: 408-411
- Hayward AC (1991) Biology and epidemiology of bacterial wilt caused by *pseudomonas solanacearum*. *Annu Rev Phytopathol* 29: 65-87
- Homma F, Huang J, Hoorn RALvd (2023) AlphaFold-multimer predicts cross-kingdom interactions at the plant-pathogen interface. *bioRxiv*: 2023.2004.2003.535425
- Hou S, Liu D, Huang S, Luo D, Liu Z, Xiang Q, Wang P, Mu R, Han Z, Chen S *et al* (2021) The Arabidopsis MIK2 receptor elicits immunity by sensing a conserved signature from phytocytokines and microbes. *Nat Commun* 12: 5494
- Hou S, Liu Z, Shen H, Wu D (2019) Damage-Associated Molecular Pattern-Triggered Immunity in Plants. *Front Plant Sci* 10: 646
- Hou S, Wang X, Chen D, Yang X, Wang M, Turra D, Di Pietro A, Zhang W (2014) The secreted peptide PIP1 amplifies immunity through receptor-like kinase 7. *PLoS Pathog* 10: e1004331
- Huang Q, Allen C (2000) Polygalacturonases are required for rapid colonization and full virulence of *Ralstonia solanacearum* on tomato plants. *Physiological and molecular plant pathology* 57: 77-83
- Huffaker A, Dafoe NJ, Schmelz EA (2011) ZmPep1, an ortholog of Arabidopsis elicitor peptide 1, regulates maize innate immunity and enhances disease resistance. *Plant Physiol* 155: 1325-1338
- Huffaker A, Pearce G, Ryan CA (2006) An endogenous peptide signal in Arabidopsis activates components of the innate immune response. *Proc Natl Acad Sci U S A* 103: 10098-10103
- Igarashi D, Tsuda K, Katagiri F (2012) The peptide growth factor, phytosulfokine, attenuates pattern-triggered immunity. *Plant J* 71: 194-204
- Inoue I, Namiki F, Tsuge T (2002) Plant colonization by the vascular wilt fungus *Fusarium oxysporum* requires *FOW1*, a gene encoding a mitochondrial protein. *Plant Cell* 14: 1869-1883
- Ishihara T, Mitsuhashi I, Takahashi H, Nakahara K (2012b) Transcriptome analysis of quantitative resistance-specific response upon *Ralstonia solanacearum* infection in tomato. *PLoS One* 7: e46763
- Jones JD, Dangl JL (2006) The plant immune system. *Nature* 444: 323-329

References

- Jorda L, Coego A, Conejero V, Vera P (1999) A genomic cluster containing four differentially regulated subtilisin-like processing protease genes is in tomato plants. *J Biol Chem* 274: 2360-2365
- Jorda L, Conejero V, Vera P (2000) Characterization of P69E and P69F, two differentially regulated genes encoding new members of the subtilisin-like proteinase family from tomato plants. *Plant Physiol* 122: 67-74
- Kashyap A, Jiménez - Jiménez ÁL, Zhang W, Capellades M, Srinivasan S, Laromaine A, Serra O, Figueras M, Rencoret J, Gutiérrez A (2022) Induced ligno - suberin vascular coating and tyramine - derived hydroxycinnamic acid amides restrict *Ralstonia solanacearum* colonization in resistant tomato. *New Phytologist* 234: 1411-1429
- Kim S, Park M, Yeom SI, Kim YM, Lee JM, Lee HA, Seo E, Choi J, Cheong K, Kim KT *et al* (2014) Genome sequence of the hot pepper provides insights into the evolution of pungency in Capsicum species. *Nat Genet* 46: 270-278
- Kumar JS, Umesha S, Prasad KS, Niranjana P (2016) Detection of quorum sensing molecules and biofilm formation in *Ralstonia solanacearum*. *Current microbiology* 72: 297-305
- Lagrimini LM, Burkhart W, Moyer M, Rothstein S (1987) Molecular cloning of complementary DNA encoding the lignin-forming peroxidase from tobacco: Molecular analysis and tissue-specific expression. *Proc Natl Acad Sci U S A* 84: 7542-7546
- Lauge R, Goodwin PH, de Wit PJ, Joosten MH (2000) Specific HR-associated recognition of secreted proteins from *Cladosporium fulvum* occurs in both host and non-host plants. *Plant J* 23: 735-745
- Li C, Yeh FL, Cheung AY, Duan Q, Kita D, Liu MC, Maman J, Luu EJ, Wu BW, Gates L *et al* (2015) Glycosylphosphatidylinositol-anchored proteins as chaperones and co-receptors for FERONIA receptor kinase signaling in Arabidopsis. *Elife* 4
- Li J, Ma X, Wang C, Liu S, Yu G, Gao M, Qian H, Liu M, Luisi BF, Gabriel DW *et al* (2022) Acetylation of a fungal effector that translocates host PR1 facilitates virulence. *Elife* 11
- Li ZT, Dhekney SA, Gray DJ (2011) PR-1 gene family of grapevine: a uniquely duplicated PR-1 gene from a Vitis interspecific hybrid confers high level resistance to bacterial disease in transgenic tobacco. *Plant cell reports* 30: 1-11
- Lincoln JE, Sanchez JP, Zumstein K, Gilchrist DG (2018) Plant and animal PR1 family members inhibit programmed cell death and suppress bacterial pathogens in plant tissues. *Mol Plant Pathol* 19: 2111-2123
- Liu H, Zhang S, Schell MA, Denny TP (2005) Pyramiding unmarked deletions in *Ralstonia solanacearum* shows that secreted proteins in addition to plant cell-wall-degrading enzymes contribute to virulence. *Molecular plant-microbe interactions* 18: 1296-1305
- Liu Z, Hou S, Rodrigues O, Wang P, Luo D, Munemasa S, Lei J, Liu J, Ortiz-Moreno FA, Wang X *et al* (2022) Phytocytokine signalling reopens stomata in plant immunity and water loss. *Nature* 605: 332-339
- Liu Z, Wu Y, Yang F, Zhang Y, Chen S, Xie Q, Tian X, Zhou JM (2013) BIK1 interacts with PEPRs to mediate ethylene-induced immunity. *Proc Natl Acad Sci U S A* 110: 6205-6210
- Lozano-Torres JL, Wilbers RH, Gawronski P, Boshoven JC, Finkers-Tomczak A, Cordewener JH, America AH, Overmars HA, Van 't Klooster JW, Baranowski L (2012) Dual disease resistance mediated by the immune receptor Cf-2 in tomato requires a common virulence

References

- target of a fungus and a nematode. *Proceedings of the National Academy of Sciences* 109: 10119-10124
- Lu S, Friesen TL, Faris JD (2011) Molecular characterization and genomic mapping of the pathogenesis-related protein 1 (PR-1) gene family in hexaploid wheat (*Triticum aestivum* L.). *Mol Genet Genomics* 285: 485-503
- Luo X, Tian T, Feng L, Yang X, Li L, Tan X, Wu W, Li Z, Treves H, Serneels F *et al* (2023) Pathogenesis-related protein 1 suppresses oomycete pathogen by targeting against AMPK kinase complex. *J Adv Res* 43: 13-26
- Macho AP, Zipfel C (2014) Plant PRRs and the activation of innate immune signaling. *Mol Cell* 54: 263-272
- Mahon P, Bateman A (2000) The PA domain: a protease-associated domain. *Protein Sci* 9: 1930-1934
- Mansfield J, Genin S, Magori S, Citovsky V, Sriariyanum M, Ronald P, Dow M, Verdier V, Beer SV, Machado MA *et al* (2012) Top 10 plant pathogenic bacteria in molecular plant pathology. *Mol Plant Pathol* 13: 614-629
- Marlatt M, Correll JC, Kaufmann P, Cooper P (1996) Two genetically distinct populations of *fusarium oxysporum* f. sp. *lycopersici* race 3 in the united states. *Plant Disease* 80: 1336
- Matsubayashi Y (2014) Posttranslationally modified small-peptide signals in plants. *Annu Rev Plant Biol* 65: 385-413
- Matsuzaki Y, Ogawa-Ohnishi M, Mori A, Matsubayashi Y (2010) Secreted peptide signals required for maintenance of root stem cell niche in Arabidopsis. *Science* 329: 1065-1067
- Mazier M, Flamain F, Nicolai M, Sarnette V, Caranta C (2011) Knock-down of both *eIF4E1* and *eIF4E2* genes confers broad-spectrum resistance against potyviruses in tomato. *PLoS One* 6: e29595
- McGarvey JA, Denny TP, Schell MA (1999) Spatial-Temporal and Quantitative Analysis of Growth and EPS I Production by *Ralstonia solanacearum* in Resistant and Susceptible Tomato Cultivars. *Phytopathology* 89: 1233-1239
- Meichtry J, Amrhein N, Schaller A (1999) Characterization of the subtilase gene family in tomato (*Lycopersicon esculentum* Mill.). *Plant Mol Biol* 39: 749-760
- Melotto M, Underwood W, He SY (2008) Role of stomata in plant innate immunity and foliar bacterial diseases. *Annu Rev Phytopathol* 46: 101-122
- Mes JJ, Weststeijn EA, Herlaar F, Lambalk JJ, Wijbrandi J, Haring MA, Cornelissen BJ (1999) Biological and Molecular Characterization of *Fusarium oxysporum* f. sp. *lycopersici* Divides Race 1 Isolates into Separate Virulence Groups. *Phytopathology* 89: 156-160
- Meyer M, Leptihn, S., Welz, M., Schaller, A. (2016) Functional Characterization of Propeptides in Plant Subtilases as Intramolecular Chaperones and Inhibitors of the Mature Protease*. *J Biol Chem* 291: 19449-19461
- Mignolet-Spruyt L, Xu E, Idanheimo N, Hoeberichts FA, Muhlenbock P, Brosche M, Van Breusegem F, Kangasjarvi J (2016) Spreading the news: subcellular and organellar reactive oxygen species production and signalling. *J Exp Bot* 67: 3831-3844
- Mirdita M, Schutze K, Moriwaki Y, Heo L, Ovchinnikov S, Steinegger M (2022) ColabFold: making protein folding accessible to all. *Nat Methods* 19: 679-+

References

- Mori Y, Hosoi Y, Ishikawa S, Hayashi K, Asai Y, Ohnishi H, Shimatani M, Inoue K, Ikeda K, Nakayashiki H (2018) Ralfuranones contribute to mushroom - type biofilm formation by *Ralstonia solanacearum* strain OE1 - 1. *Molecular plant pathology* 19: 975-985
- Mori Y, Inoue K, Ikeda K, Nakayashiki H, Higashimoto C, Ohnishi K, Kiba A, Hikichi Y (2016) The vascular plant - pathogenic bacterium *Ralstonia solanacearum* produces biofilms required for its virulence on the surfaces of tomato cells adjacent to intercellular spaces. *Molecular Plant Pathology* 17: 890-902
- Mosher S, Seybold H, Rodriguez P, Stahl M, Davies KA, Dayaratne S, Morillo SA, Wierzbica M, Favory B, Keller H *et al* (2013) The tyrosine-sulfated peptide receptors PSKR1 and PSY1R modify the immunity of Arabidopsis to biotrophic and necrotrophic pathogens in an antagonistic manner. *Plant J* 73: 469-482
- Mueller AN, Ziemann S, Treitschke S, Assmann D, Doehlemann G (2013) Compatibility in the Ustilago maydis-maize interaction requires inhibition of host cysteine proteases by the fungal effector Pit2. *PLoS Pathog* 9: e1003177
- Muller L, Cameron A, Fortenberry Y, Apletalina EV, Lindberg I (2000) Processing and sorting of the prohormone convertase 2 propeptide. *J Biol Chem* 275: 39213-39222
- Nakaho K, Inoue H, Takayama T, Miyagawa H (2004) Distribution and multiplication of *Ralstonia solanacearum* in tomato plants with resistance derived from different origins. *Journal of General Plant Pathology* 70: 115-119
- Nebes VL, Jones EW (1991) Activation of the proteinase B precursor of the yeast *Saccharomyces cerevisiae* by autocatalysis and by an internal sequence. *J Biol Chem* 266: 22851-22857
- Ngou BPM, Ahn H-K, Ding P, Jones JD (2021) Mutual potentiation of plant immunity by cell-surface and intracellular receptors. *Nature* 592: 110-115
- Niderman T, Genetet I, Bruyere T, Gees R, Stintzi A, Legrand M, Fritig B, Mosinger E (1995) Pathogenesis-related PR-1 proteins are antifungal (isolation and characterization of three 14-kilodalton proteins of tomato and of a basic PR-1 of tobacco with inhibitory activity against *Phytophthora infestans*). *Plant physiology* 108: 17-27
- Olsson V, Joos L, Zhu S, Gevaert K, Butenko MA, De Smet I (2019) Look Closely, the Beautiful May Be Small: Precursor-Derived Peptides in Plants. *Annu Rev Plant Biol* 70: 153-186
- Ottmann C, Rose R, Huttenlocher F, Cedzich A, Hauske P, Kaiser M, Huber R, Schaller A (2009) Structural basis for Ca²⁺-independence and activation by homodimerization of tomato subtilase 3. *Proc Natl Acad Sci U S A* 106: 17223-17228
- Ou Y, Lu X, Zi Q, Xun Q, Zhang J, Wu Y, Shi H, Wei Z, Zhao B, Zhang X *et al* (2016) RGF1 INSENSITIVE 1 to 5, a group of LRR receptor-like kinases, are essential for the perception of root meristem growth factor 1 in *Arabidopsis thaliana*. *Cell Res* 26: 686-698
- Passardi F, Cosio C, Penel C, Dunand C (2005) Peroxidases have more functions than a Swiss army knife. *Plant cell reports* 24: 255-265
- Patharkar OR, Walker JC (2016) Core Mechanisms Regulating Developmentally Timed and Environmentally Triggered Abscission. *Plant Physiol* 172: 510-520
- Paulus JK, Kourelis J, Ramasubramanian S, Homma F, Godson A, Horger AC, Hong TN, Krahn D, Ossorio Carballo L, Wang S *et al* (2020) Extracellular proteolytic cascade in tomato activates immune protease Rcr3. *Proc Natl Acad Sci U S A* 117: 17409-17417

References

- Pearce G, Moura DS, Stratmann J, Ryan CA, Jr. (2001) RALF, a 5-kDa ubiquitous polypeptide in plants, arrests root growth and development. *Proc Natl Acad Sci U S A* 98: 12843-12847
- Pearce G, Strydom D, Johnson S, Ryan CA (1991) A polypeptide from tomato leaves induces wound-inducible proteinase inhibitor proteins. *Science* 253: 895-897
- Pecenikova T, Pejchar P, Moravec T, Drs M, Haluska S, Santrucek J, Potocka A, Zarsky V, Potocky M (2022) Immunity functions of Arabidopsis pathogenesis-related 1 are coupled but not confined to its C-terminus processing and trafficking. *Mol Plant Pathol* 23: 664-678
- Pecenikova T, Pleskot R, Zarsky V (2017) Subcellular Localization of Arabidopsis Pathogenesis-Related 1 (PR1) Protein. *Int J Mol Sci* 18
- Perez-Lopez E, Hossain MM, Wei Y, Todd CD, Bonham-Smith PC (2021) A clubroot pathogen effector targets cruciferous cysteine proteases to suppress plant immunity. *Virulence* 12: 2327-2340
- Planas-Marques M, Bernardo-Faura M, Paulus J, Kaschani F, Kaiser M, Valls M, van der Hoorn RAL, Coll NS (2018) Protease Activities Triggered by *Ralstonia solanacearum* Infection in Susceptible and Tolerant Tomato Lines. *Mol Cell Proteomics* 17: 1112-1125
- Planas-Marques M, Kressin JP, Kashyap A, Panthee DR, Louws FJ, Coll NS, Valls M (2020) Four bottlenecks restrict colonization and invasion by the pathogen *Ralstonia solanacearum* in resistant tomato. *J Exp Bot* 71: 2157-2171
- Potato Genome Sequencing C, Xu X, Pan S, Cheng S, Zhang B, Mu D, Ni P, Zhang G, Yang S, Li R *et al* (2011) Genome sequence and analysis of the tuber crop potato. *Nature* 475: 189-195
- Poueymiro M, Cunnac S, Barberis P, Deslandes L, Peeters N, Cazale-Noel AC, Boucher C, Genin S (2009) Two type III secretion system effectors from *Ralstonia solanacearum* GMI1000 determine host-range specificity on tobacco. *Mol Plant Microbe Interact* 22: 538-550
- Power SD, Adams RM, Wells JA (1986) Secretion and autoproteolytic maturation of subtilisin. *Proc Natl Acad Sci U S A* 83: 3096-3100
- Ramirez V, Lopez A, Mauch-Mani B, Gil MJ, Vera P (2013) An extracellular subtilase switch for immune priming in Arabidopsis. *PLoS Pathog* 9: e1003445
- Ranf S, Eschen-Lippold L, Pecher P, Lee J, Scheel D (2011) Interplay between calcium signalling and early signalling elements during defence responses to microbe- or damage-associated molecular patterns. *Plant J* 68: 100-113
- Rappsilber J, Mann M, Ishihama Y (2007) Protocol for micro-purification, enrichment, pre-fractionation and storage of peptides for proteomics using StageTips. *Nat Protoc* 2: 1896-1906
- Reichardt S, Reppe D, Tuzhikov AI, Galiullina RA, Planas-Marques M, Chichkova NV, Vartapetian AB, Stintzi A, Schaller A (2018) The tomato subtilase family includes several cell death-related proteinases with caspase specificity. *Sci Rep* 8: 10531
- Rep M, van der Does HC, Meijer M, van Wijk R, Houterman PM, Dekker HL, de Koster CG, Cornelissen BJ (2004) A small, cysteine-rich protein secreted by *Fusarium oxysporum* during colonization of xylem vessels is required for I-3-mediated resistance in tomato. *Mol Microbiol* 53: 1373-1383

References

- Rhodes J, Yang H, Moussu S, Boutrot F, Santiago J, Zipfel C (2021) Perception of a divergent family of phytocytokines by the Arabidopsis receptor kinase MIK2. *Nat Commun* 12: 705
- Robert-Seilanianantz A, Grant M, Jones JD (2011) Hormone crosstalk in plant disease and defense: more than just jasmonate-salicylate antagonism. *Annu Rev Phytopathol* 49: 317-343
- Rodiuc N, Barlet X, Hok S, Perfus-Barbeoch L, Allasia V, Engler G, Seassau A, Marteu N, de Almeida-Engler J, Panabieres F *et al* (2016) Evolutionarily distant pathogens require the Arabidopsis phytosulfokine signalling pathway to establish disease. *Plant Cell Environ* 39: 1396-1407
- Rooney HC, Van't Klooster JW, van der Hoorn RA, Joosten MH, Jones JD, de Wit PJ (2005) Cladosporium Avr2 inhibits tomato Rcr3 protease required for Cf-2-dependent disease resistance. *Science* 308: 1783-1786
- Ross A, Yamada K, Hiruma K, Yamashita-Yamada M, Lu X, Takano Y, Tsuda K, Saijo Y (2014) The Arabidopsis PEPR pathway couples local and systemic plant immunity. *EMBO J* 33: 62-75
- Royek S, Bayer M, Pfannstiel J, Pleiss J, Ingram G, Stintzi A, Schaller A (2022) Processing of a plant peptide hormone precursor facilitated by posttranslational tyrosine sulfation. *Proc Natl Acad Sci U S A* 119: e2201195119
- Ryan CA, Pearce G (2003) Systemins: a functionally defined family of peptide signals that regulate defensive genes in Solanaceae species. *Proc Natl Acad Sci U S A* 100 Suppl 2: 14577-14580
- Saile E, McGarvey JA, Schell MA, Denny TP (1997) Role of extracellular polysaccharide and endoglucanase in root invasion and colonization of tomato plants by *Ralstonia solanacearum*. *Phytopathology* 87: 1264-1271
- Santiago J, Brandt B, Wildhagen M, Hohmann U, Hothorn LA, Butenko MA, Hothorn M (2016) Mechanistic insight into a peptide hormone signaling complex mediating floral organ abscission. *Elife* 5
- Sarowar S, Kim YJ, Kim EN, Kim KD, Hwang BK, Islam R, Shin JS (2005) Overexpression of a pepper basic *pathogenesis-related protein 1* gene in tobacco plants enhances resistance to heavy metal and pathogen stresses. *Plant cell reports* 24: 216-224
- Savary S, Willocquet L, Pethybridge SJ, Esker P, McRoberts N, Nelson A (2019) The global burden of pathogens and pests on major food crops. *Nat Ecol Evol* 3: 430-439
- Schaller A, Stintzi A, Rivas S, Serrano I, Chichkova NV, Vartapetian AB, Martinez D, Guamet JJ, Sueldo DJ, van der Hoorn RAL *et al* (2018) From structure to function - a family portrait of plant subtilases. *New Phytol* 218: 901-915
- Schardon K, Hohl M, Graff L, Pfannstiel J, Schulze W, Stintzi A, Schaller A (2016) Precursor processing for plant peptide hormone maturation by subtilisin-like serine proteinases. *Science* 354: 1594-1597
- Schilling O, Huesgen PF, Barre O, Auf dem Keller U, Overall CM (2011) Characterization of the prime and non-prime active site specificities of proteases by proteome-derived peptide libraries and tandem mass spectrometry. *Nat Protoc* 6: 111-120
- Schilling O, Overall CM (2008) Proteome-derived, database-searchable peptide libraries for identifying protease cleavage sites. *Nat Biotechnol* 26: 685-694

References

- Scott J, Wang J, Hanson P, 2004. Breeding tomatoes for resistance to bacterial wilt, a global view, I International Symposium on Tomato Diseases 695. pp. 161-172.
- Shin SH, Pak J-H, Kim MJ, Kim HJ, Oh JS, Choi HK, Jung HW, Chung YS (2014) An acidic PATHOGENESIS-RELATED1 gene of *Oryza grandiglumis* is involved in disease resistance response against bacterial infection. *The plant pathology journal* 30: 208
- Smith EF (1896) A bacterial disease of the tomato, eggplant, and Irish potato (*Bacillus solanacearum* sp.).
- Smith EL, Markland FS, Kasper CB, DeLange RJ, Landon M, Evans WH (1966) The complete amino acid sequence of two types of subtilisin, BPN' and Carlsberg. *J Biol Chem* 241: 5974-5976
- Song J, Win J, Tian M, Schornack S, Kaschani F, Ilyas M, van der Hoorn RA, Kamoun S (2009) Apoplastic effectors secreted by two unrelated eukaryotic plant pathogens target the tomato defense protease Rcr3. *Proc Natl Acad Sci U S A* 106: 1654-1659
- Stegmann M, Monaghan J, Smakowska-Luzan E, Rovenich H, Lehner A, Holton N, Belkhadir Y, Zipfel C (2017) The receptor kinase FER is a RALF-regulated scaffold controlling plant immune signaling. *Science* 355: 287-289
- Stegmann M, Zecua-Ramirez P, Ludwig C, Lee HS, Peterson B, Nimchuk ZL, Belkhadir Y, Huckelhoven R (2022) RGI-GOLVEN signaling promotes cell surface immune receptor abundance to regulate plant immunity. *EMBO Rep* 23: e53281
- Stenvik GE, Tandstad NM, Guo Y, Shi CL, Kristiansen W, Holmgren A, Clark SE, Aalen RB, Butenko MA (2008) The EPIP peptide of INFLORESCENCE DEFICIENT IN ABSCISSION is sufficient to induce abscission in arabidopsis through the receptor-like kinases HAESA and HAESA-LIKE2. *Plant Cell* 20: 1805-1817
- Sung YC, Outram MA, Breen S, Wang C, Dagvadorj B, Winterberg B, Kobe B, Williams SJ, Solomon PS (2021) PR1-mediated defence via C-terminal peptide release is targeted by a fungal pathogen effector. *New Phytol* 229: 3467-3480
- Tan-Wilson A, Bandak B, Prabu-Jeyabalan M (2012) The PA domain is crucial for determining optimum substrate length for soybean protease C1: structure and kinetics correlate with molecular function. *Plant Physiol Biochem* 53: 27-32
- Thaler JS, Humphrey PT, Whiteman NK (2012) Evolution of jasmonate and salicylate signal crosstalk. *Trends Plant Sci* 17: 260-270
- Tian M, Benedetti B, Kamoun S (2005) A Second Kazal-like protease inhibitor from *Phytophthora infestans* inhibits and interacts with the apoplastic pathogenesis-related protease P69B of tomato. *Plant Physiol* 138: 1785-1793
- Tian M, Huitema E, Da Cunha L, Torto-Alalibo T, Kamoun S (2004) A Kazal-like extracellular serine protease inhibitor from *Phytophthora infestans* targets the tomato pathogenesis-related protease P69B. *J Biol Chem* 279: 26370-26377
- Tian M, Win J, Song J, van der Hoorn R, van der Knaap E, Kamoun S (2007) A *Phytophthora infestans* cystatin-like protein targets a novel tomato papain-like apoplastic protease. *Plant Physiol* 143: 364-377
- Tintor N, Ross A, Kanehara K, Yamada K, Fan L, Kemmerling B, Nurnberger T, Tsuda K, Saijo Y (2013) Layered pattern receptor signaling via ethylene and endogenous elicitor peptides during Arabidopsis immunity to bacterial infection. *Proc Natl Acad Sci U S A* 110: 6211-6216

References

- Tomato Genome C (2012) The tomato genome sequence provides insights into fleshy fruit evolution. *Nature* 485: 635-641
- Tornero P, Conejero V, Vera P (1994) A gene encoding a novel isoform of the PR-1 protein family from tomato is induced upon viroid infection. *Molecular and General Genetics MGG* 243: 47-53
- Tornero P, Conejero V, Vera P (1997) Identification of a new pathogen-induced member of the subtilisin-like processing protease family from plants. *J Biol Chem* 272: 14412-14419
- Tornero P, Mayda E, Gomez MD, Canas L, Conejero V, Vera P (1996) Characterization of LRP, a leucine-rich repeat (LRR) protein from tomato plants that is processed during pathogenesis. *Plant J* 10: 315-330
- Tyanova S, Temu T, Cox J (2016) The MaxQuant computational platform for mass spectrometry-based shotgun proteomics. *Nat Protoc* 11: 2301-2319
- Vaahtera L, Brosche M, Wrzaczek M, Kangasjarvi J (2014) Specificity in ROS signaling and transcript signatures. *Antioxid Redox Signal* 21: 1422-1441
- Valls M, Genin S, Boucher C (2006) Integrated regulation of the type III secretion system and other virulence determinants in *Ralstonia solanacearum*. *PLoS pathogens* 2: e82
- van der Hoorn RA (2008) Plant proteases: from phenotypes to molecular mechanisms. *Annu Rev Plant Biol* 59: 191-223
- van der Hoorn RAL, Klemencic M (2021) Plant proteases: from molecular mechanisms to functions in development and immunity. *J Exp Bot* 72: 3337-3339
- van Kan JA, Joosten MH, Wagemakers CA, van den Berg-Velthuis GC, de Wit PJ (1992) Differential accumulation of mRNAs encoding extracellular and intracellular PR proteins in tomato induced by virulent and avirulent races of *Cladosporium fulvum*. *Plant molecular biology* 20: 513-527
- Van Loon L, Van Kammen A (1970) Polyacrylamide disc electrophoresis of the soluble leaf proteins from *Nicotiana tabacum* var. 'Samsun' and 'Samsun NN': II. Changes in protein constitution after infection with tobacco mosaic virus. *Virology* 40: 199-211
- Van Loon LC (1982) Regulation of Changes in Proteins and Enzymes Associated with Active Defence against Virus Infection. In: *Active Defense Mechanisms in Plants*, Wood R.K.S. (ed.) pp. 247-273. Springer US: Boston, MA
- Vartapetian AB, Tuzhikov AI, Chichkova NV, Taliansky M, Wolpert TJ (2011) A plant alternative to animal caspases: subtilisin-like proteases. *Cell Death Differ* 18: 1289-1297
- Vasse J, Frey P, Trigalet A (1995) Microscopic studies of intercellular infection and protoxylem invasion of tomato roots by *Pseudomonas solanacearum*. *MPMI-Molecular Plant Microbe Interactions* 8: 241-251
- Vasse J, Genin S, Frey P, Boucher C, Brito B (2000) The hrpB and hrpG regulatory genes of *Ralstonia solanacearum* are required for different stages of the tomato root infection process. *Molecular plant-microbe interactions* 13: 259-267
- Vera P, and Conejero, V (1989) The induction and accumulation of the pathogenesis-related P69 proteinase in tomato during citrus exocortis viroid infection and in response to chemical treatments. *Physiological and Molecular Plant Pathology* 34: 323-334
- Vera P, Conejero V (1988) Pathogenesis-related proteins of tomato : p-69 as an alkaline endoproteinase. *Plant Physiol* 87: 58-63

References









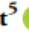



- Vera P, Yago JH, Conejero V (1989) Immunogold localization of the citrus exocortis viroid-induced pathogenesis-related proteinase p69 in tomato leaves. *Plant Physiol* 91: 119-123
- Verhage A, van Wees SC, Pieterse CM (2010) Plant immunity: it's the hormones talking, but what do they say? *Plant Physiol* 154: 536-540
- Vey M, Schafer W, Berghofer S, Klenk HD, Garten W (1994) Maturation of the trans-Golgi network protease furin: compartmentalization of propeptide removal, substrate cleavage, and COOH-terminal truncation. *J Cell Biol* 127: 1829-1842
- Wang J-F, Hanson P, Barnes J (1998) Worldwide evaluation of an international set of resistance sources to bacterial wilt in tomato. In: *Bacterial wilt disease: Molecular and ecological aspects*, pp. 269-275. Springer:
- Wang L, Einig E, Almeida-Trapp M, Albert M, Fliegmann J, Mithofer A, Kalbacher H, Felix G (2018) The systemin receptor SYR1 enhances resistance of tomato against herbivorous insects. *Nat Plants* 4: 152-156
- Wang P, Jia H, Guo T, Zhang Y, Wang W, Nishimura H, Li Z, Kawano Y (2023) The secreted immune response peptide 1 functions as a phytocytokine in rice immunity. *J Exp Bot* 74: 1059-1073
- Wang S, Xing R, Wang Y, Shu H, Fu S, Huang J, Paulus JK, Schuster M, Saunders DGO, Win J *et al* (2021) Cleavage of a pathogen apoplastic protein by plant subtilases activates host immunity. *New Phytol* 229: 3424-3439
- Wang X, Hou S, Wu Q, Lin M, Acharya BR, Wu D, Zhang W (2017) IDL6-HAE/HSL2 impacts pectin degradation and resistance to *Pseudomonas syringae* pv tomato DC3000 in Arabidopsis leaves. *Plant J* 89: 250-263
- Whitford R, Fernandez A, Tejos R, Perez AC, Kleine-Vehn J, Vanneste S, Drozdzecki A, Leitner J, Abas L, Aerts M *et al* (2012) GOLVEN secretory peptides regulate auxin carrier turnover during plant gravitropic responses. *Dev Cell* 22: 678-685
- Wydra K, Beri H (2007) Immunohistochemical changes in methyl-ester distribution of homogalacturonan and side chain composition of rhamnogalacturonan I as possible components of basal resistance in tomato inoculated with *Ralstonia solanacearum*. *Physiological and Molecular Plant Pathology* 70: 13-24
- Xiao Y, Hsiao TH, Suresh U, Chen HI, Wu X, Wolf SE, Chen Y (2014) A novel significance score for gene selection and ranking. *Bioinformatics* 30: 801-807
- Yadeta KA, J. Thomma BP (2013) The xylem as battleground for plant hosts and vascular wilt pathogens. *Frontiers in plant science* 4: 97
- Yamaguchi Y, Huffaker A, Bryan AC, Tax FE, Ryan CA (2010) PEPR2 is a second receptor for the Pep1 and Pep2 peptides and contributes to defense responses in Arabidopsis. *Plant Cell* 22: 508-522
- Yu SH, Ferretti D, Schessner JP, Rudolph JD, Borner GHH, Cox J (2020) Expanding the Perseus Software for Omics Data Analysis With Custom Plugins. *Curr Protoc Bioinformatics* 71: e105
- Yuan M, Jiang Z, Bi G, Nomura K, Liu M, Wang Y, Cai B, Zhou J-M, He SY, Xin X-F (2021) Pattern-recognition receptors are required for NLR-mediated plant immunity. *Nature* 592: 105-109
- Zhang B, Tremousaygue D, Denance N, van Esse HP, Horger AC, Dabos P, Goffner D, Thomma BP, van der Hoorn RA, Tuominen H (2014) PIRIN2 stabilizes cysteine protease

References

- XCP2 and increases susceptibility to the vascular pathogen *Ralstonia solanacearum* in *Arabidopsis*. *Plant J* 79: 1009-1019
- Zhang H, Hu Z, Lei C, Zheng C, Wang J, Shao S, Li X, Xia X, Cai X, Zhou J *et al* (2018) A Plant Phytosulfokine Peptide Initiates Auxin-Dependent Immunity through Cytosolic Ca(2+) Signaling in Tomato. *Plant Cell* 30: 652-667
- Ziegler MT, Thomas SR, Danna KJ (2000) Accumulation of a thermostable endo-1,4- β -D-glucanase in the apoplast of *Arabidopsis thaliana* leaves. *Molecular Breeding* 6: 37-46
- Ziemann S, van der Linde K, Lahrmann U, Acar B, Kaschani F, Colby T, Kaiser M, Ding Y, Schmelz E, Huffaker A *et al* (2018) An apoplastic peptide activates salicylic acid signalling in maize. *Nat Plants* 4: 172-180
- Zipfel C, Kunze G, Chinchilla D, Caniard A, Jones JD, Boller T, Felix G (2006) Perception of the bacterial PAMP EF-Tu by the receptor EFR restricts Agrobacterium-mediated transformation. *Cell* 125: 749-760
- Zuluaga AP, Sole M, Lu H, Gongora-Castillo E, Vaillancourt B, Coll N, Buell CR, Valls M (2015) Transcriptome responses to *Ralstonia solanacearum* infection in the roots of the wild potato *Solanum commersonii*. *BMC Genomics* 16: 246
- Zuluaga AP, Vega-Arreguin JC, Fei Z, Matas AJ, Patev S, Fry WE, Rose JK (2016) Analysis of the tomato leaf transcriptome during successive hemibiotrophic stages of a compatible interaction with the oomycete pathogen *Phytophthora infestans*. *Mol Plant Pathol* 17: 42-54

Annex

Induced ligno-suberin vascular coating and tyramine-derived hydroxycinnamic acid amides restrict *Ralstonia solanacearum* colonization in resistant tomato

Anurag Kashyap¹ , Álvaro Luis Jiménez-Jiménez^{1*} , Weiqi Zhang^{1*} , Montserrat Capellades^{1,2} ,
Sumithra Srinivasan³ , Anna Laromaine³ , Olga Serra⁴ , Mercè Figueras⁴ , Jorge Rencoret⁵ ,
Ana Gutiérrez⁵ , Marc Valls^{1,6}  and Nuria S. Coll^{1,2} 

¹Centre for Research in Agricultural Genomics (CRAG), CSIC-IRTA-UAB-UB, Campus UAB, 08193 Bellaterra, Spain; ²Consejo Superior de Investigaciones Científicas (CSIC), 08001 Barcelona, Spain; ³Institute of Material Science of Barcelona (ICMAB), CSIC, Campus UAB, 08193 Bellaterra, Spain; ⁴Laboratori del Suro, Biology Department, University of Girona, Campus Montilivi, 17003 Girona, Spain; ⁵Institute of Natural Resources and Agrobiology of Seville (IRNAS), CSIC, 41012 Seville, Spain; ⁶Department of Genetics, University of Barcelona, 08028 Barcelona, Spain

Summary

Author for correspondence:

Nuria S. Coll

Email: nuria.sanchez-coll@cragenomica.es

Received: 17 November 2021

Accepted: 3 January 2022

New Phytologist (2022) 234: 1411–1429

doi: 10.1111/nph.17982

Key words: bacterial wilt, feruloyltyramine, HCAAs, lignin, *Ralstonia solanacearum*, suberin, tomato, vascular coating.

- Tomato varieties resistant to the bacterial wilt pathogen *Ralstonia solanacearum* have the ability to restrict bacterial movement in the plant. Inducible vascular cell wall reinforcements seem to play a key role in confining *R. solanacearum* into the xylem vasculature of resistant tomato. However, the type of compounds involved in such vascular physico-chemical barriers remain understudied, while being a key component of resistance.
- Here we use a combination of histological and live-imaging techniques, together with spectroscopy and gene expression analysis to understand the nature of *R. solanacearum*-induced formation of vascular coatings in resistant tomato.
- We describe that resistant tomato specifically responds to infection by assembling a vascular structural barrier formed by a ligno-suberin coating and tyramine-derived hydroxycinnamic acid amides. Further, we show that overexpressing genes of the ligno-suberin pathway in a commercial susceptible variety of tomato restricts *R. solanacearum* movement inside the plant and slows disease progression, enhancing resistance to the pathogen.
- We propose that the induced barrier in resistant plants does not only restrict the movement of the pathogen, but may also prevent cell wall degradation by the pathogen and confer antimicrobial properties, effectively contributing to resistance.

Introduction

In natural environments plants are constantly exposed to diverse microbiota, including pathogenic organisms. In addition to pre-existing structural cell barriers that act as a first line of defense (Serrano *et al.*, 2014; Falter *et al.*, 2015), pathogen perception results in activation of a complex, multi-layered immune system in plants (Jones & Dangl, 2006). As part of the suite of inducible defenses, *de novo* formation of physico-chemical barriers prevents pathogen colonization and spread inside the plant. Despite their importance, the exact composition of these barriers, as well as the mechanisms that lead to their formation in the plant upon pathogen invasion remain largely unknown.

The interaction between the soil-borne bacterial wilt pathogen *Ralstonia solanacearum* and tomato offers a paradigmatic scenario to study inducible physico-chemical barriers, because of its agro-

economic impact, and the well-developed genetic and molecular tools available in both organisms. *Ralstonia solanacearum* enters the root system through wounds or at the points of emergence of lateral roots, where the epidermal and endodermal barriers may be compromised (Vasse *et al.*, 1995; Álvarez *et al.*, 2010; Ursache *et al.*, 2021). After entering the root, the bacterium moves centripetally towards the vasculature and once it reaches the xylem, it multiplies and spreads vertically within the vessels and horizontally to other vessels and the surrounding tissues (Digonnet *et al.*, 2012).

The xylem tissue is a major battleground for the interaction between vascular wilt pathogens and their hosts, where the outcome of the infection is at stake (Yadeta & Thomma, 2013). To prevent the spread of pathogenic propagules, the xylem vasculature of resistant plants undergoes intense structural and metabolic modifications, such as reinforcing the walls of xylem vessels, pit membranes and surrounding xylem parenchyma cells in response to pathogens (Street *et al.*, 1986; Benhamou, 1995). This prevents pathogen colonization of the surrounding parenchyma

*These authors contributed equally to this work.

cells, nearby vessels and inter-cellular spaces through degeneration of the vessel pit membranes or cell walls by the pathogen (Nakaho *et al.*, 2000; Liu *et al.*, 2005; Pérez-Donoso *et al.*, 2010; Dignonnet *et al.*, 2012; Lowe-Power *et al.*, 2018). This vascular confinement is an effective strategy commonly found among plants resistant to vascular wilt pathogens such as *R. solanacearum*, which otherwise spread systemically and eventually kill the plant (McGarvey *et al.*, 1999; Vasse *et al.*, 2000; Potter *et al.*, 2011; Caldwell *et al.*, 2017; Scortichini, 2020; Kashyap *et al.*, 2021).

Among the various tomato germplasms, the cultivar Hawaii 7996 (H7996) is the most effective natural source of resistance against *R. solanacearum* (Grimault *et al.*, 1994; Nakaho *et al.*, 2004). In this cultivar, resistance to *R. solanacearum* is a complex polygenic trait (2000; Thoquet *et al.*, 1996; Mangin *et al.*, 1999; Wang *et al.*, 2013). Our previous study identified the bottlenecks through which H7996 is able to limit *R. solanacearum* spread *in planta* (Planas-Marqués *et al.*, 2019), namely: (1) root colonization, (2) vertical movement from roots to shoots, (3) circular invasion of the vascular bundle and (4) radial apoplastic spread from the vessels into the cortex. Vascular cell wall reinforcements seem to play a key role in confining *R. solanacearum* into the xylem vascular bundles of resistant tomato H7996. Ultra-microscopic studies in resistant tomato showed that the pit membranes, as well as xylem vessel walls and parenchyma cells form a conspicuously thick coating in the form of an electron dense amorphous layer, as part of the defense response against *R. solanacearum* (Nakaho *et al.*, 2000; Kim *et al.*, 2016).

Among the polymers constituting vascular coating structures, lignin is the most typically found, constituting an integral part of the secondary cell wall of the xylem vasculature. Lignin is well documented as a common structural defense against vascular wilt pathogens (Novo *et al.*, 2017; Zeiss *et al.*, 2019; Kashyap *et al.*, 2021) and it is also emerging as an important inducible defense component in other diseases/pests affecting the vasculature (Jhu *et al.*, 2021; Joo *et al.*, 2021). Suberin has also been reported to be deposited in vascular coatings as a defense response (Kashyap *et al.*, 2021), although the mechanisms regulating its synthesis, spatio-temporal dynamics and inducibility remain elusive. Interestingly, root microbiota has been recently shown to shape suberin deposits in the plant, highlighting its central role in plant-microbe interactions (Salas-González *et al.*, 2021). Suberin is a polyester containing long and very long chain fatty acids and derivatives and also some aromatics, mainly ferulic acid. Cells that accumulate suberin also accumulate lignin, whose deposition has been described to precede that of suberin in phellem cells (Lulai & Corsini, 1998). This lignin is also known as a lignin-like polymer, which consists of hydroxycinnamates and monolignols (Graça, 2015). The ligno-suberin heteropolymer formed by the lignin-like polymer and suberin has been also referred to as the poly(aromatic) and poly(aliphatic) domains of suberin, respectively. Commonly, suberized cell walls also comprise soluble phenolic compounds, which share biosynthetic pathways with suberin and lignin (Bernards, 2002).

Ferulic acid present in the suberin and lignin-like fractions is proposed to link both polymers (Graça, 2010) and its continuous

production has been demonstrated essential for suberin deposition (Andersen *et al.*, 2021). Ferulic acid amides, such as feruloyl-tyramine and feruloyloctopamine, have been described as structural components of the lignin-like polymer and in the phenolic soluble fraction of suberizing wound-healing potato tuber (Negrel *et al.*, 1996; Razem & Bernards, 2002). Ferulic acid amides belong to the hydroxycinnamic acid amide (HCAA) family, which present antimicrobial activity and are considered biomarkers during plant-pathogen interactions (Zeiss *et al.*, 2021). However, the precise role of HCAs in plant defense remains to be elucidated (Macoy *et al.*, 2015a,b). Besides their direct antimicrobial activity as soluble phenols, HCAs have also been proposed to crosslink to cell wall structural polymers during infection, potentially contributing towards the formation of a phenolic barrier that can make the cell wall resilient to pathogenic degradation (Zeiss *et al.*, 2021).

In the present study, we conducted a detailed investigation of the inducibility, structure and composition of the xylem vascular wall reinforcements that restrict *R. solanacearum* colonization in resistant tomato. Using a combination of histological and live-imaging techniques, together with spectroscopy and gene expression analysis we provide important new insights into the pathogen-induced formation of vascular coatings. In particular, we show that a ligno-suberin vascular coating and tyramine-derived HCAs contribute to restriction of *R. solanacearum* in resistant tomato. In addition, we demonstrate that genes in the ligno-suberin-associated pathways can be explored to engineer resistance against *R. solanacearum* into commercial susceptible varieties of tomato.

Materials and Methods

Plant materials and growth conditions

Tomato (*Solanum lycopersicum*) varieties Marmande, Hawaii 7996 (H7996) and MoneyMaker (wild-type and 35S::FHT 1-3, generated by Campos *et al.* (2014)), were used. Plants were grown in controlled growth chambers at 60% humidity, 12 h : 12 h, day : night and 27°C (light-emitting diode (LED) lighting) or 25°C (fluorescent lighting).

Ralstonia solanacearum strains and growth conditions

Ralstonia solanacearum GMI1000 strain (Phylo type I, race 1 bio-var 3) was used, including luminescent and fluorescent reporter strains of *R. solanacearum* GMI1000 described in Cruz *et al.* (2014) and Planas-Marqués *et al.* (2019).

Cloning and stable transformation in tomato

For generation of the 35S::FHT-HA construct the FHT (Soly-c03g097500) coding sequence was amplified from tomato H7996 complementary DNA (cDNA) using the forward and reverse primers part7FHTF1 and part7FHTHAR1, respectively (Supporting Information Table S1). The amplified product was cloned into the pJET1.2/blunt cloning vector using a CloneJet

PCR cloning kit (ThermoFisher, Waltham, MA, USA) and then digested by *Sma*I and *Bam*HI. The digested products were purified using NZYGelpure (Nzytech, Lisbon, Portugal) followed by ligation into the pART7 and later to pART27 vector (Gleave, 1992). pART27 containing 35S::FHT-HA was transformed into *Marmande*. For this, the construct was transformed into *Agrobacterium tumefaciens* strain C58C1. Cotyledon explant preparation, selection, and regeneration followed the methods described by Mazier *et al.* (2011). Transformants were selected on kanamycin-containing medium. Accumulation of FHT-HA protein was assayed by immunoblot with a monoclonal HA antibody (GenScript, Piscataway, NJ, USA).

Bacterial inoculation in plants

Four- to five-week-old tomato plants were inoculated through roots with *R. solanacearum* using the soil drenching method with a 1×10^7 colony-forming unit (CFU) ml^{-1} suspension of bacteria as described in Planas-Marquès *et al.* (2018). Inoculated plants were kept in a growth chamber at 27°C. For tomato leaf infiltration, plants were vacuum-infiltrated by submerging the whole aerial part in a $c. 10^5$ CFU ml^{-1} bacterial suspension as described in Planas-Marquès *et al.* (2018). For inoculation directly onto the stem vasculature, 10 μl (5 μl at a time) of 10^5 CFU ml^{-1} bacterial suspension was placed at the node of the petiole and pin-inoculated using a sterile needle (30G \times 1/2", BD Microlance; Becton Dickinson, Franklin Lakes, NJ, USA).

Ralstonia solanacearum pathogenicity assays and quantification of bacterial growth *in planta*

Infected plants were scored for wilting symptoms using a scale from 0 to 4: 0 = healthy plant with no wilt, 1 = 25%, 2 = 50%, 3 = 75%, and 4 = 100% of the canopy wilted as described by Planas-Marquès *et al.* (2019). The relative light units per second (RLU s^{-1}) readings were converted to CFU g^{-1} tissue as described in Planas-Marquès *et al.* (2019). For bacterial colonization assays using green fluorescent protein (GFP) reporter strain, transverse stem cross-sections were made at the inoculation point and at a distance of 0.5, 1, 2 and 3 cm in both upward and downward direction, using a sterile razor blade. Quantification of mean green fluorescence was done using IMAGEJ software (Planas-Marquès *et al.*, 2019). For leaf *in planta* multiplication assays, three leaf discs of 0.8 cm^2 were homogenized in 200 μl of sterile distilled water. CFU cm^{-2} leaf tissue were calculated after dilution plating of samples with appropriate selection antibiotics and CFU counting 24 h later.

Histological methods

Thin ($c. 150 \mu\text{m}$) transverse cross-sections were obtained with a sterile razor blade from a 1.5 cm area of the taproot-to-hypocotyl transition zone located immediately below the soil line (Fig. S1a). Inoculated plants were sectioned when bacterial colonization level reached 10^5 CFU g^{-1} taproot-to-hypocotyl transition zone tissue. This corresponded to 4 d post-inoculation (dpi) in

Marmande and 9 dpi in H7996, at which stage only H7996 sections showed a localized browning at one xylem pole indicative of infection. Sections were kept in 70% ethanol at room temperature for 5 d and examined using fluorescence microscopy using a Leica DM6B-Z microscope under ultraviolet (UV) illumination (340–380 nm excitation and 410–450 nm barrier filters). Autofluorescence emitted from phenolic deposits was recorded using a Leica-DFC9000GT-VSC07341 camera and the signal was pseudo-colored green. Sections were also stained with phloroglucinol-HCl for the detection of lignin and observed under bright field (Pomar *et al.*, 2004). Photographs were taken with a DP71 Olympus digital camera. Cross-sections were also observed under UV with a Leica-DM6B-Z microscope (340–380 nm excitation and 410–450 nm barrier filters). To detect the autofluorescent blue-to-green pH-dependent color conversion of wall-bound ferulic acid cross-sections were initially mounted in 70% ethanol (neutral pH) and then in 1N potassium hydroxide (KOH) (pH above 10) adapting the protocol from Carnahan & Harris (2000), Harris & Trethewey (2010) and Donaldson & Williams (2018). A Leica DM6B-Z microscope was used to observe autofluorescence (340–380 nm excitation and 410–450 nm barrier filters). Images were recorded using a Leica MC190-HD-0518131623 digital camera. To visualize suberin aliphatics, sections were treated with 5% Sudan IV, dissolved in 70% ethanol and illuminated with UV light. These sections were subsequently treated with 1N KOH to detect ferulic acid as described earlier. For both ferulic acid and suberin, the HC PL APO or HC PL FLUOTAR objectives of the Leica DM6B-Z microscope were used and images were captured using a Leica MC190-HD-0518131623 color digital camera. The UV autofluorescence signal from xylem vessel walls and surrounding layers was measured using the LAS X Leica software and changes in ferulate accumulation were quantified using IMAGEJ software by selecting the area of xylem vessel walls showing autofluorescence. Quantifications of fluorescence intensity were normalized per micrometer of region of interest (ROI), which corresponded to a particular area of the vascular bundles, where main vessels concentrate (represented in Fig. 1b). Basically, the line is drawn at each of the four corners in the whole image and then the fluorescence is normalized by the length of the lines.

Two-dimensional nuclear magnetic resonance (2D-NMR)

The samples of a pool of 15 tomato plants (taproot-to-hypocotyl region), water treated or having a bacterial load of 10^5 CFU g^{-1} were milled and extracted sequentially with water, 80% ethanol, and with acetone, by sonicating in an ultrasonic bath during 30 min each time, centrifuging and eliminating the supernatant. Then, lignin/suberin fraction was enzymatically isolated by hydrolyzing the carbohydrates fraction with Cellulysin (Calbiochem, San Diego, CA, USA), as previously described (Rico *et al.*, 2014). Approximately 20 mg of enzymatic lignin/suberin preparation was dissolved in 0.6 ml of deuterated dimethyl sulfoxide ($\text{DMSO}-d_6$). Heteronuclear single quantum coherence (HSQC) spectra were acquired on a Bruker Avance III 500 MHz spectrometer (Bruker, Karlsruhe, Germany) equipped

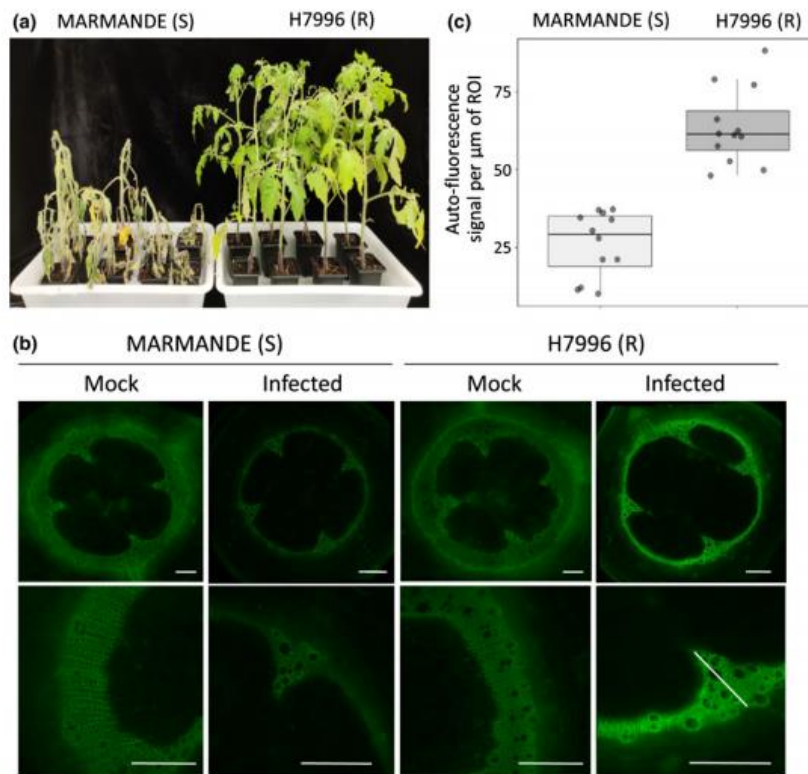


Fig. 1 Resistant H7996 tomato restricts *Ralstonia solanacearum* colonization and induces a vascular coating response with wall bound phenolics. Susceptible (Marmande) and resistant (H7996), 5-wk-old tomato plants were inoculated through roots by soil-soak with $c. 1 \times 10^7$ colony-forming unit (CFU) ml^{-1} of *R. solanacearum* GMI1000 and incubated at 28°C. (a) At 12 d post-inoculation (dpi) most Marmande plants showed severe wilting symptoms, whereas H7996 remained mostly symptomless. (b) Cross-sections of the taproot-to-hypocotyl area containing 10^5 CFU g^{-1} of *R. solanacearum* were analyzed by ultraviolet (UV) microscopy. To focus on cell wall-deposited phenolic compounds, soluble phenolic compounds were removed with ethanol prior to observation. A strong autofluorescence signal emitted from the walls of vessels and surrounding parenchyma cells in infected H7996 plants compared to Marmande or the mock controls can be observed. Fluorescence signal in white was green colored. Images from a representative experiment out of three with $n = 5$ plants per cultivar. Bar, 500 μm . (c) The UV autofluorescence signal in (b) was measured using the Leica APPLICATION SUITE X (LAS X) software. A representative region of interest (ROI) is highlighted in (b) and corresponded to a line traversing the selected vascular bundles. Data are represented with box and whiskers plots: whiskers indicate variability outside the upper and lower quartiles and boxes indicate second quartile, median and third quartile. Different letters indicate statistically significant differences ($\alpha = 0.05$, Fisher's least significant difference test).

with a 5 mm TCI cryoprobe, using the experimental conditions previously described (Rico *et al.*, 2014). HSQC cross-signals were assigned and quantified as described (del Río *et al.*, 2018; Rencoret *et al.*, 2018; Mahmoud *et al.*, 2020). In the aromatic region, the correlation signals of G_2 and $S_{2,6}$ were used to estimate the content of the respective G- and S-lignin units. The C_α/H_α signals of the $\beta-O-4'$ ethers (A_α), phenylcoumarans (B_α), and resinols (C_α) in the linkages region were used to estimate their relative abundances, whereas the C_γ/H_γ signal was used in the case of cinnamyl alcohol end-units (I_γ).

RNA extraction, cDNA synthesis and quantitative RT-PCR analysis

Taproot-to-hypocotyl transition zone sections of $c. 0.5$ mm thickness were obtained and the xylem vascular tissues (vascular bundles and surrounding parenchyma cells) were collected and kept in liquid nitrogen. Each sample comprised taproot-to-hypocotyl transition

zone xylem tissues of six plants. RNA was extracted using the Maxwell RSC Plant RNA Kit (Promega, Madison, WI, USA). Complementary DNA was synthesized from 2 μg RNA using High Capacity cDNA Reverse Transcription Kit (Applied Biosystems, Foster City, CA, USA). Complementary DNA amplification and analysis was performed using the LightCycler 480 System (Roche, Basel, Switzerland). The Elongation Factor 1 alpha housekeeping gene (*eEF1 α* , *Solyc06g005060*) was used as a reference. All reactions were run in triplicate for each biological replicates. Melting curves and relative quantification of target genes were determined using the software LIGHTCYCLER v.1.5 (Roche). The level of expression relative to the reference gene was calculated using the formula $2^{-\Delta\text{CT}}$, where $\Delta\text{CT} = (\text{CT RNA target} - \text{CT reference RNA})$.

Statistical analysis

Statistical analyses were performed using STATGRAPHICS software. All statistical tests are indicated in the respective figure legends.

Results

Resistant H7996 tomato restricts *R. solanacearum* colonization and induces a vascular coating response involving wall-bound phenolics

In order to understand the mechanisms underscoring restriction of *R. solanacearum* spread in resistant tomato varieties we used the resistant variety H7996 and compared it to the susceptible cultivar Marmande. In our assay conditions, most Marmande plants were wilted 10 d after inoculation with *R. solanacearum* GMI1000, while H7996 plants remained largely asymptomatic (Figs 1a, S2a; Planas-Marquès *et al.*, 2019). Accordingly, bacterial loads in the taproot-to-hypocotyl region were drastically reduced in H7996 compared to Marmande, confirming the remarkable bacterial restriction ability of this cultivar (Fig. S1b; Planas-Marquès *et al.*, 2019).

To identify defense-associated anatomical and physico-chemical modifications in H7996 after infection with *R. solanacearum* compared to Marmande we performed histochemical, spectroscopic and gene expression analysis. For this, plants were infected with a 10^7 *R. solanacearum* solution or mock through their roots using the soil-drench method and then we collected tissue containing 10^5 CFU g^{-1} tissue of bacteria at the taproot-to-hypocotyl transition area, located *c.* 1 cm below-ground (Fig. S1a). Marmande reached 10^5 CFU g^{-1} tissue at around 4 dpi, while the resistant H7996 took approximately 9 d to do so (Fig. S2). We have previously observed that the root-to-hypocotyl area constitutes a key bottleneck for bacterial progression inside the plant (Zuluaga *et al.*, 2015; Puigvert *et al.*, 2017; Planas-Marquès *et al.*, 2019), being thus an ideal target zone for analysis of structural defense responses.

We initially analyzed UV autofluorescence of transverse cross-sections of the taproot-to-hypocotyl region, indicative of phenolic compounds (Donaldson, 2020). To focus on cell wall-deposited phenolic compounds, soluble phenolic compounds were removed with ethanol prior to observation as reported (Pouzoulet *et al.*, 2013; Araujo *et al.*, 2014). Infection with *R. solanacearum* induced a strong UV signal emitted from the walls of the vessels, and also from surrounding xylem parenchyma cells and tracheids in resistant H7996 (Fig. 1b,c). This enhanced autofluorescence was not observed in the susceptible variety Marmande nor in mock-treated samples (Fig. 1b, c). In tissues outside the vascular area, inoculation resulted in a decrease of autofluorescence in both susceptible and resistant tomato lines.

Spectroscopic analysis reveals *R. solanacearum*-induced deposition of suberin and accumulation of tyramine-derived amides in resistant H7996 tomato and lignin structural modifications in susceptible Marmande tomato

In order to decipher the composition of the cell wall-deposited compounds we used two-dimensional (2D) HSQC nuclear magnetic resonance (NMR), one of the most powerful tools for plant cell wall structural analysis providing

information on the composition and linkages in lignin/suberin polymers (Ralph & Landucci, 2010; Correia *et al.*, 2020). The 2D-HSQC spectra of infected or mock-treated taproot-to-hypocotyl transition zones of H7996 and Marmande tomato plants were obtained and the main lignin and suberin substructures identified are shown in Fig. 2, while the chemical shifts of the assigned cross-signals are detailed in Table S2. Importantly, the aliphatic region of the 2D-HSQC spectra revealed that H7996 infected plants were more enriched in poly-aliphatic structures characteristic of suberin (magenta-colored signals), compared to its mock control (Fig. 2a). Related to this, an olefinic cross-signal of unsaturated fatty acid structures (UF, δ_C/δ_H 129.4/5.31), typical of suberin, was also found to be increased in the HSQC spectrum of the infected H7996 tomato. A rough estimate based on the integration of lignin and suberin HSQC signals, revealed that the suberin/lignin ratio in *R. solanacearum*-infected H7996 plants was doubled compared to mock-treated plants, evidencing an increase in suberin deposition as a consequence of the bacterial infection. Interestingly, signals compatible with feruloylamides (FAM₇; δ_C/δ_H 138.6/7.31) and with tyramine-derived amides (Ty in orange; δ_C/δ_H 129.3/6.92, 114.8/6.64, 40.5/3.29 and 34.2/2.62) were exclusively found in the spectrum of infected H7996 plants, suggesting the presence of feruloyltyramine exclusively in these samples (Fig. 2a). Since tyramines have been found as structural components co-occurring with suberin (Bernards *et al.*, 1995; Bernards & Lewis, 1998), which generates physically and chemically resistant barriers (He & Ding, 2020), our results substantiate the hypothesis of suberin as an important defense element against *R. solanacearum* infection in resistant tomato plants. On the contrary, the 2D-HSQC spectra from the Marmande variety did not display notable variations between mock and infected plants in the signals corresponding to suberin, tyramine-related structures nor feruloylamides (Fig. 2a).

Interestingly, 2D-HSQC-NMR spectra also revealed significant structural modifications in the composition of lignin and the distribution of linkages in tomato plants after infection. Lignins with lower S : G ratios are more branched (condensed) and recalcitrant towards pathogen attack (Iiyama *et al.*, 2020). Therefore, lignin in inoculated H7996, with an S : G ratio of 1.0 should be, a priori, more resistant than the lignin in inoculated Marmande plants (S : G ratio of 1.5). The 2D-HSQC analysis revealed that the infection of susceptible Marmande plants resulted in an increase of the S : G ratio and a clear reduction of all major lignin linkages (β -O-4', β -5' and β - β' ; reduction in roughly 9%, 43% and 46%, respectively), evidencing that a lignin depolymerization process took place (Fig. 2a). In contrast, infected H7996 tomato displayed a slight decrease of the S : G ratio, and only β -O-4' linkages (the easiest to degrade in the lignin polymer) were significantly reduced, while the β -5' and β - β' were not so affected as in the case of Marmande plants. In this context, the major reduction in lignin linkages observed in Marmande after infection could explain, at least in part, its higher susceptibility to the pathogen.

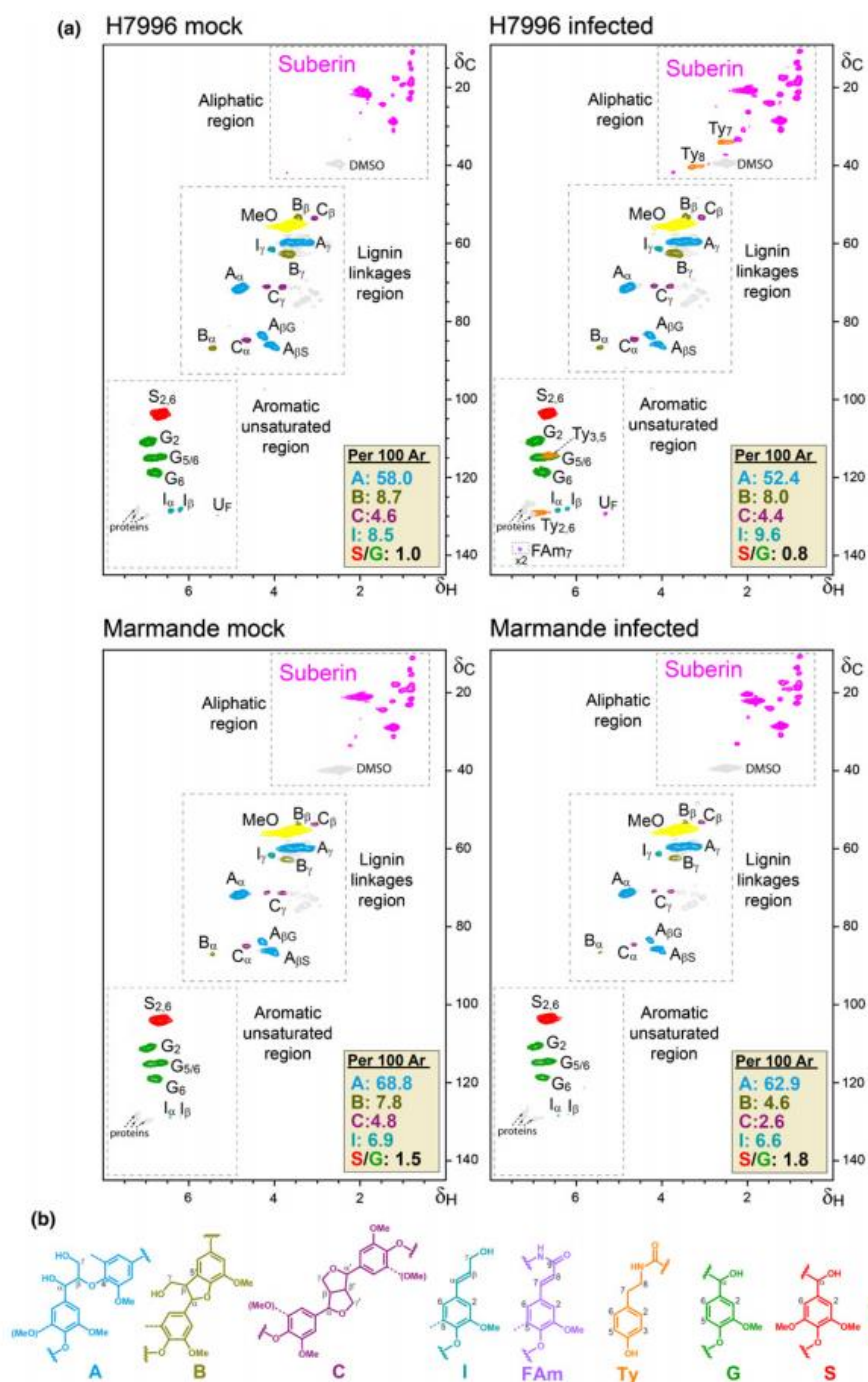


Fig. 2 Feruloylamides, tyramine-derived amides and suberin-compatible compounds are specifically enriched in resistant H7996 tomato after infection with *Ralstonia solanacearum*. (a) Two-dimensional heteronuclear single quantum correlation-nuclear magnetic resonance (2D-HSQC-NMR) spectra of enzymatically isolated lignin/suberin fractions from mock-treated and *R. solanacearum*-infected taproots (containing 10^5 colony-forming unit (CFU) g^{-1} taproot-to-hypocotyl transition tissue) of H7996 and Marmande tomato plants. The experiment was performed twice with similar results. (b) Main lignin/suberin structures identified: β -O-4' alkyl aryl ethers (A), β -5' phenylcoumarans (B), β - β' resins (C), cinnamyl alcohol end-groups (I), feruloylamides (FAm), tyramine-derived amides (Ty), guaiacyl lignin units (G), syringyl lignin units (S), as well as unassigned aliphatic signals from suberin. The structures and contours of the HSQC signals are color coded to aid interpretation. Proton (1H) and carbon-13 (^{13}C) NMR chemical shifts of the assigned signals are detailed in Supporting Information Table S2. To detect FAm₇ signal, the spectrum scaled-up to 2-fold ($\times 2$) intensity. The abundances of the main lignin linkages (A, B and C) and cinnamyl alcohol end-groups (I) are referred to as a percentage of the total lignin units (S + G = 100%).

Histochemical analysis reveals the formation of structural vascular coatings containing suberin and ferulate/feruloylamide in resistant H7996 tomato in response to *R. solanacearum* infection

To confirm our spectroscopic data, we histochemically analyzed taproot-to-hypocotyl transition zone samples of mock and infected H7996 and Marmande tomato plants. Observation of Phloroglucinol-HCl stained sections under brightfield microscopy (Wiesner staining) (Pomar *et al.*, 2002; Pradhan Mitra & Loqué, 2014), showed that mock and infected H9776 (resistant) as well as mock Marmande (susceptible) samples showed a red-purple color characteristic of the reaction of phloroglucinol-HCl in vessels and fibers, indicative of lignin (Fig. 3a). In contrast, infected Marmande sections exhibited reduced phloroglucinol-HCl staining, suggesting a change in composition of xylem lignin upon infection (Fig. 3a). This observation is in agreement with the structural changes specifically detected in the lignin structure of infected Marmande plants by 2D-HSQC-NMR (Fig. 2a), which suggest lignin depolymerization and may partly underscore the high susceptibility of this tomato variety.

UV illumination of phloroglucinol-HCl-stained samples allows quenching the autofluorescence from lignin and hence detect residual cell wall autofluorescence, which has been associated with suberin deposits (Baayen & Elgersma, 1985; Rioux *et al.*, 1998; Pouzoulet *et al.*, 2013). Under these conditions, the increased autofluorescence observed in the vascular coating regions of infected H7996 tomato plants was not quenched in phloroglucinol-HCl stained samples (Fig. 3a,b). A more detailed observation revealed that this nonquenched autofluorescence was localized in specific regions compatible with (1) intervessel and vessel-parenchyma pit membranes or pit chamber walls and (2) parenchyma coatings with fluorescent signals enriched in intracellular spaces (Fig. 3c).

Next, we analyzed whether the pathogen-induced coating of vessels observed in H7996 correlated also with an increase in ferulates, a major suberin component. We performed KOH treatment of plant tissues, which specifically shifts the UV fluorescence of ferulate/feruloylamide to green, allowing its detection (Carnachan & Harris, 2000; Harris & Trethewey, 2010; Donaldson & Williams, 2018). UV autofluorescence of vascular coatings in response to *R. solanacearum* infection in resistant H7996 shifted from blue to a strong green color upon treatment with alkali (1N KOH) (Fig. S3a). This indicated that the *R. solanacearum*-induced xylem vasculature feruloylation was specific to resistant H7996, as the fainter blue autofluorescence observed in mock-treated resistant H7996 or susceptible Marmande tissues did not change to green at high pH in either early (Fig. S3a,b) or late (Fig. S3c) stages of infection.

To corroborate that the ferulate/feruloylamide accumulation in infected H7996 tomato was related with vascular suberization, we combined the ferulate-specific UV-alkali treatment described earlier with Sudan IV staining, which binds aliphatic components of suberin to produce a reddish-brown coloration. This revealed suberization in the taproot-to-hypocotyl area of *R. solanacearum*-infected H7996 plants, xylem vessel walls as well as the layers of

vessels, parenchyma cells and tracheids in the immediate vicinity (Fig. 4). In the periphery of suberized cells, a green signal from UV-alkali was observed (Fig. 4), which may indicate ferulate/feruloylamide deposition indicative of a preceding stage towards suberization in this cell layer. In comparison, no positive Sudan IV or UV-alkali staining was detected in infected Marmande or mock-treated tomato plants. Together, suberized and feruloylated layers of parenchyma cells, vessels and tracheids might form a 'suberization zone' creating a strong physico-chemical barrier to limit *R. solanacearum* spread from the colonized xylem vessel lumen.

Ralstonia solanacearum infection activates the biosynthesis of aliphatic suberin precursors and feruloylamide, and aliphatic esterification of ferulic acid in the vasculature of resistant H7996

Since a differential accumulation of suberin-compatible compounds was specifically observed in infected H7996, we surmised that genes related to suberin and feruloylamide synthesis, as well as ferulic acid esterification to aliphatics may be upregulated in resistant tomato in response to *R. solanacearum* invasion. To test this hypothesis, we analyzed: (1) expression of genes in the phenylpropanoid and suberin biosynthesis pathways, which provide the necessary precursors for the ligno-suberin heteropolymer; (2) the feruloyl transferase FHT (ASFT/HHT in Arabidopsis), which is involved in the formation of ferulate esters of fatty acyl compounds necessary to form suberin and soluble waxes (Gou *et al.*, 2009; Molina *et al.*, 2009; Serra *et al.*, 2010); and (3) N-hydroxycinnamoyl transferases (THT), which are involved in the synthesis of HCAs such as feruloyltyramine, which is found on the lignin-like polymer and in the soluble phenolic fraction of some suberized tissues (Negrel *et al.*, 1993; Schmidt *et al.*, 1999).

Quantitative reverse transcription polymerase chain reaction (RT-PCR) from xylem vascular tissue obtained from the taproot-to-hypocotyl zone in *R. solanacearum*- or mock-treated H7996 and Marmande plants showed specific upregulation of all genes analyzed from the suberin biosynthetic pathway in H7996 infected plants compared to the mock controls (Figs 5, S4). These included essential suberin biosynthesis genes such as *CYP86A1* and *CYP86B1* (fatty acid oxidation), *FAR* (primary alcohol generation), *KCSs* (fatty acid elongases) and *GPAT5* (acylglycerol formation). In addition, feruloyl transferase *FHT* (*ASFT/HHT* in Arabidopsis), was also strongly upregulated in infected H7996 plants (Figs 5, S5b). Regarding *THT*, in tomato we identified five putative homologs (Fig. S6a), all induced by infection in the vascular tissue of H7996 (Figs 5, S6b). Among them, *S1THT1-3* showed the strongest upregulation in H7996 after infection (Figs 5, S6b). In comparison, *R. solanacearum* infection had only a modest effect on genes related to phenylpropanoid pathway as only upregulation was detected in the first enzyme of the pathway (PAL) (Figs 5, S7).

Together, these data indicate that upregulation of genes involved in the formation of aliphatic suberin precursors, ferulic acid esterification to aliphatics (FHT) and production of HCAs, such as feruloyltyramine (THT), constitute a very specific response of H7996 plants that takes place in the vasculature

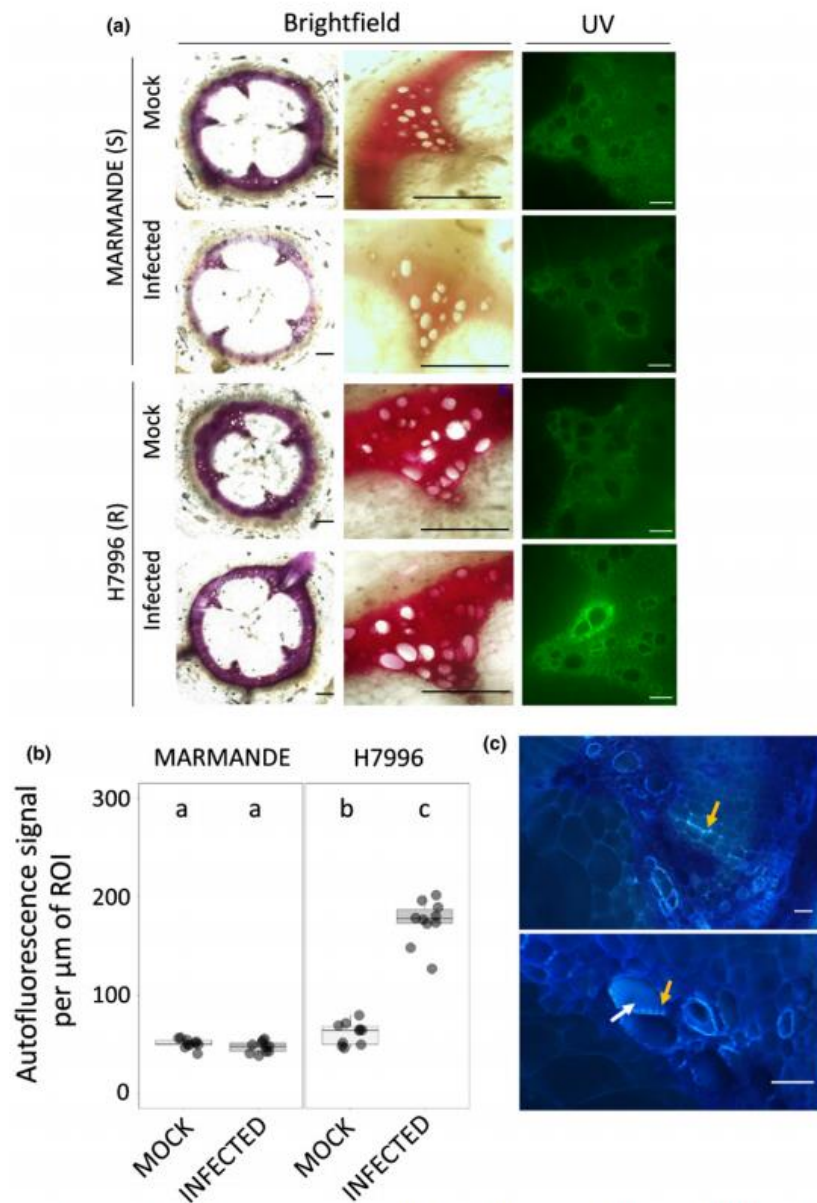


Fig. 3 Resistant H7996 tomato shows vascular autofluorescence not-quenched with phloroglucinol and susceptible Marmande shows a decrease in phloroglucinol-HCl lignin signal. Susceptible (Marmande) and resistant (H7996) 5-wk-old tomato plants were root-inoculated with a *Ralstonia solanacearum* GM1000 strain at a concentration of $c. 1 \times 10^7$ colony-forming unit (CFU) ml^{-1} or water mock. (a) Cross-sections of the taproot-to-hypocotyl area containing 10^5 CFU g^{-1} of *R. solanacearum* were stained with phloroglucinol-HCl and observed under ultraviolet (UV) to visualize other autofluorescent compounds different from lignin (not quenched with phloroglucinol-HCl) (right) and under brightfield to visualize lignin deposition (left). In infected H7996 strong UV autofluorescence could be observed in the walls of xylem vessels surrounding xylem parenchyma cells and tracheids, indicating reinforcement of walls of vascular tissue with phenolics formed *de novo* upon infection. In infected Marmande the red phloroglucinol stain was reduced especially in the intervessel areas. (b) The UV autofluorescence signal in (a) was measured using the Las X Leica software after the phloroglucinol-HCl treatment. Data are represented with box and whiskers plots: whiskers indicate variability outside the upper and lower quartiles and boxes indicate second quartile, median and third quartile. (c) Detailed observation of infected H7996 xylem after the phloroglucinol-HCl treatment shows the strong UV fluorescence concentrated in specific areas possibly corresponding to intervessel and vessel-parenchyma bordered pit membranes and/or pit chambers (yellow and white arrows, respectively). Fluorescence was also observed in parenchyma cells, specially enriched at intercellular cell corners (green arrow). Panel (b) correspond to a representative experiment out of three each with $n = 6$ plants per variety. Different letters indicate statistically significant differences ($\alpha = 0.05$, Fisher's least significant difference test). Panels (a) and (c) were representative images. Bars: (a, left), 100 μm ; (a, right) 500 μm ; (c) 50 μm .

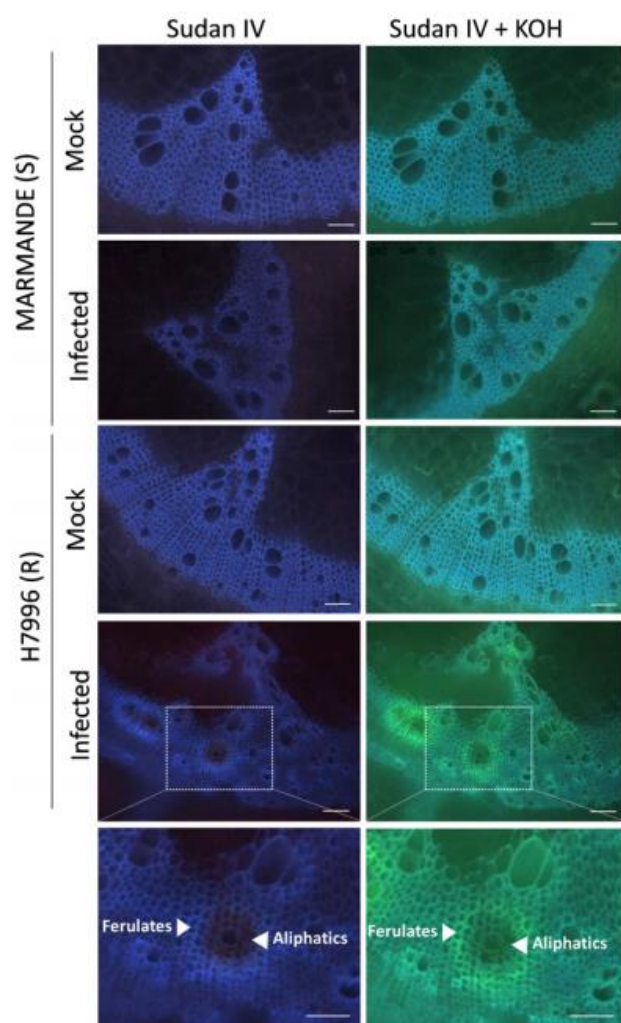


Fig. 4 Resistant H7996 tomato shows cell wall ferulate/feruloylamine and suberin deposition in restricted zones of vascular tissue upon *Ralstonia solanacearum* infection. Susceptible Marmande or resistant H7996 tomato plants were soil-inoculated with a c. 1×10^7 colony-forming unit (CFU) ml^{-1} suspension of *R. solanacearum* GMI1000 or mock-inoculated with water and incubated at 28°C. Cross-sections were obtained from taproot-to-hypocotyl transition tissue containing 10^5 CFU g^{-1} of *R. solanacearum*. Sections were stained with Sudan IV to visualize suberin aliphatics and subsequently treated with 1N potassium hydroxide (KOH) (pH above 10) to visualize ferulic acid bound to cell wall. Sudan IV positive staining (reddish-brown coloration) was observed around xylem vessels specifically in infected H7996, indicating accumulation of suberin aliphatics. Accumulation of ferulic acid bound to cell wall (blue-green coloration) appears also specifically in infected H7996 resistant tomato, surrounding Sudan IV-stained areas. White arrowheads indicate the sites of accumulation of ferulates and aliphatic compounds. Representative images from one experiment out of three with $n = 6$ plants each were taken. Bar, 100 μm .

upon *R. solanacearum* infection. Further, these data are in agreement with NMR data of infected H7996, which showed a specific increase in insoluble fatty acid structures typical of suberin as well as the appearance of signals from structural tyramine-derived amides and feruloylamides (Fig. 2a).

Overexpression of *SITH1-3* in a susceptible tomato cultivar confers resistance to *R. solanacearum*

Based on our results, we set to determine whether overexpressing genes involved in ferulic acid esterification to suberin aliphatics and feruloylamine biosynthesis, such as *SIFHT* and *SITH1-3*, respectively, would increase resistance against *R. solanacearum* in a susceptible tomato background. Initially, we obtained transgenic tomato lines stably overexpressing *SIFHT* on a susceptible Marmande background (Fig. S8). Under normal growth conditions these lines are morphologically undistinguishable from wild-type (Wt), although they display a subtle increase in fresh weight (Fig. S9). We analyzed symptom progression and bacterial colonization. *SIFHT* overexpression lines showed a slight delay in disease progression (Fig. 6a) and moderately milder symptoms. The taproot-to-hypocotyl of *SIFHT* overexpressors displayed a slight reduction in bacterial loads after soil-soak inoculation in comparison to Wt tomato (Fig. 6b).

Regarding *SITH1-3*, the corresponding tomato overexpressing line was readily available on a Moneymaker background (Campos *et al.*, 2014). This line has been shown to overaccumulate soluble HCAA such as feruloyltyramine and also the hormone salicylic acid (SA) upon infection with *Pseudomonas syringae* pv. tomato (Campos *et al.*, 2014). It is worth noting that tomato plants overexpressing *SITH1-3* display a slight decrease in fresh weight compared to wild-type plants, although with the naked eye they appear undistinguishable (Fig. S10). As expected, the Moneymaker tomato cultivar showed similar susceptibility to *R. solanacearum* as Marmande (Fig. 7a,b). In contrast, overexpression of *SITH1-3* resulted in a dramatic increase of resistance against *R. solanacearum*, with disease progressing remarkably slower in this line compared to wild-type (Fig. 7a,b). Importantly, bacterial loads were significantly lower in the taproot-to-hypocotyl and hypocotyl of the *SITH1-3* overexpressor after soil inoculation in comparison to Wt tomato (Fig. 7c). Similarly, direct leaf inoculation also showed severe bacterial growth restriction in the *SITH1-3* overexpressing line (Fig. S11a). Further, we monitored the colonization patterns of a *R. solanacearum* GFP reporter strain after stem inoculation of the *SITH1-3* overexpressing line compared to Wt. In transverse stem cross-sections of 6 dpi plants, bacteria stayed confined near the inoculation point in the *SITH1-3* line whereas they spread unrestrictedly in susceptible wild-type stems from the inoculation point and at least 3 cm up and downwards (Fig. 7d,e, S11b).

Concomitant with the observed restriction of *R. solanacearum* colonization, an increase in autofluorescence around the vasculature was observed in the *SITH1-3* overexpressor (Fig. 8a). At similar bacterial loads, Wt did not display such enhanced vascular fluorescence. Phloroglucinol-HCl staining did not quench the paravascular autofluorescence in *SITH1-3* (Fig. 8a,d), indicating that similar to what was previously observed for H7996, the observed increase in wall-bound phenolic deposits did not only correspond to lignin. To gain a deeper insight into the composition of the *R. solanacearum*-induced vascular deposits in *SITH1-3* overexpressing plants we performed combined Sudan IV-alkali staining (Fig. 8b,c,e). Treatment with alkali resulted in a clear

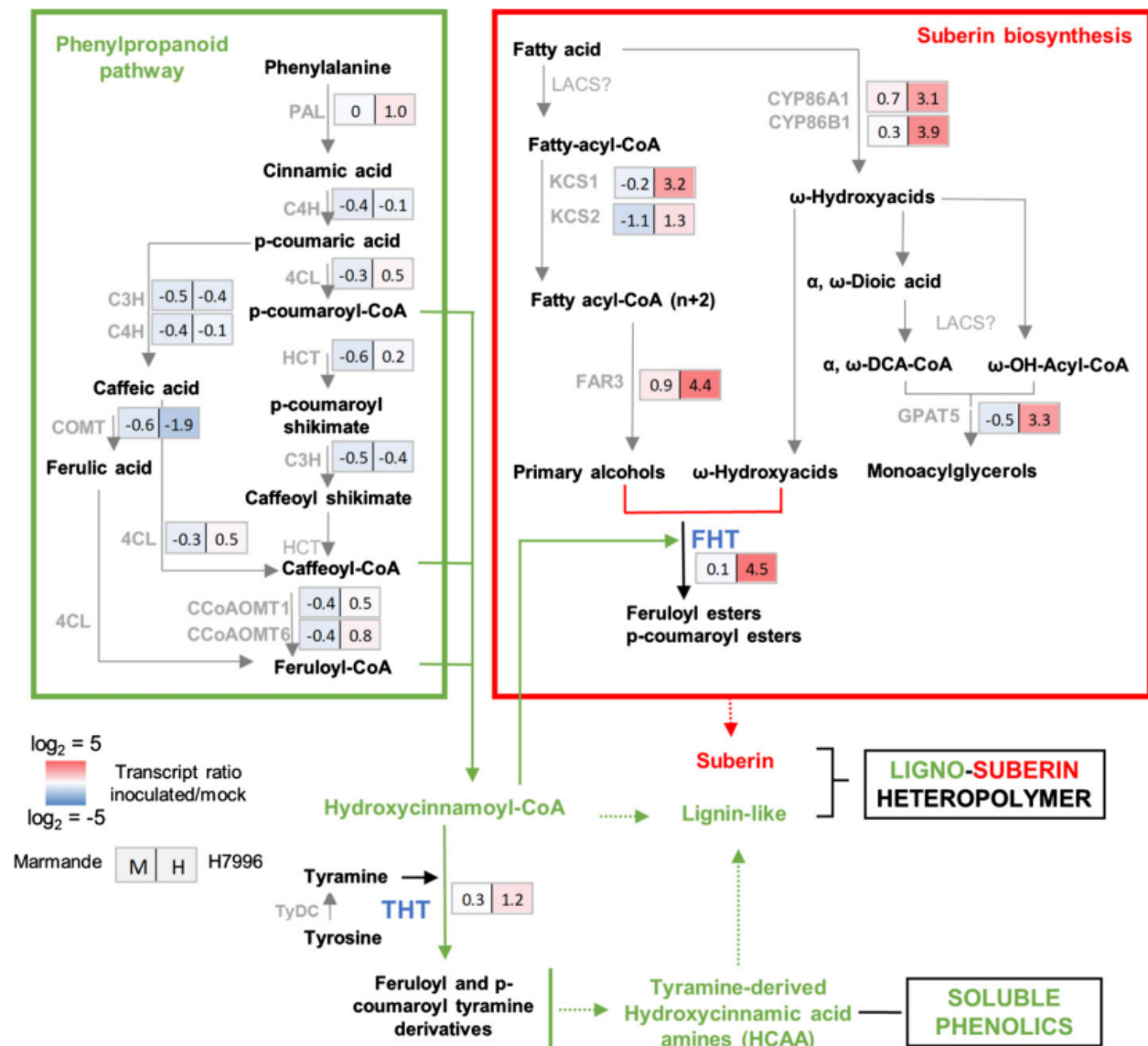


Fig. 5 Genes of the ligno-suberin heteropolymer biosynthesis pathway are specifically induced in the xylem vasculature of resistant H7996 tomato upon *Ralstonia solanacearum* infection. The levels of expression of genes belonging to metabolic pathways relevant for suberin, lignin and feruloyltyramine and related amides biosynthesis were analyzed by quantitative polymerase chain reaction (qPCR) of taproot vascular tissue in infected or mock-treated H7996 or Marmande tomato plants. Plants containing an *R. solanacearum* inoculum of 10^5 colony-forming unit (CFU) g^{-1} were selected and xylem vascular tissue from the taproot-to-hypocotyl transition zone, comprising of metaxylems and surrounding parenchyma cells was collected for RNA extraction and complementary DNA (cDNA) synthesis. In parallel, xylem tissue was collected from mock plants. Heatmaps show log₂ fold change RTA (relative transcript abundance) values of infected vs mock for Marmande (left) and Hawaii (right). The tomato gene encoding for the alpha-subunit of the translation elongation factor 1 (*SleEF1* α) was used as endogenous reference. Three biological replicates ($n = 3$) were used, and taproots of six plants were used in each replicate. All the original qPCR results can be found in Supporting Information Figs S3–S6. The scheme represents the phenylpropanoid and suberin biosynthesis pathways providing lignin-like and suberin precursors for the ligno-suberin heteropolymer. Abbreviations: PAL, phenylalanine ammonia-lyase; C4H, cinnamate-4-hydroxylase; C3H, coumarate 3-hydroxylase; 4CL, 4-coumarate-CoA ligase; HCT, hydroxycinnamoyl-CoA shikimate/quinic acid hydroxycinnamoyl transferase; COMT, caffeic acid 3-O-methyltransferase; CCoAOMT, caffeoyl CoA 3-O-methyltransferase; CYP86A1 and CYP86B1, cytochrome P450 fatty acid ω -hydroxylases; KCS1/2, 3-ketoacyl-CoA synthase; FAR 1/3/4, fatty acyl-CoA reductase; GPAT5, glycerol-3-phosphate acyltransferase 5; THT, tyramine hydroxycinnamoyl transferase; TyDC, tyrosine decarboxylase; FHT, feruloyl transferase. The question mark (?) denotes a hypothetical reaction.

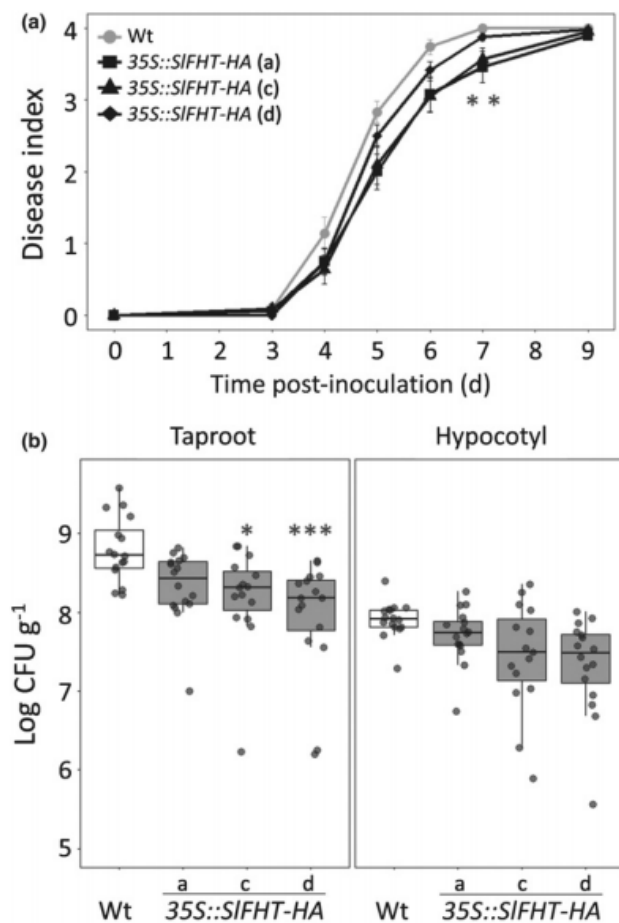


Fig. 6 Overexpression of *SIFHT-HA* in susceptible tomato slightly restricts colonization by *Ralstonia solanacearum*. (a, b) A pathogenicity assay was performed comparing wild-type (Wt) and three independent *35S::SIFHT-HA* Marmande tomato lines (a, c and d) after infection with *R. solanacearum* GMI1000 lux reporter strain. Five-wk-old plants were soil-soak inoculated with $c. 1 \times 10^7$ colony-forming unit (CFU) mL^{-1} or mock and grown at 28°C. (a) Wilting progress was monitored by rating plants daily on a 0 to 4 disease index scale where 0 = healthy and 4 = 100% wilted. Plotted values correspond to means \pm standard error of 24 independent plants ($n = 24$) from a representative experiment out of a total of three. Asterisks indicate statistically significant differences between Wt and each of the *35S::FHT-HA* analyzed using a paired Student's *t*-test (*, $P < 0.05$). (b) The level of *R. solanacearum* colonization in the taproot and hypocotyl was calculated as colony forming units per gram of fresh taproot tissue (CFU g^{-1}) at 12 d post infection (dpi). Data are represented with box and whiskers plots: whiskers indicate variability outside the upper and lower quartiles and boxes indicate second quartile, median and third quartile. Data presented are of a representative experiment out of a total of three experiments. In (a) a Kruskal–Wallis test at each dpi was conducted to examine differences in disease index among different genotypes. Significant differences among genotypes were confirmed by applying a pairwise Wilcoxon test. Asterisks indicate statistically significant differences between wild-type and *35S::FHT-HA* tomato lines in (a) (*, $P < 0.05$).

blue-to-green shift of UV autofluorescence around xylem vessels occurring specifically in the *SITH1-3* overexpressor upon infection, which reveals the presence of ferulates/feruloylamides as part of the observed vascular deposits. In contrast, no positive

Sudan IV staining was detected, indicating that a canonical suberin polyester does not seem to be part of vascular coatings in *SITH1-3* overexpressing plants. Since Sudan IV only stains specific moieties of the complex suberin heteropolymer, we cannot rule out that the observed vascular deposits in *SITH1-3* are formed by a noncanonical ligno-suberin heteropolymer that does not react with Sudan IV. Further investigation will be needed in order to ascertain the exact nature of the *R. solanacearum*-induced vascular deposits in the *SITH1-3* overexpressor. In conclusion, our data clearly show that *StTHT1-3* ectopic expression provides a very effective resistance mechanism against *R. solanacearum* – potentially mediated by accumulation of elevated amounts of HCAs such as feruloyltyramine, which drastically restricts vascular colonization, preventing bacterial spread and blocking the onset of disease.

Discussion

Ligno-suberin deposits in vascular cell walls and feruloyltyramine accumulation acts as a resistance mechanism restricting *R. solanacearum* colonization in resistant tomato

In our study, resistant tomato (H7996) was observed to react aggressively to *R. solanacearum* infection by reinforcing the walls of vessels and the surrounding parenchyma cells with UV autofluorescent phenolic deposits (Fig. 1). An increase in autofluorescence had been previously reported in another resistant tomato variety, LS-89, although its composition was not precisely defined (Ishihara *et al.*, 2012). Histochemical analysis of vascular coatings in resistant tomato upon *R. solanacearum* infection showed that suberin-associated autofluorescence was prominent in the vasculature, in line with previous reports using transmission electron microscopy (TEM) that showed thickening of the pit membranes accumulating electron-dense material in tomato plants resistant to *R. solanacearum* (Nakaho *et al.*, 2000, 2004). The suberin nature of these coatings was further supported by the positive Sudan IV staining of vessels and surrounding parenchyma cells of H7996 taproot-to-hypocotyl transition zone upon infection (Fig. 4). These results are in agreement with coatings detected in tomato plants resistant to *Verticillium albo-atrum* (Robb *et al.*, 1991), where suberin and lignin were both deposited in intercellular spaces between parenchyma cells adjoining a xylem vessel or infusing and occluding pit membranes coatings (Street *et al.*, 1986; Robb *et al.*, 1991). Besides, inhibition of the phenylpropanoid pathway inhibited the formation of both lignin and suberin coatings (Street *et al.*, 1986), in agreement with the ferulic acid requirement to correctly deposit suberin (Andersen *et al.*, 2021) and reinforcing our observations of the presence of a ferulate/feruloylamide-derived polymer detected in H7996 *R. solanacearum* (Fig. 4). In line with this, NMR data of resistant H7996 tomato vascular tissue revealed the presence of tyramine-derived amides and feruloylamides incorporated into the cell wall and also an enrichment in poly-aliphatic structures characteristic of suberin (Fig. 2) (Graça, 2015; Legay *et al.*, 2016; Figueiredo *et al.*, 2020).

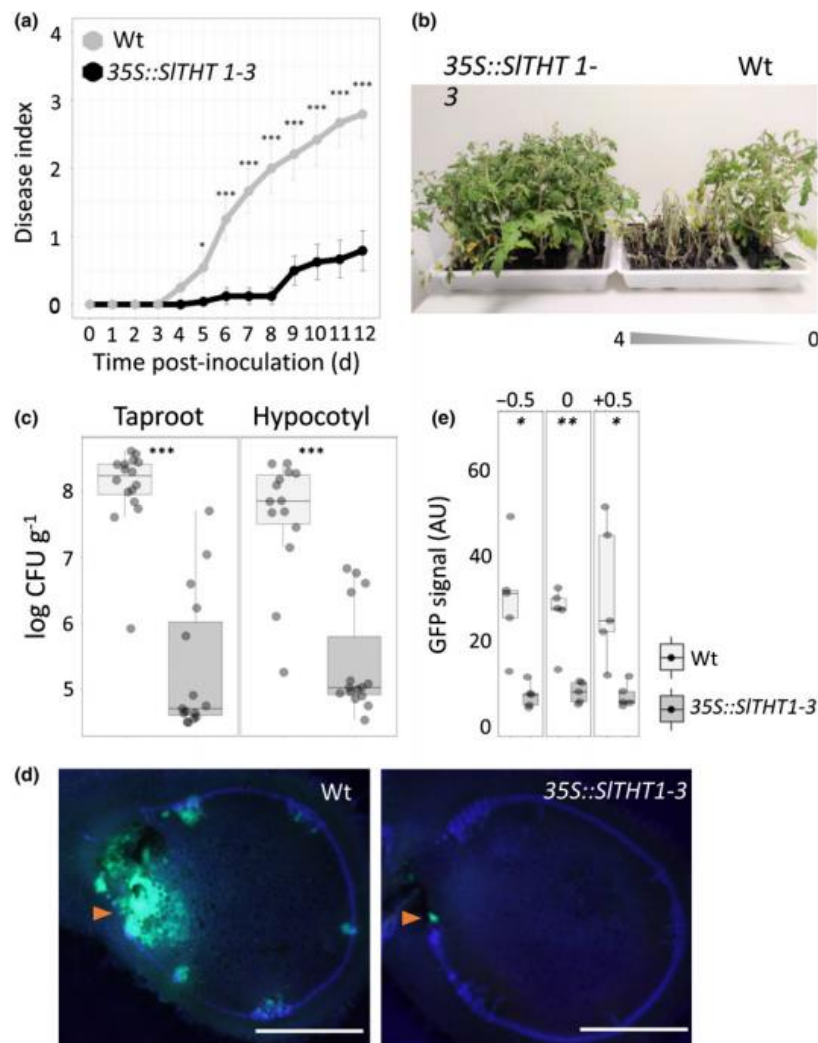


Fig. 7 Overexpression of *SITH1-3* in susceptible tomato confers resistance to *Ralstonia solanacearum*. (a, b) A pathogenicity assay was performed comparing wild-type (Wt) and *35S::SITH1-3* tomato lines (MoneyMaker background) after infection with *R. solanacearum* lux reporter GMI1000 strain. Five-wk-old plants were soil-soak inoculated with c. 1×10^7 colony-forming units (CFU) ml^{-1} and grown at 28°C. (a) Wilting progress was monitored by rating plants daily on a 0 to 4 disease index scale where 0 = healthy and 4 = 100% wilted. Plotted values correspond to means \pm standard error of 24 independent plants ($n = 24$) from a representative experiment out of a total of three. Asterisks indicate statistically significant differences between Wt and *35S::SITH1-3* using a Kruskal–Wallis test at each day post infection (dpi) was conducted to examine differences in disease index among different genotypes. Significant differences among genotypes were confirmed by applying a pairwise Wilcox test (*, $P < 0.05$; ***, $P < 0.0001$). (b) Pictures were taken 12 dpi. Wt plants were arranged according to the degree of symptom severity (from 4 to 0). (c) Transgenic *35S::SITH1-3* tomato significantly restricted *R. solanacearum* colonization in both the taproot-to-hypocotyl transition zone and hypocotyl compared to Wt. Five-wk-old tomato plants were root-inoculated with a *R. solanacearum* GMI1000 luciferase reporter strain at a concentration of c. 1×10^7 CFU ml^{-1} or water mock. The level of *in planta* colonization by *R. solanacearum* was calculated as colony forming units per gram of fresh taproot tissue (CFU g^{-1}) at 12 dpi. Data are represented with box and whiskers plots: whiskers indicate variability outside the upper and lower quartiles and boxes indicate second quartile, median and third quartile. Box-and-whisker plots show data from a representative experiment out of three ($n = 14$ –16) (***, $P < 0.0001$). (d) Transverse stem cross-sections of Wt and transgenic *35S::SITH1-3* tomato lines were imaged under a confocal microscope 6 d after infection with a *R. solanacearum* GMI1000 green fluorescent protein (GFP) reporter strain. *Ralstonia solanacearum* at a concentration of 10^5 CFU ml^{-1} was injected directly into the xylem vasculature of the first internode thorough the petiole. Orange arrow points the site of inoculation. Representative images of *R. solanacearum* colonization progress at the point of inoculation are shown. Bar, 2 mm. (e) Mean green fluorescence of the GFP signal emitted from *R. solanacearum* at cross-sections obtained as described in (d) at the point of inoculation (0), below the point of inoculation (–0.5 cm) and above the point of inoculation (+0.5 cm) was measured using IMAGEJ. Data are represented with box and whiskers plots: whiskers indicate variability outside the upper and lower quartiles and boxes indicate second quartile, median and third quartile. Data from a representative experiment out of a total of three, with $n = 5$ plants per condition. In (a) a Kruskal–Wallis test at each dpi was conducted to examine differences in disease index among different genotypes. Significant differences among genotypes were confirmed by applying a pairwise Wilcox test. Asterisks indicate statistically significant differences between wild-type and *35S::SITH1-3* tomato lines in (a) (*, $P < 0.05$; **, $P < 0.001$).

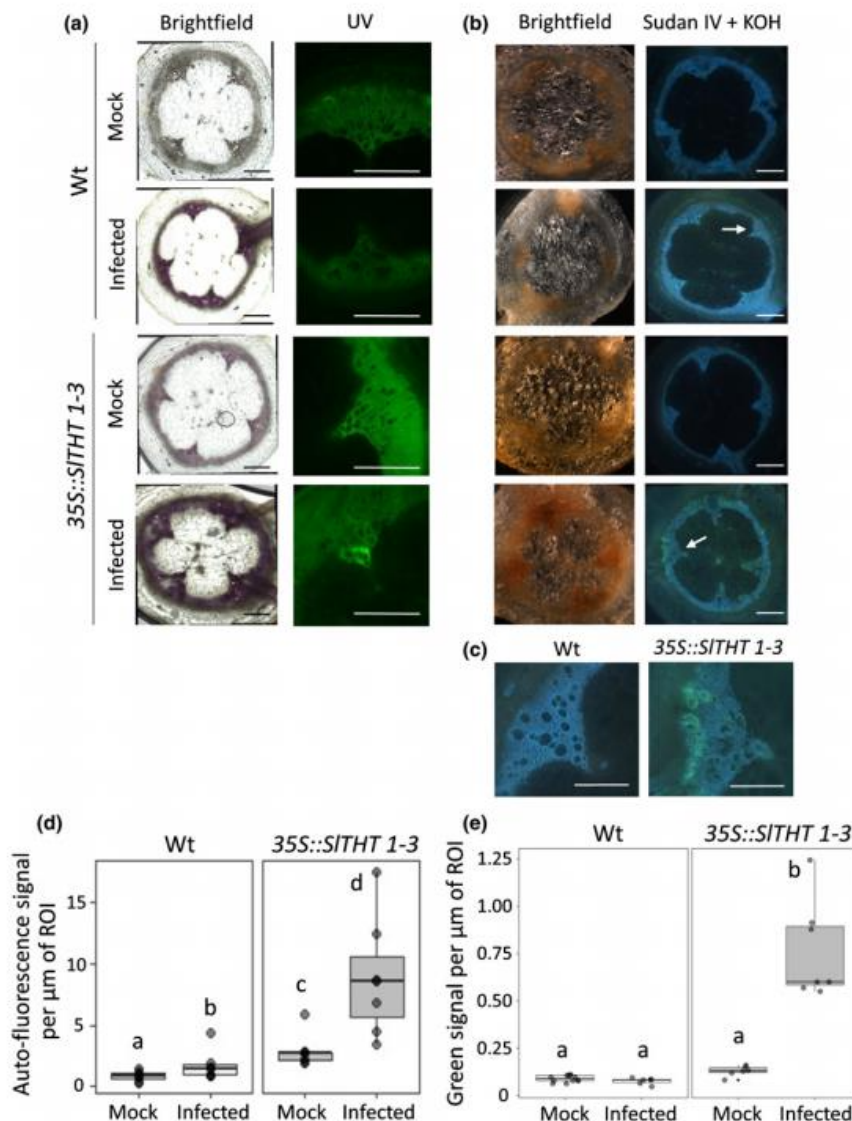


Fig. 8 Overexpression of *SITH1-3* in susceptible tomato results in vascular autofluorescence not-quenched with phloroglucinol and cell wall ferulate/feruloylamine deposition in restricted zones of vascular tissue upon *Ralstonia solanacearum* infection. Susceptible wild-type Moneymaker (Wt) or resistant 35S::SITH1-3 overexpressing tomato plants were soil-inoculated with a c. 1×10^7 colony-forming unit (CFU) ml^{-1} suspension of *R. solanacearum* GM1000 lux reporter strain. Cross-sections were obtained from taproot-to-hypocotyl of both genotypes tissue containing 10^5 CFU g^{-1} of *R. solanacearum*. (a) Cross-sections were stained with phloroglucinol-HCl and observed under brightfield to visualize lignin deposition (left) and under ultraviolet (UV) to visualize other autofluorescent compounds different from lignin (not quenched with phloroglucinol-HCl) (right). (b) Combined Sudan IV+KOH treatment showed no positive suberin aliphatic signal in *SITH1-3*, but a significant increase in ferulate/feruloylamine accumulation upon infection. (c) Close-ups (10×) of the vascular bundles of Wt and 35S::SITH1-3 infected plants pointed with a white arrow in (b) are also shown. Images from a representative experiment out of three with $n = 6$ plants per cultivar. (d) Quantification of UV fluorescence after phloroglucinol-HCl staining as shown in (a, right) were performed with Las X software by selecting the vascular areas surrounding main vessels with strong localized fluorescence or green signal. (e) Quantification of UV green fluorescence from ferulate deposits after Sudan IV+KOH staining as shown in (a, right) were performed with Las X software by selecting the vascular areas surrounding main vessels with strong localized fluorescence or green signal. Data in (d, e) are represented with box and whiskers plots: whiskers indicate variability outside the upper and lower quartiles and boxes indicate second quartile, median and third quartile. Different letters indicate statistically significant differences ($\alpha = 0.05$, Fisher's least significant difference test). Bar, 500 μm .

Beyond histochemistry and spectroscopic signature detections, further evidence supporting the nature of these ligno-suberin coatings as responsible of the resistance observed in H7796 to *R. solanacearum* was unequivocally provided transcriptionally using gene markers. Tissues undergoing suberization have to go

through a complex reprogramming involving a network of metabolic pathways, in order to produce the precursors of the polymer and their polymerization into the matrix (Lashbrooke *et al.*, 2016). Transcriptional reprogramming associated to suberin biosynthesis was clearly observed in the taproot-to-

hypocotyl transition zone vascular tissue of resistant H7996 tomato upon infection with *R. solanacearum* (Fig. 5). Interestingly, PAL, which showed modest upregulation in resistant H7996, had been previously defined as a rate-limiting enzyme of phenylpropanoid pathway (Faragher & Brohier, 1984; Howles *et al.*, 1996). Considering this, the observed upregulation could provide more tyramine and feruloyl-CoA, which together with the upregulation of *THT* would be in agreement with the increased presence of feruloyltyramine detected by 2D-HSQC-NMR (Fig. 2a).

The 2D-HSQC-NMR also revealed differences in the composition and structure of lignin between resistant and susceptible tomato cultivars after infection (Fig. 2). The amounts and the level of lignin of a particular tissue affect wall strength, degradability and pathogen resistance (Cho *et al.*, 2012; Mnich *et al.*, 2020). However, its role in resistance/susceptibility responses is not fully understood. Part of the challenge lies in the fact that its composition seems to be less static than what was previously established. A large variety of lignin-like polymers may co-exist in plants depending on the developmental or environmental context. This becomes particularly relevant in plant–pathogen interactions, where a large variety of compounds linked to lignin differentially accumulate upon infection (Cho *et al.*, 2012; Zeiss *et al.*, 2019). The observed lignin structural differences after infection indicate that (1) under basal conditions the two tomato varieties display differences in the composition and structure of lignin and (2) *R. solanacearum* infection affects very differently the lignin fraction in the two varieties: resistant tomato shows only a slight decrease in the S : G ratio that may be linked to an accumulation of the ligno-suberin heteropolymer, while susceptible Marmande undergoes pronounced depolymerization that correlates with a decrease in ferulate/feruloylamide (Fig. 3a). Although *R. solanacearum* has not been shown to be able to specifically depolymerize lignin, the pathogen secretes enzymes that can degrade cell wall polysaccharides and could participate in the observed Marmande stem collapse phenotype (Fig. 1a). In resistant H7996, however, vascular ligno-suberin-containing coatings would allow to create a hydrophobic barrier to prevent enzymes from accessing the cell wall substrates and at the same time create reinforcements, contributing to resistance to the pathogen. The fact that these reinforcements are rich in tyramine/feruloyltyramine, may further reinforce the structural barrier, providing rigidity and hampering cell wall digestibility by the pathogen's hydrolytic enzymes (Macoy *et al.*, 2015a,b; Zeiss *et al.*, 2021). In addition to that, resistant H7996 may have evolved yet undiscovered mechanisms that directly prevent lignin degradation by the pathogen.

Overall, our data indicate that vascular coating with wall-bound ligno-suberized compounds may restrict horizontal spread of the bacterium (Fig. 1). In comparison, susceptible tomato is either not able to induce such vascular coating upon *R. solanacearum* infection or induces a very weak response (Figs 1, 3), potentially predisposing its vascular walls to disruption by the pathogen's cell wall degrading enzymes. Considering that both varieties seem to possess the metabolic components to build such barriers, the difference in response may be a direct effect of the

differential transcriptional activation of the pathway in vascular tissue of H7996 compared to Marmande. The fact that varieties with moderate resistance to *R. solanacearum* show intermediate restriction of colonization (Planas-Marquès *et al.*, 2019), indicate that the formation of these barriers may be a quantitative trait. However, this also opens the possibility that the differential transcriptional activation of the ligno-suberin pathway observed in resistant tomato may have evolved as an effective mechanism to execute defense responses triggered by activation of an immune receptor upon *R. solanacearum* recognition. Very few immune receptors involved in perception of vascular wilt pathogens have been identified so far, and the mechanisms involved in translating this recognition into effective defense responses in the vasculature remain vastly unknown. Considering that the xylem is a dead tissue, it is expected that the surrounding parenchyma cells will have a pivotal role in perception of the pathogen as well as the signaling leading to the synthesis and wall-binding of the metabolites involved in vascular coating structures, such as the one described here. In fact, xylem parenchyma cells have been shown to synthesize vascular coating components in response to the wilt pathogen *V. albo-atrum* (Street *et al.*, 1986). However, how suberin is synthesized and deposited in the xylem is still poorly defined. Exciting research currently ongoing in this area will certainly help understanding the origin and transport of ligno-suberin components to form inducible vascular deposits in response to pathogens. This will also help determine the exact point of perception of the pathogen (at a cell type or tissular level). Identification of pathogen-inducible pathways specifically occurring in resistant varieties such as the one presented here open new avenues of research to shed light on this biologically and agronomically relevant question.

Based on the earlier observations, we propose the following model (Fig. 9). When reaching the xylem vessels of resistant H7996, *R. solanacearum* multiplies and tries to invade the surrounding healthy vessels and parenchyma cells by degradation of the xylem pit membranes and walls. Resistant tomato plants respond to *R. solanacearum* vascular invasion depositing feruloyltyramine and other HCAA-tyramine derived compounds, and suberin. These deposits would block the pit membrane access and serve as coatings of the vessel walls and parenchyma cells present in the immediate vicinity of colonized vessels, compartmentalizing the infection. These ligno-suberized layers together form a 'zone of ligno-suberization' creating a strong physico-chemical barrier to limit *R. solanacearum* spread.

Engineering tomato resistance against *R. solanacearum* by inducing the tyramine-HCAA pathway

Considering the observed accumulation of ligno-suberin and cell wall-linked feruloyltyramine in resistant H7996 tomato in response to *R. solanacearum* infection, we sought to understand the implications of overexpressing genes involved in the synthesis of these compounds in susceptible tomato cultivars upon *R. solanacearum* infection. We focused on *FHT* and *THT* and because their corresponding transcripts are upregulated in the xylem vasculature of resistant tomato upon *R. solanacearum*

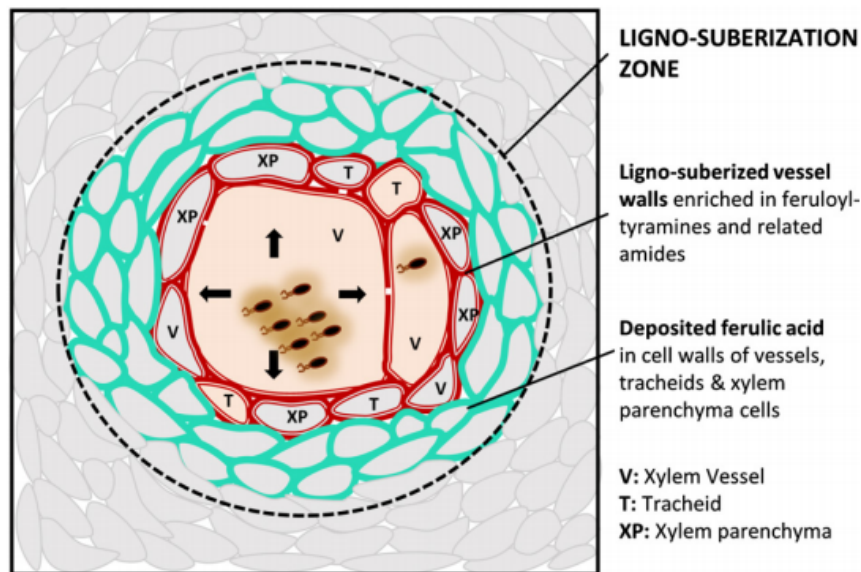


Fig. 9 Schematic representation of the vascular ligno-suberization process potentially taking place in infected vessels of resistant H7996 tomato upon *Ralstonia solanacearum* infection. Colonization of the vasculature by *R. solanacearum* in resistant tomato plants induces a ligno-suberization process in the walls of the infected vessel (V) and of the adjacent tracheids (T) and parenchyma cells (XP) (red). The lignin-like polymer accompanying suberin would be enriched in structural feruloyltyramine and related amides. The signal of structural ferulic acid (ester or as amide) would extend to the walls of peripheral parenchyma cells, vessels and tracheids (green), indicating a stage preceding suberization or a final layered pattern, still to be resolved. Together, the red and green areas, would form a 'zone of ligno-suberization' (black dashed line) potentially creating a physico-chemical barrier to limit *R. solanacearum* spread from the colonized xylem vessel lumen.

infection (Fig. 5) and they are the enzymes related with the synthesis of suberin ferulates and ether linked feruloyltyramine, respectively.

SIFHT overexpression had a small effect on the responses of susceptible tomato against *R. solanacearum*, showing a slight delay in wilting symptoms together with a slight decrease of bacterial loads in the plant (Fig. 6). The fact that increasing the levels of FHT in Marmande does only result in a marginal increase in resistance might be linked to a shortfall of aliphatic precursors in this variety (Fig. 5), which constrain a subsequent increase in suberin synthesis. In contrast, transgenic tomato overexpressing *SIFHT1-3* on a susceptible background was highly resistant to *R. solanacearum* (Fig. 7). Importantly, this transgenic line was previously shown to accumulate elevated amounts of soluble HCAAs such as feruloyltyramine and also SA upon infection with the bacteria *Pseudomonas syringae* pv. *tomato* (Pto) and to slightly but significantly restrict bacterial growth (Campos *et al.*, 2014). Since SA does not seem to play a major role in defense responses against *R. solanacearum* (Hirsch *et al.*, 2002; Hernández-Blanco *et al.*, 2007; Hanemian *et al.*, 2016), accumulation of this hormone in *SIFHT1-3* overexpressing line may not be the major underlying cause of the observed increase in resistance in this line. Alternatively, enhanced production of tyramine-derived HCAAs may constitute an important defense strategy against *R. solanacearum*. Feruloyltyramines exhibit antimicrobial activity (Fattorusso *et al.*, 1999; Novo *et al.*, 2017) and that they can be involved in plant priming or an adaptive strategy where plants are in a physiological state with improved defensive capacity (Zeiss *et al.*, 2021). These tyramine-derived

HCAAs overproduced in *SIFHT1-3* overexpressing plants may interfere with *R. solanacearum* colonization by becoming incorporated into the vascular and perivascular cell walls, providing a stronger crosslinking and restricting the movement of the pathogen inside the plant (Fig. 8) but also partly by remaining soluble and acting as direct antimicrobial agents against the pathogen. *Ralstonia solanacearum* possesses a hydroxycinnamic acid degradation pathway and it has been shown that mutants that cannot degrade hydroxycinnamic acids are less virulent on tomato (Lowe-Power *et al.*, 2015; Zhang *et al.*, 2019), which clearly underscores the importance of HCAAs in the arms race taking place in this pathosystem. Considering that the ligno-suberin pathway and HCAAs are well-conserved across the plant kingdom (Philippe *et al.*, 2020; Kashyap *et al.*, 2021; Zeiss *et al.*, 2021), these findings open the possibility to engineer disease resistance in other *R. solanacearum* hosts by manipulating these pathways. Interestingly, ligno-suberin deposits and accumulation of HCAAs have been reported in response to drought (Macoy *et al.*, 2015a,b; Zhang *et al.*, 2020). Therefore, engineering these pathways could have a double impact both on biotic and abiotic stress responses, improving plant performance in the field under adverse conditions.

In conclusion, we have provided evidence of the formation of a 'ligno-suberization zone' enriched in ether-linked feruloyltyramine and possibly related amides as an effective strategy to confine *R. solanacearum* into infected vessels of resistant tomato plants, preventing horizontal spread of the pathogen into healthy tissues and delaying disease symptoms. Resistance against *R. solanacearum* can be attained in susceptible tomato

background by stably overexpressing *THT* potentially contributing. In the future, it will be interesting to investigate the contribution of HCAs and suberin to resistance against the pathogen, the mechanisms whereby *R. solanacearum* perception leads to the formation of a ligno-suberin coatings around the vasculature in resistant tomato varieties. Increasing the spatio-temporal resolution of the tomato–*R. solanacearum* interaction will be instrumental to reach a deeper insight into structural resistance mechanisms. Also, since vascular confinement has been reported in different plant species as a means of resistance against various vascular wilt pathogens (De Ascensao & Dubery, 2000; Martín *et al.*, 2008; Xu *et al.*, 2011; Sabella *et al.*, 2018), the level of conservation of vascular ligno-suberin deposition and HCAs as a constituent of vascular coatings and part of a resistance mechanism remains to be determined.

Acknowledgements

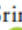
The authors would like to thank Gabriel Castrillo and Nico Geldner for inspiring discussions. The authors also thank Marc Planas-Marqués for helpful comments and María Pilar López Gresa (IBMCP-UPV) for kindly sharing the tomato *THT* seeds. Research is funded by MCIN/AEI/10.13039/501100011033 (NSC, MV), MCIN/AEI/PID2019-110330GB-C21 (MF, OS), MCIN/AEI/PID2020-118968RB-I00 (JR), through the 'Severo Ochoa Programme for Centres of Excellence in R&D' (SEV-2015-0533, CEX2019-000917 and CEX2019-000902-S funded by MCIN/AEI/ 10.13039/501100011033), and by the Spanish National Research Council (CISC) pie-201620E081 (JR, AG) and the Generalitat de Catalunya (2017SGR765 grant). AK is the recipient of a Netaji Subhas – Indian Council of Agricultural Research International Fellowship. SS acknowledges financial support from DOC-FAM, European Union's Horizon 2020 research and innovation programme under the Marie Skłodowska-Curie grant agreement no. 754397. This work was also supported by the CERCA Program/Generalitat de Catalunya.

Author contributions

AK designed and performed experiments, interpreted data and wrote the manuscript. ÁLJ-J performed the experiments required for the second submission of the manuscript. WZ performed experiments. MC performed experiments, interpreted data and reviewed the manuscript. SS conducted preliminary spectroscopy experiments and reviewed the manuscript. JR isolated the lignin/suberin fractions and conducted the 2D-HSQC-NMR analysis, including data interpretation. AG isolated the lignin/suberin fractions and conducted the 2D-HSQC-NMR analysis, including data interpretation. AL conducted preliminary spectroscopy experiments and reviewed the manuscript. OS conducted histopathology staining experiments, interpreted data and reviewed the manuscript. MF interpreted data and reviewed the manuscript. MV designed experiments, interpreted data and reviewed the manuscript. NSC conceptualized the research, designed experiments,

interpreted data and wrote the manuscript. ÁLJ-J and WZ contributed equally to this work.

ORCID

Montserrat Capellades  <https://orcid.org/0000-0001-9514-2885>
 Nuria S. Coll  <https://orcid.org/0000-0002-8889-0399>
 Mercè Figueras  <https://orcid.org/0000-0002-6288-1830>
 Ana Gutiérrez  <https://orcid.org/0000-0002-8823-9029>
 Álvaro Luis Jiménez-Jiménez  <https://orcid.org/0000-0002-9406-4595>
 Anurag Kashyap  <https://orcid.org/0000-0003-2622-8209>
 Anna Laromaine  <https://orcid.org/0000-0002-4764-0780>
 Jorge Rencoret  <https://orcid.org/0000-0003-2728-7331>
 Olga Serra  <https://orcid.org/0000-0002-1678-0932>
 Sumithra Srinivasan  <https://orcid.org/0000-0002-0473-9801>
 Marc Valls  <https://orcid.org/0000-0003-2312-0091>
 Weiqi Zhang  <https://orcid.org/0000-0002-2535-1398>

Data availability

The data that support the findings of this study are available from the corresponding author upon reasonable request.

References

- Álvarez B, Biosca EG, López MM. 2010. On the life of *Ralstonia solanacearum*, a destructive bacterial plant pathogen. In: Méndez-Vilas A, ed. *Technology and education topics in applied microbiology and microbial biotechnology*. Badajoz, Spain: Formatec, 267–279.
- Andersen TG, Molina D, Kilian J, Franke RB, Ragni L, Geldner N. 2021. Tissue-autonomous phenylpropanoid production is essential for establishment of root barriers. *Current Biology* 31: 965–977.
- Araujo L, Bispo WMS, Cacicque IS, Moreira WR, Rodrigues FA. 2014. Resistance in mango against infection by *Ceratocystis fimbriata*. *Phytopathology* 104: 820–833.
- Baayen RP, Elgersma DM. 1985. Colonization and histopathology of susceptible and resistant carnation cultivars infected with *Fusarium oxysporum* f. sp. *dianthi*. *Netherlands Journal of Plant Pathology* 91: 119–135.
- Benhamou N. 1995. Ultrastructural and cytochemical aspects of the response of eggplant parenchyma cells in direct contact with *Verticillium*-infected xylem vessels. *Physiological and Molecular Plant Pathology* 46: 321–338.
- Bernards MA. 2002. Demystifying suberin. *Canadian Journal of Botany* 80: 227–240.
- Bernards MA, Lewis NG. 1998. The macromolecular aromatic domain in suberized tissue: a changing paradigm. *Phytochemistry* 47: 915–933.
- Bernards M, Lopez M, Zajicek J, Lewis N. 1995. Hydroxycinnamic acid-derived polymers constitute the polyaromatic domain of suberin. *Journal of Biological Chemistry* 270: 7382–7386.
- Caldwell D, Kim B, Iyer-Pascuzzi AS. 2017. *Ralstonia solanacearum* differentially colonizes roots of resistant and susceptible tomato plants. *Phytopathology* 107: 528–536.
- Campos L, Lisón P, López-Gresa MP, Rodrigo I, Zacarés L, Conejero V, Bellés JM. 2014. Transgenic tomato plants overexpressing tyramine N-hydroxycinnamoyltransferase exhibit elevated hydroxycinnamic acid amide levels and enhanced resistance to *Pseudomonas syringae*. *Molecular Plant-Microbe Interactions* 27: 1159–1169.
- Carnachan SM, Harris PJ. 2000. Ferulic acid is bound to the primary cell walls of all gymnosperm families. *Biochemical Systematics and Ecology* 28: 865–879.
- Cho K, Kim Y, Wi SJ, Seo JB, Kwon J, Chung JH, Park KY, Nam MH. 2012. Nontargeted metabolite profiling in compatible pathogen-inoculated tobacco

- (*Nicotiana tabacum* L. cv. Wisconsin 38) using UPLC-Q-TOF/MS. *Journal of Agriculture and Food Chemistry* 60: 11015–11028.
- Correia VG, Bento A, Pais J, Rodrigues R, Haliński P, Frydrych M, Greenhalgh A, Stepnowski P, Vollrath F, King AWT *et al.* 2020. The molecular structure and multifunctionality of the cryptic plant polymer suberin. *Materials Today Bio* 5: 100039.
- Cruz APZ, Ferreira V, Pianzola MJ, Siri MI, Coll NS, Valls M. 2014. A novel, sensitive method to evaluate potato germplasm for bacterial wilt resistance using a luminescent *Ralstonia solanacearum* reporter strain. *Molecular Plant-Microbe Interactions* 27: 277–285.
- De Ascensao ARDCF, Dubery IA. 2000. Panama disease: cell wall reinforcement in banana roots in response to elicitors from *Fusarium oxysporum* f. sp. *cubense* race four. *Phytopathology* 90: 1173–1180.
- Digonnet C, Martinez Y, Denancé N, Chasseray M, Dabos P, Ranocha P, Marco Y, Jauneau A, Goffner D. 2012. Deciphering the route of *Ralstonia solanacearum* colonization in *Arabidopsis thaliana* roots during a compatible interaction: focus at the plant cell wall. *Planta* 236: 1419–1431.
- Donaldson L. 2020. Autofluorescence in plants. *Molecules* 25: 2393.
- Donaldson L, Williams N. 2018. Imaging and spectroscopy of natural fluorophores in pine needles. *Plants* 7: 10.
- Falter C, Ellinger D, Von Hulsen B, Heim R, Voigt CA. 2015. Simple preparation of plant epidermal tissue for laser microdissection and downstream quantitative proteome and carbohydrate analysis. *Frontiers in Plant Science* 6: 194.
- Faragher JD, Brohier RL. 1984. Anthocyanin accumulation in apple skin during ripening: regulation by ethylene and phenylalanine ammonia-lyase. *Scientia Horticulturae* 22: 89–96.
- Fattorusso E, Lanzotti V, Tagliatalela-Scafati O. 1999. Antifungal N-feruloylamides from roots of two *Allium* species. *Plant Biosystems* 133: 199–203.
- Figueiredo R, Portilla Llerena JP, Kiyota E, Ferreira SS, Cardeli BR, de Souza SCR, dos Santos Brito M, Sodek L, Cesarino I, Mazzafera P. 2020. The sugarcane ShMYB78 transcription factor activates suberin biosynthesis in *Nicotiana benthamiana*. *Plant Molecular Biology* 104: 411–427.
- Gleave AP. 1992. A versatile binary vector system with a T-DNA organisational structure conducive to efficient integration of cloned DNA into the plant genome. *Plant Molecular Biology* 20: 1203–1207.
- Gou J-Y, Yu X-H, Liu C-J. 2009. A hydroxycinnamoyltransferase responsible for synthesizing suberin aromatics in *Arabidopsis*. *Proceedings of the National Academy of Sciences, USA* 106: 18855–18860.
- Graça J. 2010. Hydroxycinnamates in suberin formation. *Phytochemistry Reviews* 9: 85–91.
- Graça J. 2015. Suberin: the biopolyester at the frontier of plants. *Frontiers in Chemistry* 3: 62.
- Grimault V, Anais G, Prior P. 1994. Distribution of *Pseudomonas solanacearum* in the stem tissues of tomato plants with different levels of resistance to bacterial wilt. *Plant Pathology* 43: 663–668.
- Hanemian M, Barlet X, Sorin C, Yadeta KA, Keller H, Favory B, Simon R, Thomma BPHJ, Hartmann C, Crespi M *et al.* 2016. *Arabidopsis* CLAVATA1 and CLAVATA2 receptors contribute to *Ralstonia solanacearum* pathogenicity through a miR169-dependent pathway. *New Phytologist* 211: 502–515.
- Harris PJ, Trethewey JAK. 2010. The distribution of ester-linked ferulic acid in the cell walls of angiosperms. *Phytochemistry Reviews* 9: 19–33.
- He M, Ding N. 2020. Plant unsaturated fatty acids: multiple roles in stress response. *Frontiers in Plant Science* 11: 562785.
- Hernández-Blanco C, Feng DX, Hu J, Sánchez-Vallet A, Deslandes L, Llorente F, Berrocal-Lobo M, Keller H, Barlet X, Sánchez-Rodríguez C *et al.* 2007. Impairment of cellulose synthases required for *Arabidopsis* secondary cell wall formation enhances disease resistance. *Plant Cell* 19: 890–903.
- Hirsch J, Deslandes L, Feng DX, Balagué C, Marco Y. 2002. Delayed symptom development in ein2-1, an *Arabidopsis* ethylene-insensitive mutant, in response to bacterial wilt caused by *Ralstonia solanacearum*. *Phytopathology* 92: 1142–1148.
- Howles PA, Sewalt VJH, Paiva NL, Elkind Y, Bate NJ, Lamb C, Dixon RA. 1996. Overexpression of 1-phenylalanine ammonia-lyase in transgenic tobacco plants reveals control points for yada into phenylpropanoid biosynthesis. *Plant Physiology* 112: 1617–1624.
- Iiyama K, Lam TBT, Stone B. 2020. Covalent cross-links in the cell wall. *Plant Physiology* 104: 315–320.
- Ishihara T, Mitsuhashi I, Takahashi H, Nakaho K. 2012. Transcriptome analysis of quantitative resistance-specific response upon *Ralstonia solanacearum* infection in tomato. *PLoS ONE* 7: e46763.
- Jhu M, Farhi M, Wang L, Philbrook RN, Belcher MS, Nakayama H, Zumstein KS, Rowland SD, Ron M, Shih PM *et al.* (2021). Lignin-based resistance to *Cuscuta campestris* parasitism in Heinz resistant tomato cultivars. *bioRxiv*. doi: 10.1101/706861.
- Jones JDG, Dangl JL. 2006. The plant immune system. *Nature* 444: 323–329.
- Joo Y, Kim H, Kang M, Lee G, Choung S, Kaur H, Oh S, Choi JW, Ralph J, Baldwin IT *et al.* 2021. Pith-specific lignification in *Nicotiana attenuata* as a defense against a stem-boring herbivore. *New Phytologist* 232: 332–344.
- Kashyap A, Planas-marqués M, Capellades M, Valls M, Coll NS. 2021. Blocking intruders: inducible physico-chemical barriers against plant vascular wilt pathogens. *Journal of Experimental Botany* 72: 184–198.
- Kim SG, Hur OS, Ro NY, Ko HC, Rhee JH, Sung JS, Ryu KY, Lee SY, Baek HJ. 2016. Evaluation of resistance to *Ralstonia solanacearum* in tomato genetic resources at seedling stage. *Plant Pathology Journal* 32: 58–64.
- Lashbrooke J, Cohen H, Levy-Samocho D, Tzfadia O, Panizel I, Zeisler V, Massalha H, Stern A, Trainotti L, Schreiber L *et al.* 2016. MYB107 and MYB9 homologs regulate suberin deposition in angiosperms. *Plant Cell* 28: 2097–2116.
- Legay S, Guerriero G, André C, Guignard C, Cocco E, Charton S, Boutry M, Rowland O, Hausman JF. 2016. MdMyb93 is a regulator of suberin deposition in russeted apple fruit skins. *New Phytologist* 212: 977–991.
- Liu H, Zhang S, Schell MA, Denny TP. 2005. Pyramiding unmarked deletions in *Ralstonia solanacearum* shows that secreted proteins in addition to plant cell-wall-degrading enzymes contribute to virulence. *Molecular Plant-Microbe Interactions* 18: 1296–1305.
- Lowe-Power TM, Ailloud F, Allen C. 2015. Hydroxycinnamic acid degradation, a broadly conserved trait, protects *Ralstonia solanacearum* from chemical plant defenses and contributes to root colonization and virulence. *Molecular Plant-Microbe Interactions* 28: 286–297.
- Lowe-Power TM, Khokhani D, Allen C. 2018. How *Ralstonia solanacearum* exploits and thrives in the flowing plant xylem environment. *Trends in Microbiology* 26: 929–942.
- Lulai EC, Corsini DL. 1998. Differential deposition of suberin phenolic and aliphatic domains and their roles in resistance to infection during potato tuber (*Solanum tuberosum* L.) wound-healing. *Physiological and Molecular Plant Pathology* 53: 209–222.
- Macey DM, Kim WY, Lee SY, Kim MG. 2015a. Biosynthesis, physiology, and functions of hydroxycinnamic acid amides in plants. *Plant Biotechnology Reports* 9: 269–278.
- Macey DM, Kim WY, Lee SY, Kim MG. 2015b. Biotic stress related functions of hydroxycinnamic acid amide in plants. *Journal of Plant Biology* 58: 156–163.
- Mahmoud AB, Danton O, Kaiser M, Han S, Moreno A, Algaffar SA, Khalid S, Oh WK, Hamburger M, Mäser P. 2020. Lignans, amides, and saponins from *Haplophyllum tuberculatum* and their antiprotozoal activity. *Molecules* 25: 2825.
- Mangin B, Thoquet P, Olivier J, Grimsley NH. 1999. Temporal and multiple quantitative trait loci analyses of resistance to bacterial wilt in tomato permit the resolution of linked loci. *Genetics* 151: 1165–1172.
- Martín JA, Solla A, Domingues MR, Coimbra MA, Gil L. 2008. Exogenous phenol increase resistance of *Ulmus minor* to Dutch elm disease through formation of suberin-like compounds on xylem tissues. *Environmental and Experimental Botany* 64: 97–104.
- Mazier M, Flamin F, Nicolai M, Sarnette V, Caranta C. 2011. Knock-down of both eIF4E1 and eIF4E2 genes confers broad-spectrum resistance against potyviruses in tomato. *PLoS ONE* 6: e29595.
- McGarvey JA, Denny TP, Schell MA. 1999. Spatial-temporal and quantitative analysis of growth and EPS I production by *Ralstonia solanacearum* in resistant and susceptible tomato cultivars. *Phytopathology* 89: 1233–1239.
- Mnich E, Bjarnholt N, Eudes A, Harholt J, Holland C, Jørgensen B, Larsen FH, Liu M, Manat R, Meyer AS *et al.* 2020. Phenolic cross-links: building and deconstructing the plant cell wall. *Natural Products Reports* 37: 919–961.

- Molina I, Li-Beisson Y, Beisson F, Ohlrogge JB, Pollard M. 2009. Identification of an Arabidopsis feruloyl-coenzyme A transferase required for suberin synthesis. *Plant Physiology* 151: 1317–1328.
- Nakaho K, Hibino H, Miyagawa H. 2000. Possible mechanisms limiting movement of *Ralstonia solanacearum* in resistant tomato tissues. *Journal of Phytopathology* 148: 181–190.
- Nakaho K, Inoue H, Takayama T, Miyagawa H. 2004. Distribution and multiplication of *Ralstonia solanacearum* in tomato plants with resistance derived from different origins. *Journal of General Plant Pathology* 70: 115–119.
- Negrel J, Javelle F, Paynot M. 1993. Wound-induced tyramine hydroxycinnamoyl transferase in Potato (*Solanum tuberosum*) tuber discs. *Journal of Plant Physiology* 142: 518–524.
- Negrel J, Pollet B, Lapiere C. 1996. Ether-linked ferulic acid amides in natural and wound periderms of potato tuber. *Phytochemistry* 43: 1195–1199.
- Novo M, Silvar C, Merino F, Martínez-Cortés T, Lu F, Ralph J, Pomar F. 2017. Deciphering the role of the phenylpropanoid metabolism in the tolerance of *Capsicum annuum* L. to *Verticillium dahliae* Kleb. *Plant Science* 258: 12–20.
- Pérez-Donoso AG, Sun Q, Caroline Roper M, Carl Greve L, Kirkpatrick B, Labavitch JM. 2010. Cell wall-degrading enzymes enlarge the pore size of intercellular pit membranes in healthy and *Xylella fastidiosa*-infected grapevines. *Plant Physiology* 152: 1748–1759.
- Philippe G, Sørensen I, Jiao C, Sun X, Fei Z, Domozych DS, Rose JK. 2020. Cutin and suberin: assembly and origins of specialized lipidic cell wall scaffolds. *Current Opinion in Plant Biology* 55: 11–20.
- Planas-Marqués M, Bernardo-Faura M, Paulus J, Kaschani F, Kaiser M, Valls M, Van Der Hoorn RAL, Coll NS. 2018. Protease activities triggered by *Ralstonia solanacearum* infection in susceptible and tolerant tomato lines. *Molecular & Cellular Proteomics* 17: 1112–1125.
- Planas-Marqués M, Kressin JP, Kashyap A, Panthee DR, Louws FJ, Coll NS, Valls M. 2019. Four bottlenecks restrict colonization and invasion by the pathogen *Ralstonia solanacearum* in resistant tomato. *Journal of Experimental Botany* 71: 2157–2171.
- Pomar F, Merino F, Barceló AR. 2002. O-4-linked coniferyl and sinapyl aldehydes in lignifying cell walls are the main targets of the Wiesner (phloroglucinol-HCl) reaction. *Protoplasma* 220: 17–28.
- Pomar F, Novo M, Bernal MA, Merino F, Barceló AR. 2004. Changes in stem lignins (monomer composition and crosslinking) and peroxidase are related with the maintenance of leaf photosynthetic integrity during *Verticillium* wilt in *Capsicum annuum*. *New Phytologist* 163: 111–123.
- Potter C, Harwood T, Knight J, Tomlinson I. 2011. Learning from history, predicting the future: the UK Dutch elm disease outbreak in relation to contemporary tree disease threats. *Philosophical Transactions of the Royal Society of London. Series B: Biological Sciences* 366: 1966–1974.
- Pouzoulet J, Jacques A, Besson X, Dayde J, Mailhac N. 2013. Histopathological study of response of *Vitis vinifera* cv. Cabernet Sauvignon to bark and wood injury with and without inoculation by *Phaeomoniella chlamydospora*. *Phytopathologia Mediterranea* 52: 313–323.
- Pradhan Mitra P, Loqué D. 2014. Histochemical staining of *Arabidopsis thaliana* secondary cell wall elements. *Journal of Visualized Experiments* 87: e51381.
- Puigvert M, Guarischi-Sousa R, Zuluaga P, Coll NS, Macho AP, Setubal JC, Valls M. 2017. Transcriptomes of *Ralstonia solanacearum* during root colonization of *Solanum commersonii*. *Frontiers in Plant Science* 8: 370.
- Ralph J, Landucci L. (2010). NMR of lignins. In: Heitner JA, Dimmel C, Schmidt DR, eds. *Lignin and lignans: advances in chemistry*. Boca Raton, FL, USA: CRC Press, Taylor & Francis, 137–243.
- Razem FA, Bernards MA. 2002. Hydrogen peroxide is required for poly (phenolic) domain formation during wound-induced suberization. *Journal of Agriculture and Food Chemistry* 50: 1009–1015.
- Rencoret J, Kim H, Evaristo AB, Gutiérrez A, Ralph J, Del Río JC. 2018. Variability in lignin composition and structure in cell walls of different parts of macaúba (*Acrocomia aculeata*) Palm Fruit. *Journal of Agriculture and Food Chemistry* 66: 138–153.
- Rico A, Rencoret J, Del Río JC, Martínez AT, Gutiérrez A. 2014. Pretreatment with laccase and a phenolic mediator degrades lignin and enhances saccharification of *Eucalyptus* feedstock. *Biotechnology for Biofuels* 7: 6.
- del Río JC, Rencoret J, Gutiérrez A, Kim H, Ralph J. 2018. Structural characterization of lignin from Maize (*Zea mays* L.) fibers: evidence for diferuloylputrescine incorporated into the lignin polymer in Maize kernels. *Journal of Agriculture and Food Chemistry* 66: 4402–4413.
- Rioux D, Nicole M, Simard M, Ouellette GB. 1998. Immunocytochemical evidence that secretion of pectin occurs during gel (gum) and tylosis formation in trees. *Phytopathology* 88: 494–505.
- Robb J, Lee SW, Mohan R, Kolattukudy PE. 1991. Chemical characterization of stress-induced vascular coating in tomato. *Plant Physiology* 97: 528–536.
- Sabella E, Luvisi A, Aprile A, Negro C, Vergine M, Nicoli F, Miceli A, De Bellis L. 2018. *Xylella fastidiosa* induces differential expression of lignification related-genes and lignin accumulation in tolerant olive trees cv. Leccino. *Journal of Plant Physiology* 220: 60–68.
- Salas-González I, Rey G, His P, Custódio V, Gopalchian D, Bakhoun N, Dew TP, Suresh K, Franke RB, Dangl JL et al. 2021. Coordination between microbiota and root endodermis supports plant mineral nutrient homeostasis. *Science* 371: eabd0695.
- Schmidt A, Grimm R, Schmidt J, Scheel D, Strack D. 1999. Cloning and expression of a potato cDNA encoding hydroxycinnamoyl-CoA:tyramine N-(hydroxycinnamoyl)transferase. *Journal of Biological Chemistry* 274: 4273–4280.
- Scortichini M. 2020. The multi-millennial olive agroecosystem of salento (Apulia, Italy) threatened by *Xylella fastidiosa* subsp. Pauca: a working possibility of restoration. *Sustain* 12: 6700.
- Serra O, Figueras M, Franke R, Prat S, Molinas M. 2010. Unraveling ferulate role in suberin and periderm biology by reverse genetics. *Plant Signaling & Behavior* 5: 953–958.
- Serrano M, Coluccia F, Torres M, L'Haridon F, Métraux JP. 2014. The cuticle and plant defense to pathogens. *Frontiers in Plant Science* 5: 274.
- Street PFS, Robb J, Ellis BE. 1986. Secretion of vascular coating components by xylem parenchyma cells of tomatoes infected with *Verticillium albo-atrum*. *Protoplasma* 132: 1–11.
- Thoquet P, Olivier J, Sperisen C, Rogowsky P, Laterrot H, Grimsley N. 1996. Quantitative trait loci determining resistance to bacterial wilt in tomato cultivar Hawaii 7996. *Molecular Plant-Microbe Interactions* 9: 826–836.
- Unsach R, Vieira Teixeira CDJ, Tendon VD, Gully K, Bellis DD, Schmidt-Siebert E, Andersen TG, Shekhar V, Calderon S, Pradervand S et al. 2021. GDSL-domain proteins have key roles in suberin polymerization and degradation. *Nature Plants* 7: 353–364.
- Vasse J, Frey P, Trigalet A. 1995. Microscopic studies of intercellular infection and protoxylem invasion of tomato roots by *Pseudomonas solanacearum*. *Molecular Plant-Microbe Interactions* 8: 241–251.
- Vasse J, Genin S, Frey P, Boucher C, Brito B. 2000. The hrpB and hrpG regulatory genes of *Ralstonia solanacearum* are required for different stages of the tomato root infection process. *Molecular Plant-Microbe Interactions* 13: 259–267.
- Wang JF, Ho FI, Truong HTH, Huang SM, Balatero CH, Dittapongpich V, Hidayati N. 2013. Identification of major QTLs associated with stable resistance of tomato cultivar “Hawaii 7996” to *Ralstonia solanacearum*. *Euphytica* 190: 241–252.
- Xu L, Zhu L, Tu L, Liu L, Yuan D, Jin L, Long L, Zhang X. 2011. Lignin metabolism has a central role in the resistance of cotton to the wilt fungus *Verticillium dahliae* as revealed by RNA-seq-dependent transcriptional analysis and histochemistry. *Journal of Experimental Botany* 62: 5607–5621.
- Yadeta KA, Thomma BPHJ. 2013. The xylem as battleground for plant hosts and vascular wilt pathogens. *Frontiers in Plant Science* 4: 97.
- Zeiss DR, Mhlongo MI, Tugizimana F, Steenkamp PA, Dubery IA. 2019. Metabolomic profiling of the host response of tomato (*Solanum lycopersicum*) following infection by *Ralstonia solanacearum*. *International Journal of Molecular Sciences* 20: 3945.
- Zeiss DR, Piater LA, Dubery IA. 2021. Hydroxycinnamate amides: intriguing conjugates of plant protective metabolites. *Trends in Plant Science* 26: 184–195.
- Zhang L, Merlin I, Pascal S, Bert PF, Domergue F, Gambetta GA. 2020. Drought activates MYB41 orthologs and induces suberization of grapevine fine roots. *Plant Direct* 4: 278.
- Zhang Y, Zhang W, Han L, Li J, Shi X, Hikichi Y, Ohnishi K. 2019. Involvement of a PadR regulator PrhP on virulence of *Ralstonia solanacearum* by controlling detoxification of phenolic acids and type III secretion system. *Molecular Plant Pathology* 20: 1477–1490.

Zuluaga AP, Solé M, Lu H, Góngora-Castillo E, Vaillancourt B, Coll N, Buell CR, Valls M. 2015. Transcriptome responses to *Ralstonia solanacearum* infection in the roots of the wild potato *Solanum commersonii*. *BMC Genomics* 16: 246.

Supporting Information

Additional Supporting Information may be found online in the Supporting Information section at the end of the article.

Fig. S1 Tissue used for analysis and bacterial dynamics.

Fig. S2 H7996 plants show mild symptoms upon challenge inoculation of *Ralstonia solanacearum*.

Fig. S3 Vascular coating response to *Ralstonia solanacearum* infection with wall bound phenolics.

Fig. S4 Expression of suberin biosynthetic genes in xylem vasculature of taproots upon infection of *Ralstonia solanacearum*.

Fig. S5 Phylogeny of feruloyl transferase (FHT) orthologs in different plant species and expression of the putative tomato FHT ortholog in response to *Ralstonia solanacearum* infection.

Fig. S6 Phylogeny of tyramine hydroxycinnamoyl transferase (THT) orthologs in different plant species and expression of the

tomato THT gene family members in response to *Ralstonia solanacearum* infection.

Fig. S7 Expression of phenylpropanoid pathway genes in xylem vasculature of taproots upon invasion of *Ralstonia solanacearum*.

Fig. S8 Immunoblot of 35S::SIFHT-HA in independent Marmande tomato lines expressing 35S::SIFHT-HA (Marmande).

Fig. S9 Fresh weight of 35S::SIFHT-HA plants.

Fig. S10 Fresh weight of 35S::SITHT1-3 plants.

Fig. S11 Overexpression of SITHT1-3 in tomato results in restricted colonization by *Ralstonia solanacearum*.

Table S1 List of primers used in this study.

Table S2 Assignments of the correlation signals in the two-dimensional heteronuclear single quantum coherence (2D HSQC) spectra.

Please note: Wiley Blackwell are not responsible for the content or functionality of any Supporting Information supplied by the authors. Any queries (other than missing material) should be directed to the *New Phytologist* Central Office.

Determination of de novo suberin-lignin ferulate deposition in xylem tissue upon vascular pathogen attack

Running head: Xylem ligno-suberin ferulate determination upon vascular pathogen attack

WeiQi Zhang^{1,‡}, Álvaro Jiménez-Jiménez^{1,‡}, Montserrat Capellades^{1,2}, Jorge Rencoret³, Anurag Kashyap^{2,‡}, Núria S. Coll^{1,2,*}

¹ Centre for Research in Agricultural Genomics (CRAG), CSIC-IRTA-UAB-UB, Campus UAB, 08193 Bellaterra, Spain

² Consejo Superior de Investigaciones Científicas (CSIC), 08001 Barcelona, Spain

³ Institute of Natural Resources and Agrobiological Sciences (IRNAS), CSIC, 41012 Seville, Spain

⁴ Department of Plant Pathology, Assam Agricultural University, Jorhat, Assam, India, 785013

[‡] These authors contributed equally to the work

* Corresponding authors:

Núria S. Coll,

Centre for Research in Agricultural Genomics (CRAG), CSIC-IRTA-UAB-UB, Campus UAB, 08195 Bellaterra, Spain

e-mail: nuria.sanchez-coll@cragenomica.es

Anurag Kashyap

Department of Plant Pathology, Assam Agricultural University, 785013 Jorhat, Assam, India

e-mail: anuragkashyap11@gmail.com

1. Introduction

Vascular plant pathogens cause some of the most devastating diseases in plants, ranging from annual herbaceous to big trees (Yadeta & Thomma, 2013). These pathogens adopt different strategies to make their way into xylem vessels. Once the pathogen reaches the vasculature it multiplies profusely inside the xylem tissue and spread vertically and horizontally to the neighboring tissues, resulting in dreadful wilting of the infected plants and eventual death (Bae *et al.*, 2015). However, resistant plants have evolved mechanisms in the xylem vasculature to sense invading pathogens and mount an array of defense responses against these aggressors (Yadeta & Thomma, 2013). One of the major defense mechanisms conferring resistance against vascular pathogens can be attributed to the genesis of physio-chemical blockades (Kashyap *et al.*, 2021). Plants have evolved effective structural defense mechanisms to prevent vessel colonization or movement between vessels, once vascular colonization has occurred (Beckman & Roberts, 1995). Structural barricades such as gels and tyloses prohibit vertical movement of xylem vascular pathogens inside the lumen of vessels. Similarly, vascular pathogen induced reinforcements in secondary cell wall of vascular tissue act as a potent barrier against colonization (Ferreira *et al.*, 2017). Wall reinforcements with phenolic polymers such as lignin and suberin contribute towards preventing horizontal spread of the pathogens to the apoplast and the contiguous active tissues and vessels (Kashyap *et al.*, 2022). Hence, these horizontal and vertical barricades compartmentalize vascular pathogens at the site of infection (Kashyap *et al.*, 2021). Timely formation of these physico-chemical vascular barriers early upon pathogen perception can lead to confinement of the vascular pathogen at the infected vessel, avoiding the spread of wilt diseases (Robb *et al.*, 2008; Zaini *et al.*, 2018; Planas-Marquès *et al.*, 2019). Also, the occurrence of these defense responses are highly intertwined, both spatial and temporally, for avoidance of deleterious repercussions (embolism and cavitation). Hence, these anatomical shifts act as a hallmark of plant defense response against xylem vascular pathogens, which can be vital while exploring resistant germplasms. Such structural defense responses vary based on the host-pathogen interaction but are conserved across the plant kingdom (Kashyap *et al.*, 2021). Hence, an in-depth histopathological characterization gives important insights on the defense responses employed by the host against a pathogen.

We present here protocols based on staining along with bright field and fluorescence microscopy, and on two-dimensional nuclear magnetic resonance (2D-NMR)

spectroscopy, standardized in our laboratory, to visualize wall reinforcements with phenolic wall polymers namely, lignin, ferulates and suberin that occur in xylem vasculature, in response to pathogen attack. Staining of cross-sections with Phloroglucinol-HCl gives an accurate visualization of changes in lignin accumulation of xylem vasculature in response to infection. Likewise, Sudan IV staining can accurately detect deposition of aliphatic domain of suberin in walls of xylem vasculature in response to pathogen attack. Another important phenolic player in wall reinforcements is ferulate which not only imparts strength to walls by cross-linking but it may also act as lignin-like poly-phenolic domain of suberin. Ferulates constitute a crucial component of the suberin polyphenolic domain and are one of the first compounds deposited in a suberizing tissue, potentially acting as nucleating site for suberin matrix polymerization (Negrel *et al.*, 1996; Graça, 2010, 2015; Boher *et al.*, 2013). Here we also present a simple technique to detect ferulate deposition in walls of vasculature as defense response to pathogens, based on a pH dependent blue to green color conversion of UV autofluorescence. On the other hand, 2D-NMR experiments such as the Heteronuclear Single Quantum Coherence (HSQC) can provide additional valuable information on suberin/lignin structure. 2D-HSQC NMR is considered one of the most powerful tools for plant cell wall structural analysis providing information on the composition and linkages in lignin/suberin polymers (Ralph and Landucci 2010; Correia *et al.* 2020).

2. Materials

2.1 Plant Varieties and Plant Growth Materials

1. Tomato (*Solanum lycopersicum*) plants cultivars Marmande and Moneymaker were used as susceptible control; cultivar Hawaii was used as a resistant control. Transgenic Moneymaker tomatoes overexpressing hydroxycinnamoyl-CoA:tyramine N-hydroxycinnamoyl transferase (THT), a key enzyme in the synthesis of hydroxycinnamic acid amides (Campos *et al.*, 2014) were also used. Plants were grown in controlled growth chambers at 60% humidity, neutral day photoperiod (12 h day-12 h night) and 27°C (when grown under light-emitting diode (LED) lighting) or 25°C (when grown under fluorescent lighting).
2. Soil mix: 5 parts peat + 3 small parts sand + 3 small part vermiculite.

2.2 Bacterial Strains and Bacterial Culture

1. *Ralstonia solanacearum* strain GMI1000 (Phylotype I, race 1 biovar 3) was used, including luminescent and fluorescent reporter strains previously described in Planas-Marques *et al.*, 2019.

2. Rich B medium: 10 g/L Bacteriological peptone, 1 g/L yeast extract, and 1 g/L casamino acids. For solid media 1.5% agar should be added before autoclaving. Before plating, 0.5% glucose and 0.005% triphenyltetrazolium chloride (TTC) should be added. pH should be adjusted to 7.0. Gentamycin (10 µg/ml) should be supplemented in liquid and solid cultures for selection of reporter strains.

3. Sterile petri dishes.

4. Sterile 50 ml tubes.

5. Spectrophotometer.

2.3 Tissue Sectioning

1. Sterile carbon steel surgical blades.

2. Sterile 2 ml tubes.

3. Ethanol 70%.

2.4 Histological materials

1. Ethanol 70%.

2. Phloroglucinol-HCl: 100 mg of Phloroglucinol dissolved in 8 ml of 95% Ethanol and 8 ml of HCl 37%, stored at room temperature covered in aluminum foil.

3. 1N potassium hydroxide (KOH) (pH above 10).

4. 5% Sudan IV solution: 2,5 g of Sudan IV in 50 ml of Ethanol 70%, filtered and stored at room temperature covered in aluminum foil.

5. Leica DM6B-Z microscope with ultraviolet (UV) illumination (340–380 nm excitation and 410–450 nm barrier filters).

6. Leica MC190-HD-0518131623 digital camera and Leica-DFC9000GT-VSC07341 camera.

3. Methods

3.1 Bacterial inoculation in planta (soil-drenching method)

1. Four- to five-week-old tomato plants are used for inoculation. Two days before inoculation, plants are transferred to a new chamber adapted for infection (27°C, 60% RH, 12 h/12 h). Do not overwater the plants so the soil is dry enough for the plants to absorb all the inoculum through the roots.

2. One day prior inoculation, set an overnight culture of the *R. solanacearum* strain(s) of interest in Rich B medium (+antibiotics) in an Erlenmeyer flask (see **Note 1**). The amount of inoculum needed depends on the experiment and number of plants you want to inoculate, as well as the final bacterial concentration in the inoculum.

Typically, a concentration of 10⁸ colony forming units (CFU)/ml is used for resistant

varieties and 10^7 CFU/ml for susceptible ones. Calculations can be made according to the initial concentration in the liquid culture, and the fact that 40 ml of inoculum per plant are used.

3. On the day of inoculation, measure the optical density (OD_{600}) of the culture, and prepare the inoculation solutions by diluting with sterile distilled water to the desired bacterial concentration (see **Note 2**). Poke the soil with a blue pipette tip at each corner of the pot (4 punctures) to inflict root wounding, which facilitates infection.

4. Pour 40 ml of bacterial suspension in each pot, and do not water the plants until they have time to absorb the inoculum (1-2 days, depending on plant size).

4. Afterwards, keep watering the plants regularly (see **Note 3**) and start scoring symptoms at 3 days post infection (dpi), when the susceptible backgrounds begin to show wilting symptoms.

3.2 Histochemical analysis

1. When the desired stage of infection for analysis has come, take the plants, wash the roots with 1% v/v bleach and eliminate the adventitious roots (**Note 4**).

2. Take thin (150 μ m) cross-sections with a sterile razor blade or a microtome, at the transition zone between the taproot and the basal hypocotyl, 1.5 cm below the soil line approximately (**Figure 1**).

2. Transfer the sections to tubes containing 300-500 μ l of ethanol 70% and incubate at room temperature (RT) 2-5 days (at least) before analysis. This incubation ensures that the components not bound to the cell wall become solubilized with the ethanol and are thus removed from cell wall structures.

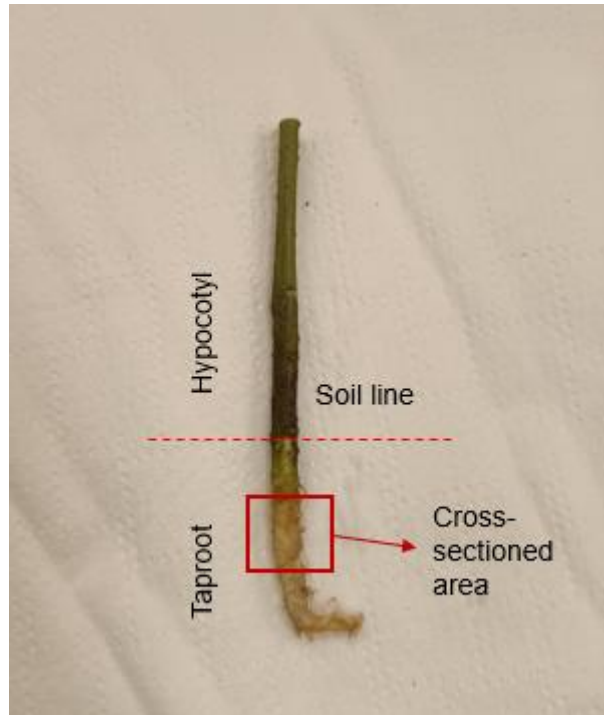


Figure 1. Region of interest for histological analysis. The lower portion of a 4-week-old tomato plant is shown, after throughout washing and eliminating adventitious roots, specifying in red the region of interest for the histochemical analysis

3.4 Lignin staining

For lignin detection, Phloroglucinol, (**Note 5**), is used for direct visualization of lignin (cinnamaldehyde end-groups of lignin units) (Pomar *et al.*, 2004) as a red-purple coloration in the vasculature (**Figure 2**).

A drop of staining solution is added to the cross-sections and incubated 5 mins at room temperature, until the purple color has appeared. Then, sections are mounted for microscopy using 70% ethanol and subsequently visualized under bright field light in a stereomicroscope (see **Note 6**).

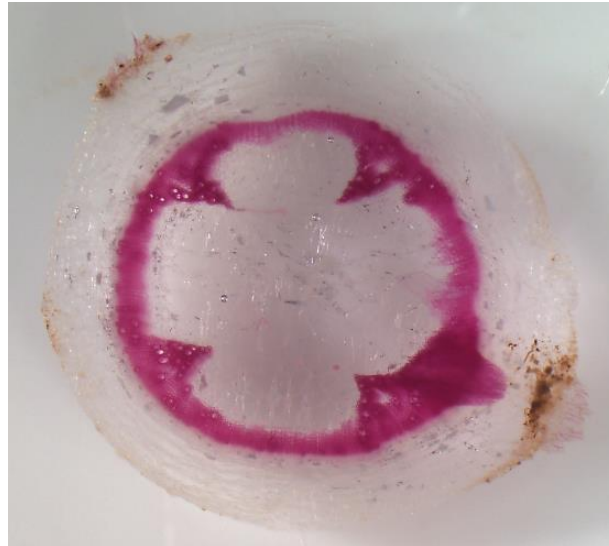


Figure 2. Phloroglucinol-stained samples. Examples cases of cross-sections stained with only Phloroglucinol-HCl observed under brightfield in a stereomicroscope Olympus SX16.

3.5 Detecting ferulate deposition

1. To detect ferulate accumulation (**Note 7**) alkali treatment can be performed, adding one drop of 1N KOH (pH=10) in the cross-sections of interest.
2. After 2 minutes of incubation at room temperature, samples can be mounted in microscopy slides with the KOH and ferulates can be visualized as green regions under UV light with an epifluorescence microscope. The basic pH is responsible for the blue-to-green shift in fluorescence observed specifically for ferulate deposits (Harris and Trethewey, 2010).

3.6 Detecting suberin aliphatics

1. To detect aliphatic suberin the Sudan IV stain is used. To prepare the samples, put the slices in a tube containing 300 μ l of Sudan IV and incubate 15 mins at room temperature.
2. Perform two washes with ethanol 70%, or until the samples do not release more dye.
3. After this, samples can be mounted on slides with ethanol 70% for microscopy. Under UV light in an epifluorescence microscope, suberin deposits can be visualized as brownish regions surrounding the vessels. Alternatively, the same samples can be directly mounted with 1N of KOH instead of ethanol, to combine the techniques in order to localize both parts of suberin barriers (**Figure 3**).

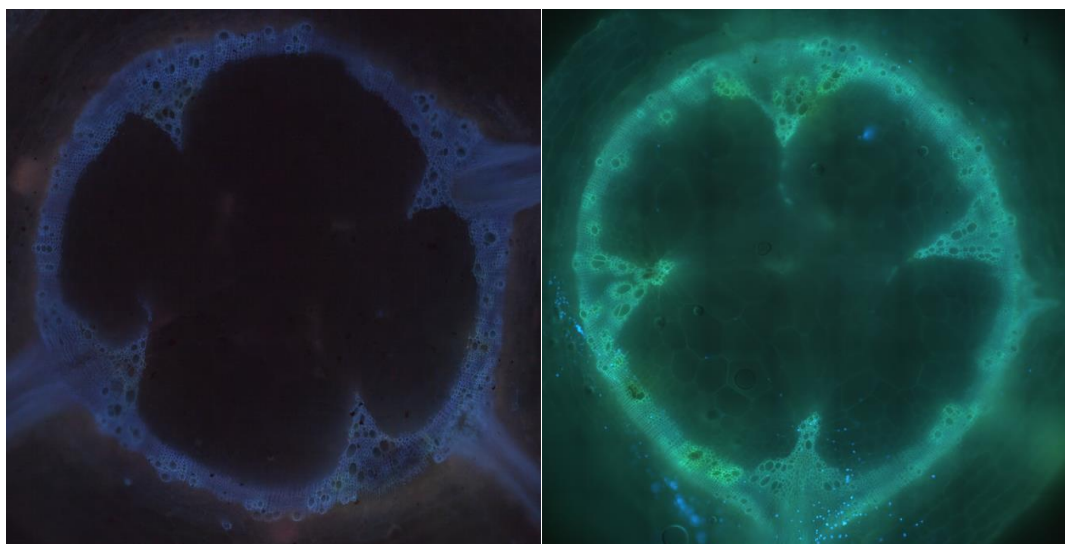


Figure 3. Sudan IV+KOH stained samples. Examples cases of cross-sections stained with only Sudan IV (left) and Sudan IV+KOH (right), observed under UV light in an epifluorescence microscopy Leica DM6.

3.7 Deciphering the composition and structure of the cell wall-deposited compounds

To obtain additional information on suberin and lignin present in tomato plant cell walls, fractions enriched in both polymers were isolated and analyzed by two-dimensional nuclear magnetic resonance spectroscopy (2D-NMR), which currently represents the most powerful tool for the structural analysis of plant cell-wall components (Ralph & Landucci, 2010; Correia *et al.*, 2020). Prior to 2D-NMR analysis of suberin/lignin polymers, it is necessary to remove the non-structural components of the plant cell wall, as well as the structural polysaccharides that form it.

- Solvent extraction for removing non-structural plant cell-wall components. Samples of a pool of tomato plants (taproot-to-hypocotyl region), infected or water-treated, are knife milled and extracted sequentially with distilled water, 80% ethanol, and finally with acetone, by sonicating in an ultrasonic bath, centrifuging and discarding the supernatant.

1. Add ~300 mg of plant material to a 50-ml PTEF Nalgene® centrifuge tubes.
2. Add 40 ml of distilled water and sonicate for 30 min.
3. Centrifuge the samples for 20 min at 8228 $\times g$ at 4 °C.
4. Remove the supernatant by decanting and discard it.
5. Repeat the water addition, sonication, centrifugation, and supernatant removal two additional times.
6. Add 40 ml of 80% (vol/vol) ethanol and sonicate for 30 min.
7. Centrifuge the samples for 20 min at 8228 $\times g$ at 4 °C.

8. Remove the supernatant by decanting and discard it.
9. Repeat the addition of 80% (vol/vol) ethanol, sonication, centrifugation, and supernatant removal two additional times.
10. Add 40 ml of 100% acetone and sonicate for 30 min.
11. Centrifuge the samples for 20 min at 8228 x *g* at 4 °C.
12. Remove the supernatant by decanting and then discard.
13. Oven-dry the extract-free tomato plant roots at ~45-50 °C (generally, 24 h is sufficient).

- Ball-milling. Grind extract-free tomato plant roots (around 200 mg) using a Retsch PM100 planetary mill (Retsch, Haan, Germany) fitted with one 50 ml agate grinding jar and 10 x10 mm ball bearings, set at 600 rpm. A total ball milling time of 3 h, alternating 20 min of grinding with 10 min of rest to avoid heating the sample, is sufficient.

- Lignin/suberin isolation by enzymatic removal of polysaccharides. The lignin/suberin fraction can be isolated by enzymatically hydrolyzing the structural polysaccharides that form the plant cell-wall, as described by Chang *et al.* (1975). For this, cellulysin cellulase (Calbiochem), a crude cellulase preparation from *Trichoderma viride* also containing hemicellulase activities, with activity $\geq 10,000$ FPUg⁻¹ of dry weight, is used.

1. Add ~200 mg of extractives-free ball-milled tomato roots to a 50-ml PTEF Nalgene® centrifuge tube.
2. Add 30 ml of 20 mM sodium acetate (pH 5.0) buffer and 7.5 mg of Cellulysin cellulase.
3. Incubate the reaction slurry at 30°C for 48 h, with constant agitation.
4. Centrifuge the samples (8228 x *g*, 4°C, 20 min) and discard the solvent by decantation.
5. Repeat the process with fresh buffer (30 ml) and enzyme (7.5 mg) two additional times.
6. Finally, wash the residue (enriched lignin/suberin fraction) with distilled water, recover it by centrifugation and freeze dry it.

- 2D-NMR analysis. Transfer approximately 20 mg of enzymatically isolated lignin/suberin preparation to a 5 mm NMR tube and add 0.6 ml of DMSO-*d*₆. Sonicate the NMR tube in an ultrasonic bath for 30-60 min until complete sample dissolution. Acquire 2D ¹H–¹³C Heteronuclear Single Quantum Coherence (HSQC) spectra on a cryoprobe-equipped Bruker Avance III 500 MHz instrument, using a standard Bruker adiabatic-pulse program ('hsqcetgpsisp.2') that enabled a semiquantitative analysis of the different ¹H–¹³C- correlation signals. 2D-HSQC spectra are acquired from 10 to 0 ppm in F2 (1H) using 1000 data points for an acquisition time (AQ) of 100 ms, an

interscan delay (D1) of 1 s, and from 200 to 10 ppm in F1 (^{13}C) using 256 increments of 32 scan, for a total experiment time of 2 h 34 min. The $^1J_{\text{CH}}$ used is 145 Hz. Processing uses typical matched Gaussian apodization in ^1H (LB=-0.1 and GB=0.001) and a squared cosine bell in ^{13}C (LB=0.3 and GB=0.1). The central residual DMSO peak ($\delta_{\text{C}}/\delta_{\text{H}}$ 39.5/2.49) is used as an internal reference.

- *Assignment and quantitation of 2D-HSQC correlation signals.* HSQC cross-signals are assigned by literature comparison (Rencoret *et al.*, 2018; del Río *et al.*, 2018; Mahmoud *et al.* 2020; Youngsung *et al.*, 2021). A semiquantitative analysis of the volume integrals of the HSQC correlation peaks can be performed using Bruker's Topspin or other equivalent NMR-processing software such as MNova. The ^1H - ^{13}C correlation signals from the aromatic/unsaturated region ($^1\text{H}/^{13}\text{C}$ 5-8/90-150 ppm) of the spectrum are used to estimate the lignin composition in terms of guaiacyl (G) and syringil (S) units (**Figure 4**). The correlation signals of G_2 and $\text{S}_{2,6}$ are used to estimate the content of the respective G- and S-lignin units (as the signal $\text{S}_{2,6}$ involves two proton-carbon pairs, its volume integral is halved). The $\text{C}\alpha/\text{H}\alpha$ correlation signals of the $\beta\text{-O-4'}$ alkyl aryl ethers ($\text{A}\alpha$), phenylcoumarans ($\text{B}\alpha$), and resinols ($\text{C}\alpha$) in the aliphatic-oxygenated region of the spectra (**Figure 4**) are used to estimate their relative abundances (as per 100 aromatic units), whereas the $\text{C}\gamma/\text{H}\gamma$ correlation signal of the cinnamyl alcohol end-units ($\text{I}\gamma$) is used to estimate its relative abundance (as per 100 aromatic units); as signal $\text{I}\gamma$ involves two proton-carbon pairs, its volume integrals is also halved. Suberin/lignin (Sub/L) ratio can be roughly estimated by integration of all the HSQC signals in the aliphatic region (in which most of suberin signals appear) and referring this value to the total aromatic lignin units (G+S) integration.

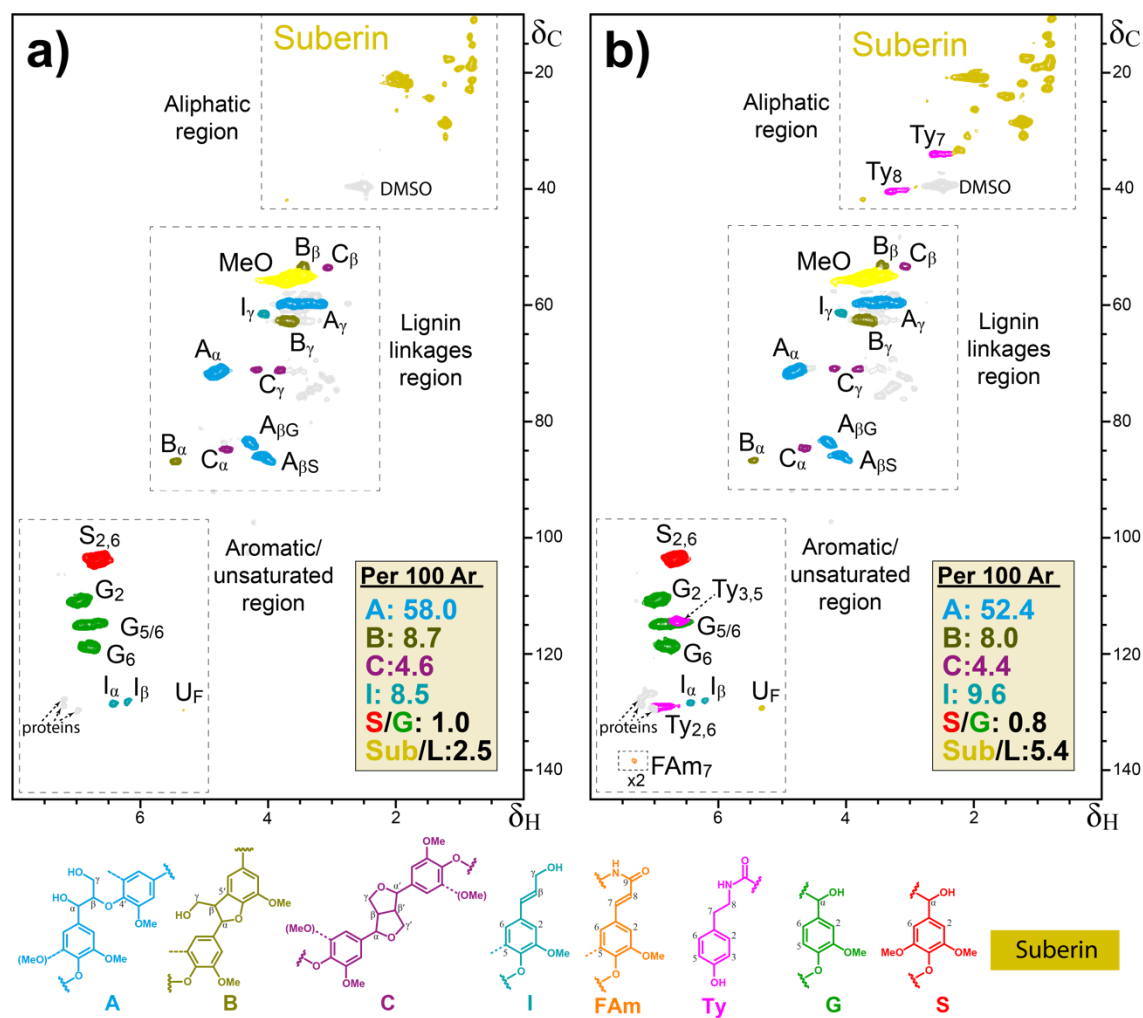


Figure 4. 2D-HSQC spectra of enzymatically isolated lignin/suberin fractions from mock-treated and *R. solanacearum*-infected taproots of resistant H7996 tomato. **(b)** Main lignin/suberin structures identified: β -O-4' alkyl aryl ethers (A), β -5' phenylcoumarans (B), β - β' resinols (C), cinnamyl alcohols end-groups (I), feruloyl amides (FAm), amides of tyramine (Ty), guaiacyl lignin units (G), syringyl lignin units (S), as well as unassigned aliphatic signals from suberin. The structures and contours of the HSQC signals are color coded to aid interpretation. To detect the FAM7 signal, the spectrum scaled-up to 2-fold ($\times 2$) intensity. The abundances of the main lignin linkages (A, B and C) and cinnamyl alcohol end-groups (I) are referred to as a percentage of the total lignin units ($S + G = 100\%$). Image reproduced from Kashyap *et al.*, 2022 with permission.

4. Notes

1. Always use a bigger Erlenmeyer than the desired volume (2.5 times-5 times) to ensure a good aeration of bacterial culture.
2. Do not use tap water, that can contain hypochlorite and other compounds toxic to bacteria.

3. Drought stress interferes with the response to bacterial wilt disease, so it is essential to ensure proper watering of the plants during infection.
4. In terms of analyzing the contribution of barrier formation on resistance, always take samples where both susceptible and resistant lines carry the same bacterial load.
5. Phloroglucinol is also known as the Weisner stain.
6. Phloroglucinol is easily oxidized (green coloration starts to appear) after a couple of weeks, so always use freshly stained samples.
7. At the molecular level, suberin is generally divided into an aromatic fraction composed mainly of ferulates, metabolic derivatives from the phenylpropanoid pathway, and an aliphatic part composed of long carbon chains (Nomberg *et al.*, 2022).

5. Acknowledgements

Research was funded through MCIN/AEI/ 10.13039/501100011033 and “ERDF A way of making Europe” with grants PID2019-108595RB-I00 (NSC) and PID2020-118968RB-I00 (JR) and with the fellowship PRE2020-092086 (ALJ-J). WZ is a recipient of a China Scholarship Council fellowship (CSC NO.201906990041). Research at CRAG is also funded through the “Severo Ochoa Programme for Centres of Excellence in R&D” (CEX2019-000902-S by MCIN/AEI/ 10.13039/501100011033) and through the CERCA Programme / Generalitat de Catalunya.

6. Figure legends

Figure 1. Region of interest for histological analysis. The lower portion of a 4-week-old tomato plant is shown, after throughout washing and eliminating adventitious roots, specifying in red the region of interest for the histochemical analysis.

Figure 2. Phloroglucinol stained samples. Examples cases of cross-sections stained with only Phloroglucinol-HCl observed under brightfield in a stereomicroscope Olympus SX16.

Figure 3. Sudan IV+KOH stained samples. Examples cases of cross-sections stained with only Sudan IV (left) and Sudan IV+KOH (right), observed under UV light in an

epifluorescence microscopy Leica DM6.

Figure 4. 2D-HSQC spectra of enzymatically isolated lignin/suberin fractions from mock-treated and *R. solanacearum*-infected taproots of resistant H7996 tomato. **(b)** Main lignin/suberin structures identified: β -O-4' alkyl aryl ethers (A), β -5' phenylcoumarans (B), β - β' resinols (C), cinnamyl alcohols end-groups (I), feruloyl amides (FAm), amides of tyramine (Ty), guaiacyl lignin units (G), syringyl lignin units (S), as well as unassigned aliphatic signals from suberin. The structures and contours of the HSQC signals are color coded to aid interpretation. To detect FAm₇ signal, the spectrum scaled-up to 2-fold ($\times 2$) intensity. The abundances of the main lignin linkages (A, B and C) and cinnamyl alcohol end-groups (I) are referred to as a percentage of the total lignin units ($S + G = 100\%$). Image reproduced from Kashyap *et al.*, 2022 with permission.

7. References

- Bae C, Han SW, Song YR *et al.* (2015) Infection processes of xylem-colonizing pathogenic bacteria: possible explanations for the scarcity of qualitative disease resistance genes against them in crops. *Theor Appl Genet* 128: 1219–1229.
- Beckman CH, Roberts EM. (1995) On the nature and genetic basis for resistance and tolerance to fungal wilt diseases of plants. *Adv Bot Res* 21: 35–77.
- Boher P, Serra O, Soler M *et al.* (2013) The potato suberin feruloyl transferase *FHT* which accumulates in the phellogen is induced by wounding and regulated by abscisic and salicylic acids. *J Exp Bot* 64: 3225–3236.
- Chang H, Cowling EB, Brown W *et al.* (1975). Comparative studies on cellulolytic enzyme lignin and milled wood lignin of sweetgum and spruce. *Holzforschung* 29:153–159.
- Correia VG, Bento A, Pais J, Rodrigues R, Haliński P, Frydrych M, Greenhalgh A, Stepnowski P, Vollrath F, King AWT *et al.* 2020. The molecular structure and multifunctionality of the cryptic plant polymer suberin. *Mater Today Bio* 5: 100039.
- Campos L, Lisón P, López-Gresa MP *et al.* (2014) Transgenic tomato plants overexpressing tyramine N-hydroxycinnamoyltransferase exhibit elevated hydroxycinnamic acid amide levels and enhanced resistance to *Pseudomonas syringae*. *Mol Plant Microbe Interact.* 27:1159-69.
- del Río JC, Rencoret J, Gutiérrez A *et al.* (2018) Structural characterization of lignin from Maize (*Zea mays* L.) fibers: evidence for diferuloylputrescine incorporated into the lignin polymer in Maize kernels. *Journal of Agricultural and Food Chemistry* 66: 4402-4413.
- Ferreira V, Pianzola MJ, Vilaró FL *et al.* (2017) Interspecific potato breeding lines display differential colonization patterns and induced defense responses after *Ralstonia*

- solanacearum* infection. Front Plant Sci 8: 1–14.
- Graça J. (2010) Hydroxycinnamates in suberin formation. Phytochem Rev 9: 85–91.
- Graça J. (2015) Suberin: The biopolyester at the frontier of plants. Frontiers in Chemistry 3: 1–11.
- Harris PJ and Trethewey JAK. (2010). The distribution of ester-linked ferulic acid in the cell walls of angiosperms. Phytochem Rev 9: 19–33.
- Kashyap A, Jimenez-Jimenez AL, Zhang W *et al.* (2022) Induced ligno-suberin vascular coating and tyramine-derived hydroxycinnamic acid amides restrict *Ralstonia solanacearum* colonization in resistant tomato. New Phytol 234: 1411-1429
- Kashyap A, Planas-Marquès M, Valls M. (2021) Blocking intruders: inducible physico-chemical barriers against plant vascular wilt pathogens. J Exp Bot 72: 184–198.
- Mahmoud AB, Danton O, Kaiser M *et al.* (2020) Lignans, amides, and saponins from *Haplophyllum tuberculatum* and their antiprotozoal activity. Molecules 25:2825.
- Negrel J, Pollet B, Lapierre C. (1996) Ether-linked ferulic acid amides in natural and wound periderms of potato tuber. Phytochemistry 43: 1195–1199.
- Nomberg, G, Marinov, O, Arya, GC *et al.* (2022) The key enzymes in the suberin biosynthetic pathway in plants: an update. Plants 11: 392.
- Planas-Marquès M, Kressin JP, Kashyap A *et al.* (2019) Four bottlenecks restrict colonization and invasion by the pathogen *Ralstonia solanacearum* in resistant tomato. J Exp Bot 71: 2157–2171.
- Pomar F, Novo M, Bernal MA *et al.* (2004) Changes in stem lignins (monomer composition and crosslinking) and peroxidase are related with the maintenance of leaf photosynthetic integrity during Verticillium wilt in *Capsicum annuum*. New Phytol 163: 111–123.
- Ralph J, Landucci L (2010) NMR of lignins. In: Heitner JA, Dimmel C, Schmidt DR, eds. Lignin and lignans: Adv chem. Boca Raton, FL, USA: CRC Press, Taylor & Francis, 137–243.
- Rencoret J, Kim H, Evaristo AB *et al.* (2018) Variability in lignin composition and structure in cell walls of different parts of macaúba (*Acrocomia aculeata*) palm fruit. J Agri Food Chem 66: 138–153.
- Robb J, Lee S-W, Mohan R, Kolattukudy PE (2008) Chemical characterization of stress-induced vascular coating in tomato. Plant Physiol 97: 528–536.
- Yadeta KA, Thomma BPHJ (2013) The xylem as battleground for plant hosts and vascular wilt pathogens. Front Plant Sci 4: 97.
- Youngsung J, Kim H, Kang M *et al.* (2021) Pith-specific lignification in *Nicotiana attenuata* as a defense against a stem-boring herbivore. New Phytol 232: 332–44.
- Zaini PA, Nascimento R, Gouran H *et al.* (2018) Molecular profiling of Pierce's disease outlines the response circuitry of *Vitis vinifera* to *Xylella fastidiosa* infection. Front Plant Sci 9: 771.